(21)

Heat Pipe Dehumidification for Supermarket Energy Savings

by
Eric M. Oliver
S.B. Art and Design, M.I.T.
Cambridge, Massachusetts
June, 1990

SUBMITTED TO THE DEPARTMENT OF ARCHITECTURE
IN PARTIAL FULFILLMENT OF THE REQUIREMENTS FOR THE DEGREE
MASTER OF SCIENCE IN BUILDING TECHNOLOGY
AT THE
MASSACHUSETTS INSTITUTE OF TECHNOLOGY
JUNE 1994

© Eric M. Oliver 1994. All rights reserved.

The author hereby grants to M.I.T. permission
to reproduce and to distribute publicly paper and
electronic copies of this thesis document in whole or in part.

Signature of the
author_____
Eric M. Oliver, Department of Architecture
February 16, 1994

Certified by_____
Leslie K. Norford
Assistant Professor, Building Technology
Thesis Supervisor

Accepted
by_____
Leon Glicksman
Professor, Building Technology
Chairman, Department Committee on Graduate Students

Rotch
MASSACHUSETTS INSTITUTE
OF TECHNOLOGY
JUL 14 1994

MIT Libraries
Document Services

Room 14-0551
77 Massachusetts Avenue
Cambridge, MA 02139
Ph: 617.253.2800
Email: docs@mit.edu
http://libraries.mit.edu/docs

DISCLAIMER OF QUALITY

Due to the condition of the original material, there are unavoidable flaws in this reproduction. We have made every effort possible to provide you with the best copy available. If you are dissatisfied with this product and find it unusable, please contact Document Services as soon as possible.

Thank you.

Images contained in this document are of the best quality available.

Heat Pipe Dehumidification for Supermarket Energy Savings
by
Eric Oliver

Submitted to the Department of Architecture on February 15, 1994
in partial fulfillment of the requirements for the Degree of
Master of Science in Building Technology

ABSTRACT

This thesis examines the possibility of using a heat pipe installed in the air conditioning unit of a supermarket to increase the level of dehumidification of the inside air. This dehumidification is expected to reduce the energy consumption of the refrigeration system due to an improved efficiency of the heat transfer at the display case. This increase in efficiency will be due to reduced frost buildup on the refrigeration coils. Chapter two includes a physical and psychrometric analysis of the heat pipe, proving that for any system where direct evaporation dehumidification is used, at any given time when dehumidification is being performed, the addition of a heat pipe will increase the amount of moisture being removed by the cooling coil.

For this thesis, a heat pipe was installed in a supermarket in Worcester, Massachusetts. Over a period of the summer from the beginning of June to the end of October, various air temperatures and relative humidities, refrigeration line temperatures, pressures, and mass flows, and compressor power consumption were monitored for fifteen minute periods. The monitoring period included two months before the installation and three months after the installation to determine changes in the air system and refrigeration system due to the presence of the heat pipe. Chapters two through five describe the equipment, site and strategy used in the analysis. Chapter six describes the results of the monitoring, and Chapters seven and eight give the results of the air system and refrigeration system models. The systems were modelled using monitored data and engineering equations to predict humidity levels and power consumption based on ambient conditions.

The analysis was unique in that a heat pipe application had never been previously studied in a Northeast location, since the mild summers made dehumidification less of an issue than in Southern states. This study was also considerably more in depth than previous studies (summarized in Chapter 2), for which savings estimates do not account for large potential errors. This study concluded that potential savings estimates (0-8% reduction in supply air humidity, ~1% reduction in refrigeration power) were within statistical error (9% for specific humidity, 4% for refrigeration power), and therefore inconclusive. Further studies with superior equipment and modelling strategies are needed to substantiate heat pipe dehumidification.

Thesis Supervisor: Leslie K. Norford
Title: Associate Professor of Building Technology

Dedication:

To Tracy, My sister and best friend

"You MIT people are the dumbest smart people in the world"

Acknowledgements

The compilation of this thesis involved five months of monitoring, one month of data organization, and ten weeks of writing, the last four of which was the most intense period of concentration on any one subject in my life, pushing the edges of physical and emotional balance. Along the way I learned more about refrigeration and air systems than any class could teach, more about written communication and report organization than in the previous 21 years since I learned how to write my name, and more about the people around me than I could ever have expected. Some people were with me part of the way, some all of the way, and I want to thank them all.

First I'd like to thank Scott Englander of New England Electric, my supervisor and friend, who introduced me to the project and was always there to help and offer ideas.

Second I'd like to thank Les Norford, my advisor who helped me make decisions and made sure I didn't compromise the quality of my work.

Third I'd like to thank Leon Glicksman, for his helpful advice and thoughtful comments.

And I'd like to thank Glenn Deming and Beth Poulin of Aspen Systems for taking on the thankless job of monitoring the site, and for adding extra effort to provide the best possible data, and Andy Hayes of Shaws Supermarkets for providing a facility for the project and for supplying answers to the many questions raised along the way.

I'd like to thank the students of the building technology group for continuous support and friendship when things got tough.

As well I'd like to thank friends at New England Electric, especially the other interns who have seen the best and worst, and made sure I never stopped having fun.

And an MCI salute to Friends and Family , too numerous to list here, who helped me keep my sanity and *joie de vivre* .

I hope this thesis provides helpful insight to anyone interested in supermarket dehumidification, or energy conservation in general, because the importance of reducing the consumption of our resources cannot be stressed enough as we barrel into the twenty-first century.

Table of Contents

List of Figures

List of Tables

Chapter 1 Introduction

As electric utilities become more competitive and environmental concerns necessitate that steps be taken to preserve our natural resources, energy conservation has become one of the most important tasks of society today. The field of demand side management (DSM), has assumed a large role in reducing the amount of electricity generated each year. DSM involves engineers, designers, and utility planners who work to try and improve electrical efficiency where it is actually consumed. This usually occurs in the form of equipment retrofits, equipment replacements, or new construction design using the most energy efficient components. In this field, new technologies and advanced research have allowed more creative methods of energy conservation to play a significant part of total load reduction. One field of recent advancement involves reducing electricity consumption in supermarkets.

Supermarkets consume a significant amount of energy due to lighting, air conditioning, and refrigeration. The refrigeration of food, necessary to preserve freshness and marketability, is a complex process which consumes nearly 40 percent of total supermarket electricity consumption. A significant part of refrigeration electricity consumption goes to defrosting refrigeration coils which have accumulated frost from inside air. Previous studies have shown that dehumidifying inside air reduces the rate that frost builds up on these coils, therefore reducing the cooling load and power consumption of the refrigeration system. One method of dehumidifying inside air involves installing a heat pipe in the air conditioning system. A heat pipe is a device which pre-cools air before it enters the cooling coils, allowing the incoming air to reach saturation quicker which allows cooling coils to remove more moisture. The other end of the heat pipe reheats the

post-coil air closer to supply conditions. The process is accomplished by alternating evaporation and condensation of a liquid refrigerant contained within the heat pipe.

In this thesis, I analyze the issue of whether or not heat pipe dehumidification can play a significant role in energy conservation in the Northeast. Most previous studies have involved installations in the South, where dehumidification is an important issue due to the long high humidity season. In the Northeast, and specifically New England, the summers are milder and humidity levels are not as important an issue. Nevertheless, for supermarkets any amount of dehumidification is important in increasing the efficiency of the refrigeration system, as will be explained later in the thesis. To accomplish dehumidification, I feel heat pipes are the best alternative due to the fact that they are completely passive, requiring no energy input without significantly changing the existing air conditioning system. Heat pipes, as opposed to dessicant dehumidifying systems, can be retrofit into existing air conditioning units without changing setpoints or considerably increasing the unit's energy consumption. Heat pipes do, however, create an additional pressure drop in the airflow due to resistance, and if existing airflows are to be maintained, the fan blower will require an adjustment, increasing its power consumption slightly. While dessicant systems consume gas and electricity while in operation, heat pipes provide free humidity reduction, which is important in a location where humidity reduction is expected to be small.

The next five sections will further explain the consumption of energy in supermarkets, the need for dehumidification, types of dehumidification, and finally a map of how the remaining chapters will accomplish the analysis

1.1 Supermarket Energy Consumption

Supermarkets are increasingly becoming targets for DSM energy efficiency projects in utilities' efforts to reduce electricity consumption and demand in the commercial sector. According to estimates by the Electric Power Research Institute (EPRI), supermarkets account for approximately ten percent of the total electricity consumption in the commercial sector, which accounts for about thirty percent of all electricity use in the United States (Blatt 1992). Typical supermarket energy consumption breaks down to about 40% for refrigeration, 25% for lighting, 20% for heating, ventilation and air conditioning, and 15% for miscellaneous. These figures will vary according to many factors such as climate, store size, operating hours and equipment efficiency, but it is clear that attacking refrigeration energy consumption is a good way to cut electricity costs.

Refrigeration energy consumption consists of three main components. A certain portion of refrigeration energy is consumed at the display cases (in the form of fan power, case lighting, and anti-sweat heaters), some energy is consumed by compressors, and a smaller amount of energy is used by the condensers. For a typical multiplex refrigeration system, compressor power represents 87% of overall refrigeration system energy consumption (Walker et al 1989). For the site monitored in this thesis, this percentage is not known, as only compressor power is monitored. The energy consumed at the display cases is somewhat constant, as fan power and lighting do not vary with ambient conditions, and anti-sweat heaters operate as a function of dew point temperature, which may or may not be controlled. Condenser fan power is a function of outside temperature, as higher air temperatures require increased fan power to provide adequate condensation. Compressor power is a function of load conditions on the refrigeration circuit and ambient air conditions. It is compressor power that would benefit the most from indoor air dehumidification.

1.2 Need For Dehumidification

Humidity levels in supermarkets are a problem for three reasons. First, there is a higher level of moisture introduction in supermarket buildings than most other buildings due to the constant entering and exiting of customers, in part because the average person emits about a half pound of water per hour through breathing and perspiration, and also because infiltration due to constant opening of doors introduces moisture when outside humidity levels are higher than indoor humidity levels. Second, high humidity levels can cause mold, mildew, and frost on shelved, refrigerated, and frozen food products. Third, moisture from indoor air makes its way into refrigerated food display cases, which causes frost buildup on refrigeration coils, thereby reducing their efficiency. Although this is usually only a problem during the summer, when outdoor humidity levels are substantially higher than desired indoor humidity levels, it is this third problem that I will focus on.

Due to the extremely low temperatures of refrigeration coils, moisture in the air surrounding them will condense and then freeze on the pipes. For any given air system with a specific temperature and relative humidity there is a dew point temperature, lower than the existing temperature, for which relative humidity is 100 percent. When an object in this system is at a temperature lower than the dew point, the surrounding air reaches 100 percent humidity and further cooling results in condensation of moisture on the object. If the object is lower than 32 degrees Fahrenheit, as is the case with many refrigeration coils, the condensed water will freeze. The latent energy of freezing condensate is absorbed by the refrigerant, requiring additional cooling. Also, as the ice builds up on the coils, it creates both an added insulation (thereby reducing the heat transfer from the air to the coils) and added surface area (which creates resistance to the airflow).

A typical multideck display case is shown in Figure 1. Cooling coils and circulation fans are located below and behind the products. This set up provides three air curtains

protecting the merchandise from the ambient air. The innermost flow path (path 1), contains the refrigeration coils. The fan forces air through the coils and out through the top of the case, supplying cold air into the case. At the bottom of the case is an inlet duct which draws the slightly warmed air into the fan based on negative pressure. The secondary air curtain (path 2) serves as a buffer between the cold air curtain and the ambient air curtain. The fan, located at the top of the case, draws air into the inlet duct and blows it out through the top, just outside the cold air outlet. The ambient air curtain (path 3) simply draws air from above the display case and blows it out an outlet just out side the secondary air curtain outlet. This air is not recirculated, but just allowed to spill out into the aisle. The paths, though, are theoretical and there is substantial air mixing prior to the inlet ducts. Because of this mixing, a significant amount of humid building air is drawn into the cases (Bittner 1992).

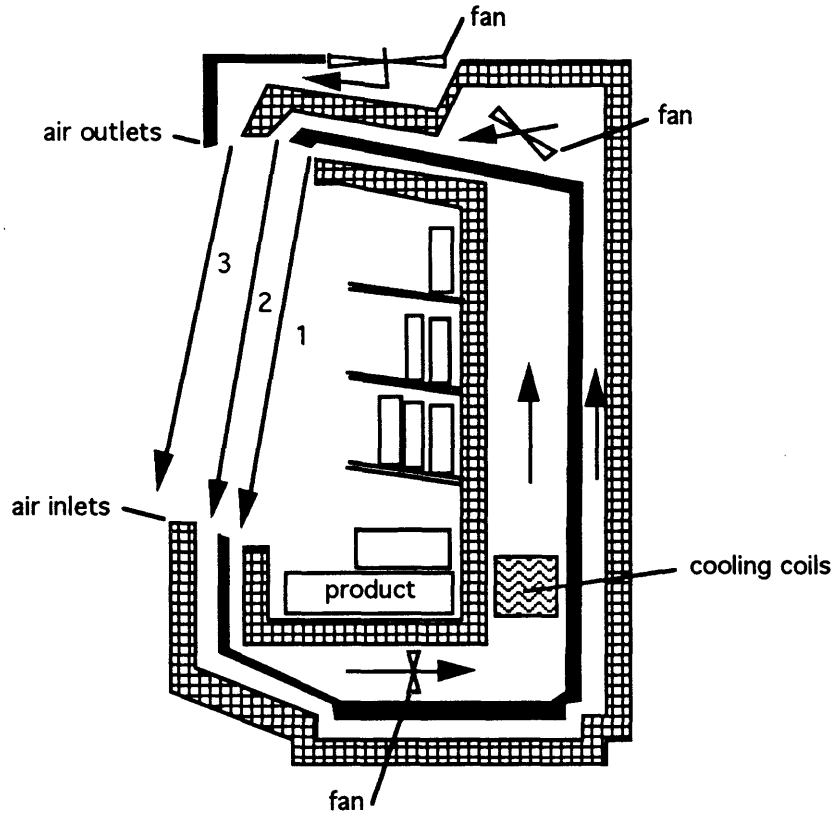

Figure 1. Section of a Typical Display Case

As this is an unavoidable problem, all refrigeration systems include a defrost cycle during which the ice is allowed (or forced) to melt off the coils. There are three typical types of defrost currently used. Off-time defrost shuts off the refrigerant flow and allows the ice to warm up and melt. Electric heat defrost shuts off the refrigerant flow and blows air warmed with an electric resistance heater over the ice. Hot gas defrost redirects hot refrigerant gas out of the compressor back into the coils, heating the pipes and melting the ice. All methods result in an undesirable warming of the display cases, and when the defrost cycle is done the refrigeration system picks up an extra load to cool the case back down to the desired temperature.

1.3 Types of Dehumidification

There are three main methods used to dehumidify air in supermarkets. Direct evaporation uses a cooling coil located right after the mixed air filters in the air conditioning duct (Figure 2) The coil cools air past the saturation point to condense moisture while evaporating the refrigerant. The cold, drier air is then heated through a reheat coil section (usually hot gas out of the refrigeration compressor before the condenser) to desired supply conditions.

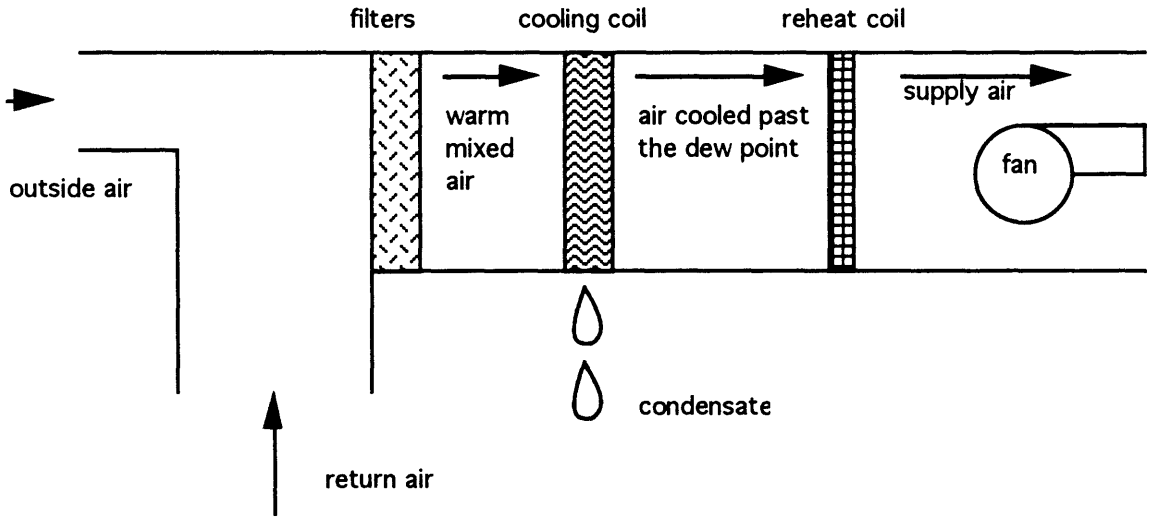

Figure 2. Diagram of Direct Evaporation Dehumidification

Gas-fired dessicant dehumidification uses a dessicant wheel which absorbs moisture from the mixed return air (Figure 3). The act of removing moisture passively from an air system increases its temperature, so the air needs to be cooled down to desired supply conditions. Sections of the dessicant wheel which have absorbed water need to be regenerated by blowing 250^{o} air through it to dry out the absorbed moisture. This is usually accomplished by gas heating outside air, blowing it through a section isolated in a separate

duct (accomplished by rotating the dessicant wheel), and dumping the wetter, cooler air back outside. Regeneration heating coils are designed to heat air from 95 degrees to 250 degrees at about 2,500 cfm, which requires 418,500 Btu/hr of energy. This corresponded to a moisture removal rate of 90 lbw/hr, which was described as typical for a 30,000 ft^2 supermarket (Banks 1992). If the ambient air being used for regeneration is cooler, more energy is needed. The rest of the energy used in the dessicant system is for the cooling coils to bring the warm, dried air down to supply air temperature. This process is somewhat energy intensive but reliable in dehumidifying. The third method, studied in this thesis and explained further in Chapter 2, is heat pipe dehumidification.

We can use a psychrometric chart to describe the differences between the three processes for typical design conditions (Figure 4). The dessicant process is represented by the dashed line, and the evaporative and heat pipe process is represented by the solid line. For a 30,000 cfm airflow and mixed air conditions of 70 degrees F and 70% RH (point 1) and supply air conditions of 65 degrees F and 55% RH,The dessicant wheel would need to remove moisture corresponding to a specific humidity drop of 0.004 lbw/lba.. At constant enthalpy, this action brings the air to point 2. Then, sensible cooling corresponding to an enthalpy drop of 5.4 Btu/lba (714,690 Btu/hr) is needed to bring the air to a dry bulb temperature of 65 degrees (point 4).

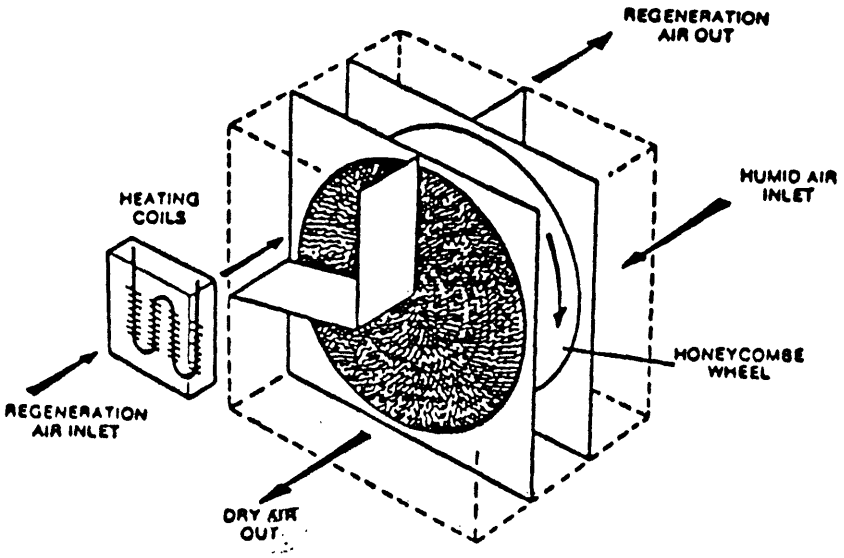

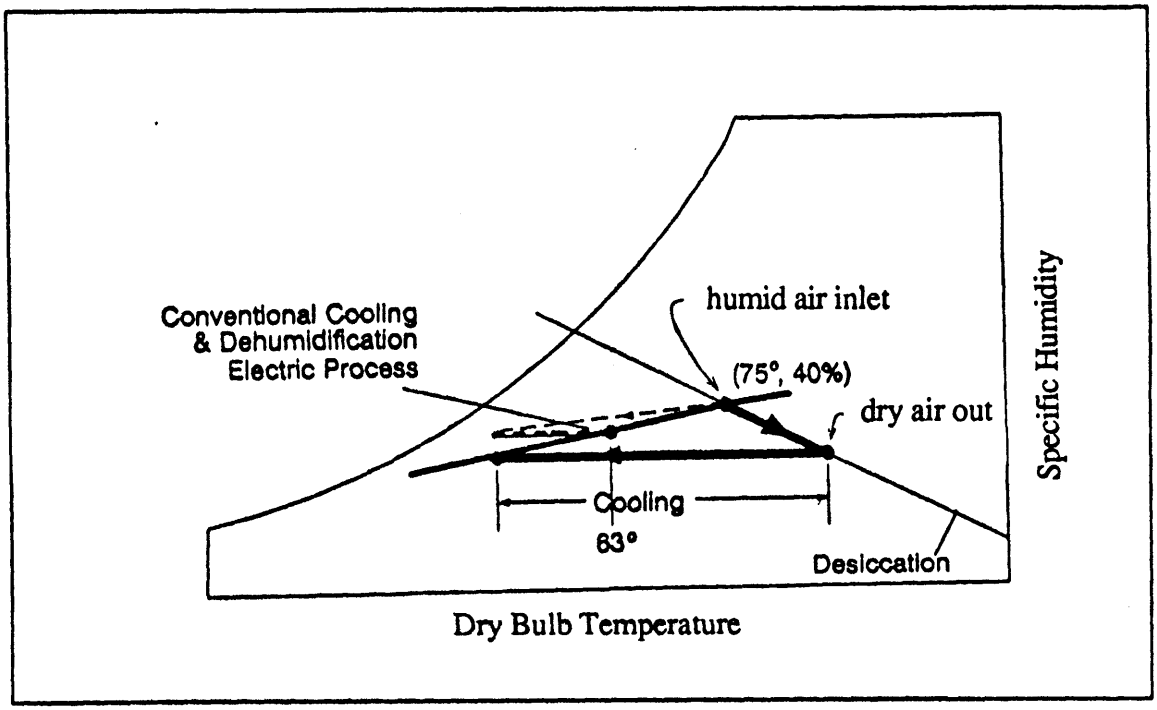

Figure 3. Dessicant Dehumidification Process

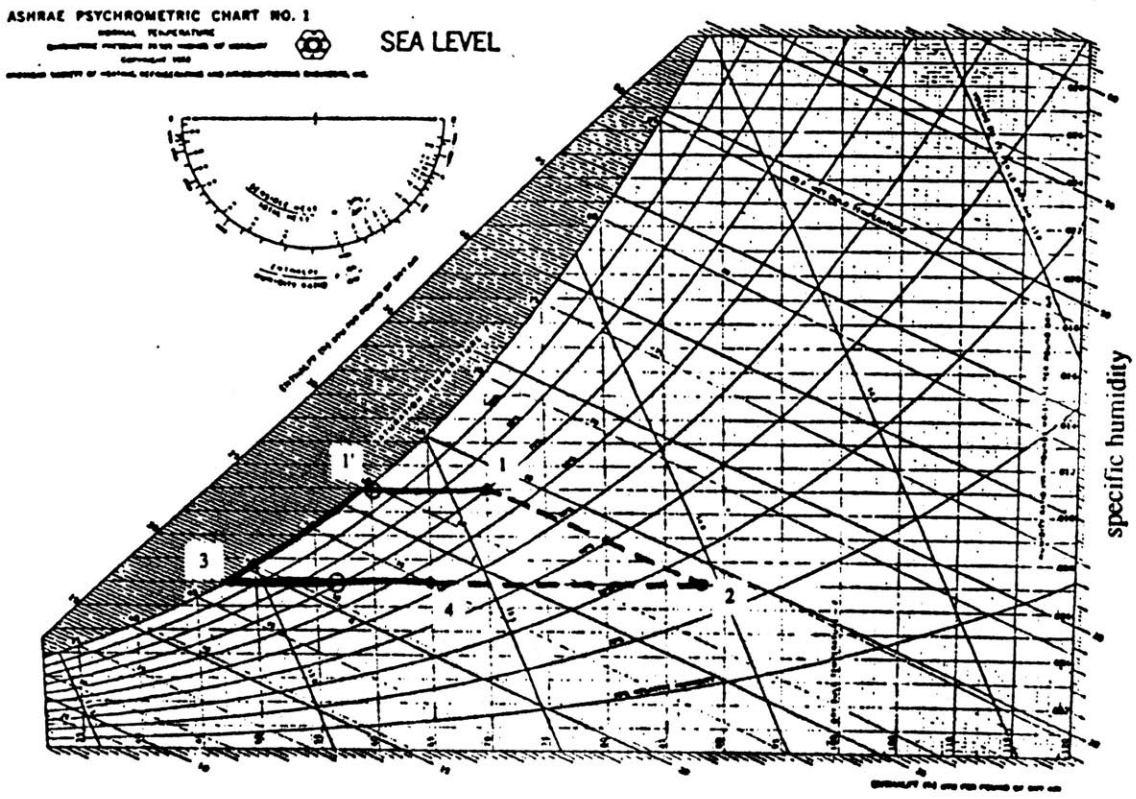

Figure 4. Psychrometric Chart with Dessicant, Direct Evaporative, and Heat Pipe Dehumidification

For the same mixed air conditions, if only a cooling coil were used to condense moisture, the air would need to be cooled to point 3. This corresponds to a enthalpy drop of 9.8 Btu/lba (1,297,030 Btu/hr). The reheat to bring the air to point 4 can generally be reclaimed from the refrigeration system for free. If a heat pipe were installed which had the capability of providing 10 degrees of sensible pre-cooling and reheat, the air would originally be cooled by the pre-cooling section of the heat pipe to point 1'. Then, the cooling coil would need to provide an enthalpy drop of 7.4 Btu/lba (979,390 Btu/hr) to bring the air to point 3. The reheat section of the heat pipe and free heat reclaim would bring the air to the supply conditions at point 4. Therefore, using each of these three methods to bring mixed air at point 1 to supply air at point 4 would necessitate the following energy rates:

Direct Evaporation	1,297,030 Btu/hr
Dessicant Wheel	1,133,190 Btu/hr
Heat Pipe	979,390 Btu/hr

Therefore, provided the added resistance in the air system doesn't require an increase in fan power corresponding to 153,800 Btu/hr, the most energy efficient method for bringing the air from point 1 to point 4 is the heat pipe.

A study was done by the University of Wisconsin comparing the different types of dehumidification for a typical supermarket in the Miami climate (Khattar 1992). The study used TRNSYS, a dynamic simulation program that uses typical inputs and system parameters to model the energy consumption of the HVAC and refrigeration systems. The analysis assumed a 40,000 square foot supermarket with a 30,000 square foot sales area. The original conditions, which the dehumidification systems were compared to, assumed a conventional DX system in which the air was supercooled to condense moisture and then reheated to supply conditions at 55% relative humidity. The output of the analysis was

yearly energy costs for the HVAC and refrigeration systems combined, including electricity and gas costs.

The results of the simulation predicted that energy costs with this conventional system would be $93,000 a year. If this system had used a dessicant wheel to accomplish 55% relative humidity conditions, energy costs would come to $91,000 a year. Next, the study analyzed total energy costs for reducing the humidity level to 40%. For the conventional system, the costs come to $96,000 a year, meaning that the increase in air conditioning load exceeded the reduction in refrigeration load due to dehumidification. The yearly costs of the dessicant system decreased to $84,000, meaning that air system energy increases were small compared to refrigeration savings. When the simulation was run with a heat pipe installed to decrease humidity to 40%, the annual energy costs were estimated to be $81,000, about $3,000 lower than the dessicant simulation

Although this simulation was run for a high humidity climate (Miami's high humidity season is about ten months), it is expected that similar results (on a smaller scale) would occur for a climate with a short humid season, such as that in the Northeast. It is for this reason that supermarket energy managers, utility load planners, and energy engineers would be interested in the effectiveness of heat pipe installations.

1.4 Analysis Summary

For the analysis we monitored various air temperatures and humidity levels, refrigeration line temperatures and pressures, and compressor power consumption for fifteen minute averages over most of the cooling season (June 2 through October 31). The heat pipe was installed on August 2, which allowed us to compare pre-installation points with post-installation points.

As a result of this analysis, we are able to predict reductions in inside relative humidity due to the installation of a heat pipe based on outside weather conditions. We also predict savings in the refrigeration system based on reductions in inside humidity levels. This is accomplished by creating a model of the system for which inputs of monitored data points result in outputs of indoor air conditions and refrigeration system energy consumption. The conclusion will examine whether or not this method is a successful way of determining the effectiveness of a heat pipe, and whether or not heat pipes are an efficient tool for energy savings in the New England climate.

There will be six steps in this analysis, covered in the following eight chapters. The conclusion will summarize the results of the process, as well as give suggestions as to how future studies can be improved based on problems and successes of this thesis. The steps are outlined below:

Step One. Chapter two will explain heat pipe dehumidification and why it was chosen as a method of energy savings. First the heat pipe process will be explained, with a physical description and examples of how they might be used in an installation. Then, a summary of three previous studies will show how heat pipe analyses have been handled before, and what kind of results to expect. Third, a psychrometric analysis will prove that engineering equations back up the hypothesis that heat pipes are guaranteed to reduce humidity levels for a given supply air temperature and ambient conditions as long as some dehumidification is being performed. Finally, the effects of dehumidification on the refrigeration cycle will be modelled based on an ideal Carnot cycle.

Step Two. This step, covered in chapters three and four describes the strategy that was used to obtain the information necessary for the analysis. Chapter three describes the method of analysis, explaining how monitored data will be combined with models based on

appropriate engineering equations in an attempt to predict refrigeration system energy consumption based on ambient conditions. Chapter four describes the monitoring strategy, including the site which is being monitored, what equipment was installed, and where the sensors were located. This step is summarized at the end of chapter four.

Step Three. This step serves to describe the existing conditions of the building being monitored. Since heat pipe performance varies based on air conditioning and refrigeration system configuration, it is important that the results of this analysis be tied to this specific setup. This chapter includes air conditioning unit description and specifications, as well as the refrigeration system description.

Step Four. This step, covered in chapter six, describes the measured data that was presented to us by the monitoring contractor. For each point where temperature or relative humidity was measured, sensor location and calibration are covered, as well as maintenance or location problems associated with the data we received. For the refrigeration system measurements, the location of sensors and plans on how the data are to be used are discussed. The end of the chapter explains how monitored data met expectations and how they will fit in to the system models.

Step Five. This step is the meat of the analysis, and is covered in chapters seven and eight. Chapter seven combines the monitored data from step four with the air system models in step one to predict supply air temperature and specific humidity based on return air and outside air data compiled over the monitoring period. This is accomplished by creating a spreadsheet model in which each step in the air conditioning unit is calculated based on regressions of monitored data, psychrometric equations, and numbers derived in the previous step. In the model, mixed air parameters are predicted based on return air, outside air, and airflow measurements. Post-cooling coil air is predicted based on mixed air and cooling load. Supply air is predicted based on post-cooling coil air and reheat. The

equations predicting supply air before and after heat pipe installation are compared to determine to what extent the heat pipe further reduced humidity levels. These savings are compared to potential margin of error to determine the statistical accuracy.

Chapter eight describes the loads in the refrigeration system, based on monitored data and engineering equations. Data from monitored points and calculations are compared to each other to determine a correlation between factors within the cycle and with ambient conditions. Factors within the cycle are compared to attempt to relate temperatures, pressure, and loads of adjacent stages in the cycle to each other, and are compared to ambient conditions to attempt to predict variations in the cycle. The end of the chapter summarizes the results and problems in relating the air system and refrigeration system models, and in predicting refrigeration compressor power.

Step Six. The last step ties the models and data together to resolve the question of whether or not the installation of the heat pipe actually generated any energy savings. Chapter nine includes the energy analysis, in which monitored refrigeration compressor power is examined to see if consumption was reduced. Also, the issue of air conditioning fan power penalties is raised, as with the heat pipe comes added airflow resistance, and should come with a fan power penalty. Finally, the unrealized energy savings are discussed to show how the presence of the heat pipe warrants changes in the system which will generate energy savings without compromising building operating conditions.

As a result of this analysis, it is hoped that there will be a better understanding of how heat pipes can be effective in a mild summer climate such as the one in the Northeast, and also how a successful analysis of an installation can be achieved by correcting problems incurred in this and other studies.

Chapter 2 Heat Pipe Dehumidification

This chapter, as explained above in step one, will tell the reader more about how the heat pipe works and what types of results to expect in this analysis. The section on previous studies shows that, even for installations in high humidity climates, problems associated with the complexity of estimating refrigeration system energy savings affect conclusions attempting to justify heat pipe dehumidification. The psychrometric analysis shows that the addition of the heat pipe not only lowers supply air specific humidity for a given supply air temperature and cooling coil load, but also reduces the amount of heat reclaim necessary. The refrigeration system analysis shows that, for evaporator load reduction (which is expected with dehumidification), compressor load based on the Carnot cycle decreases. The chapter summary addresses how these issues will affect the rest of the analysis.

2.1 The Heat Pipe Process

A heat pipe is a sealed metal tube bent in a rectangular shape to be placed around a cooling coil which is evacuated to an absolute vacuum and half filled with a liquid refrigerant. The design is based on the principle that the liquid refrigerant will evaporate when warm air is blown over it, and the vapor will condense when supercooled air is blown over it. The condensation creates a negative pressure relative to the warm air side, which draws the evaporated vapor from the warm air side. The lower section of the heat pipe is tilted towards the warm air side of the cooling coil, so when the condensed refrigerant reaches the bottom as a liquid, it settles on the warm air side of the cooling coil where it is evaporated again. Several metal fins are attached to the pipe to increase the heat transfer

rate. The heat pipe kit is placed around the cooling coil it is being applied to, with the pipe tilted so that the liquid end settles on the pre-cooling side (Figure 5).

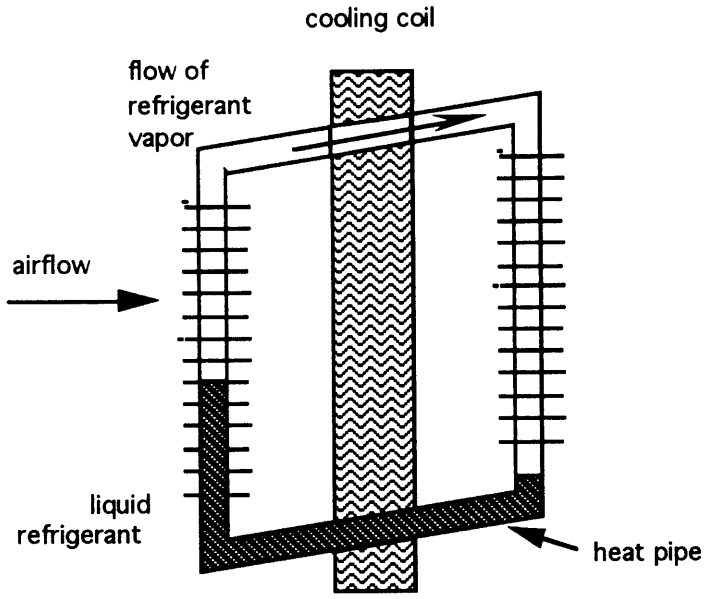

Figure 5. Heat pipe and cooling coil section

When the heat pipe system is in use, mixed return and fresh air entering the cooling section first passes through the pre-cooling side of the heat pipe. The warm air is cooled down as it evaporates the refrigerant in the heat pipe. The evaporated refrigerant rises to the other end of the heat pipe, flowing around the cooling coil to the re-heat side. If the air entering the heat pipe is close to saturation, it is possible that there would be some latent cooling (in the form of condensation on the heat pipe) after sensible cooling to 100 percent humidity. The cooled air now enters the cooling coil, where the heat transfer of the coil provides initially some sensible cooling, and after saturation provides latent cooling in the form of moisture removal. This cool air at high relative humidity leaves the cooling coil and passes over the re-heat end of the heat pipe, where it receives heat as it condenses the refrigerant vapor. The energy gain across the re-heat section of the heat pipe is identical to

the energy loss across the pre-cooling end. The air leaving the condensing end of the heat pipe is at a slightly higher dry bulb temperature and a significantly lower absolute humidity than if the heat pipe were not present. The heat pipe is completely passive, requiring no energy input. The flow of the refrigerant is completely driven by alternating evaporation and condensation. A psychrometric description of this process is show below in section 2.3.

Although heat pipes have been installed in many different types of buildings, they are used in different ways in supermarkets than in office buildings. In office buildings, designers take advantage of the fact that comfort levels for humans are as dependent on humidity levels as temperature levels. For lower humidity levels, the cutoff point for what is considered a comfortable temperature is higher than the cutoff point for higher humidity levels (Olgyay 1963). Heat pipes are installed in these applications to reduce humidity levels so that supply air can be cooled to a higher temperature. The higher the temperature of the supply air, the less cooling is needed, and the air conditioning system runs at a lower level during the cooling season. For supermarkets, heat pipes are installed to reduce humidity levels while keeping supply air temperature the same. The savings are not realized in the air conditioning system, but in the refrigeration system, where reduced inside humidity levels have the effect of reducing the load on refrigeration coils. Because the equipment where energy is to be saved is not connected to the system where the heat pipe is installed, it becomes a difficult problem to calculate the effects of having a heat pipe installed.

The first study of a heat pipe supermarket installation for which savings were calculated was conducted by the Georgia Power company in July of 1989. Another evaluation of an installation was sponsored by the Duke Power Company in 1991.

Another study was performed by ASHRAE involving six different installations in 1992. All three of these studies will be discussed in the next section.

The heat pipe used in our installation was manufactured by Heat Pipe Technology of Alachua, Florida. Figure 6 shows a photograph of the heat pipe used in the installation. The refrigerant used is R22, the pipes are made of copper, and the fins are continuous plate aluminum. The heat pipe was factory assembled in four sections, two pre-cooling sections and two re-heating sections. The kit was designed to transfer 205,630 Btu/hr of energy, corresponding to a sensible pre-cooling and reheat of 5.7 degrees Fahrenheit at the same air mass flow.

2.2 Previous Heat Pipe Studies

An analysis of the successes and problems of three earlier studies should give insight into how my study could be improved. The first heat pipe study was sponsored by the Georgia Power Company and the Electric Power Research Institute (EPRI) in 1989 (Keebaugh 1992). A heat pipe was installed in a 40-ton rooftop air conditioning unit at a 35,000 sq ft supermarket in Lithonia Georgia, and allowed to function for one full year. The heat pipe was installed in July 1989, and the monitoring equipment was installed August 1989. In this store, refrigeration energy represented about 39% of total energy consumption. Inside air conditions were controlled by maintaining a 57 degree dew point, corresponding to 75 degree dry bulb temperature and 55% relative humidity. Approximately one month after the heat pipe was installed, the setpoint was changed to maintain a 47 degree dew point (75 degrees dry bulb, 38% relative humidity). The study used condensate removal as a benchmark for cooling coil condensation by measuring the amount of water draining out of the cooling section during dehumidification. The conclusion of the analysis is that, as shown in Figure 7a, condensate volume per kWh of

air conditioning compressor consumption seems to be lower without the heat pipe than with the heat pipe, but the data seem to be too scattered to quantify the difference. Refrigeration compressor demand and energy consumption was estimated as a function of inside dew point and inside and outside dry bulb temperature (Figures 7b and 7c) for a time period after the heat pipe was installed. . Although the study did not supply regression coefficients and standard errors, it used the accuracy of this prediction equation to show that the reduction in interior air humidity reduced refrigeration energy consumption by about 24 kWh (1 percent) for every 1 degree drop in dew point.

The second study, conducted by the Duke Power Company, was completed in December of 1991 (Abrams et al 1992). This study analyzed a heat pipe installation in a 24-hour, 33,000 square foot supermarket in Spartanburg, South Carolina. In this supermarket, refrigeration accounted for 36% of overall energy consumption. Again, this study focused on condensate removal efficiency in terms of lb/kWh compressor energy consumption. For this study, conditions with and without the heat pipe were simulated by disabling the heat pipe. This was easily accomplished by tilting the heat pipe in the other direction, so the cold liquid settled on the other side of the cooling coil. With the heat pipe tilted this way, the liquid refrigerant changed temperature with the cooled air and did not evaporate, therefore providing no heat transfer. Figure 8a shows the data points for the moisture removal efficiency with and without the heat pipe. As with the Georgia Power study, the points show a lower efficiency without the heat pipe, but the results are not quantifiable. The authors of this study attempted to predict daily refrigeration compressor energy consumption as a function of average daily indoor dew point, and this scatter plot is shown in Figure 8b. This plot includes points for every day in the year, including days when no cooling or dehumidification was performed. A regression of these points resulted in a savings estimate of 1.66% per degree dew point, with a standard error of 148 kWh per

day (about 7%). Over the course of the year, the simulation assumed a reduction of indoor dew point due to the heat pipe of 10 to 12 degrees, resulting in an overall energy savings of 5.4% to 6.5% respectively. For additional energy savings, the store owners disabled the anti-sweat heaters for five days and did not encounter any condensation problems while saving approximately 350 kWh per day. The defrost cycles were timer activated and were not reprogrammed for their analysis. However, changing defrost cycle times was included in their recommendations for future energy savings.

The third study was performed by the Georgia Power Company and ASHRAE in 1992 (Hill et al 1993). Heat pipes were installed in six different locations, three in Wisconsin, one in Pennsylvania, one in South Carolina, and one in Georgia. Refrigeration energy consumption varied from 20% of total energy consumption at the Pennsylvania site to 46% of total energy consumption at the Wisconsin site. For this study, indoor dry bulb and dew point temperatures were monitored and compared to refrigeration compressor power consumption, and the cooling coil moisture removal rate (in lb/kWh) was analyzed before and after installation. The Pennsylvania site and two of the Wisconsin sites used dual path air conditioning systems and the rest of the sites used single path systems. The study claimed that moisture removal efficiency increased by 21% for the Pennsylvania site, and that moisture removal comparisons were unable to be completed at the Wisconsin sites. For the single path systems, the study claimed a 27% removal efficiency increase for the South Carolina site, 18% for the Georgia site, and not found for the Wisconsin site. As a conclusion, the study predicted a mean value of energy savings for all sites, which was 17.3 kWh per day per degree drop in inside air dew point (a mean relative savings of 0.65% of refrigeration energy use). Although the authors recommended that heat pipes were not effective in dual path systems, they determined that the complexities of the

analysis prevented general or specific conclusions on the benefits of the heat pipe installation.

Neither of these studies addressed many of the issues important in a heat pipe analysis. All of the studies focused on measuring condensate removal at the cooling coil, yet all of them determined that the results were not quantifiable. All of the energy savings estimates were significantly smaller than total refrigeration consumption, yet none of the analyses addressed errors in the estimates. Each of the three studies agreed that dehumidification was accomplished by the presence of the heat pipe, yet none of them were able to satisfactorily predict savings based on ambient conditions.

As was determined in this thesis also, complexities in combining air system estimates with refrigeration system estimates make savings estimates inconclusive. Suggestions for achieving a successful study will be addressed in chapter 10.

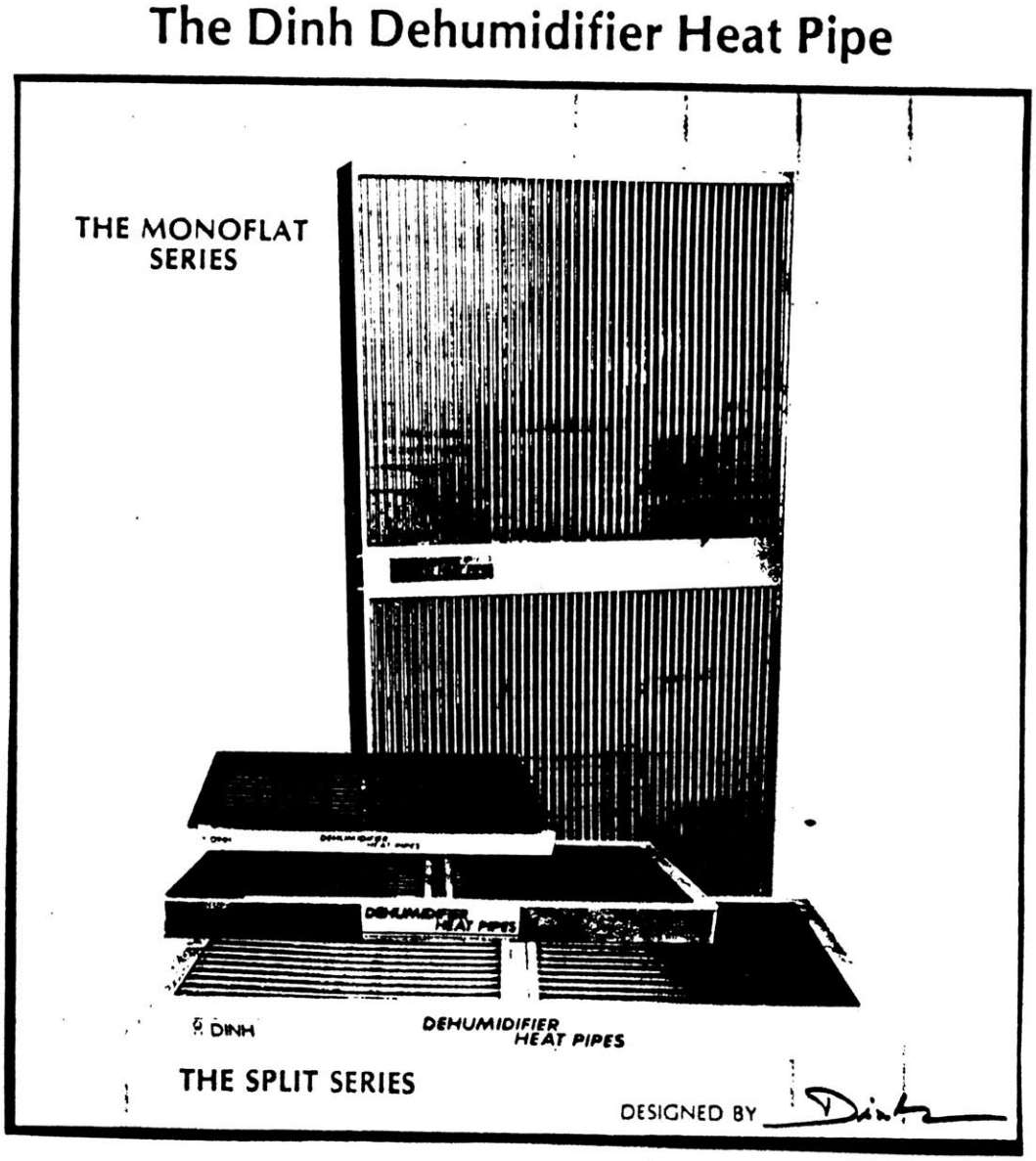

Figure 6. Dehumidifier Heat Pipe Used in Worcester Installation

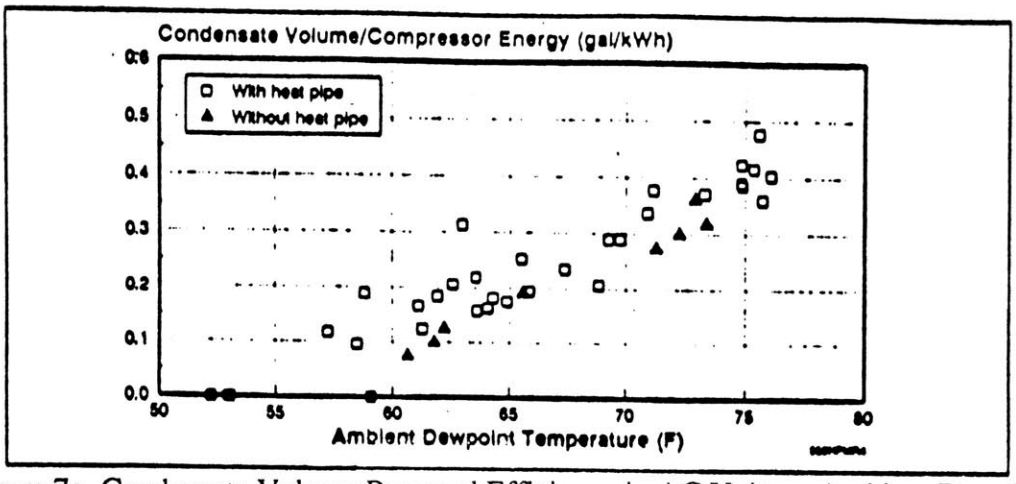

Figure 7a. Condensate Volume Removal Efficiency in AC Unit vs. Ambient Dew Point Temperature, Georgia Power Study.

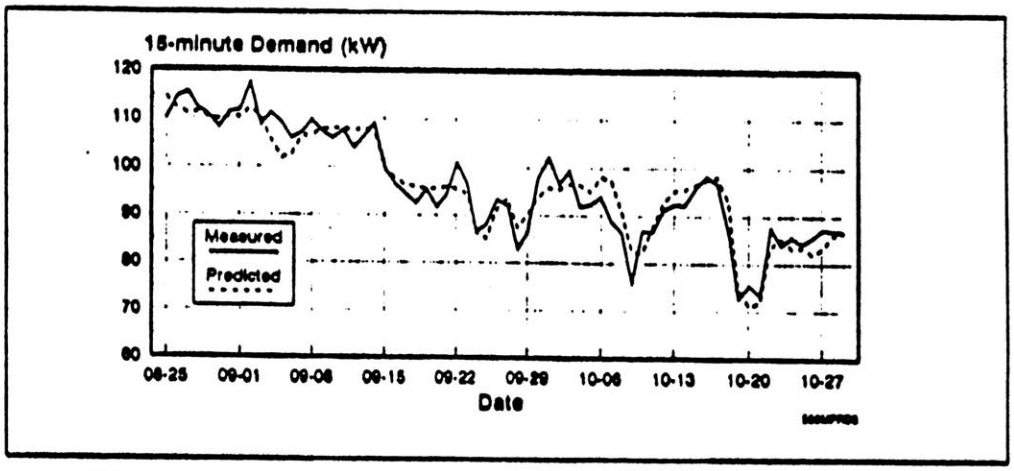

Figure 7b. Measured and Predicted Refrigeration System Demand, Georgia Power Study.

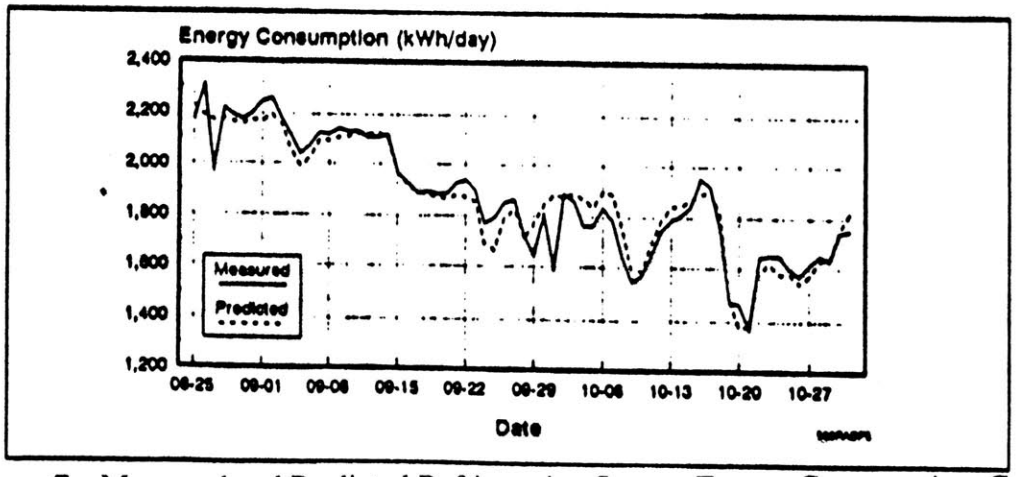

Figure 7c. Measured and Predicted Refrigeration System Energy Consumption, Georgia Power Study.

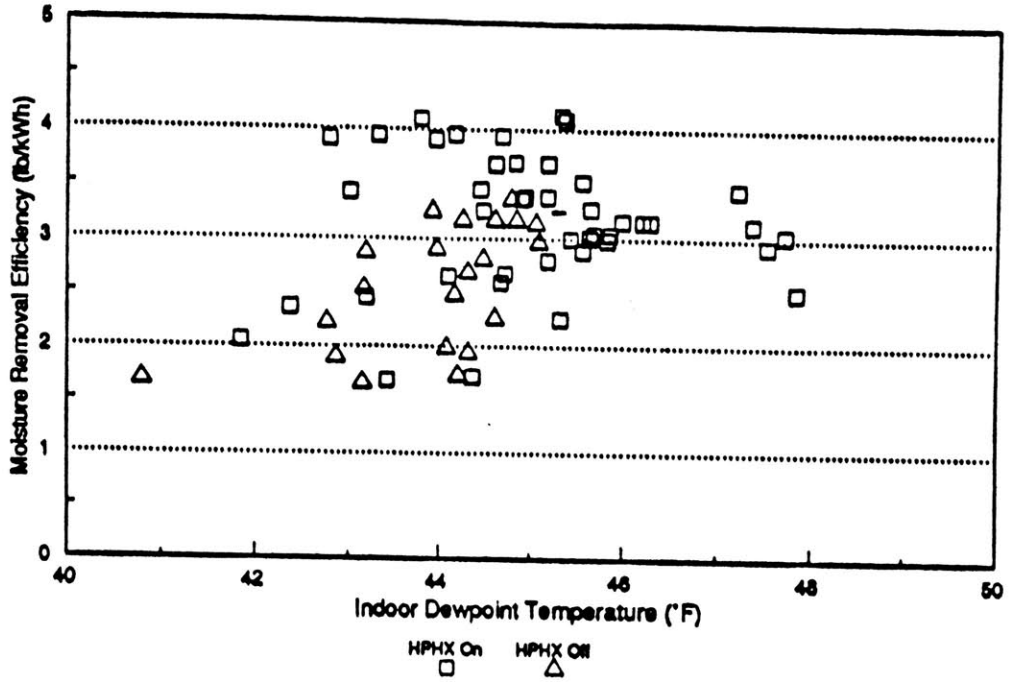

Figure 8a. Condensate Volume Removal Efficiency in AC Unit vs. Indoor Dew Point Temperature, Duke Power Study.

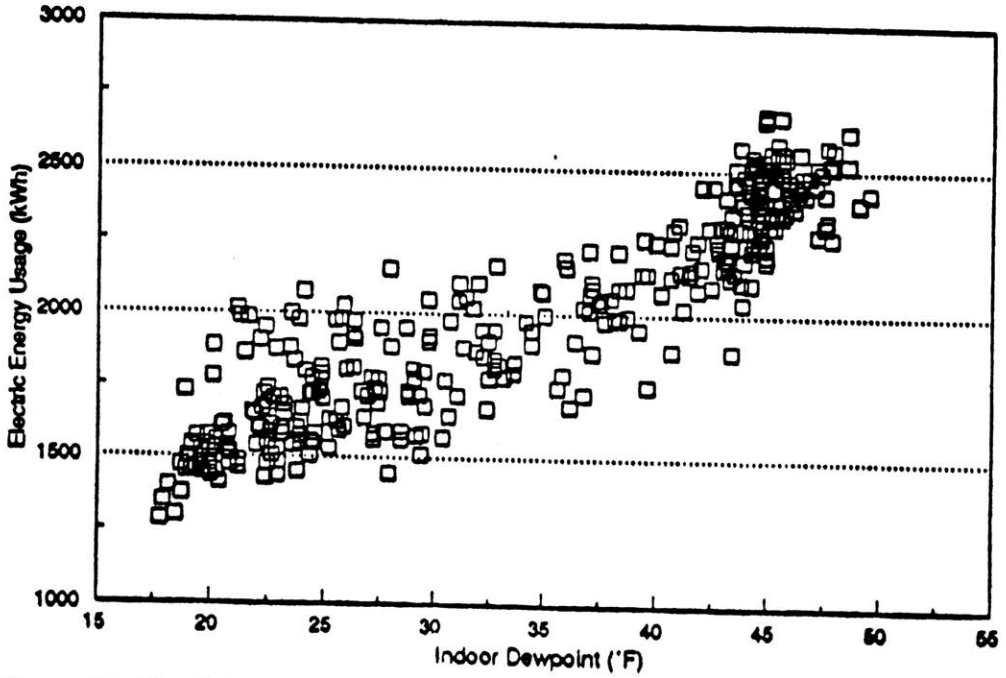

Figure 8b. Total Refrigeration Energy Consumption vs. Indoor Dew Point, Duke Power Study.

2.3 Psychrometric analysis

To further explain how the presence of a heat pipe reduces humidity levels in the air, this section will describe the process using psychrometric equations and models of the air conditioning system with and without the heat pipe. The first part of this section explains specific humidity, a variable used throughout the analysis which describes the ratio of the mass of water vapor per unit mass of dry air in an airflow. The second part of this section shows two examples of airflow in this air conditioning configuration, one with the heat pipe and one without the heat pipe. By comparing the two examples, the reader can see how the heat pipe reduces supply air specific humidity while maintaining the same dry bulb temperature. The AC compressor power does not change, as the energy management system controlling the compressor power is still receiving the same inside air temperature as a control point, yet the amount of heat reclaim necessary to maintain the design supply air temperature decreases due to the lower enthalpy of the supply air.

2.3.1 Specific Humidity

The specific humidity (or absolute humidity or humidity ratio) of an air system is defined by the 1993 ASHRAE Fundamentals Handbook as the ratio of the mass of water vapor to the mass of dry air. As opposed to relative humidity, which varies as dry bulb temperature changes, specific humidity is independent of temperature.

For a supermarket application, comparing the specific humidity of the supply air and the return air would give a good indication of how much moisture is removed from or added to the air system as a function of the supermarket. Moisture can be removed from the store mixed air by absorption, condensation, and most importantly, freezing on the refrigeration coils. Moisture can be added to the system by customers, infiltration, or

evaporation (from produce, sinks, or other water sources. Specific humidity can be calculated from dry bulb temperature and relative humidity using the following equations (ASHRAE 1993) :

$$W = 0.62198 * (p_w / p\text{-}p_w) \quad (2.1)$$

W = specific humidity (lb water / lb air)

p = atmospheric pressure (psi)

p_w = partial water vapor pressure (psi)

$$p_w = p_{ws} * RH \quad (2.2)$$

RH = relative humidity

p_{ws}=partial water vapor saturation pressure (psi)

$$p_{ws}=C_0+C_1(T)+C_2(T^2)+C_3(T^3)+C_4(T^4)+C_5(lnT) \quad (2.3)$$

T = dry bulb temperature (R)

The partial water vapor saturation pressure calculated in equation 2.3 is the saturation pressure over water. The saturation pressure over ice is an equation similar to equation 2.3 with different constants. The saturation pressure over ice is important in determining the buildup of frost on the refrigeration coils. The constants used in this equation can be found in Appendix C-2. The measurement error in specific humidity calculations, as shown in Appendix D, is 2.4%.

2.3.2 Air Conditioning System Models

The best way to understand how the heat pipe affects the dehumidification of the airflow is to follow the process on a psychrometric chart. Figure 9 shows charts with the path outlined from mixed air conditions to supply air conditions for typical design conditions, a theoretical heat pipe design which provides 12 degrees of sensible cooling and reheating, and a desired supply air temperature of 65 degrees (ASHRAE 1993). The top graph simulates direct evaporative cooling without the heat pipe, and the lower graph simulates direct evaporative cooling with a heat pipe. In both graphs mixed air conditions occur at point A, corresponding to 75 degrees dry bulb and 55% relative humidity. In the top graph, the cooling coil removes heat from the airflow dropping its enthalpy (Δh) to point B. In the lower graph, the cooling section of the heat pipe pre-cools the air 12 degrees, bringing it to point B. The cooling coil then removes heat corresponding to the same enthalpy drop (Δh), bringing the air to point C. Point C in this graph has a lower specific humidity and dry bulb temperature than point B in the top graph, although they both represent post-cooling-coil air conditions. In the top graph, reheat corresponding to a sensible temperature rise of 15 degrees is needed to bring supply air (point C) to 65 degrees. In the lower graph, the reheat section of the heat pipe raises the air temperature 12 degrees to point D. From this point, only 10 degrees of reheat is needed to bring the supply air to 65 degrees (point E). The specific humidity at this point is lower than in the top graph by ΔW.

A psychrometric chart analysis for four different types of ambient conditions can show what affect the heat pipe is expected to have. The above analysis was done for four different mixed air conditions based on four climate types: hot and humid (80 degrees, 60% RH), warm and humid (70 degrees, 85% RH), hot and dry (80 degrees, 45% RH), and warm and dry (70 degrees, 65% RH). These runs used the same supply temperature

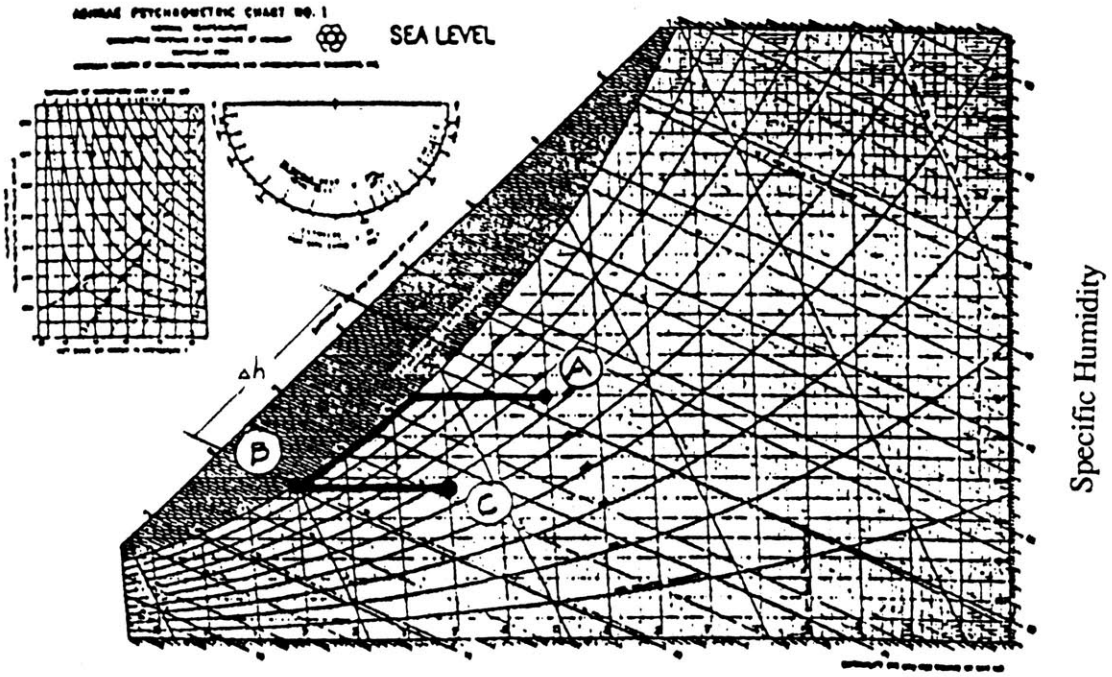

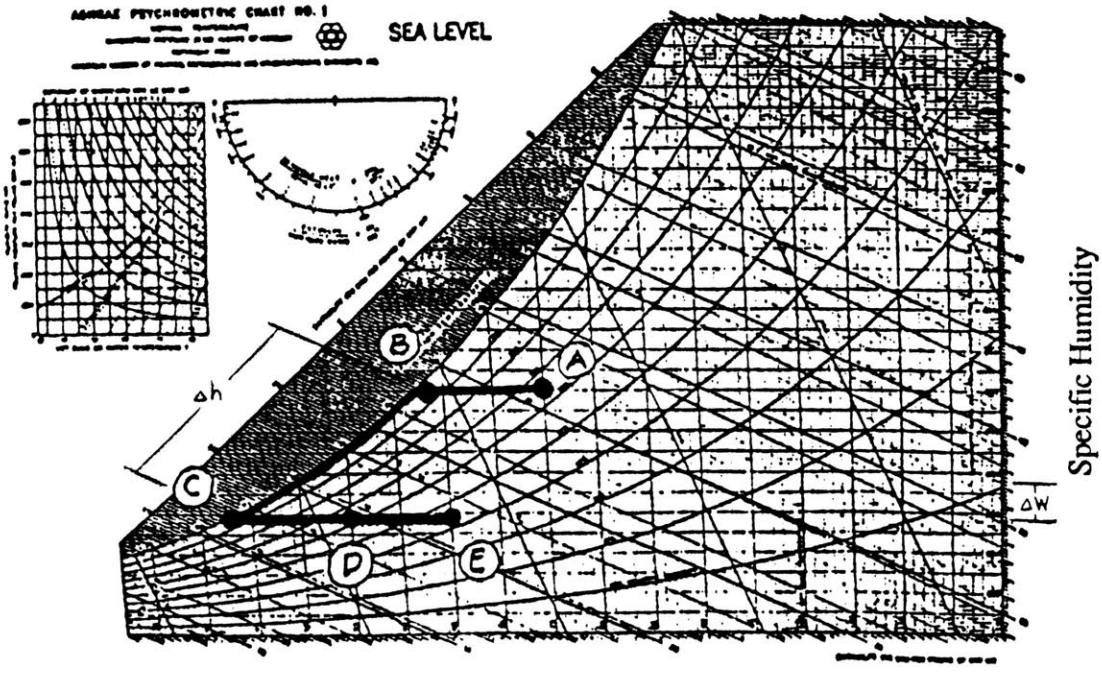

Figure 9. Psychrometric Charts Showing Dehumidification with and without Heat Pipe

(65 degrees), same cooling coal load (Δh = 12 Btu/lb), and the same heat pipe cooling and reheat load (3 Btu/lb). The results are in Table 1. In the table, the left column describes the climate type (H/H = hot/humid, W/D = warm/dry), the column marked W is specific humidity, and L/S is the latent/sensible cooling ratio for the cooling coil for each condition in Btu/lb latent / Btu/lb sensible. What this showed was that the difference in specific humidity drop was greater in humid climates than in dry climates, because the heat pipe has a larger affect on the system when more dehumidification is being done.

Table 1. Psychrometric Analysis for Varying Ambient Conditions

				Supply Air				
	Temp (deg F)	RH	W (lbw/lba)	Temp (deg F)	W w/o heat pipe	W with heat pipe	L/S w/o heat pipe	L/S with heat pipe
H/H	80	60%	0.0134	65	0.0085	0.0070	2.0	11.0
W/H	70	85%	0.0134	65	0.0072	0.0057	7.6	∞
H/D	80	45%	0.0100	65	0.0066	0.0052	1.0	3.0
W/D	70	65%	0.0100	65	0.0054	0.0041	2.8	29.5

On one extreme, if the combined cooling of the pre-cooling section of the heat pipe and the cooling coil doesn't bring the air temperature to the saturation point, no dehumidification is being done and the heat pipe is useless. On the other extreme, if the air entering the pre-cooling section of the heat pipe is at saturation, then the heat pipe and the cooling coil are providing entirely latent cooling, and the heat pipe provides its maximum possible

dehumidification. The rest of this section quantifies this analysis using energy balance equations in examples. Example 1 is a simulation without the heat pipe, and example 2 is a simulation with the heat pipe.

Example 1

One way of predicting the effect of the heat pipe is by performing an energy balance with and without the heat pipe. Figure 10 shows a schematic of the duct before the heat pipe was installed. In the figure, m represents the mass flow (lb/hr), h represents the enthalpy of the moist air (Btu/lb), and q represents rate of heat extraction at the cooling coil and insertion at the reheat coil (Btu/hr). For all points between heat exchangers calculated heat flow (q') is described by the equation:

$$q' = mh \qquad (2.4)$$

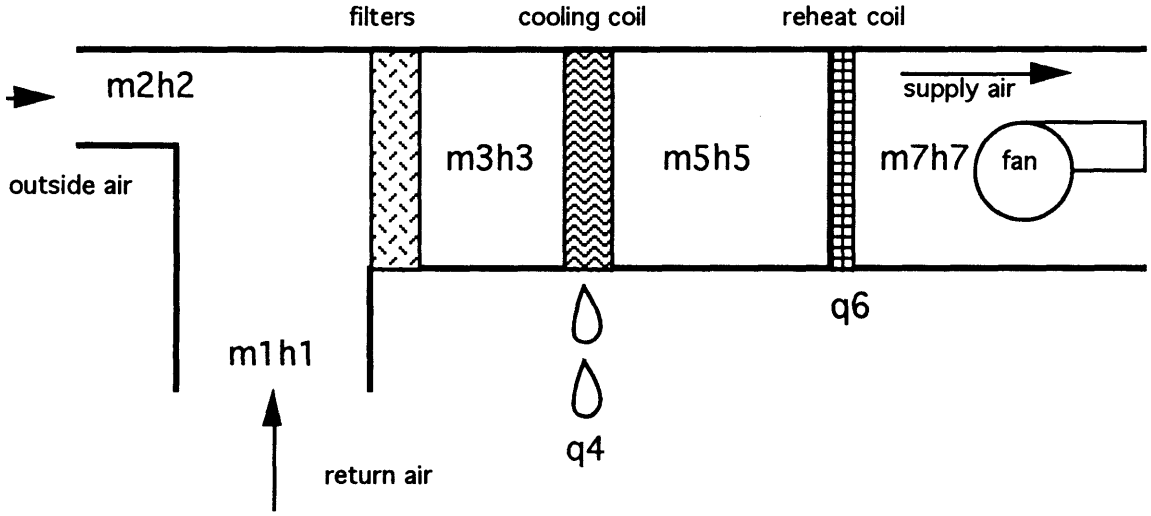

Figure 10. Energy Flows in System Without Heat Pipe

For each of the points, mass flow is calculated as the volumetric flow rate (v) divided by specific volume (u) as described below:

$$m\ [lb/hr] = v\ [cfm] * 60\ [min/hr] / u\ [ft^3/lb] \quad (2.5)$$

The specific volume is a function of dry bulb temperature in degrees Rankine (T) and humidity ratio (W) as described below:

$$u\ [ft^3/lb] = 53.352\ [ft\ lb/lb\ R] * T\ [R] * (1+1.6078*W)/ (14.91*144\ [lb/ft^2]) \quad (2.6)$$

Enthalpy of moist air is a function of dry bulb temperature and humidity ratio:

$$h = .240*T + W*(1061 + 0.444*T) \quad (2.7)$$

For this example we will assume a supply airflow of 33,200 cfm and a return airflow of 28,700 cfm, resulting in the following airflows:

$$v_1 = 28{,}700 \text{ cfm}$$

$$v_2 = 4{,}500 \text{ cfm}$$

$$v_3 = v_5 = v_7 = 33{,}200 \text{ cfm}$$

We will also assume the following existing conditions:

$$T_1 = 70 \quad rh_1 = 45\% \quad W_1 = 0.006974$$

$$T_2 = 90 \quad rh_2 = 55\% \quad W_2 = 0.016635$$

where the humidity ratios are calculated as a function of the temperatures and relative humidities (rh).

Our desired supply conditions will be:

$$T_7 = 65 \quad rh_7 = 55\% \quad W_7 = 0.007178$$

The equation that will give us our mixed air conditions (m3h3) is an energy balance of the outside air and return air:

$$m1h1 + m2h2 = m3h3 \tag{2.8}$$

$$u_1 = 13.3094 \ [ft^3/lb]$$

$$\text{therefore} \quad m1 = 129{,}382 \ [lb/hr]$$

$$h1 = 24.416 \ [Btu/lb]$$

$$u_2 = 14.0241 [ft^3/lb]$$

$$\text{therefore} \quad m2 = 19{,}253 \ [lb/hr]$$

$$h2 = 39.914 \ [Btu/lb]$$

$$\text{and} \quad m3h3 = 3{,}927{,}473 \ [Btu/hr]$$

and mixed air humidity ratio can be found by:

$$(W_2 - W_3)/(W_3 - W_1) = m1 / m2 \tag{2.9}$$

$$W_3 = 0.0082253$$

Using the previous equations for m and h (2.5, 2.6, and 2.7), we can now solve for T_3, and then h3, knowing the product m3h3 and W_3.

$$T_3 = 72.6$$

$$h3 = 26.416$$

The cooling coil (q4) is designed for a capacity of 940,000 Btu/hr. The amount of heat removal needed to bring the mixed air to saturation is proportional to the enthalpy difference at constant humidity ratio and a temperature drop of 20.54 degrees (72.6 - 52.06 from the iteration shown for saturation temperature for W=0.008225 in Table 1 in Appendix C-1).

$$\Delta h_{3\text{-}5} = 0.24*\Delta T_{3\text{-}5} + W_3*(0.444*\Delta T_{3\text{-}5}) \qquad (2.10)$$

$$\Delta h_{3\text{-}5} = 5.0046$$

From Table 1, the energy flow at this point is 3,310,278 Btu/hr, which is 617,195 btu/hr less than point 3. Since the desired humidity ratio is 0.007178, the remainder of the cooling must bring the air down to that level. Another iteration (Table 2 in Appendix C-1) shows that this ratio at saturation can be achieved at 48.439 degrees. The energy flow at this point (point 5) is 3,025,116 Btu/hr. Therefore, the total heat flow from the cooling coil comes to q4 = 3,927,480-3,025,116 = 902,357 Btu/hr, which is within its capacity.

The final energy flow m7h7 can be calculated using equations 2.5, 2.6, and 2.7 and desired conditions, and it comes to 3,537,899 Btu/hr. Therefore 512,783 Btu/hr of reheat is required.

Example 2

Figure 11 shows a schematic of the duct with the heat pipe installed. In this case, m1h1, m2h2, and m3h3 are the same conditions as before. The heat pipe provides the same amount of heat flow removed before the cooling coil and added after the cooling coil. The

goal is to see, for the same amount of heat removal across the cooling coil, at what humidity level and amount of reheat a 65 degree supply temperature can be provided.

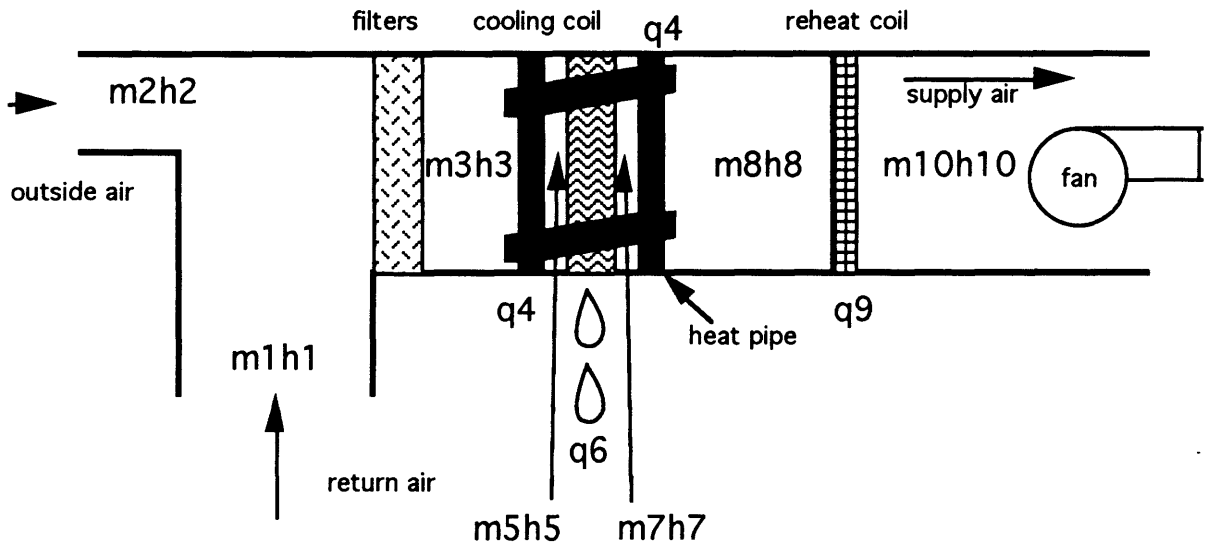

Figure 11. Energy Flows in System With Heat Pipe

With the heat pipe installed, point 3 still has the same characteristics:

$$W_3 = 0.0082253$$

$$T_3 = 72.6\ [^oF]$$

$$h3 = 26.416\ [Btu/lb]$$

$$m3h3 = 3{,}927{,}473\ [Btu/hr]$$

However, the heat pipe provides an initial 205,630 Btu/hr of cooling. This corresponds to a Δh of 1.383 Btu/lb at m3=148,678 lb/hr. Equation 2.4 gives a temperature $T_5 = 66.9$.

With this pre-cooling, the heat flow needed to bring the air to saturation at 52.06 degrees (the same point that was found in Table 1) is only 411,565 Btu/hr. The cooling coil, responding to the same ambient conditions as if the heat pipe were not present, will provide the same heat removal as in Example 1, which was 902,357 Btu/hr. Therefore, the cooling coil will provide 490,792 Btu/hr of extra heat removal at saturation.

At point 7, the energy flow will be 2,819,486 Btu/hr. Another iteration of saturation points (Table 3), shows that this corresponds to about 45.7 degrees at saturation. The humidity ratio, $W_7 = 0.006466$ and the mass flow, m7 = 156,993 lb/hr.

At this point, the air enters the reheat section of the heat pipe, and is provided with 205,630 Btu/hr of heating. Since there was no latent cooling done by the heat pipe, the temperature difference will be the same, 5.7 degrees. The air conditions leaving the cooling section will be as follows:

$$W_8 = 0.006466$$

$$T_8 = 51.4\ [^oF]$$

$$h8 = 19.342\ [Btu/lb]$$

$$m8h8 = 3,025,116\ [Btu/hr]$$

The final supply condition m10h10 will have a dry bulb temperature of 65 degrees and a humidity ratio $W_{10} = W_8 = 0.006466$. Using equations 2.5, 2.6, and 2.7, this corresponds to an energy flow of 3,453,295 Btu/hr. Therefore, the necessary reheat q_9 can be determined by the following equation:

$$m8h8 + q_9 = m10h10$$

$$q_9 = 428,179\ Btu/hr$$

As was expected, the reheat needed to bring the over-cooled air to supply conditions is 84,604 Btu/hr less than what was needed without the heat pipe. The relative humidity at the supply temperature in this example can be calculated as the ratio of the partial water pressure divided by the partial water pressure at saturation:

$$RH_{10} = p_w / p_{ws} \tag{2.11}$$

$$p_w = 0.153407 \text{ psig}$$

$$p_{ws} = 0.309271 \text{ psig}$$

$$\text{Therefore } RH_{10} = 49.6\%$$

This supply air relative humidity is less than in Example 1 by 5.4%. The reduction in relative humidity will be greater if the heat pipe performs more cooling, allowing the cooling coils to perform more latent heat removal. Our data showed that the heat pipe provided about 7 degrees of pre-cooling at maximum cooling conditions and about 9 degrees of reheat. The difference is due to the fact that some latent heat removal done by the pre-cooling section meant less sensible cooling (ASHRAE 1993).

Table 2. Example 1 variables

point	T	u	W	m	h	q	EF
1	70	13.3094	.006974	129,382	24.416		3,159,018
2	90	14.0241	.016635	19,253	39.914		768,455
3	72.6	13.4013	.008225	148,642	26.416		3,927,473
4						-902,357	
5	48.4	12.7718	.007178	155,969	19.396		3,025,116
6						512,783	
7	65	13.1880	.007178	151,046	23.423		3,537,899

Table 3. Example 2 variables

point	T	u	W	m	h	q	EF
1	70	13.3094	.006974	129,382	24.416		3,159,018
2	90	14.0241	.016635	19,253	39.914		768,455
3	72.6	13.4013	.008225	148,642	26.416		3,927,473
4						-205630	
5	66.9	13.2578	.008225	148,677	25.033		3,721,843
6						-902357	
7	45.7	12.6885	.006466	156993	17.959		2,819,486
4						205630	
8	51.4	12.8317	.006466	156,401	19.342		3,025,116
9						428,179	
10	65	13.1731	.006466	151,217	22.647		3,453,295

T = dry bulb temperature [F]
u = specific volume [ft^3/lb]
W = humidity ratio
m = mass flow [lb/hr]
h = enthalpy [Btu/lb]
q = heat removal/addition [Btu/hr]
EF = Energy Flow [Btu/hr]

2.4 Refrigeration System Models

To further explain how dehumidification of inside air reduces the load on the refrigeration system, this section includes an energy balance on the refrigerant as it flows through the vapor compression cycle. The basis of the refrigeration system model will be to show how reductions in evaporator cooling load (which is display case load) affect the rest of the cycle, including compressor power. For this model, reductions in evaporator load will be caused by increased heat transfer efficiency due to a reduction in the rate of frost buildup on the cooling coils.

2.4.1 Energy Balance

For each of the components of the vapor compression cycle, an energy balance can be performed by comparing enthalpy, mass flow, and work put into or taken out of the refrigerant flow. Each point in the pressure vs enthalpy curve representing the refrigeration cycle (Figure 12) is a state of refrigerant, and each path connecting two points is a change in state, due to compression, condensation, expansion, and evaporation. The energy balance associated with each change of state is given by four equations which will be used later in the refrigeration system model (ASHRAE 1993):

Compression	$W = -(h_2-h_1)*m$	(2.12)
Condensation	$Q_{23} = -(h_2-h_3)*m$	(2.13)
Expansion	$h_3 = h_4$	(2.14)
Evaporation	$Q_{14} = (h_1-h_4)*m$	(2.15)

where h is enthalpy, m is mass flow, and Q and W are energy. Compressor energy is given as W, corresponding to work on the compressor, which is negative because work is being taken from the compressor and added to the refrigerant

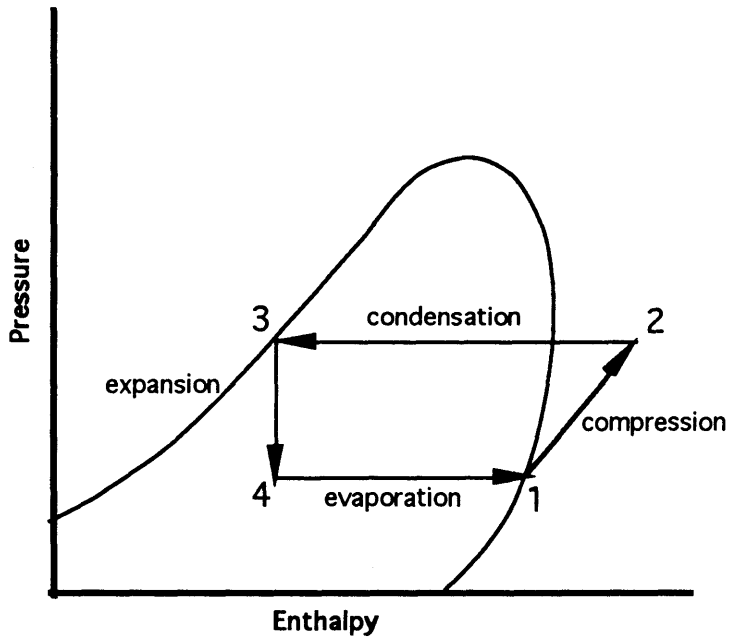

Figure 12. Pressure-Enthalpy Diagram for Vapor Compression Cycle

Evaporation, which in our study occurs at the display case, is an enthalpy gain to the refrigerant at constant pressure (in an ideal cycle). The refrigerant enters the evaporator as a low temperature, low pressure vapor and evaporates by removing heat from the air flowing around it. It exits the evaporator as a saturated vapor.

The refrigerant, now at point 1, enters the compressor. Here the refrigerant is compressed adiabatically (at constant entropy), becoming a high temperature, high pressure, superheated vapor.

The refrigerant vapor, now at point 2, enters the condensing stage. There are possibly two parts to the condensing stage. First, the vapor may be used for heat reclaim in the air conditioning system. In a system like the one in our study, air is supercooled to condense moisture, and then is reheated to desired supply conditions. A valve in the refrigeration line between the compressor and the condenser diverts superheated vapor up

to the air conditioning system where it gives some of its heat to the air. The amount of heat given varies depending on how much reheat is needed. This process reduces the temperature, and therefore enthalpy of the refrigerant at constant pressure. The second part of the condensing stage is the condenser, where the vapor is desuperheated and condensed. Both reclaim and condensation (or only condensation at times when there is no heat reclaim) reduce the refrigerant's enthalpy at constant pressure (in an ideal cycle), until it leaves the condenser as a saturated liquid at high pressure.

From this stage (point 3), the refrigerant enters the expansion valve. This process increases the refrigerant's volume while decreasing its temperature and pressure. This occurs at constant enthalpy, as heat is neither added nor removed from the refrigerant. Now, the supercooled liquid enters the evaporator at point 4, and the cycle is repeated.

2.4.2 Refrigeration System Model

For the purpose of this study, we will model the rack A refrigeration cycle on a pressure versus enthalpy chart to determine what effect reductions on display case load have on compressor and condenser power. Figure 13 shows the pressure versus enthalpy chart for R-502 with lines of constant entropy and constant density. We will assume an ideal cycle, although actual conditions may vary slightly due to entrance and exit pressure drops.

To model this rack, we will use data taken during peak conditions which occurred on July 10 at 6:00 pm. The refrigerant entered the compressor rack from the suction manifold at 13.3 psia pressure and 84.9 Btu/lbm enthalpy, shown in the figure as point 1. From there it traveled up the path of constant entropy until it reached the discharge pressure of 213.0 psia, at point 2. At this point the refrigerant has an enthalpy of 115 Btu/lbm. With a single-compressor-per-circuit configuration, this path can be easily predicted using

compressor efficiency and manufacturers equations. For a multideck configuration such as ours, this is impossible because there are several different types of compressors in the rack, and they cycle on and off alternately during the course of the day based on load needed. The condensation stage ended at the liquid manifold at 206.3 psia pressure and 36 Btu/lbm enthalpy. Then the refrigerant entered the expansion valve, where its pressure dropped to 13.3 psia along the line of constant enthalpy.

For this situation, the enthalpy gain across the evaporator is 48.9 Btu/lbm, while the enthalpy gain across the compressor is 29.1 Btu/lbm. The enthalpy drop which occurs in the condensing section is equal to the combined enthalpy gains in the evaporator section and the compressor, which is 78.0 Btu/lbm.

Considering similar ambient conditions, a theoretical reduction in display case load corresponding to a reduction in enthalpy gain of 10 Btu/lbm would result in suction manifold conditions described by point 1' on the figure. The compressor then compresses the refrigerant, as it travels up the chart at constant entropy to the discharge pressure of 213.0 psia. At this point the refrigerant's enthalpy is 100 Btu/lbm. With the reduction in display case load, the enthalpy gain from the compressor for this pressure increase is 25 Btu/lbm, which is less than the enthalpy gain from the compressor before the reduction (115 - 85 Btu/lbm = 30 Btu/lbm). This means that the compressor needs to work less to provide the same discharge pressure. Although the reduction in display case load due to dehumidification of inside air is not expected to be this drastic for given conditions, this model shows that this type of reduction results in compressor load reduction.

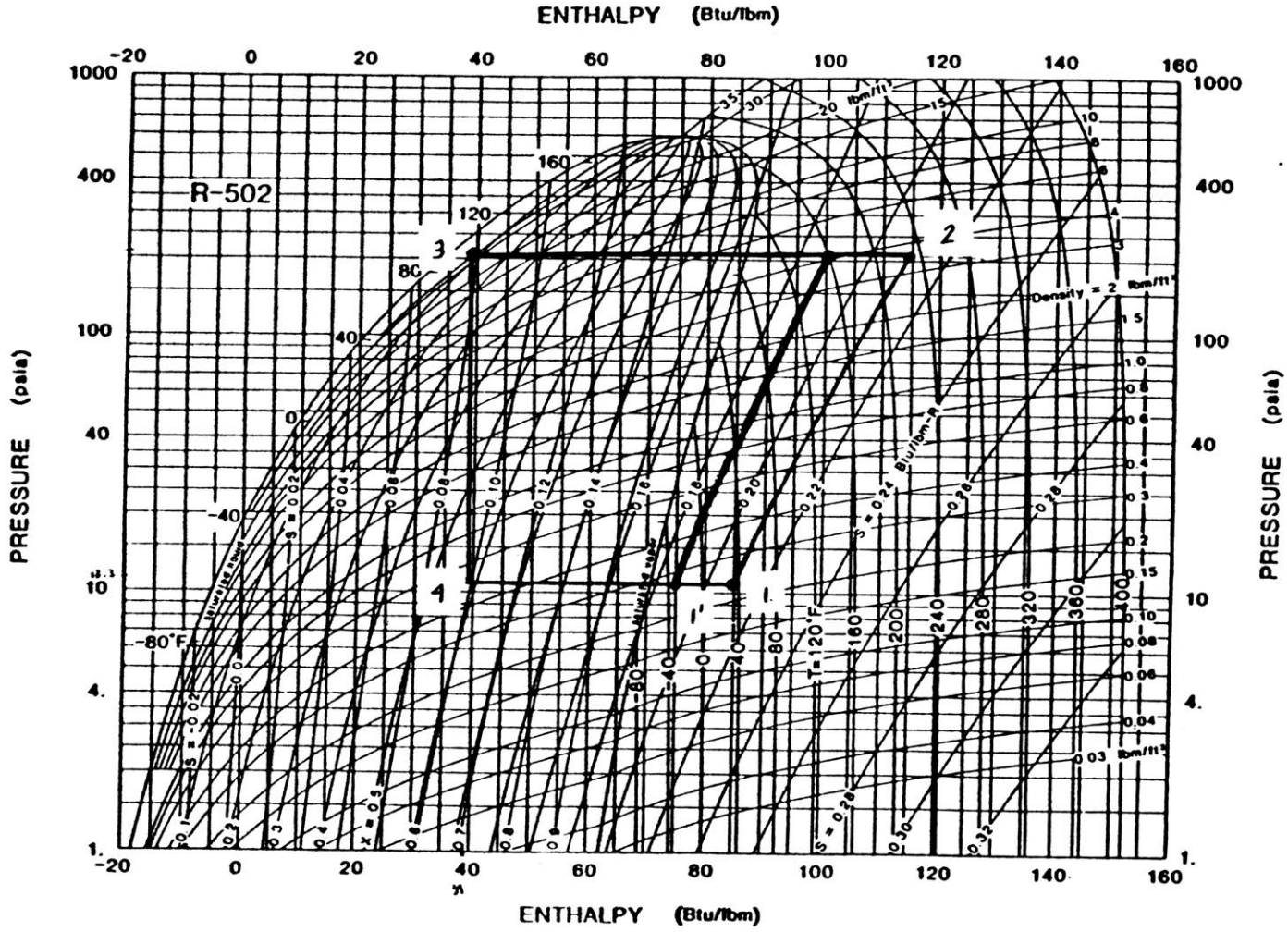

Figure 13. Pressure vs. Enthalpy chart for R-502.

Chapter 3 Method of Analysis

The goal of the project is to determine the effect on refrigeration system energy consumption by dehumidification of inside air caused by installation of a heat pipe. Another goal is to normalize energy savings based on outside air temperature and relative humidity in a model that could be applied to any location. Therefore, the analysis will be accomplished by monitoring air system and refrigeration line parameters ranging from refrigeration compressor power to outside air temperature and relative humidity.

System Modelling. The first step in the analysis is to model the air system and the refrigeration system based on an existing configuration. Using design conditions, it is possible to predict supply air temperature and humidity using return air and outside air parameters. Then we include the heat pipe in the model and see how supply conditions are changed. The refrigeration system is modelled to show the heat gains and losses at different points in the circuit. Then, with the introduction of the heat pipe and inside air dehumidification, variations in display case load are introduced into the model to determine their effect on compressor load.

Inclusion of Monitored Data. Monitored data are used to compare points in the system that would be expected to be affected by each other, and to set up links between the air system and the refrigeration system and within each system. For instance, variation in outside air intake due to opening and closing of the dampers are predicted using the model and monitored return, outside, and mixed air parameters. Temperature differences across the heat pipe were monitored to aid in determining the actual energy transfer from air to heat pipe and back during pre-cooling and re-heat. Mixed air specific humidity and supply air specific humidity are compared to see exactly how much more water vapor is removed

from the air after installation. Supply air specific humidity is compared to return air specific humidity and outside air specific humidity to determine what affect air circulation through the supermarket has on humidity. Inside air and outside air parameters are compared to various parts of the refrigeration circuit and then included in the model to determine how much the heat pipe actually affected the refrigeration system, if at all.

Comparison of Pre-installation and Post-installation Models. It is certain that the installation of the heat pipe will produce lower supply air specific humidity levels than if it weren't installed, as long as the air is cooled past saturation. Physically, this is because the initial cooling of the air by the heat pipe decreases the amount of cooling coil load which is sensible, therefore increasing the amount of cooling load which is latent (since total cooling load is unaffected by the presence of the heat pipe). Whether or not the supply air relative humidity is decreased depends on the amount of reheat added and the supply temperature. By combining the model with monitored data, we can determine how much the supply air specific humidity is reduced for a given mixed air specific humidity level. This is accomplished by performing separate regressions using pre-installation data and post-installation data and applying the equations to monitored data over the cooling season. Inside air is modelled as a function of supply air, outside air, and time of day (as customer traffic, and therefore moisture introduction, is a function of time of day).

The type of refrigeration system used is a multideck system in which three racks (A,B,and C) containing multiple compressors draw refrigerant from a common suction manifold and compress the refrigerant to be distributed to the condenser. The refrigeration cycle for rack A is modelled using monitored data and thermodynamic equations. We vary evaporator load in the model, simulating a reduction in frost buildup on the evaporator (display case) coils, to determine its effect on the rest of the cycle. Compressor load is modelled as a function of evaporator load, condenser load, outside conditions, and time of

day. Condenser load is modelled as a function of outside air conditions. Compressor load is compared to monitored compressor power to determine their relationship. When compressor power has been modelled as a function of evaporator load and outside air conditions, evaporator load will be compared to inside air conditions from the air system model. If there is a definite correlation between compressor power and inside air conditions, and the difference between the pre-installation loads and the post-installation loads are greater than potential calculation and monitoring errors, then savings will be estimated. The set of equations applying to pre-installation conditions will be applied to the whole monitored period, and then the post-installation equations will be applied to the same period.

Prediction of Energy Savings. Energy savings will be estimated and compared to monitored refrigeration compressor power changes. Energy savings are compared to standard monitoring, calculation and regression errors to determine the statistical accuracy.

Scatter plots and regression analyses are performed using SYSTAT, a statistical software package for use with MicroSoft Windows. Engineering calculations and time graphs are performed using Lotus version 3.1 software. Two dimensional graphs are configured using Sigmaplot graphics software.

Chapter 4 Monitoring Strategy

4.1 Monitoring Site Specifics

The site that was monitored is a supermarket located in Worcester, Mass. It was chosen because the managers agreed through New England Electric System's Custom Design program to have a heat pipe installed and monitored. They purchase their electricity from the Massachusetts Electric Company (a subsidiary of NEES) under the G-4 rate, which is a general time-of-use rate based on demand charges of $8.45/kW and energy charges of $0.04283/kWh on-peak and $0.02558/kWh off-peak. The supermarket's annual energy consumption for 1992 was 2,359 MWh and for 1991 was 2,361 MWh. The monthly billing demand in 1992 (which is the peak demand for the month) ranged from 280 kW in January to 410 kW in June (see Figure 14). The total floor space is 57,700 ft^2 including about 39,000 ft^2 of sales area.

4.2 Monitoring Equipment

Monitoring equipment was installed on June 2, 1993. Data were collected and stored on a Campbell Scientific 21X Microdatalogger with a data multiplexer and modem. The datalogger uses up to 16 differential channels of analog input. Up to 16 differential channels can be multiplexed into one input channel. At this site, one Model AM32 Relay Scanner was used to multiplex 32 points of input into two channels, and ten input channels recorded direct measurements. One other channel was used to track panel temperature for overheating, and one channel was used as a reference temperature input. Two input

channels were not used. Manufacturers level of accuracy for voltage measurements is given as 0.05% of full scale range.

Relative humidity / temperature sensors are Omega HX10 Series transmitters. They measure humidity using a thin film capacitor and temperature using a precision integrated circuit. Manufacturers level of accuracy is given as ±2% for relative humidity and ±1°F for temperature.

Thermocouples are Omega Model FF-T-24-TWSH type T shielded wires with teflon insulation. Pressure sensors are Omega PX602 Series transducers with a manufacturers accuracy of ±0.4 %. Watt transducers are Ohio Semitronics GW5 Series using split-core current transformers. Manufacturers level of accuracy is given as ±0.25%. A Kflow Model number K-20 non-intrusive direct mass flow meter was used to measure refrigerant flow. This device uses pulse counts (one pulse for each pound of refrigerant flowing) to track mass flow. The pulse counts are based on the Coriolis effect, for which the acceleration of flows through bends in piping oscillates over time, which deforms the piping proportional to the mass flow. Manufacturer's level of accuracy is given as ±0.2% ±zero stability. Zero stability for the K-20 model is given as 0.004 lb/min. Calibration of the sensors is addressed in chapter 6.

Aspen Systems Inc. of Marlborough MA bought and installed the monitoring equipment. They downloaded monitored data by modem daily and delivered the data to us monthly. The data were received in daily files in Lotus version 3.1 spreadsheet format, and were copied onto hard drive as backup.

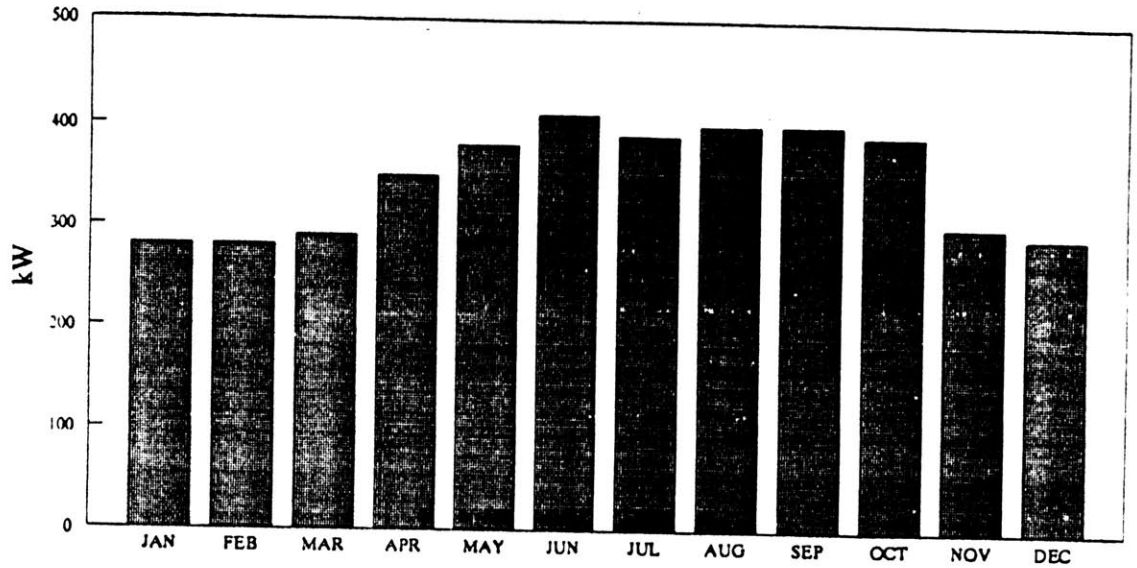

1992 Monthly Peak Demand

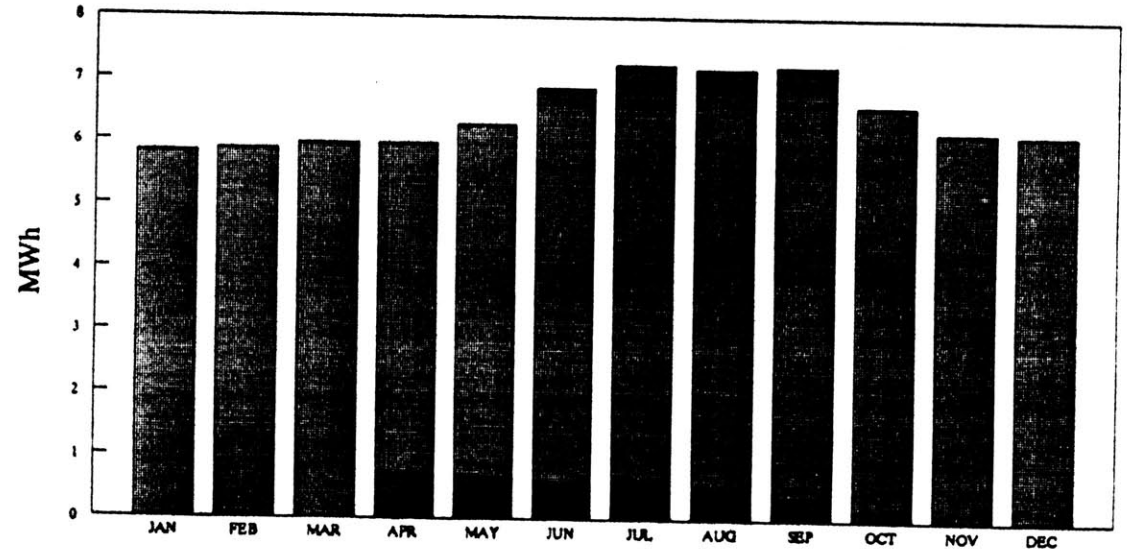

1992 Average Energy Consumption per Day

Figure 14. 1992 Monthly Billing Demand and Energy Consumption

4.3 Measurement Device Locations

For the air conditioning system, temperature and relative humidity sensors were installed to determine air conditions at various points throughout the roof-top air conditioning cabinet. Compressor power was also monitored to measure the level at which the cooling coils were being used. A grid of temperature sensors was installed before and after both the upper and lower cooling coils. Each grid contained four thermocouples, located in the center of each quadrant before and after the coil. A diagram showing where each sensor was located is shown in Figure 15. A schematic showing where all sensors are located is on the next page in Figure 16.

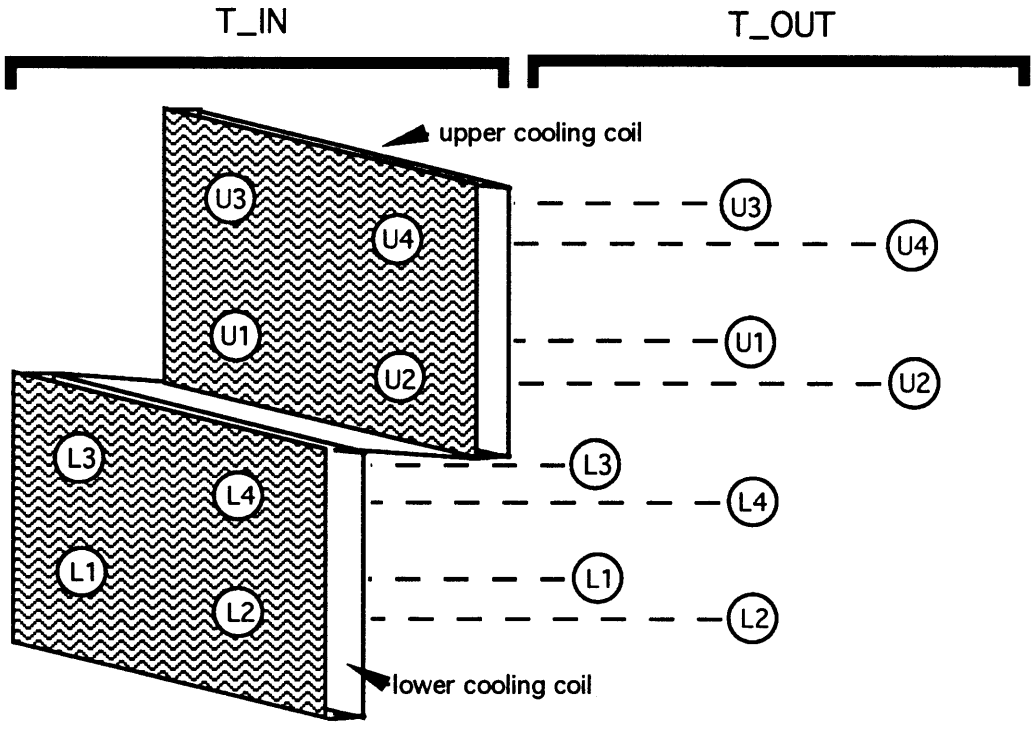

Figure 15. Location of Thermocouples Before and After Cooling Coils

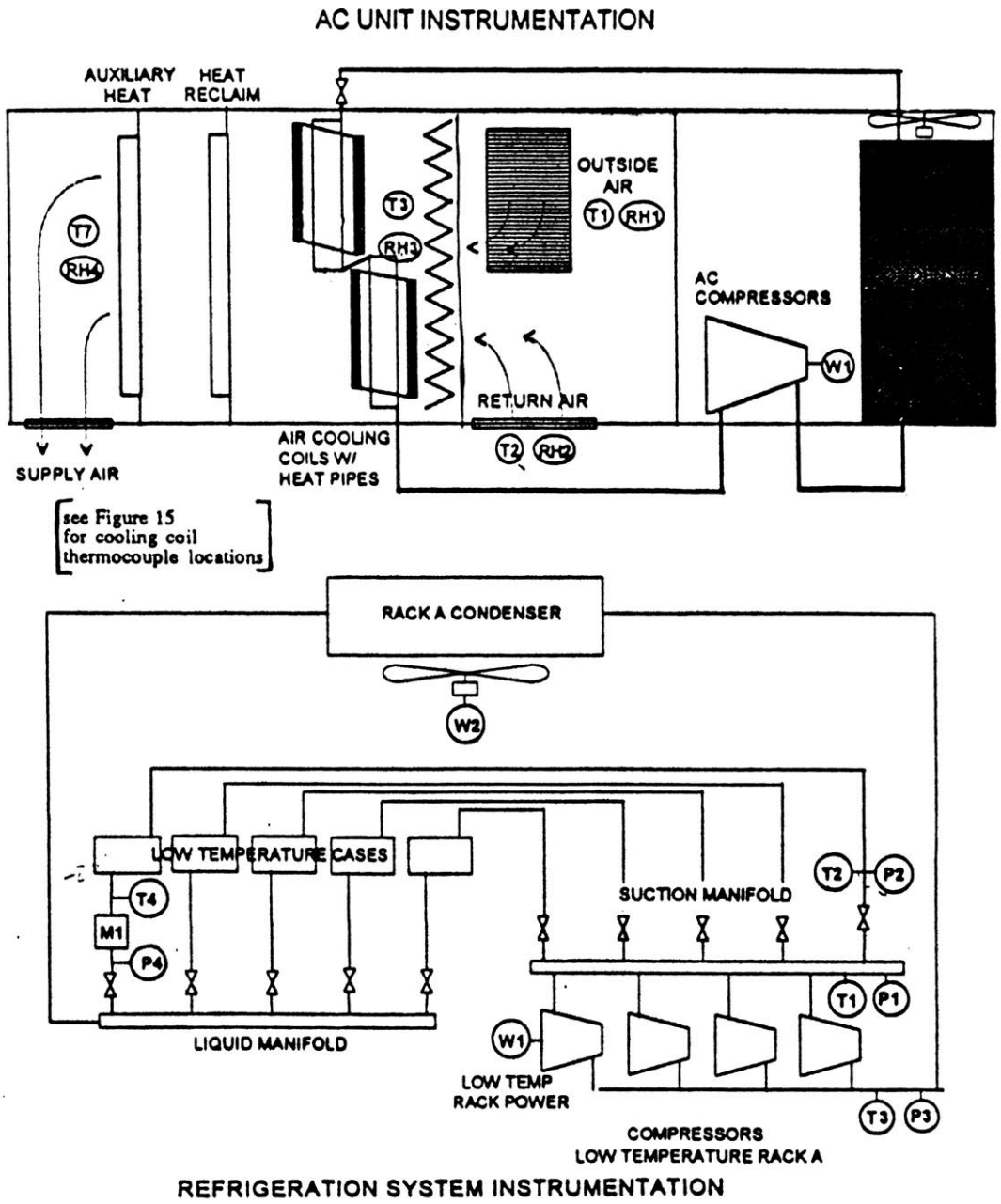

Figure 16. Air Conditioning Unit and Refrigeration System Monitoring Locations.

Since the return air vent was at floor level and the outside air vent was near the top of the duct; and the cooling coils were located so close to these vents, there was expected to be some temperature gradient over the area of the cooling coils. Figure 17 shows graphs of the eight thermocouples located before the cooling coil during typical A/C operation. The graphs show that the temperature gradient is not evident in the lower coil, but is visible from the bottom of the upper coil (TIN_U1 and TIN_U2) to the top of the upper coil (TIN_U3 and TIN_U4). This is to be expected, since the amount of outside air coming in is small compared to the amount of return air. Therefore, only the air near the top of the duct would show any effects of outside air temperature.

After the installation of the heat pipe, a single thermocouple was installed outside the pre-cooling side of the heat pipe and outside the reheat side of the heat pipe for each coil. It was assumed that the temperature difference across the heat pipe was independent of location, and that the difference monitored at one location could be applied to all other locations. This, however, turned out to be a faulty assumption, as temperature differences for these four locations varied considerably (section 7.3).

In addition to these locations, relative humidity / temperature sensors were installed to monitor return air, outside air, supply air, and mixed air prior to the cooling section. Total compressor power (for two compressor motors, one controlling the lower cooling coil and one controlling the upper coil) was also monitored. Table 4 shows the list of all points measured with description and range.

For the refrigeration system, compressor power for all three racks was monitored, as well as line pressures and temperatures for rack A and circuit 4 (servicing a low temperature, open coffin style frozen food display case) and refrigerant mass flow for circuit 4. Circuit 4 evaporator suction and liquid pressures and temperatures were

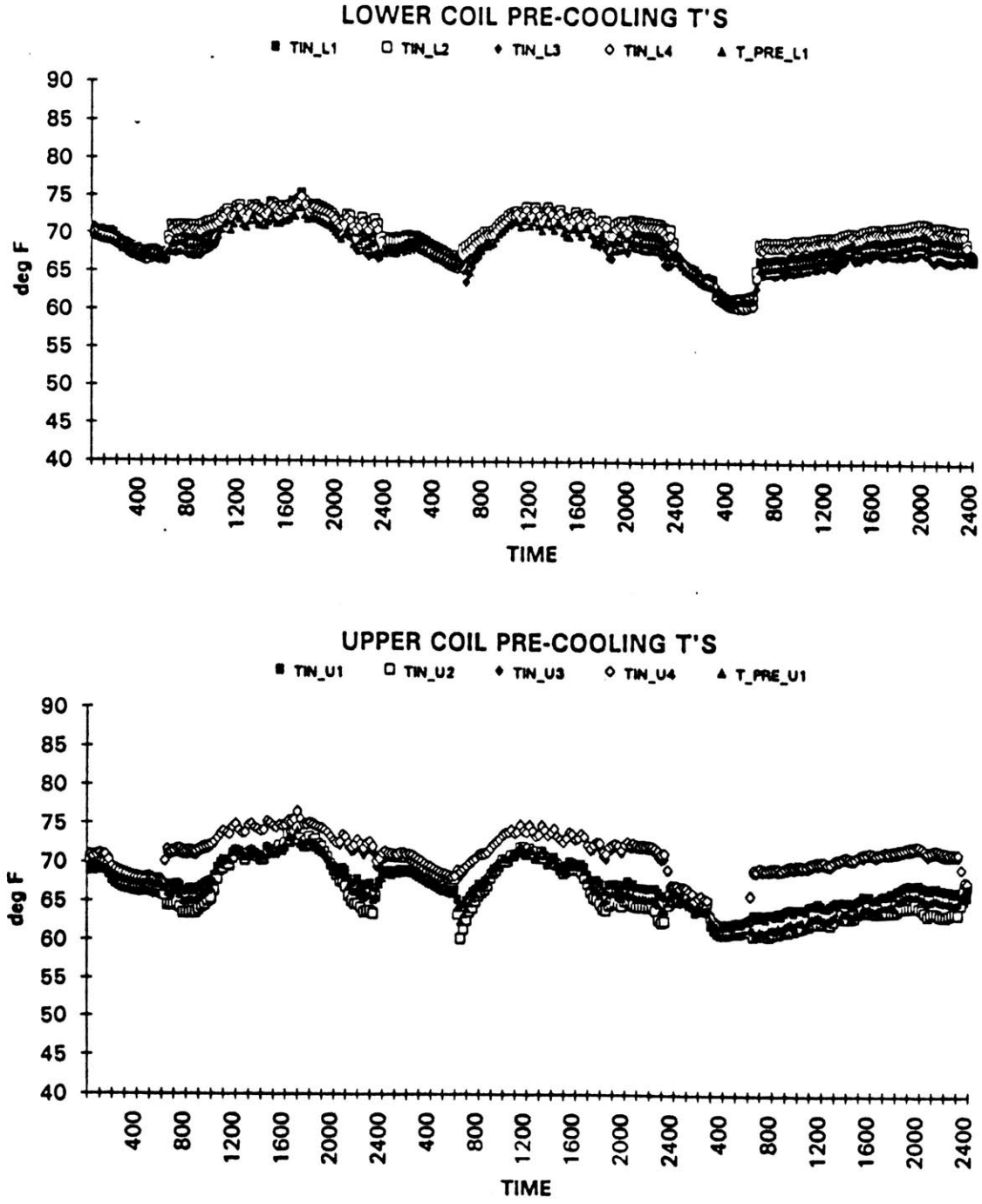

Figure 17. Three-Day Temperature Readings for Eight Pre-Coil Thermocouples

HEAT PIPE RETROFIT MONITORING INSTRUMENT LIST

CHANNEL	INPUT	PARAMETER	DESCRIPTION	RANGE	UNITS
1	21X-3	P1	RACK A COMPRESSOR SUCTION PRESSURE	0 - 100	PSIG
2	21X-4	P2	CIRCUIT 4 SUCTION PRESSURE	0 - 100	PSIG
3	MUX-2.15	P3	RACK A COMPRESSOR DISCHARGE PRESSURE	0 - 300	PSIG
4	MUX-2.16	P4	CIRCUIT 4 LIQUID PRESSURE	0 - 300	PSIG
5	21X-5H	T1	RACK A COMPRESSOR SUCTION TEMPERATURE	TC TYPE T	DEG F
6	21X-5L	T2	CIRCUIT 4 SUCTION TEMPERATURE	TC TYPE T	DEG F
7	21X-6H	T3	RACK A COMPRESSOR DISCHARGE TEMPERATURE	TC TYPE T	DEG F
8	21X-6L	T4	CIRCUIT 4 LIQUID TEMPERATURE	TC TYPE T	DEG F
9	21X-1P	M1	CIRCUIT 4 REFRIGERANT MASS FLOW RATE	0 - 1200	LB/HR
10	21X-7H	W1	RACK A COMPRESSOR POWER	0 - 45	KW
11	21X-7L	W2	RACK A CONDENSER POWER	0 - 18	KW
12	21X-8H	W3	RACK B COMPRESSOR POWER	0 - 30	KW
13	MUX-1.1	W4	RACK C COMPRESSOR POWER	0 - 80	KW
14	MUX-2.1	W5	AC COMPRESSOR POWER	0 - 80	KW
15	MUX 1.2	RH1	INDOOR AIR (RETURN) RELATIVE HUMIDITY	0 - 100	% RH
16	MUX-1.3	RH2	OUTDOOR AIR RELATIVE HUMIDITY	0 - 100	% RH
17	MUX-1.4	RH3	MIXED AIR RELATIVE HUMIDITY BEFORE HEAT PIPE	0 100	% RH
18	MUX-1.5	RH4	SUPPLY AIR RELATIVE HUMIDITY AFTER HEAT PIPE AND REHEAT	0 - 100	% RH
19	MUX-2.2	T5	INDOOR AIR (RETURN) TEMPERATURE	32 - 212	DEG F
20	MUX-2.3	T6	OUTDOOR AIR TEMPERATURE	32 - 212	DEG F
21	MUX-2.4	T7	MIXED AIR TEMP BEFORE HEAT PIPE	32 - 212	DEG F
22	MUX-2.5	T8	SUPPLY AIR TEMP AFTER HEAT PIPE AND REHEAT	32 - 212	DEG F
23	MUX-1.6	T9	UPPER COIL INLET, 1ST QUADRANT	TC TYPE T	DEG F
24	MUX-1.7	T10	UPPER COIL INLET, 2ND QUADRANT	TC TYPE T	DEG F
25	MUX-1.8	T11	UPPER COIL INLET, 3RD QUADRANT	TC TYPE T	DEG F
26	MUX-1.9	T12	UPPER COIL INLET, 4TH QUADRANT	TC TYPE T	DEG F
27	MUX-1.10	T13	UPPER COIL AFTER HEAT PIPE EVAP, 1ST QUADRANT	TC TYPE T	DEG F
28	MUX-1.11	T14	UPPER COIL AFTER DX EVAP, 1ST QUADRANT	TC TYPE T	DEG F
29	MUX-1.12	T15	UPPER COIL OUTLET, 1ST QUADRANT	TC TYPE T	DEG F
30	MUX-1.13	T16	UPPER COIL OUTLET, 2ND QUADRANT	TC TYPE T	DEG F
31	MUX-1.14	T17	UPPER COIL OUTLET, 3RD QUADRANT	TC TYPE T	DEG F
32	MUX-1.15	T18	UPPER COIL OUTLET, 4TH QUADRANT	TC TYPE T	DEG F
33	MUX-1.16	T19	LOWER COIL INLET, 1ST QUADRANT	TC TYPE T	DEG F
34	MUX-2.6	T20	LOWER COIL INLET, 2ND QUADRANT	TC TYPE T	DEG F
35	MUX-2.7	T21	LOWER COIL INLET, 3RD QUADRANT	TC TYPE T	DEG F
36	MUX-2.8	T22	LOWER COIL INLET, 4TH QUADRANT	TC TYPE T	DEG F
37	MUX-2.9	T23	LOWER COIL AFTER HEAT PIPE EVAP, 1ST QUADRANT	TC TYPE T	DEG F
38	MUX-2.10	T24	LOWER COIL AFTER DX EVAP, 1ST QUADRANT	TC TYPE T	DEG F
39	MUX-2.11	T25	LOWER COIL OUTLET, 1ST QUADRANT	TC TYPE T	DEG F
40	MUX-2.12	T26	LOWER COIL OUTLET, 2ND QUADRANT	TC TYPE T	DEG F
41	MUX-2.13	T27	LOWER COIL OUTLET, 3RD QUADRANT	TC TYPE T	DEG F
42	MUX-2.14	T28	LOWER COIL OUTLET, 4TH QUADRANT	TC TYPE T	DEG F
45	21X		PANEL TEMPERATURE		
46	21X-8L		MULTIPLEXER REFERENCE TEMPERATURE		
	21X-1		MULTIPLEXER CHANNEL 1 INPUT		
	21X-2		MULTIPLEXER CHANNEL 2 INPUT		

Table 4. Monitoring Instrument List

monitored to determine the refrigerant enthalpy, and combined with the mass flow to determine display case (evaporator) load as shown by the equation below,

$$\text{Display case load } Q = m * (h_2 - h_1) \tag{4.1}$$

m = mass flow (lb/hr)

h_2=enthalpy of suction gas

h_1=enthalpy of liquid

Compressor power and suction and discharge temperatures and pressures were monitored for one minute intervals on July 22 between the hours of midnight to 8:30 am to observe a more detailed performance of the defrost cycle. Defrost cycles and types vary depending on location and evaporating temperature, and are listed in Table 5.

4.4 Summary

The points chosen to be monitored were selected based on all of the factors which would be needed to model the airflow and refrigeration cycle with a limitation of input channels available. The specific points to monitor were chosen by representatives of NEES, Aspen Systems, the supermarket managers, and myself as a group. Monitoring devices were chosen by Aspen Systems, who also performed the calibrations, sensor maintenance, and data reduction. All regressions, psychrometric analyses, graphics, and other data manipulation (including calculation of specific humidity, energy flows, enthalpies, etc.) were performed by me. Ideally, we would have liked to have monitored more points in the cross section of the mixed air and supply air flow, and more points before and after the heat pipe, but in that case we would have needed another datalogger. The depth of this analysis is much greater than any other I have read about, and the fact that the results are still statistically inconclusive means that either this strategy is ineffective,

more advanced technology needs to be used with this strategy, or current technology is incapable of providing a sufficient heat pipe analysis. These issues will be addressed in chapter 10.

Description	Type	Start times	Duration
MEAT C18	Hot Gas	04:00 AM	18 min
		10:00 AM	18 min
		04:00 PM	18 min
		10:00 PM	18 min
MEAT C19	Hot Gas	05:00 AM	18 min
		11:00 AM	18 min
		05:00 PM	18 min
		11:00 PM	18 min
FMTZ 20	Hot Gas	08:00 AM	30 min
MEATWKIN 21	Hot Gas	01:00 AM	20 min
		01:00 PM	20 min
POULWKIN C22	Hot Gas	02:00 AM	20 min
		02:00 PM	20 min
DELMEAT C23	Hot Gas	03:00 AM	18 min
		09:00 AM	18 min
		03:00 PM	18 min
		09:00 PM	18 min
S/DELI C24	Off-cycle	04:30 AM	90 min
CHEESE C25	Off-cycle	02:30 AM	45 min
		10:30 AM	45 min
		06:30 PM	45 min
PROD C26	Off-cycle	01:00 AM	50 min
		07:00 AM	50 min
		01:00 PM	50 min
		07:00 PM	50 min
FISH WALKIN	Off-cycle	04:00 AM	60 min
		04:00 PM	60 min
DELI WALKIN	Off-cycle	03:00 AM	60 min
		03:00 PM	60 min
BAKWKN C29	Off-cycle	06:00 PM	60 min
PRODWN	Off-cycle	03:00 AM	60 min
		07:00 PM	60 min
		11:00 PM	60 min
MEAT PREP	Off-cycle	05:00 AM	120 min
DELI 4' BAR	Off-cycle	12:30 AM	60 min
		04:30 AM	60 min
		08:30 AM	60 min
		12:30 PM	60 min
		04:30 PM	60 min
		08:30 PM	60 min
CHEESE C33	Off-cycle	11:00 AM	60 min
		11:00 PM	60 min
BAKFRZ D35	HEAT	01:00 AM	45 min
		07:00 AM	45 min
		01:00 PM	45 min
		07:00 PM	45 min

Table 5. Defrost Cycles and Types

Chapter 5 Building Operating Conditions

This chapter, as mentioned above in step three, serves to describe the existing building conditions and air system and refrigeration system configuration. Heat pipe dehumidification has different effects on different systems, and it is important to note that the findings of this thesis apply to this building's configuration. The air conditioning system is a single path, direct evaporative cooling system and the refrigeration system is a multideck configuration with remote condensation. The sections of this chapter describe the units in more detail.

5.1 Air Conditioning Unit

The air conditioning unit is a 77 ton Seasons 4 rooftop model, shown in Figure 18. It includes a condensing section, a service vestibule, a return air plenum, an evaporator section, a supply air blower section, auxiliary reheat, and a supply air plenum. The condensing section contains counter-flow condensers with liquid sub-cooling, and direct drive fans with pressure switches to provide floating head pressure control. The service vestibule contains the compressors and electrical panels. The return air plenum receives return air through the bottom and outside air from dampers located on the top half of the wall opposite the service door. The evaporator section contains air filters and two cooling coils, one each in the upper half and lower half, which are offset slightly. The blower section contains heat-reclaim coils across the upper half of the duct with bypass dampers on the lower half, and a centrifugal fan, controlled by a forty-horsepower open drip-proof motor.

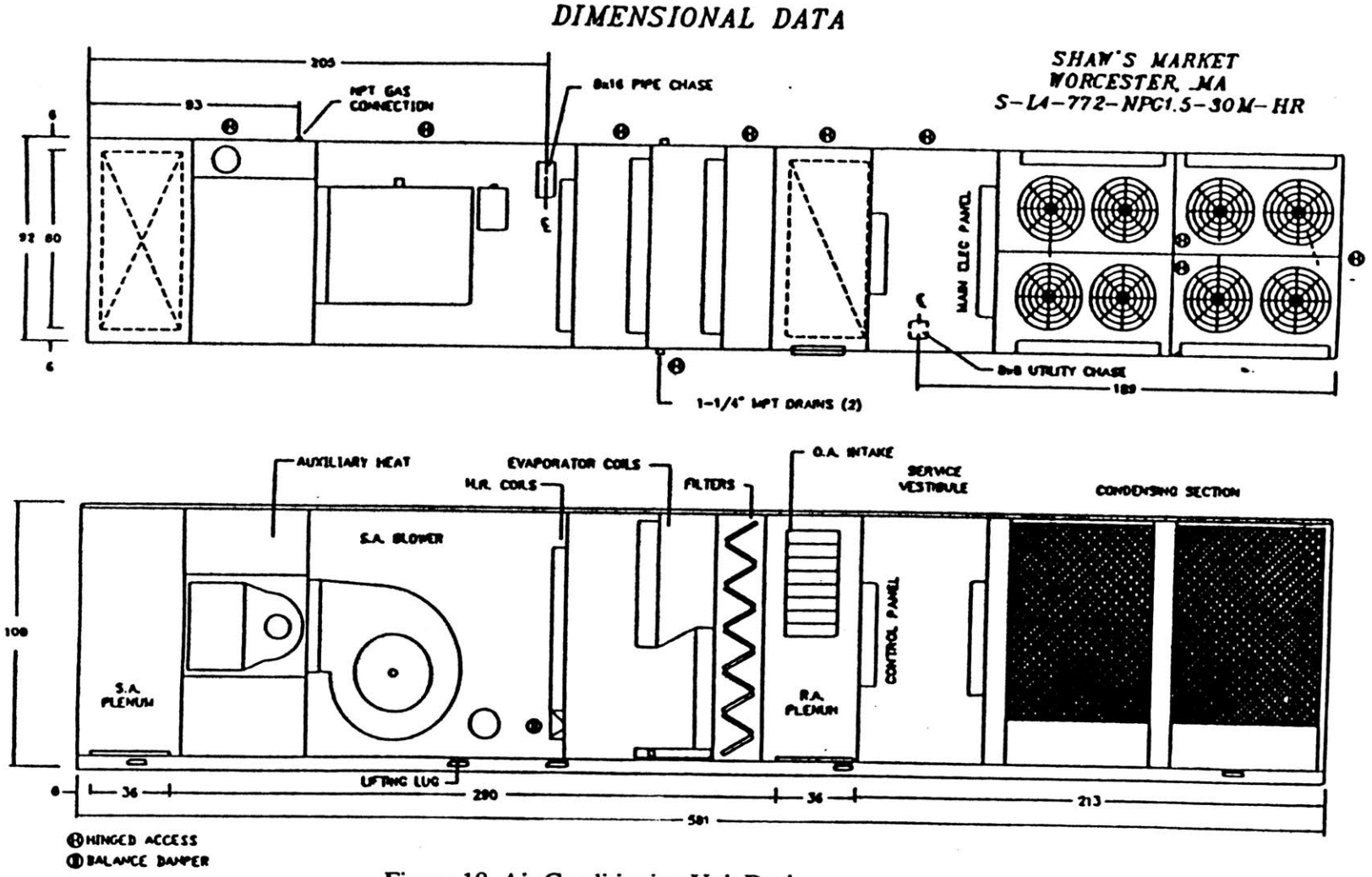

Figure 18. Air Conditioning Unit Design.

5.1.1 Air Conditioning Specifications

There are two semi-hermetic compressors in the cooling section, manufactured by Copelametic Discus, each using R-22 refrigerant. The first compressor serves the lower cooling coils, and it is the first one activated when cooling is needed. When maximum power has been reached and additional cooling is needed, the second compressor drives the upper cooling coil. The cooling coils have a design capacity of 940,000 Btuh. Compressor power is controlled through a CPC Intelligent Environmental Control panel which monitors inside air dry bulb temperature and turns the compressors on and off accordingly. The control setpoints change at night (12:00 am to 6:00 am) when less cooling is needed. For the summer months the first compressor is designed to turn on when the inside temperature reaches 72 degrees during the day (74 at night), and the second compressor comes on when the temperature reaches 73 degrees during the day (75 at night). The second compressor shuts off when the temperature drops to 72 degrees (73 at night), and the first compressor shuts off when the temperature drops below 71 degrees (72 at night). For each setpoint there is a delay of five minutes.

There are eight fans in the condensing section, each of which are 1-1/2 horsepower operating at 1.4 kW. The fans are cycled to provide head pressure control when the ambient temperature drops below the setpoint.

The supply air fan is a Barry Blower 40 inch centrifugal fan designed for 924 rpm and 30,000 cfm of air supply. At 30,000 cfm, the fan generates a static pressure rise of 5.0 (in. water). During the months of April through October, the fan is on a schedule which turns it on at 6:00 am and shuts it off at 11:59 pm. On extremely warm nights, the fan comes on if the cooling coil compressors are activated.

Equipment specification sheets and fan curve can be found in Appendix B.

5.1.2 Airflow Measurements

The unit was designed for a total airflow of 30,000 cfm, with an outdoor air intake of 4,500 cfm. On August 2, 1993 just before the heat pipe was installed, HEC Energy Services assisted in an air flow measurement test in the evaporator section of the duct just before the reheat coils and bypass dampers. The test was accomplished by using a vane anemometer, an instrument which uses rotating blades to measure distance covered by moving air for a given amount of time. By traversing the entire area of the duct while the blower was in operation, we were able to obtain an average velocity for the airflow, and using cross sectional area we were able to calculate volumetric airflow. The test resulted in an estimated airflow of 33,200 cfm as calculated below in Table 6.

Table 6. Airflow Measurements Performed August 2.

	Over heat Reclaim Coils - Upper Half			Bypass Damper-Lower Half	
	Test 1	**Test 2**	**Test 3**	**Test 1**	**Test 2**
Feet measured	505	510	520	1000	1040
Seconds	60	60	60	60	60
Ft/Sec	8.42	8.50	8.67	16.67	17.33
Ft/min	505	510	520	1000	1040
CFM	9789	9886	10080	22847	23761

Average of readings over upper half 9,918 cfm

Average of readings over lower coil 23,304 cfm

Total Airflow 33,200 cfm

On September 30 we measured the airflow through the outside air dampers during fan operation using a velometer. A velometer is a device which covers inflow dampers and channels the flow into a known cross-sectional area, and uses fan blades to measure air speed. The device converts the air speed into volumetric flow using the given area. Airflow through the upper damper was measured at 2550 cfm and through the lower damper was measured at 2500 cfm, for a total of 5050 cfm.

5.2. Refrigeration System Description

The refrigeration system consists of three compressor racks and four satellite compressors, remote condensers on the roof, and 35 individual display units. The system was manufactured by Hussman Northeast in 1988. There are two compressor rooms, one located behind the dairy storage room which houses compressor racks A and B, and one behind the meat storage housing compressor rack C. Rack A includes five compressors supplying eight low temperature circuits, Rack B includes four compressors supplying five medium temperature circuits, and Rack C includes seven compressors supplying thirteen medium temperature circuits. Compressors are manufactured by Copeland. All three racks use R502 refrigerant and have a remote condenser. The condenser for rack A contains two rows of three fans, designed for 318,000 Btuh of total heat rejection. The rack B condenser has three fans and 229,200 Btuh of design heat rejection, and the rack C condenser has two rows of four fans and 667,600 Btuh of design heat rejection. For a list of design loads and evaporating temperatures see Tables 7 and 8.

Circuit 4 provides refrigeration for an open tub display case for frozen dinners and juices. It was chosen for monitoring because of its low operating temperature and high

level of exposure to the indoor air. Circuit 4 is connected to rack A compressors which supply the low temperature refrigeration for ice cream and frozen foods.

5.3 Summary

The end of this chapter concludes step three of the analysis. Since different refrigeration configurations and quantities will result in different savings estimates, and different air system will require different heat pipe designs, an extensive background of the existing setup and operating conditions has been provided. The first three steps were mainly used to set up the last three steps, which are the quantitative part of the thesis. The analytic steps start with the introduction of the monitored data, and how it was used in the analysis. Then the air system and refrigeration system are modelled and energy savings are analyzed.

Table 7
Refrigerated display cases

Circuit no.	Circuit desc.	Design Load(Btu/hr)	Evap. Temp	Disch. Air temp.
4	frozen food	21,450	-20	-10
5	frozen food	9,900	-20	-10
6	ice cream	15,400	-19	-12
7	ice cream	15,400	-19	-12
8	frozen food	24,200	-19	-5
9	frozen food	24,200	-19	-5
10	frozen food (spare)			
11	dairy	11,445	15	29
12	dairy	33,000	21	37
13	dairy	27,000	21	37
14	dairy	21,000	21	37
17	produce (spare)			
18	meat cases	73,200	11	22
19	meat cases	24,400	11	22
20	frozen food	18,700	-20	-10
23	deli	43,840	20	32
24	deli	14,880	22	26
25	cheese	19,280	20	32
26	produce	49,680	21	37
32	deli	6,240	17	32
33	cheese	7,980	25	30

Table 8
Refrigerated walk-in coolers and freezers

Circuit no.	Circuit desc.	Design Load(Btu/hr)	Evap. Temp	Room Temp.
2	ice cream	20,100	-22	-15
3	ice cream	20,100	-22	-15
15	dairy	20,575	25	36
16	dairy	20,575	25	36
21	meat storage	34,500	18	28
22	poultry storage	8,900	18	28
27	fish	6,500	25	34
28	deli	9,800	24	34
29	bakery	9,000	28	36
30	produce	31,100	33	40
31	meat preparation	54,600	35	55

Chapter 6 Monitored Data

As was mentioned in Step 4, this chapter summarizes the data that were monitored and calibrated by Aspen Systems. Each section corresponds to a monitoring location in the air system, and circuit 4 and rack A in the refrigeration system. Sensor calibration is addressed in this chapter, as well as sensor maintenance and problems associated with data collection. For sensor calibration, several methods were used including ice water baths and boiling water baths for thermocouples and saturated salt solutions for relative humidity sensors. The original mixed air, return air, outside air, and supply air sensors were sealed in a jar for a three day period before testing to determine their relative accuracies. Since the supply air sensor was the only one that remained at the same location until the end of testing, it was calibrated alone at the end of testing and the other sensors were calibrated based on their relationship to the supply air sensor. The results are the source of calibration for the temperature readings in each corresponding section. The graphs of all air system calibrations and calibration equation derivations are included in Appendix E.

This chapter sets the stage for chapter 7, which includes the models, as it describes the data which are being inserted into the models, and clarifies their accuracy. In general the collection of data was not as successful as expected, due to many reasons which will be discussed in the summary and in the Conclusions in chapter 10.

6.1 Return Air Temperature and Relative Humidity

The return air was included in the analysis for two reasons. By modelling mixed air as a function of return air and outside air using known equations and airflows, we can evaluate the accuracy of the sensors involved. Also, the return air is a good representation

of the inside air in its final mixed state. The inside air goes through many changes after the supply vents, receiving heat and moisture from customers, losing moisture due to frost buildup on refrigeration coils, and cooling down due to contact with display cases, before entering the return duct. Although the exact relationship between return air and inside air cannot be determined, a good indication that they are related can be seen by comparing AC compressor power and return air temperature.

6.1.1 Return Air vs AC Compressor Power

Since the air conditioning compressor activates based on inside air dry bulb temperature (which is also a function of location in the store, as the inside air is not isothermal), trends in AC power should be seen in trends in return air temperature. This is evident in Figure 19, a time line of return temperature and AC compressor power over a typical four day period. At the beginning of the graph, the return air temperature is rising as the first compressor is on full power. when the return air temperature reaches 68, the second compressor kicks in, dropping the return temp. When the temperature drops below 66, the second compressor shuts off and the temperature rises again. This occurs throughout the graph for daytime hours (6:00 to 23:30), corresponding to daytime EMS setpoints of 73 for the second compressor to come on, and 72 for it to shut off. The first compressor seems to turn on at the beginning of each day, and shuts off when the return air temperature falls below 64. It then seems to turn on when the temperature rises above 66.

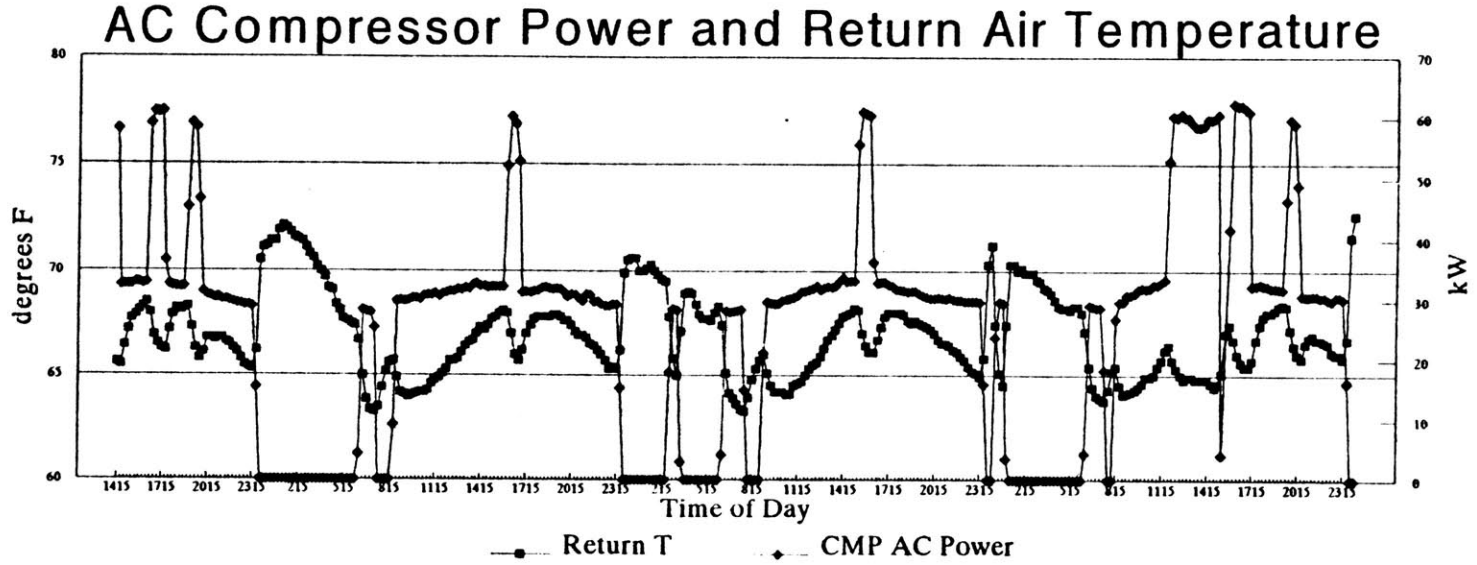

Figure 19. Typical Four Day Period with AC Compressor Power and Return Air Temperature

Although this is not a quantifiable or exact relationship, the reoccurrence of these reactions lead to the assumption that there is a relationship between return air and inside air.

6.1.2 Return Air Sensor Location and Calibration

The return air temperature and relative humidity sensors were installed at the return air inlet to the rooftop air conditioning cabinet. The temperature sensor was checked against a hand held thermometer for multiple three minute periods on June 14 and June 25. The differences between readings and sensor measurements varied considerably, so this calibration was considered unusable. A pre-installation test with all sensors in a sealed jar for three days revealed that, for a temperature range of 70 degrees to 90 degrees:

$$T\_RTRNraw = T\_SUPPraw + 0.4 \text{ [F]}$$

and given the supply air calibration (section 6.3), the calibrated results are:

$$T\_RTRNcalibrated = T\_RTRNraw - 5.8 \text{ [F]}$$

$$Standard\ error = 0.857 \text{ [F]}$$

On August 19 the relative humidity sensor was calibrated in a salt solution against reference humidities of 75.5% and 11.3%. The resulting equation is as follows:

$$RH\_RTRNcalibrated = 1.458*(RH\_RTRNraw) - 6.6$$

$$(R^2 = 1.0)$$

These adjustments were applied to return air data before September 22. The replacement sensors were calibrated on September 28 , which gave the relationships:

$$T\_RTRNcalibrated = T\_RTRNraw - 3.1 \text{ [F]}$$

$$RH\_RTRNcalibrated = 1.351(RH\_RTRNraw) - 25.3$$

6.2 Mixed Air Temperature and Relative Humidity

The mixed air temperature and relative humidity sensors were located approximately 3/4 of the way from the floor of the duct to the roof, and between the air filters and the cooling coil. In retrospect, it would be a better idea to use multiple sensors in a cross-section for this location, but availability of resources at the time allowed only one sensor. It was obvious from the data that there was an error with either the location, the sensor, or the calibration (see below), as calibrated mixed air temperature readings were consistently higher than both the return air and outside air readings. This issue is addressed in the next chapter when mixed air is modelled.

6.2.1 Sensor Location

The mixed air temperature and relative humidity sensors were installed between the air filters and the cooling coils. There is very little distance between the filters and the coils, and also between the filters and return air plenum. Since the return air inlet is at the bottom of the duct, and the outside air inlet is on the side and near the top of the duct, there is still expected to be some cross-sectional variation in air temperature and humidity when the air has reached the cooling coil. Therefore, the air is not completely mixed at the location of the sensor, but we felt that a location after the filters and near the middle of the upper cooling coil would give the most accurate data.

The original sensor was at this location until August 11, when it was used to replace the failed sensor outside the air conditioning unit. The second sensor was installed at the original location on August 11 and remained until the end of monitoring

6.2.2 Sensor Calibration

Calibrations resulting from data recorded in a sealed jar during a three day period show that this sensor was reading 1.3 degrees lower than the supply sensor. Since the supply temperature sensor, as shown below, reads 5.4 degrees higher than actual temperature, the mixed air temperature sensor was reading 4.1 degrees higher than actual temperature. This calibration was applied to mixed air temperature data before August 11.

The second temperature sensor was calibrated on September 28 and revealed that raw temperature was 1.8 degrees higher than the reference temperature. This calibration was applied to mixed air temperature data after August 11.

The original relative humidity sensor was calibrated only in a low RH salt solution on June 1. It was assumed at that time by the monitoring contractor that a one-point calibration would be sufficient, but it was later found that sensor error varied considerably with humidity levels. Therefore, this calibration is determined to be inconclusive, and no adjustments were made to data before August 11.

The relative humidity sensor installed on August 11 was calibrated on September 28 against reference relative humidities of 75.5% and 11.3 % and the following relationship was discovered:

$$RH\_MIXcalibrated = 1.351(RH\_MIXraw) - 25.3$$

$$(R^2 = 1.0)$$

mixed air relative humidity data after August 11 was adjusted accordingly.

6.3 Supply Air Temperature and Relative Humidity

The supply air temperature and relative humidity were monitored to track any changes of the air being supplied to the store after the heat pipe was installed. Although

the temperature is not expected to change, the specific humidity calculated from temperature and relative humidity is expected to decrease due to extra dehumidification.

The supply air temperature and relative humidity sensors were installed at the end of the air conditioning cabinet, after the auxiliary heating coils. The original sensors remained until the end of monitoring, and were calibrated on September 28. The temperature sensor was calibrated against a reference temperature range of 52 degrees to 80 degrees. The relative humidity sensor was calibrated against reference relative humidities of 75.5% and 11.3 %. As a result of the calibration, the following adjustments were applied to all supply air data:

$$T\_SUPLcalibrated = 0.97(T\_SUPLraw) - 3.1 \text{ [F]}$$

$$Standard\ Error = 0.857 \text{ [F]}$$

$$RH\_SUPLcalibrated = 1.553(RH\_SUPLraw) - 1.4$$

$$(R^2 = 1.0)$$

Since the supply air sensor was included in the original sealed jar containing all of the sensors, this calibration was combined with the relative relationship between this sensor's readings and other sensors readings to calibrate the other sensors.

6.4 Outside Air Temperature and Relative Humidity

The outside air temperatures and relative humidities were the most important data being collected, and they unfortunately resulted in the most trouble. Outside air conditions were the key factor separating this analysis from other analyses, since milder conditions during the cooling season in Worcester were expected to lessen the effect of dehumidification. Accurate data were necessary to normalize savings as a factor of outside temperature and humidity levels. Also, several factors including condenser power, mixed air specific humidity, and inside air temperature and humidity (due to infiltration) are

expected to be a factor of outside condition, and regressions against accurate data would be useful in predicting these parameters.

As is further explained in the next sections, outside air temperature and relative humidity as they were recorded were insufficient for the analysis. Many periods of data were removed due to poor readings. Bad readings were either due to poor location, inadequate sensor protection, or general sensor failure. In order to obtain the most complete outside air data for the entire monitoring period, dry bulb and wet bulb temperatures for Worcester MA were obtained from the National Climatic Data Center in Asheville, North Carolina.

6.4.1 Sensor Location and Maintenance

The temperature and relative humidity sensors used to measure outside air conditions were originally placed just inside the outside air dampers in the return air duct. We had originally been informed by the store's managers that the supply air blower operated 24 hours a day, seven days a week, and therefore this location would always be an inlet for outside air, yet the sensors would be protected from rain and solar radiation.

During several of the early days of monitoring, the data for these points sharply dropped at 11:30 pm to the levels of the return air data, and remained there until approximately 6:00 am, when the data jumped back to expected conditions. After further investigation, we determined that during these hours the supply air blower shut off, leaving the air in the duct stagnant. Outside air was no longer being drawn in through the damper and the sensors were reading return air conditions. Although the blower sometimes came on over the course of the summer at night when cooling was needed, this never happened in the first few weeks. As a result of this problem, the sensors were moved to outside the air supply cabinet. Over the next several weeks, there occurred several problems related to

sensor location and performance. On some occasions, the sensors were heated due to inadequate shielding for solar radiation and therefore read too high, sometimes as high as 160 degrees. When this happened , these data were deleted and the sensor was moved to a location shaded from the sun. The sensor was relocated several times by an employee of Aspen Systems, who determine over the course of several site visits that the sensor location was either affected by sunlight, rain or wind (as this was originally at an inside location, the sensor chosen was not protected for outside conditions), or measured air conditions that were different than the air entering the inlet dampers. Because of this there are gaps in recorded data, either due to relocation of the sensor or sensor failure. The weather station data which were acquired to fill in these gaps will be discussed in section 6.4.3.

On August 11, the outside sensors were replaced with the original mixed air sensors. On August 26, these sensors were replaced with sensors designed for outside conditions. These sensors remained until the end of monitoring

6.4.2 Sensor Calibration

The original temperature sensor (used June 2 to August 10) was calibrated before sensor installation and after removal. This sensor was calibrated against a dry bulb thermometer over three minute intervals on June 14 and June 25. This comparison produced inconsistent results, so the calibration was accomplished by comparing data recorded with the supply temperature sensor when both sensors were placed in a sealed jar for three days, This analysis showed that the outside air temperature sensor was reading 0.8 degrees lower than the supply air temperature sensor. Using the supply air sensor calibration, the calibration for this sensor can be described as follows:

$$T\_OUTcalibrated = 0.97(\ T\_SUPPraw) - 3.1 \quad [F]$$

$$T\_OUTcalibrated = 0.97(T\_OUTraw + 0.8) - 3.1 \quad [F]$$

$$or \quad T\_OUTcalibrated = 0.97(T\_OUTraw) - 3.9 \quad [F]$$

$$Standard\ Error = 0.857 \quad [F]$$

This calibration was applied to all data before August 10.

The temperature sensor used from August 11 to August 26 was the sensor used previously for mixed air. This sensor failed from August 20 to August 27, showing readings considerably different than local temperature readings, and these data were deleted. Calibration of this sensor (section 6.2.2) showed that actual temperature was 4.1 degrees lower than measured temperature, so this calibration was applied to data for this period.

The original relative humidity sensor was calibrated on June 14 and 25. Sensor readings over separate three minute periods were compared to reference relative humidity values obtained with a sling psychrometer. Results obtained with the sling psychrometer varied considerably during the test period. This, combined with the small range of relative humidity values represented in this test, resulted in an inconclusive calibration, and therefore it was recommended that raw data be used.

The humidity sensor used from August 11 to August 26 was the sensor used previously for mixed air. This sensor failed from 3:45 pm on August 20 to the end of August 26, when the new sensor was installed. Data for this period were deleted. The calibration for this sensor as shown above gave calibrated relative humidity by the equation below:

$$RH\_MIXcalibrated = 1.351(RH\_MIXraw) - 25.3$$

$$(R^2 = 1.0)$$

This calibration was applied to data for the period when the sensor had not failed.

The calibration for the relative humidity sensor used from August 27 to the end of monitoring resulted in the following equation:

$$RH\_OUTcalibrated = 1.406(RH\_OUTraw) - 29.7$$

6.4.3 Monitored Data vs. Weather Station Data

Because there are gaps in recorded outside temperature and relative humidity data, we obtained hourly dry bulb and wet bulb temperature conditions for Worcester MA from the National Climatic Data Center for the period of monitoring. Our goal was to compare monitored data to weather station data to fill in blank areas. As outside temperature is used as a controlled variable, a factor that affects the air system as well as the refrigeration system, but is unchanged by installation of the heat pipe, it is important that the data be as complete and accurate as possible. Figure 20 shows the results of the comparison of weather station outside temperature data vs. monitored outside temperature data for June through September. The diagonal lines on the graph are lines of unity, marking points where the measured temperatures are equal.

The plots for July, August and September fall relatively close to the line, within a margin of error of a few degrees. This may be due to sensor margin of error and geographical distance between the weather station and the supermarket. The data for June are more scattered, yet this is mainly due to the period when the sensor was located inside the outside air damper and the supply blower was shut off, resulting in erroneous readings. A regression applied to all data after the original outside air sensor was moved outside the return air plenum shows that the standard error is 3.3 degrees F. When the equation of mixed air conditions as a combination of return air flow and outside air flow is run with design conditions (70°F, 40% return, 90°F, 30% outside), and then with a 3.3 degree error added to the outside temperature, the difference is 0.7% (0.5 to 0.7 degrees) in mixed air temperature. Therefore, since this error is within the sensor error given by the manufacturer, we concluded that weather station dry bulb temperature could be directly

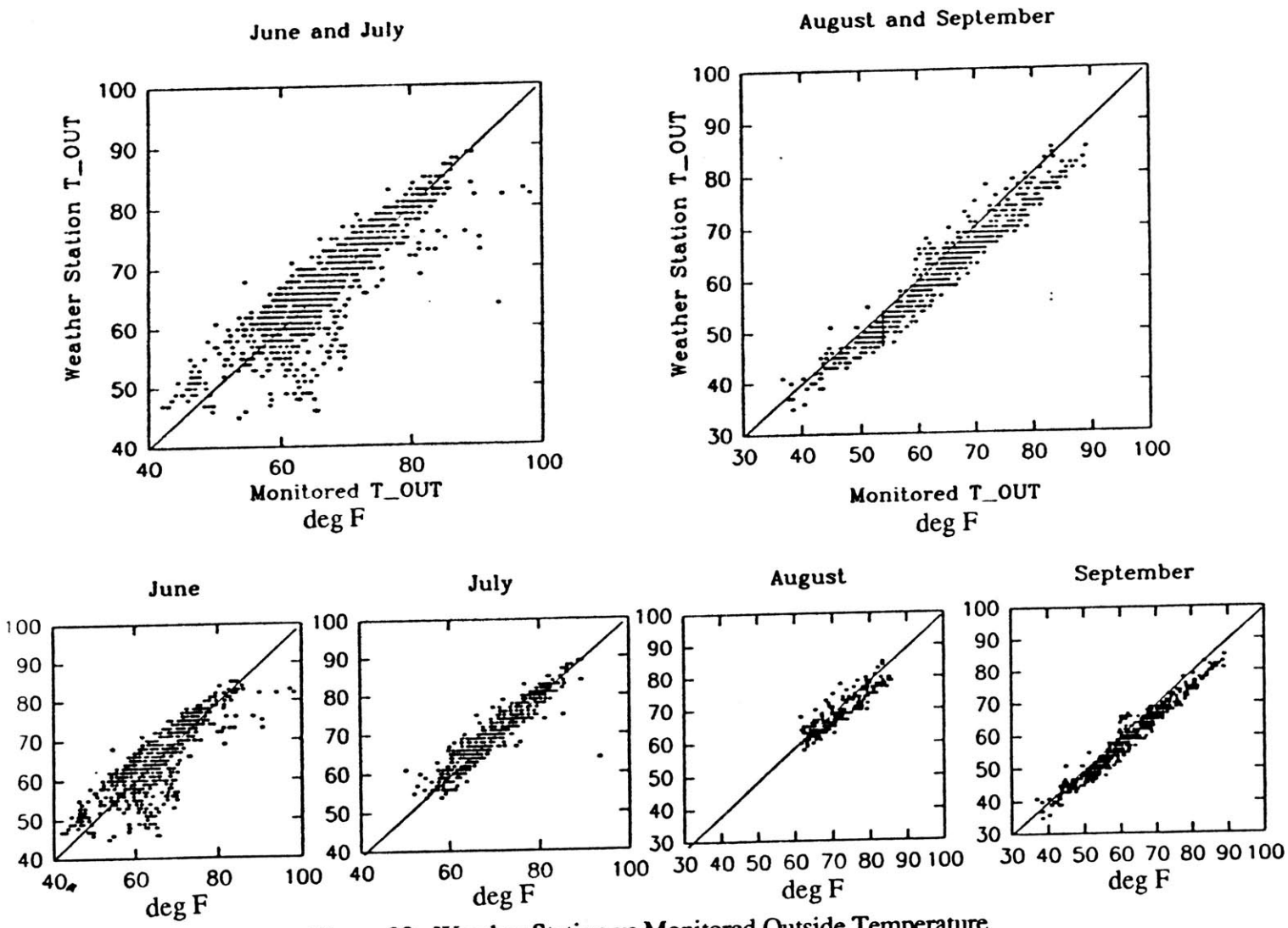

Figure 20. Weather Station vs Monitored Outside Temperature

inserted into missing data periods. (Note: since the weather station data are hourly, for gaps in which data were filled in, there are still missing data corresponding to the fifteen minute intervals between the hours.)

Weather station relative humidity was derived from dry bulb temperature and wet bulb temperature using psychrometric equations given in the ASHRAE Handbook. Partial water vapor saturation pressure for the dry bulb temperature and wet bulb temperature was calculated using the equation described in section 2.3. Specific humidities for dry bulb and wet bulb temperatures at saturation were calculated by the following equations:

$$W_S = 0.62198(p_{WS} / p\text{-}p_{WS})$$

Ws = specific humidity at saturation for dry bulb

p = atmospheric pressure (psi)

p_{WS} = partial water vapor saturation pressure for dry bulb

$$W^*_S = 0.62198\ (p^*_{WS} / p\text{-}p^*_{WS})$$

W^*s = specific humidity at saturation for wet bulb

p = atmospheric pressure (psi)

p^*_{WS} = partial water vapor saturation pressure for wet bulb

Specific humidity for the given dry bulb and wet bulb temperature can be calculated as:

$$W = ((1093 - 0.556\ t^*)W^*_S - 0.240(t - t^*)) / (1093 + 0.444\ t - t^*)$$

t = dry bulb temperature

t^* = wet bulb temperature

Therefore, the degree of saturation is u = (W/Ws) and the relative humidity can be expressed as:

$$RH = u / (1 - (1 - u)(p_{WS} / p))$$

Figure 21 shows the relationship between monitored relative humidity and weather station relative humidity for the first sensor (used June 2 through August 27) and for the second sensor (used August 28 through the end of the monitoring period). It is evident from looking at the graphs that there is a much less definitive correlation between monitored and weather station relative humidity. A regression of this data, using only points where both temperature and relative humidity for monitored and weather station data are accounted for, shows that monitored relative humidity can be related to weather station relative humidity as follows:

<u>First Sensor</u>

$$RH\_OUT\ mon = 0.062 + 0.702(RH\_OUT\ ws)$$

$$(R^2 = 0.701)$$

$$Average\ Error = 0.078$$

<u>Second Sensor</u>

$$RH\_OUT\ mon = -0.122 + 1.191(RH\_OUT\ ws)$$

$$(R^2 = 0.781)$$

$$Average\ Error = 0.086$$

When this error is applied to the model with the temperature error, the result is a mixed air error of ±3.9% in specific humidity. This is a significant percentage, and this issue will be further addressed in the next chapter when modelled mixed air conditions are compared to monitored mixed air conditions.

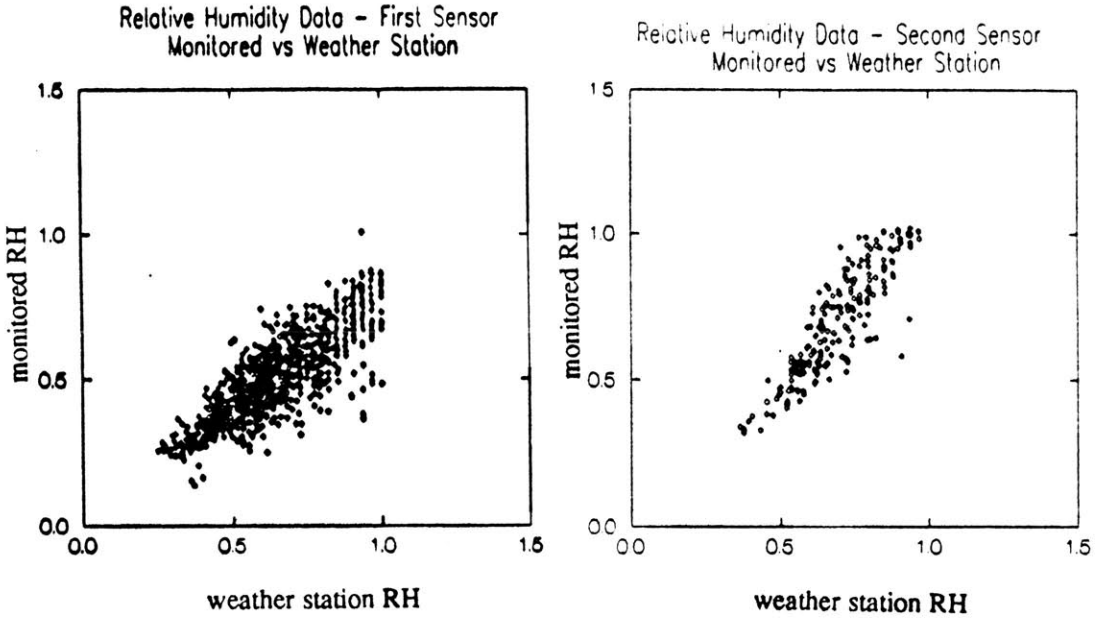

Figure 21. Monitored vs. Weather Station Outside Relative Humidity.

These equations were applied to weather station relative humidities to be filled in where monitored data was missing.

6.5 Pre- and Post- Cooling Coil Temperature

The original grid of sensors installed before and after each of the cooling coils (see Figure 15) remained until the end of monitoring, with the exception of TIN_L4, which was the thermocouple located before the lower cooling coil on the top right corner of the grid. This sensor was removed from this location on August 10 and installed outside as a backup to record outside temperature while there was trouble with the outside sensor. This sensor was re-installed at its original location on August 26 when new sensors were installed for outside air. All sensors were calibrated in an ice bath and a boiling distilled water bath on May 28 and August 2. On May 28, all thermocouples were calibrated in an ice bath for 20 minutes, and read between 1.4 and 2.7 degrees low. On August 2, the same test was performed, and the range of temperatures recorded was from 1 degree below to 1 degree above reference temperature. These results, added to the boiling water calibration, gave the equation :

$$Tcalibrated = -1.4 + 1.024(Traw)$$

which results in a variation of no more than 0.2 degrees for the 50 degree to 70 degree range. This error can be attributed to sensor error (±1 degree) so no additional changes were made to raw data.

6.6 Circuit 4 Temperatures and Pressures

As mentioned before, Circuit 4 is a refrigeration line serving open-tub frozen-food cases using compressors in rack A. The line comes off the liquid manifold from the condenser, runs through the evaporators in the low temperature display cases, and enters

the suction manifold feeding the rack A compressors (see Figure 16 for a schematic). Temperature and pressure sensors were installed after the liquid manifold before the expansion valve and after the evaporators before the suction manifold. For the first few weeks of the installation the temperature sensor located just after the liquid manifold was found to be fluctuating significantly with the variation in mass flow through the circuit. This was determined not to be a monitoring problem, but a result of fifteen minute average readings. The temperature recorded for the fifteen minute average was not the temperature of the refrigerant flowing through the circuit when the valve was open, but an average between this temperature and whatever temperature was recorded when the valve was off. As we were afraid that these fluctuations would be "double-counted" in the load equation when mass flow is multiplied by temperature, the temperature sensor was moved to the liquid manifold on June 28. In this case, the temperature measured is the actual temperature of the liquid refrigerant when the mass flow is greater than zero. The mass flow measuring device was installed before the expansion valve to assist in calculating display case load. The fluctuations in flow measurements are simply due to the fact that the number is a fifteen minute average, and that mass flow rates should be either maximum or zero at any given instant.

6.7 Compressor Rack Temperatures, Pressures, and Power Measurements

Temperature and pressure sensors were installed at the suction manifold and in the line leading from the compressors to the condenser for rack A. Power meters were installed at the rack A power line and at the condenser fan power line, and also at the rack B and rack C power line. The compressor rack power meters measure the combined power consumption of all of the compressors. Although individual compressors cycle on and off

at different times, the power consumption of the whole rack should give a good indication of the load on the system.

6.8 Summary

Although some of the problems encountered couldn't have been prevented at the time of monitoring (if the supply fan was on 24 hours as originally expected, there theoretically would have been no problems with the outside air sensor), some of them could have been prevented. Relative humidity sensors, important in a dehumidification analysis, should have required more care in calibration. All sensors should have been calibrated against a low and high reference humidity before and after installation. The return air, mixed air, and supply air temperature sensor locations should have been checked against cross-sectional temperature readings to determine the relationship with the single reading and what the average reading should have been.

A significant amount of data were deleted for all sensors. This was done by Aspen Systems, when it was felt that recorded numbers were unreasonable and therefore attributable to sensor error. With the exception of these gaps, the calibrated data should be sufficient to now create an airflow model and a refrigeration system model. Furthermore, data used from now on will be the calibrated monitored data, but will be referred to as 'monitored data'. Although it was determined that calibrated data is obviously in error in some cases (as when supply air specific humidity is higher than mixed air specific humidity), the models included in the next two chapters should provide further adjustments needed to obtain reasonable results.

Chapter 7 Air System Model

The original method of analysis was to simply compare monitored supply air humidity levels and mixed air humidity levels before and after installation. We expected supply air specific humidity to be always either the same or lower than mixed air specific humidity, and we expected the difference between the two to increase after the heat pipe was installed. We planned to predict supply air specific humidity as a function of mixed air humidity and cooling coil load with two different equations, one using pre-installation data and one using post-installation data. Then we would apply the two equations to the same data, and the difference between the results would determine how much more dehumidification was accomplished by the heat pipe. When we became aware that, due to sensor, calibration, and data collection errors, monitored data alone would not be sufficient, we decided to combine data with engineering calculations to predict mixed air, and then supply air conditions based on return and outside air temperatures and relative humidities. We expected that the equations predicting supply air specific humidity would be different with and without inclusion of the heat pipe. These two equations were then applied to the same return and outside air data for the post-installation period to determine the amount of extra dehumidification accomplished.

In this chapter, the first two sections relate to a spreadsheet model which was set up to predict mixed air and then supply air conditions based on monitored inputs, and engineering equations. The spreadsheet is set up so that the fifteen-minute data can simply be copied to the appropriate columns in files which can accommodate a week's worth of data. The calculated vs monitored graphs are derived from this spreadsheet. By relating calculated to monitored data, pre- and post-installation calculations can be applied to data

from the whole cooling season. The third section analyzes the temperature difference generated by the heat pipe, which, due to insufficient monitoring, is a rough estimate. The fourth section summarizes the chapter.

As a result of the modelled analysis, specific humidity differences due to the installation of the heat pipe are evident, but within statistical margin of error. This issue will be further discussed in the conclusion.

7.1 Mixed Air

As mentioned above, monitored mixed air and supply air data are insufficient because they show a higher supply air humidity than mixed air humidity. At this point it is not certain whether or not the mixed air readings are in error, the supply readings are in error, or both. It is definite if the return air and outside air sensors are accurate, that calculating mixed air as a mixture of two moist air streams will be accurate (ASHRAE 1993). If the calculated results follow the same trends as the monitored results with a constant difference, it can be concluded that the mixed air sensors account almost entirely for the error. If the difference between the two lines varies considerably, either of the three sensors could be in error. If only the mixed air sensor is in error, a regression should give an equation which can be applied to monitored mixed air specific humidity for all points.

7.1.1 Calculated vs Monitored

The mixed air specific humidity is a function of return air specific humidity, outside air specific humidity, and return and outside air volume flows. For the model the airflows used were the ones obtained from site measurements described in section 5.1.2. Supply airflow is 33,200 cfm, outside airflow is 5,050 cfm, and therefore return airflow is 28,150 cfm.

The pre-installation mixed air temperature and specific humidity were calculated using the first section of the spreadsheet for which input columns were return and outside air monitored temperatures and relative humidities. The method used is the same as the one described in chapter two. The calculated mixed air columns were compared to monitored mixed air temperature and mixed air specific humidity (calculated from mixed air temperature and relative humidity). Figures 22, 23, and 24 show graphs comparing calculated and monitored mixed air temperature and specific humidity for three pre-installation weeks, the first and second week in June and the fourth week in July. What these graphs show, especially for specific humidity, is that monitored points follow very closely the paths that are expected as a mixture of two moist air streams. Points where the difference between the lines varies include times of the day when the supply fan was off, which changed the airflow assumptions. Scatter plots comparing calculated and monitored mixed air temperature and specific humidity when the supply fan was on are shown in Figure 25. A simple linear regression gives the following equations:

$$C\_MIX\_W = -0.001 + 1.492(M\_MIX\_W)$$

$$(R^2 = 0.868)$$

$$C\_MIX\_T = -7.494 + 1.111(M\_MIX\_T)$$

$$(R^2 = 0.918)$$

C_MIX_W : calculated mixed air specific humidity

M_MIX_W : monitored mixed air specific humidity

C_MIX_T : calculated mixed air temperature

M_MIX_T : monitored mixed air temperature

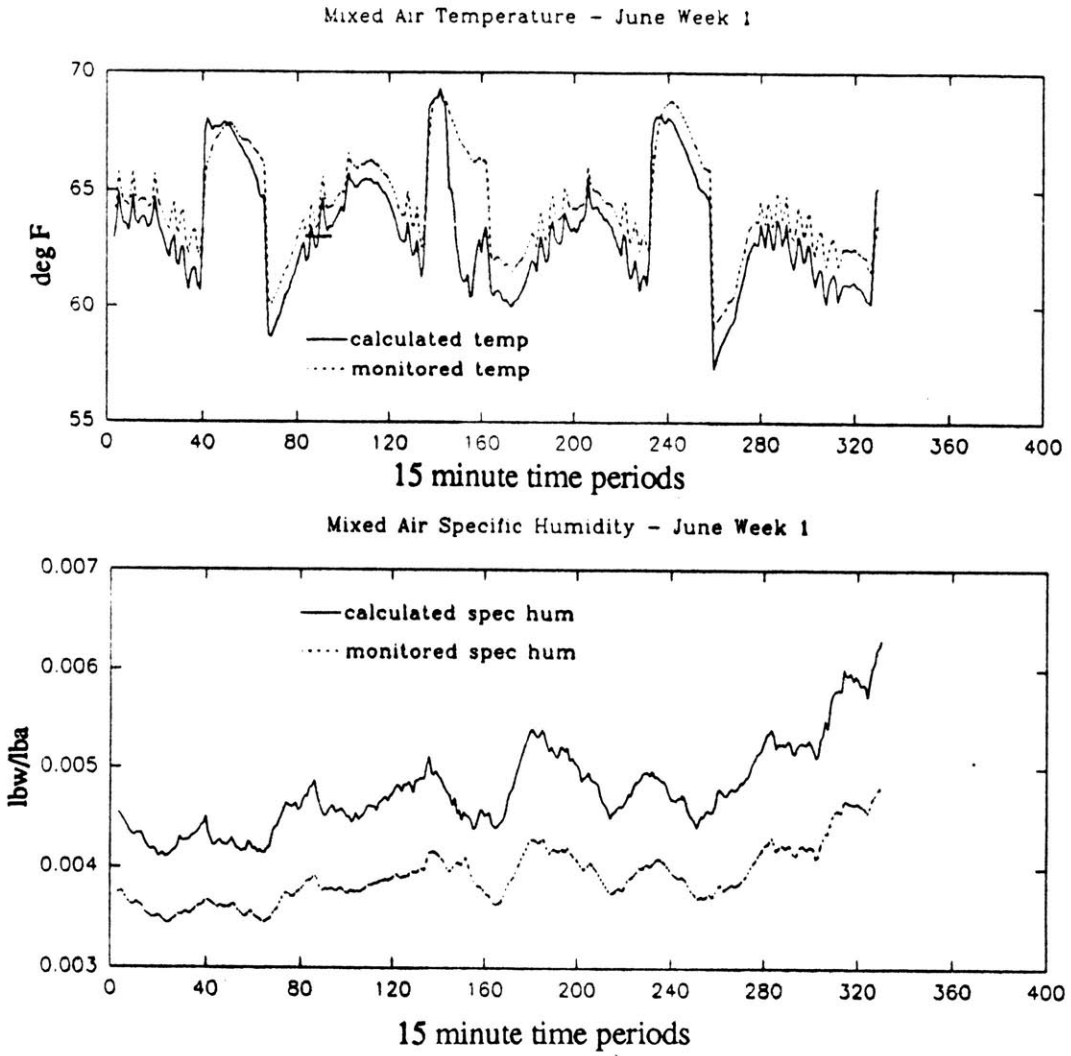

Figure 22. Calculated and Monitored Mixed Air Temperature and Specific Humidity June Week 1.

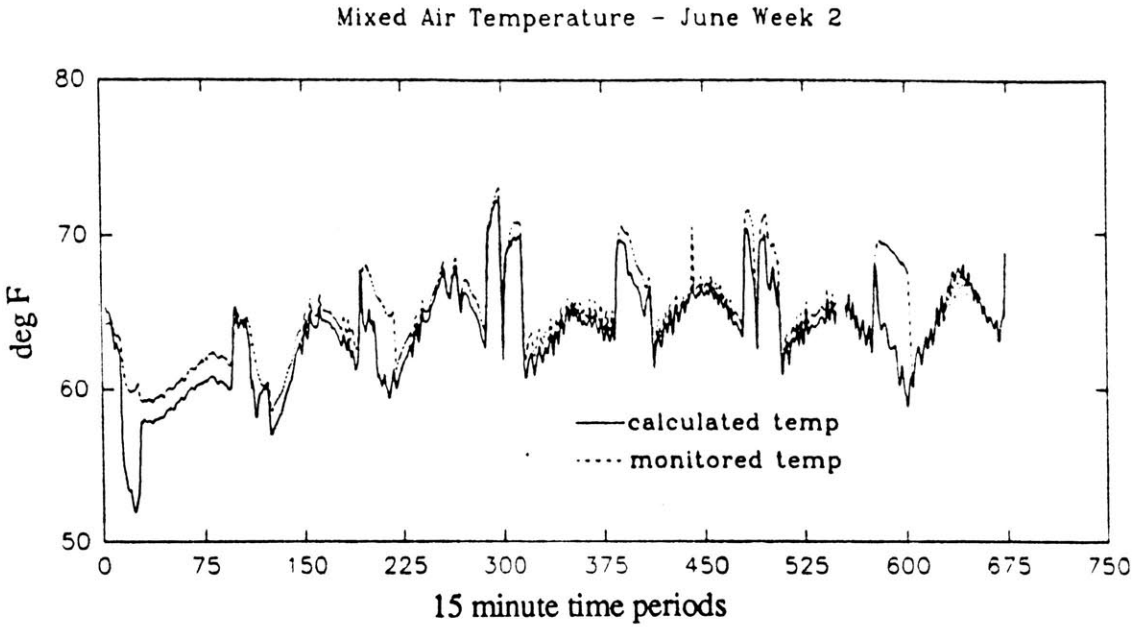

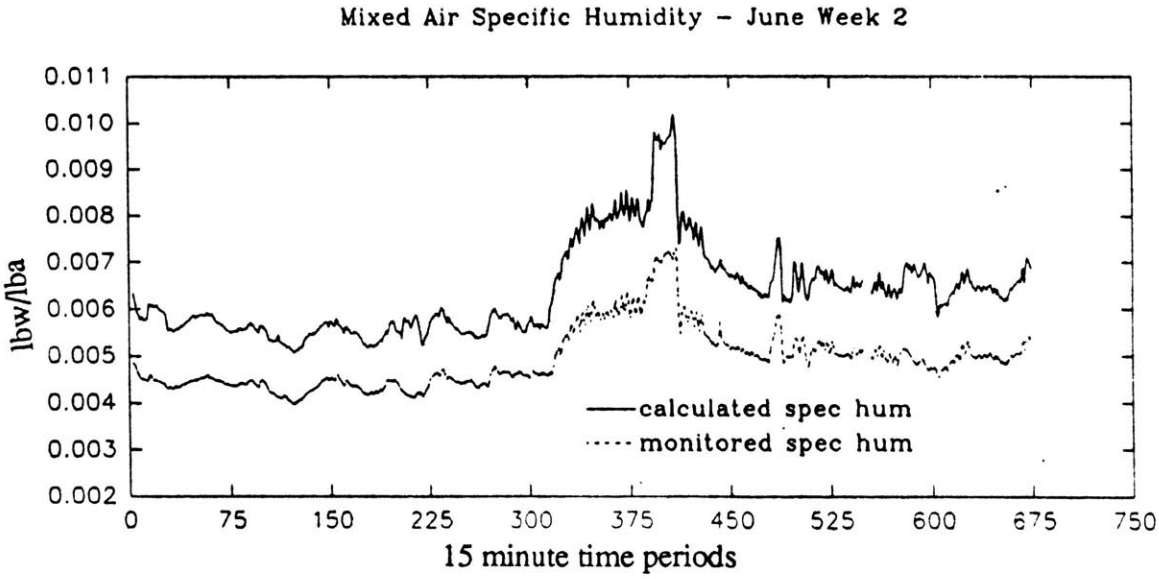

Figure 23. Calculated and Monitored Mixed Air Temperature and Specific Humidity June Week 2.

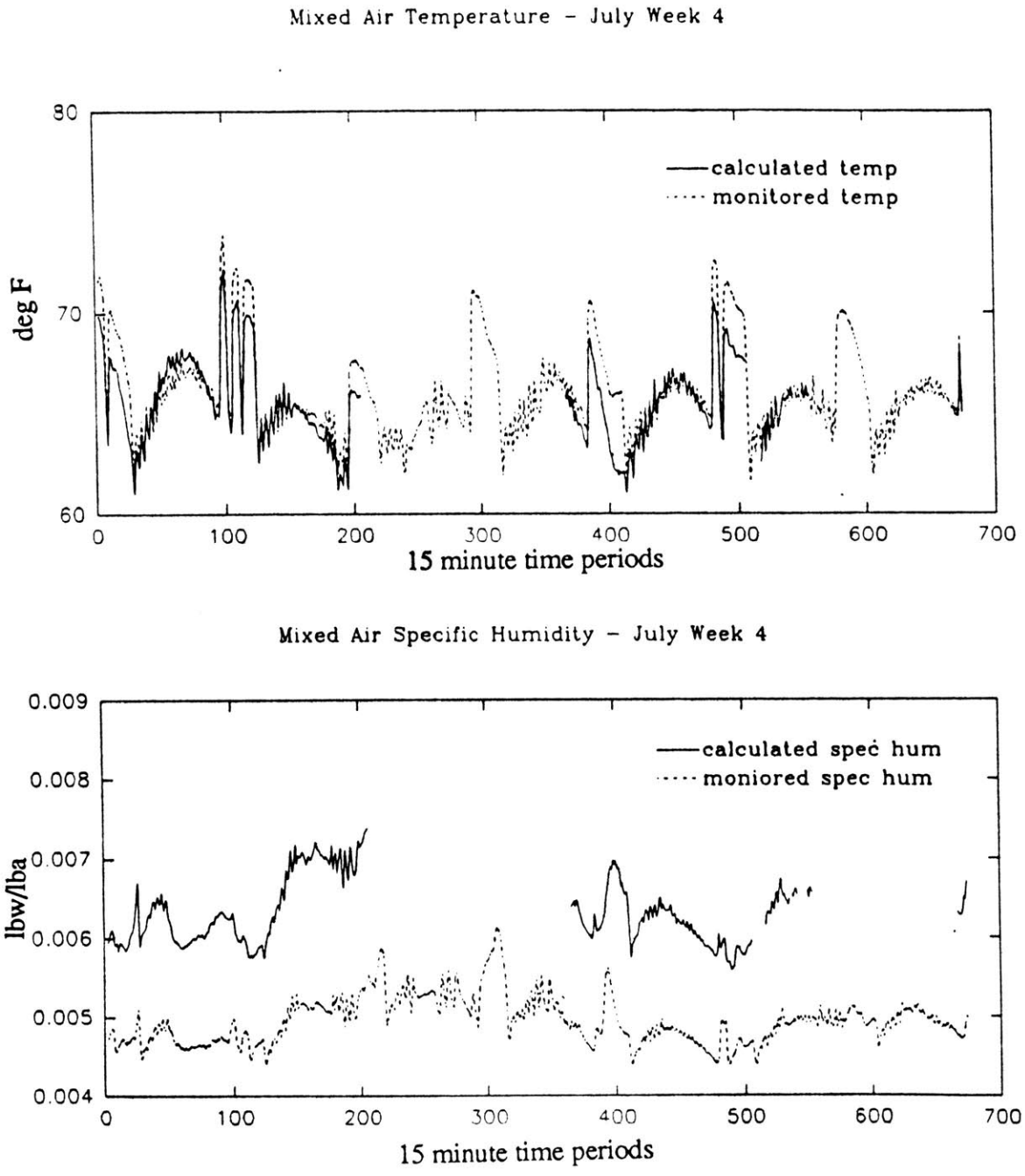

Figure 24. Calculated and Monitored Mixed Air Temperature and Specific Humidity July Week 4.

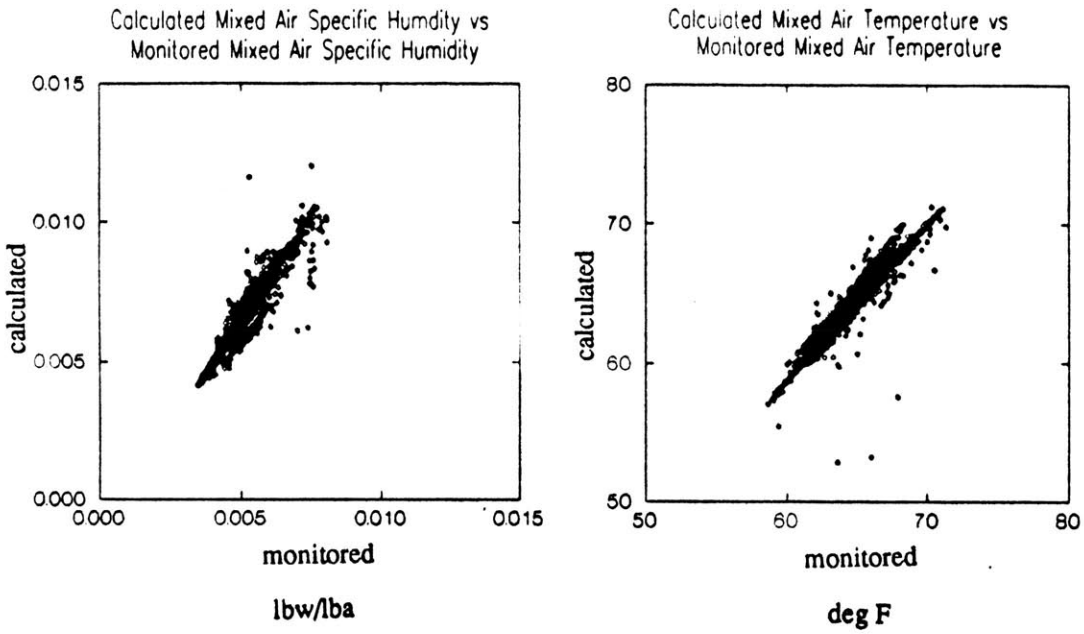

Figure 25. Calculated vs. Monitored Mixed Air Specific Humidity and Temperature.

The standard error for each of these equations is 0.0004 lbw/lba (5-10%) for specific humidity and 0.6 degrees for temperature. Since sensor error for each of these variables, as described in Appendix D, is 2.4% for specific humidity and 1 degree for monitored temperature, the calculated differences for specific humidity is larger than manufacturer's sensor error, and cannot be attributed to it. The calculated error for temperature is close to sensor error, and therefore the uncertainty of this equation can be calculated as the root mean square of the two uncertainties (see Appendix D), which is 0.8 degrees.

Figure 26 shows two graphs comparing monitored and calculated mixed air specific humidity with monitored supply air specific humidity for the pre-installation period. The top graph shows the two lines taken directly from monitored data. Although the lines in the two graphs seem to fall into similar trends, the supply air specific humidity is always higher than the mixed air specific humidity. This is impossible, since no moisture is introduced into the system between these two points, and at the worst case the two should be the same (no dehumidification). The lower graph shows the same comparison with the mixed air specific humidity adjusted based on the calculated conditions described above. Unfortunately, the supply air specific humidity is still higher than the mixed air specific humidity, which means that there must be an error in the supply air readings.

Figures 27 and 28 show graphs of two typical post-installation weeks. Although the graphs for the most part seem to follow similar trends, there is not the same obvious linear correlation as there was in the pre-installation comparison. Since the mixed air conditions should not be affected by the presence of the heat pipe, there must have been a change in the parameters of the equation. The difference may be due to the fact that outside relative humidity sensors failed during this period and may not have yielded accurate results while they were functioning. This also may be due to a change in outside air intake due to shifting of the dampers. Several times during the installation period and

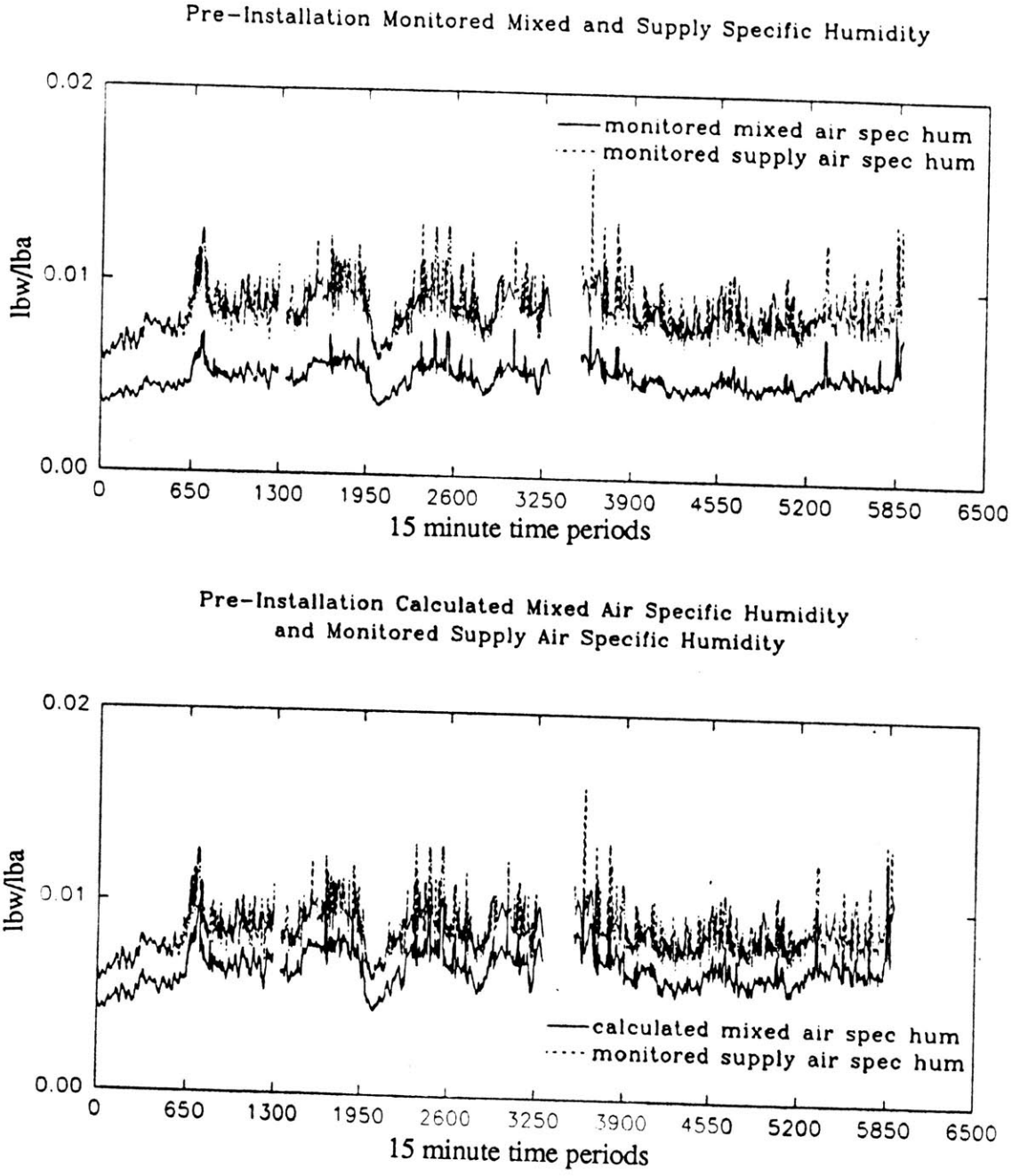

Figure 26. Pre-Installation Monitored and Calculated Mixed Air Specific Humidity vs. Monitored Supply Air Specific Humidity.

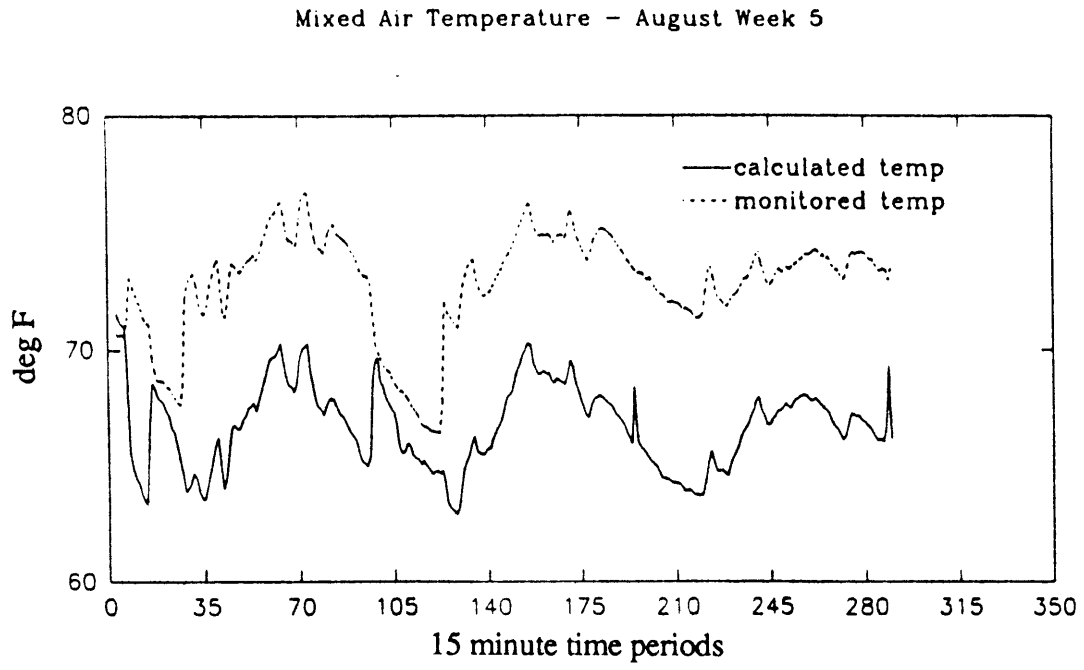

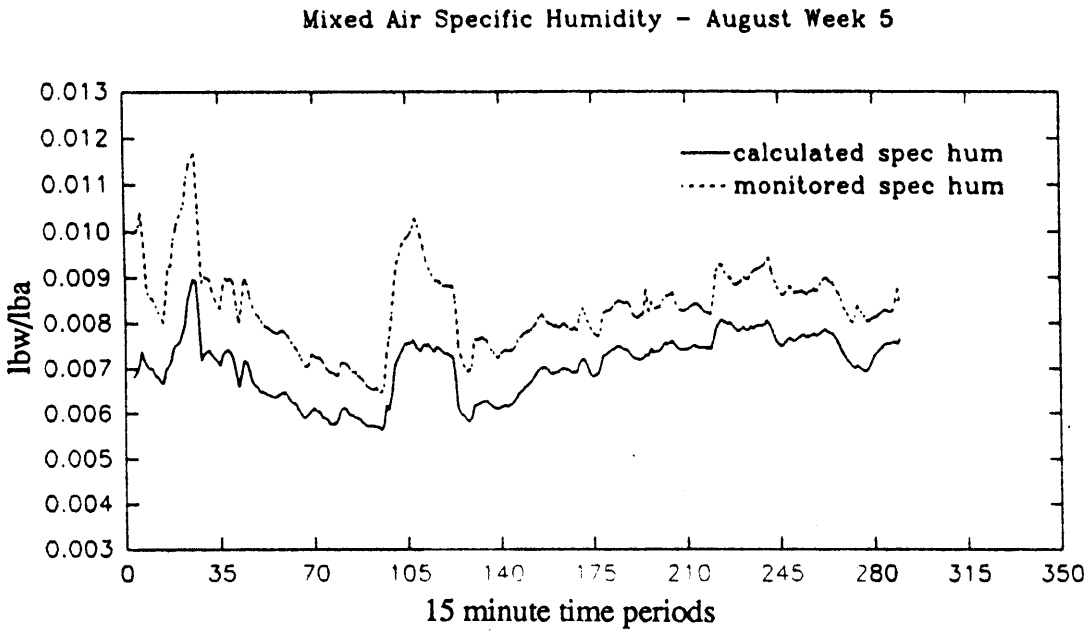

Figure 27. Calculated and Monitored Mixed Air Temperature and Specific Humidity August Week 5.

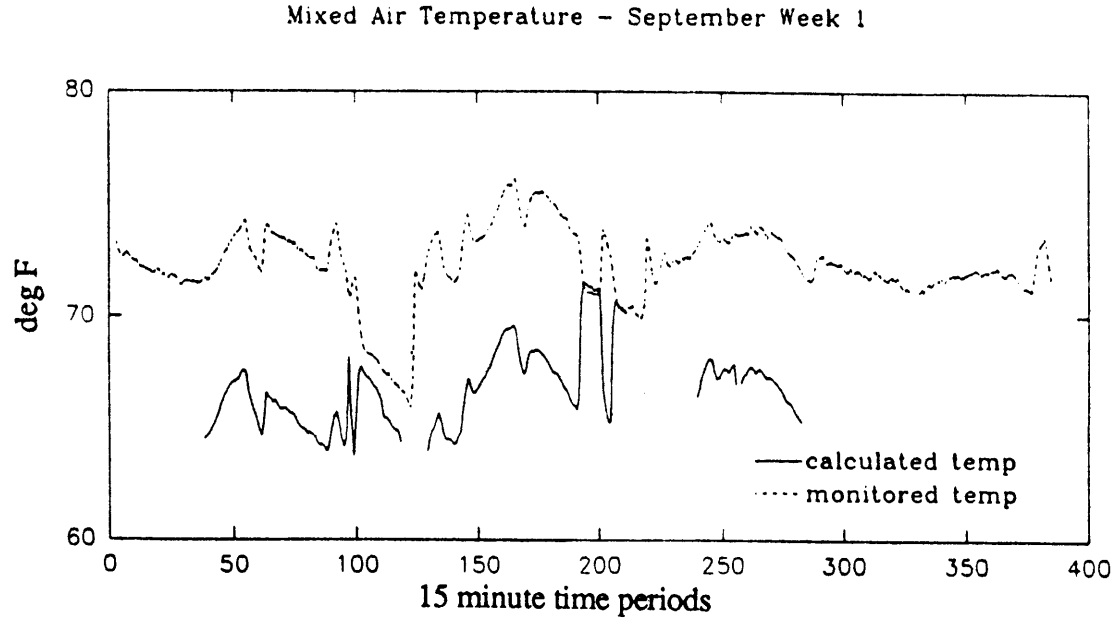

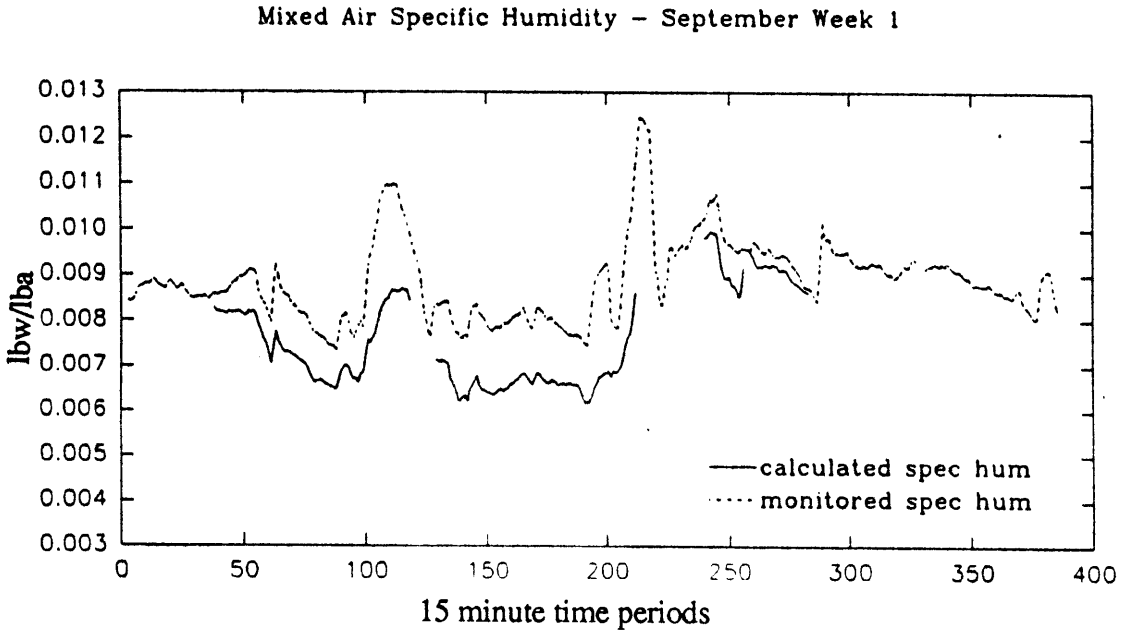

Figure 28. Calculated and Monitored Mixed Air Temperature and Specific Humidity September Week 1.

shortly after, the outside air dampers were opened and closed to measure intake over the range of positions (1,260 cfm at closed position, and 5,500 cfm at fully opened position).

7.1.2 Error Analysis

The errors in monitored specific humidity, as shown in Appendix D, are 2.5%. Therefore the maximum error in calculated vs monitored mixed air specific humidity difference, for which the regression error ranges from 5% to 10%, is 12.5 percent (±0.0005 for W=0.004). This is smaller than the difference between the monitored and calculated mixed air specific humidity time lines, which was an average of 27.5 percent (0.0014 lbw/lba), meaning that the difference cannot be attributed to statistical error.

The reasons for the errors could be either in the data collection or in the model assumptions. The calibrations are all two point calibrations, which eliminates uncertainty in that aspect, but relative humidity sensors were only calibrated once, and it is possible that the readings over the course of the monitoring drifted from the calibrated results. Where the trends in the two lines mimic each other exactly, the equations would not be the source of the error, and the difference would probably stem from sensor readings which were different than the calibration. Where the slopes in the two graphs are different (as in the first few hours of August week 5 in Figure 27) the error is probably due to variations in the equations parameters, such as outside air inflow. Since the source of the error at this point is unknown, and the trends in the two lines do in fact mimic each other when the supply fan is on, the difference is probably due to the mixed air sensors. If this were to be true, a correction factor applied to monitored data would produce a line almost exactly along the calculated line. Since this correction factor is unknown, and the engineering equations are very reliable, we will accept the monitored return air and outside air temperatures and

relative humidities for the analysis, and the calculated mixed air temperature and specific humidity will be used for the rest of the spreadsheet model.

7.2 Supply Air

Since there is no way for air to escape or enter the airflow between the mixed air sensor and supply air sensor (the air conditioning unit is well sealed), the temperature and humidity difference can be easily computed using the known factors, cooling coil load and heat reclaim. Although all of the factors in the cooling section were monitored, temperature difference across the heat reclaim was not. For this analysis, the specific humidity of the supply air was more important than the temperature of the supply air, and humidity would not change across the heat reclaim. Therefore the specific humidity of the air after the cooling coil can be calculated and compared to the specific humidity derived from the supply air sensors. This process will give the same insight to the accuracy of the monitored data outside of statistical errors as was found in the mixed air analysis.

This section is divided into three parts. The first part describes the process accomplished by the spreadsheet for predicting supply air conditions. The second part summarizes the analysis which attempted to relate the monitored temperature difference across the cooling coils with compressor power. Based on the success of this analysis, for future studies at this site, compressor power, usually an accurate measurement, can be used to predict the temperature drop and subsequent cooling load (sensible if dew point is not reached, sensible and latent if dew point is reached) across the cooling coils. The third part completes the analysis by comparing pre-installation and post-installation conditions.

7.2.1 Calculated vs Monitored

The supply air specific humidity should be a function of mixed air specific humidity and cooling coil load. Heat reclaim and auxiliary reheat would affect supply air temperature, but not its specific humidity (since reheat is a sensible gain). It would be expected that the cooling coil would reduce the amount of moisture in the air by condensation proportional to its load, and that the cooling coil load would be proportional to the temperature drop across the coils. This would not be a consistent proportion, however, since the temperature difference is expected to be smaller for a given load when latent cooling is being performed. As is shown in the next section, the relationship does not vary much from linearity, meaning that a consistent amount of latent cooling was performed over the summer.

Since the supply air specific humidity derived from monitored data is higher than the calculated mixed air specific humidity, it is obviously in error. By calculating the specific humidity using the model and comparing the results with monitored data, it may be possible to determine the source of the error. The spreadsheet model was extended to calculate air conditions after the cooling coil based on the temperature difference measured across the coil for the pre-installation period. Since the thermodynamic energy flow equations are different for sensible and latent cooling, the calculations had to be accomplished in two parts. Also, since the airflow is divided into two halves, and condensation on the lower coil could happen while there was no cooling through the upper coil, the analysis was split into four parts: upper coil sensible cooling, upper coil latent cooling, lower coil sensible cooling, and lower coil latent cooling.

For the first step, the dew point temperature for the mixed air was calculated using the following equations (ASHRAE 1993):

$$T_d = 79.047 + 30.5790\alpha + 1.8893\alpha^2 \quad (7.1)$$

$$\alpha = ln(p_W) \quad (7.2)$$

$$p_W = (p*W) / (0.62198 + W) \quad (7.3)$$

W = specific humidity

p = atmospheric pressure [in. Hg]

p_W = water vapor partial pressure [in. Hg]

The dew point temperature is the temperature at which condensation starts (100% relative humidity) for a constant specific humidity. The statistical error, as calculated in Appendix D, is 1.37 degrees F.

For the second step, the post-coil temperatures were calculated for the upper coil and the lower coil using the monitored temperature difference and the calculated mixed air temperature. If the post coil temperature for either section was greater than the dew point temperature, there was no condensation and the specific humidity didn't change. If the post-coil temperature was lower than the dew point temperature, then there was some condensation and a drop in specific humidity, which was then calculated using the post-coil temperature and 100% relative humidity. Although the air at this point would not be at exactly 100% rh, the difference between the overall air flow and the air in contact with the coils (which is at 100% relative humidity) is only in temperature and the specific humidity is the same, Since resistances are the same for both coils, the airflow would split half through the upper coil and half through the lower coil, so therefore the post-coil specific humidity would be the average of the two calculated specific humidities. Due to the fact that the air is only being heated between this point and the supply fan, this specific humidity is the same as the supply air specific humidity.

Figure 29 and 30 show graphs of calculated vs monitored supply air specific humidity for July weeks three and four. As was expected, monitored humidity is higher than what the model predicts. As with the mixed air comparison, the graphs seem to follow similar trends except for periods at night when the blower is off. Figure 31 shows a scatter plot of calculated vs monitored specific humidity for pre-installation times when the blower is on (during the day and at night when cooling is needed). This graph also shows a strong linear correlation. A regression gives the following equation:

$$CALSUPW = 0.0004 + 0.6849(MONSUPW)$$

$$(R^2 = 0.929)$$

CALSUPW = calculated supply specific humidity

MONSUPW = monitored supply specific humidity

The standard error in this regression is 0.0002 (2-2.5%). Since the statistical error for specific humidity is 2.5 percent, errors in the regression can be attributed to the sensors as they are calibrated now.

7.2.2 Cooling Coil Load

As shown in Figure 32, the total power consumed by the two compressors has a linear relationship with the sum of the temperature drops across the upper and lower cooling coils. Summing the temperature drops is realistic because the lower compressor is constant (at maximum) whenever the upper compressor is on, and the upper compressor power is at zero whenever the lower compressor power is less than maximum. This is evident from examining compressor power and temperature differences for June 19 (Figure 33). What this relationship doesn't account for, though, is the fact that when latent cooling is being performed, the temperature difference across the cooling coil will be different than if only sensible cooling is being performed. When moisture is being

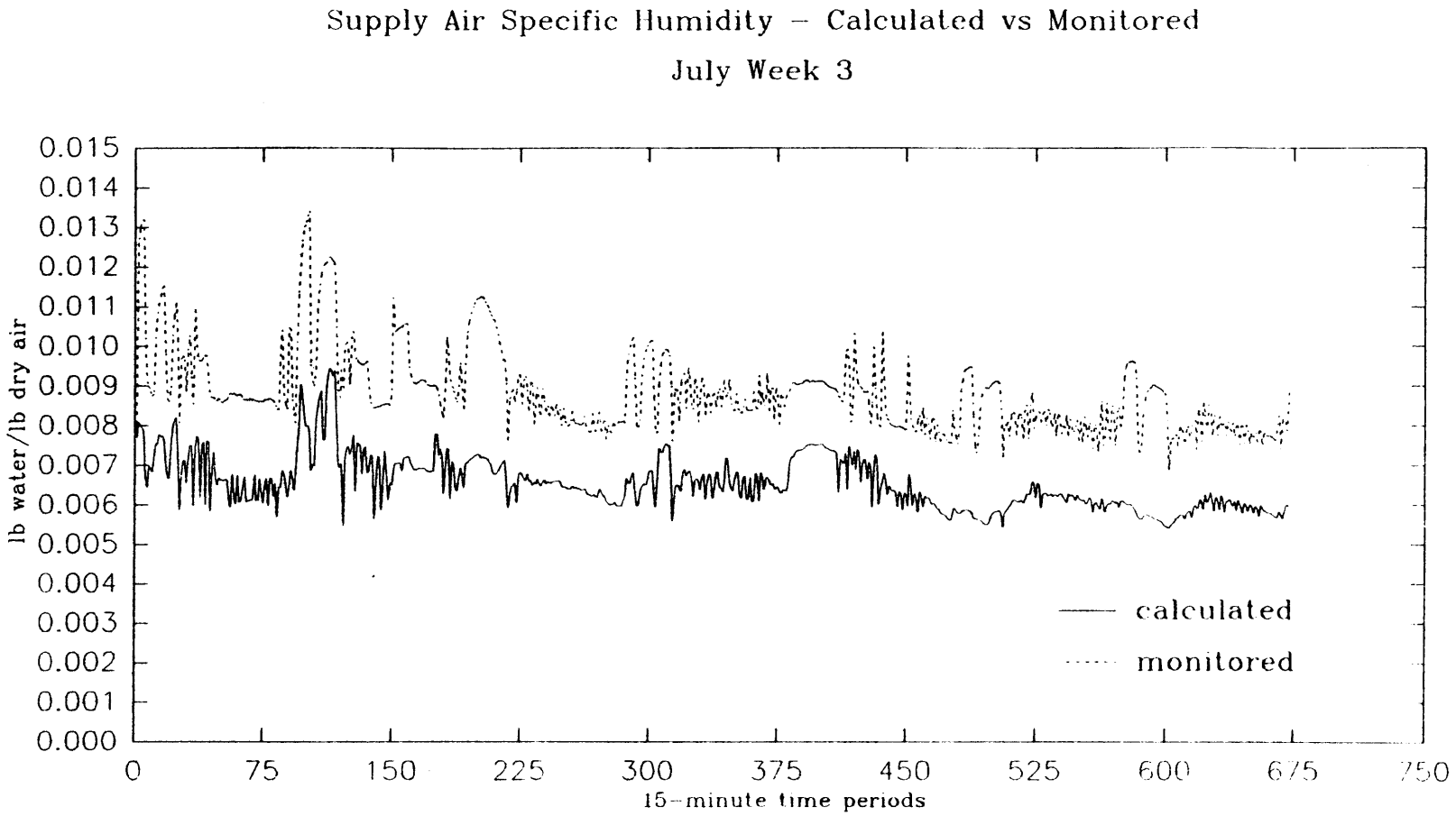

Figure 29. Calculated vs. Monitored Supply Air Specific Humidity for July Week 3.

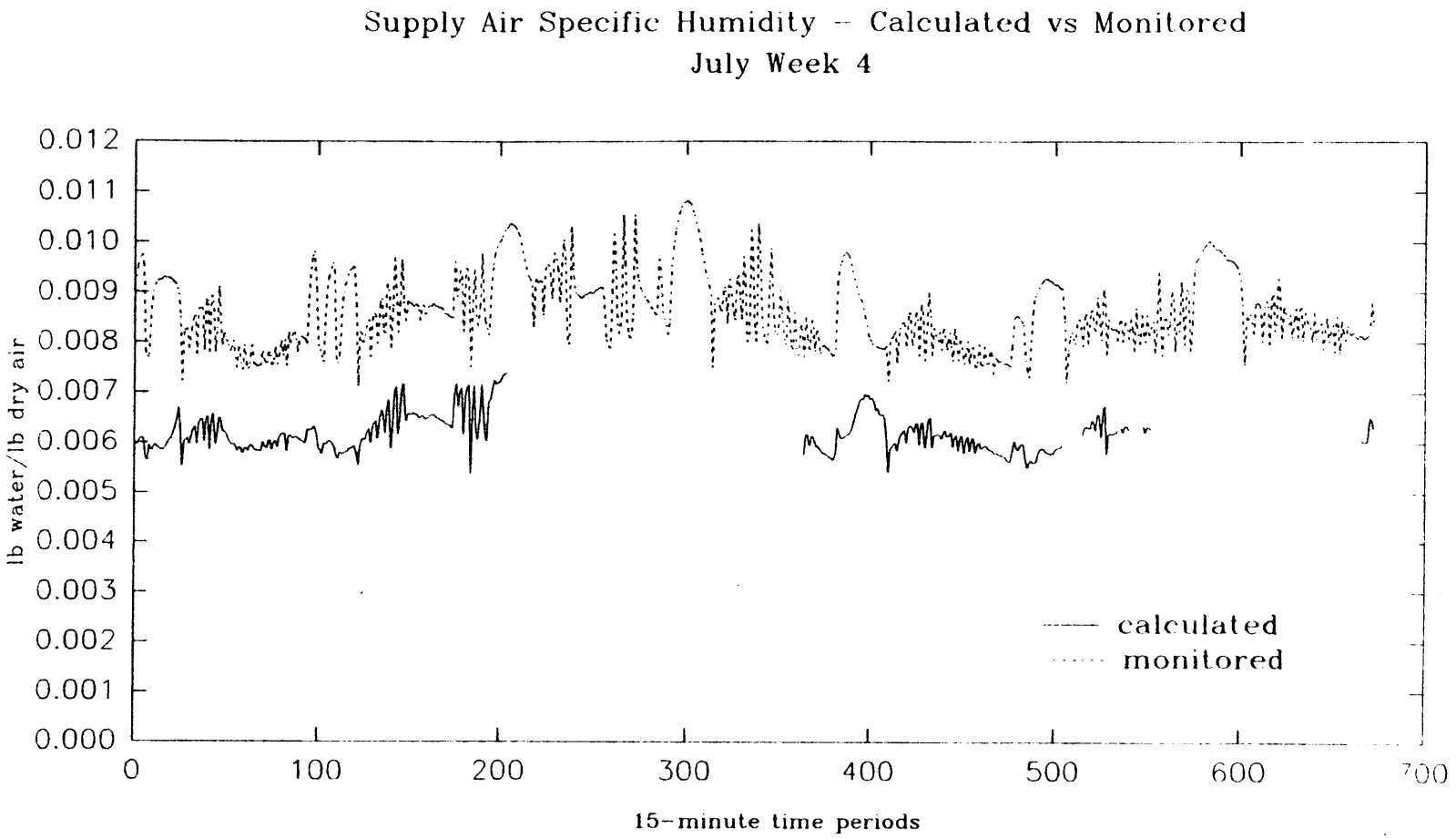

Figure 30. Calculated vs. Monitored Supply Air Specific Humidity for July Week 4.

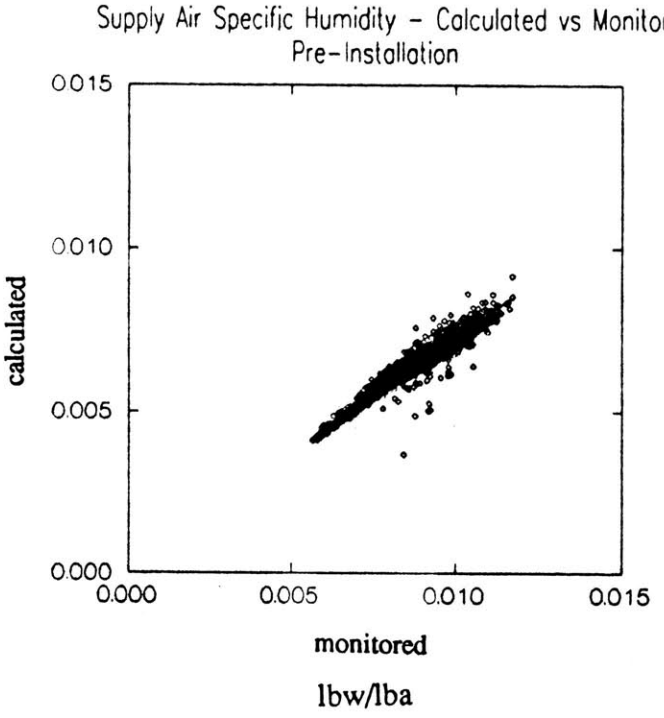

Figure 31. Pre-Installation Calculated vs. Monitored Supply Air Specific Humidity.

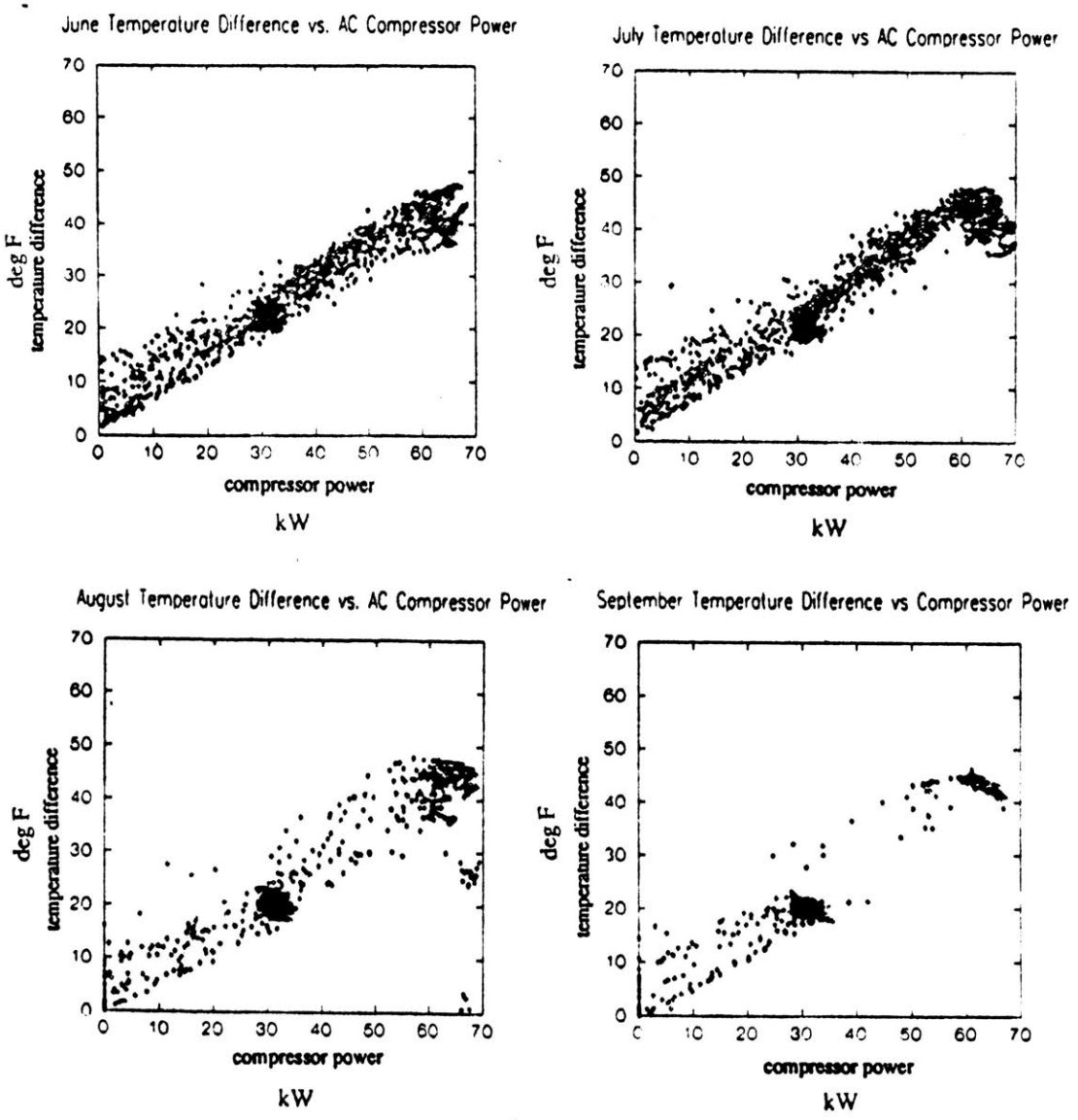

Figure 32. Cooling Coil Temperature Difference vs. AC Compressor Power.

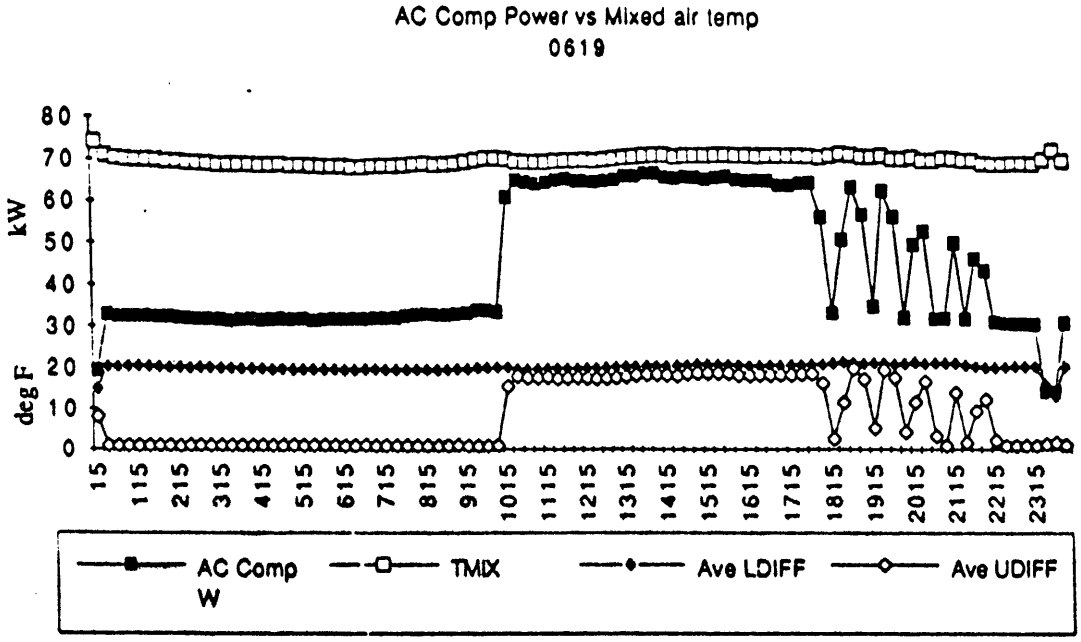

Figure 33. AC Compressor Power and Cooling Temperature Differences for June 19.

removed from the air, there will be a smaller temperature drop for a given load (as part of the load is being used to remove the moisture), than when no moisture is being removed. This accounts for some of the scatter in the graphs, which still is fairly well concentrated due to the fact that there was not much latent cooling over the summer (as will be shown later). A regression of data for before and after heat pipe installation, fixed at the origin, gives the following equations:

Pre Installation

$$June\ TDIFF = 0.695(CMP\_AC)$$

$$(R^2=0.984)$$

$$July\ TDIFF = 0.691(CMP\_AC)$$

$$(R^2=0.983)$$

Post Installation

$$August\ TDIFF = .662(CMP\_AC)$$

$$(R^2=0.977)$$

$$September\ TDIFF = .682(CMP\_AC)$$

$$(R^2=0.988)$$

CMP_AC = total compressor power

TDIFF=sum of temperature drops across lower and upper coils

After the heat pipe was installed, the average slope of the graphs decreases, due to the fact that the cooling coil is performing more latent cooling and less sensible cooling. Therefore, for a given compressor load there is a smaller temperature difference. This is most evident in the cluster of data points which occur when the lower coil compressor is on full power, around 30 kW. The cluster of points varies from 28 to 35 kW, due to the fact that the reading is a fifteen minute average and includes times when the first compressor is off for a small part of the time or the second compressor is on for a small part of the time.

Before the heat pipe installation, this range of points corresponds to a range of temperature differences between 19.5 degrees and 25 degrees. After the installation, the cluster ranges from 17 degrees to 22 degrees, since more of the cooling load is latent.

There are several occasions where there is a significant temperature drop when compressor power is zero. This situation occurs at night, when the fan blower is off. When the building does not need cooling and the compressors shut off, the pipes remain ool for a while and still generate a temperature drop. To calculate a more accurate analysis, these data were excluded from the regression.

7.2.3 Pre-Installation Mixed Air vs. Supply Air

Figure 34 shows the graph of modelled mixed air and supply air specific humidity as well as the graph of monitored mixed and supply air specific humidity for both the pre- and post- installation period. For the pre-installation section of the modelled graph, supply air is always equal to or slightly lower than the mixed air, which was expected. From this graph it can be determined that not much dehumidification was performed during the pre-installation period, as the lines do not vary by much. The average fifteen minute specific humidity difference over this period is 0.0003 ± 0.00014 lbw/lba (the only uncertainties in this specific analysis are in the engineering equations supplied by ASHRAE and in the temperature sensors, which is 2% or 0.00014 for W=0.007, as explained in section IV of Appendix D).

A regression analysis will allow us to predict supply air specific humidity for calculated mixed air conditions. Since the supply air specific humidity is actually a function of compressor load as well as mixed air specific humidity, it is necessary to include it. Since compressor power has been already determined to have a linear relationship with the temperature difference across the coil, it can be assumed that there is a

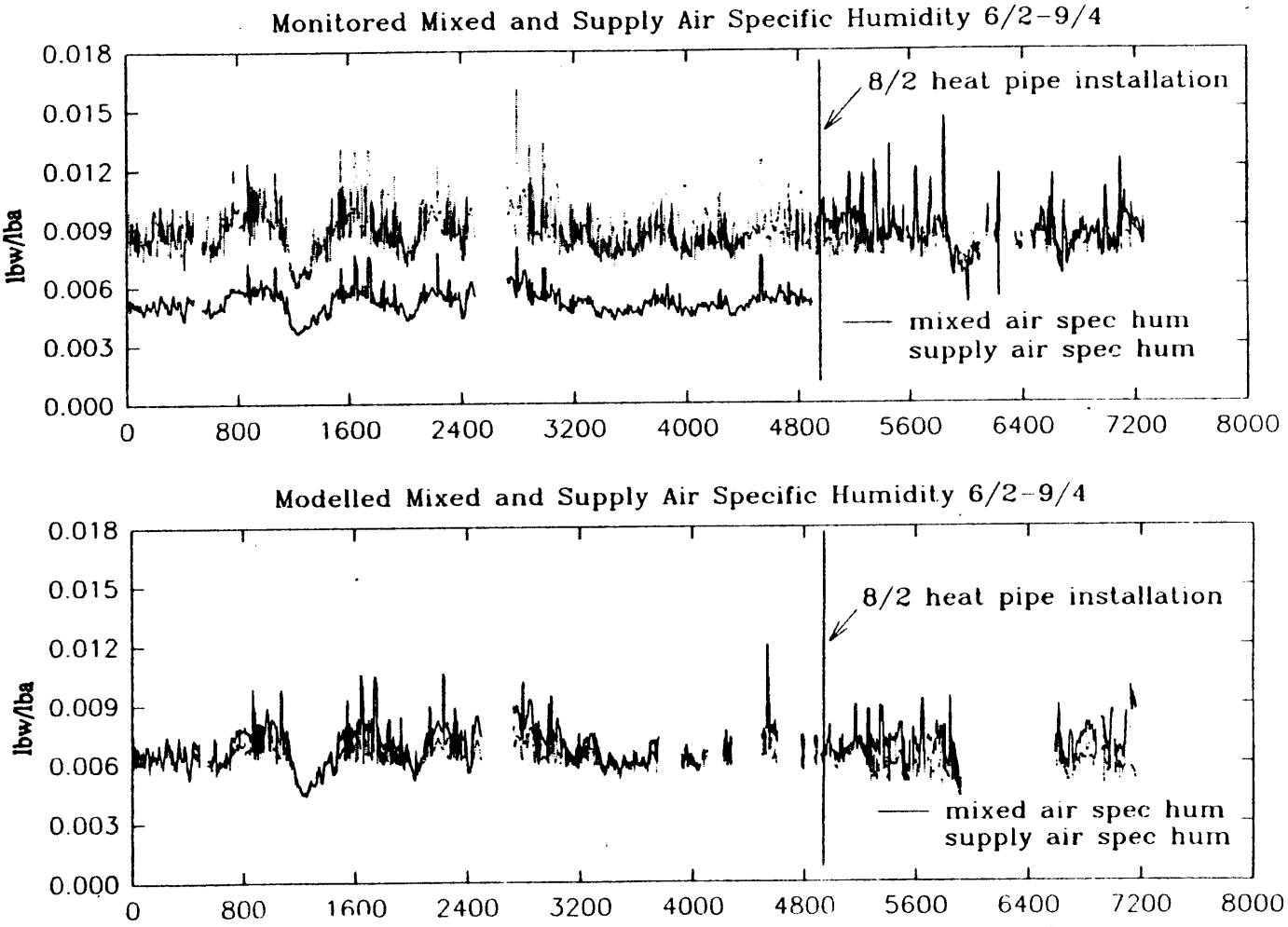

Figure 34. Monitored and Modelled Mixed and Supply Air Specific Humidities

relationship between compressor power and specific humidity difference (since specific humidity is a function of temperature). A regression gives the following equation of supply specific humidity as a function of mixed air specific humidity and compressor power:

Pre Installation

$$SUPP\ SPH = 0.001187 + 0.827(MIX\ SPH) - 0.000012(CMP\_AC)$$

$$(R^2=0.909)$$

$$Standard\ Error\ of\ Estimate = 0.000257$$

This error, which falls in the range of 2.3% to 3.7%, is generally larger than the statistical error (2.5%).

7.2.4 Post-Installation Mixed Air vs Supply Air

After installation of the heat pipe, as has been explained before, the difference between supply air specific humidity and mixed air specific humidity is expected to increase. The top graph in Figure 34 shows calibrated monitored mixed and supply specific humidities. Immediately after the installation, the mixed air humidity jumps considerably while the supply air humidity doesn't change much from the pre-installation levels. The sensor which recorded mixed air temperature and relative humidity was moved to record outside conditions and a new sensor was installed in the mixed air location. It is probably a calibration error or a recording error which accounts for the jump.

The bottom graph shows a time line of modelled mixed and supply air specific humidity levels before and after installation. To model post-installation conditions, temperature drops across the pre-cooling section of the heat pipe were included in the model. For this, the temperature of the air after the pre-cooling section of the heat pipe was calculated by subtracting the monitored temperature drop for the lower coil and upper coil

from the calculated mixed air temperature. A comparison of temperature differences against mixed air temperatures showed that this temperature was never below the dew point, meaning that only sensible cooling should be accounted for. Therefore, the specific humidity of the air system did not change across the pre-cooling section. The temperature drop across the cooling coils for the upper and lower section was then applied to this cooler temperature, which increased the probability that the post-cooling coil temperature was below the dew point. The specific humidity of this airflow was calculated in the same manner as in the pre-installation model, resulting in supply air specific humidity levels shown in the bottom graph in Figure 34. Figure 35 shows scatter plots of modelled supply and mixed air specific humidity before and after installation. Data points along the straight line (the line of unity) are times when there was no dehumidification and specific humidity levels didn't change. Although there is little correlation between calculated and monitored quantities below this line, it is evident that for a given mixed air specific humidity, calculated supply air specific humidities are lower in the post-installation graph.

A multivariate regression will be based on the energy balance before and after the cooling section given below:

$$W_{in}m(H + C_wT_{in}) + mC_aT_{in} = \alpha(CMPAC) + W_{out}m(H + C_wT_{out}) + mC_aT_{out}$$

W = specific humidity [lbw/lba]

m = mass flow of air [lba/hr]

H = heat of vaporization [Btu/lbw]

C_w=heat capacity of water [Btu/lbw ^oF]

C_a=heat capacity of air [Btu/lba ^oF]

α=coefficient relating compressor power (CMPAC) to energy removed [Btu/hr kW]

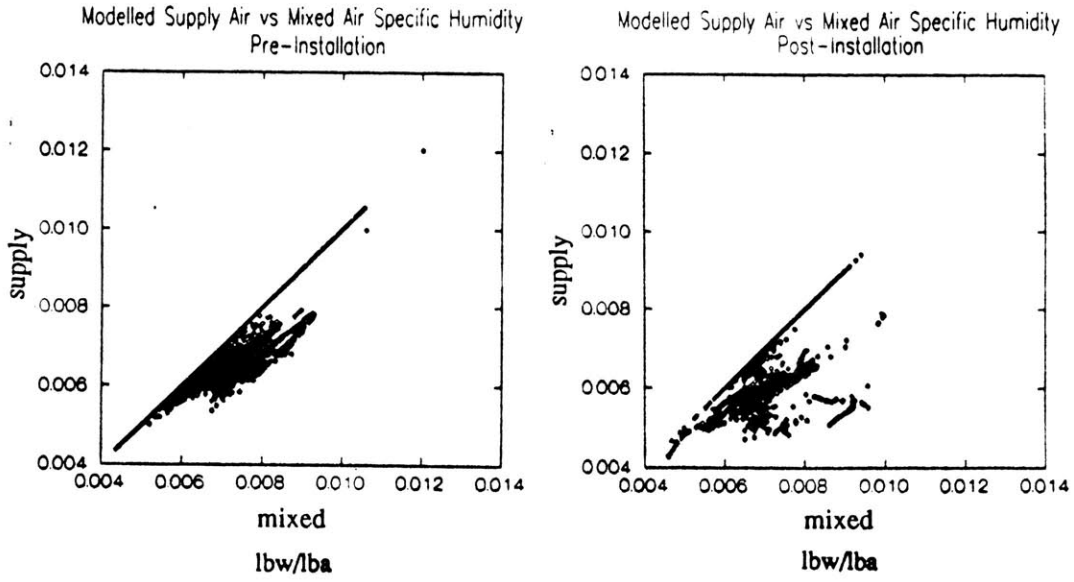

Figure 35. Modelled Supply Air vs. Mixed Air Specific Humidity.

The regression estimates calculated supply air specific humidity (W_{out}) as a function of calculated mixed air specific humidity (W_{in}), average temperature difference over all four heat pipe sections, and AC compressor power results in the following equation:

Post Installation

$$SUPP\ SPH = 0.002704 - 0.636(MIX\ SPH) - 0.000069(AVETDIFF) - 0.000022(CMP\_AC)$$

$$(R^2 = 0.758)$$

$$Standard\ Error\ of\ Estimate = 0.000450$$

The reason the average temperature difference across all heat pipe sections was used as well as the reason the error is so significant (nearly 7.5%), will be explained in the next section.

7.3 Heat Pipe Temperature Differences

Because the heat pipe is a completely passive system, and because it only provides sensible cooling and heating in this application, the temperature differences should be the same across both pre-cooling sections and reheat sections. Due to limitations in input channels in the datalogger, only one thermocouple was installed between each of the heat pipe sections and the cooling coil, hoping that it would give a good representation of the average temperature drop across each section. An analysis of the data, however, showed that temperature differences varied considerably not only from the pre-cooling section to the re-heat section, but also over the upper and lower coils.

Figure 36 includes a graph for each of the four sections of the heat pipe, showing the temperature differences across the coils as a function of time of day. For the pre-cooling sections a positive number represents cooling, and for the re-heat sections a positive number represents heating. During the day when the supply fan was supposed to be continuously on, the lower coil shows relatively consistent (although different) temperature changes while the upper coil shows a wide variation in temperature changes. For all of the sections, temperature changes are abnormal during night hours (12:00 am to 6:00 am), and fifteen minute time periods when the fan was on for part of the time (scattered data between the maximum and zero). The only explanation for the variation is that temperature changes are not independent of location, as was originally assumed. Heat pipes are designed for an average temperature exchange, which is integrated over the entire cross-section. Using the data from these four points only, it is unlikely that the true effect of the heat pipe can be accurately predicted. As this is an important factor in modelling the post-installation supply air specific humidity, there will probably be some inconsistencies in modelled output. Since the heat pipe sections are of identical design, the most accurate temperature representation we could arrive at is to apply the average fifteen minute temperature difference for all four sections to the model.

7.4 Summary

Although by observation and reasoning the assumption that the installation of the heat pipe must reduce supply air specific humidity levels has been proven, the physical differences from before to after are too small to be considered as evidence. The statistical sensor errors alone are larger than the predicted reductions, and regression errors compound on the problem. Figure 37 shows the time line of the difference between the pre-installation model and the post-installation model applied to post-installation data.

Although the difference is almost always positive, the combined standard error of estimate for these two calculations is 0.0007, and most of the calculated differences fall below this line. For this application, the air system model therefore is inconclusive.

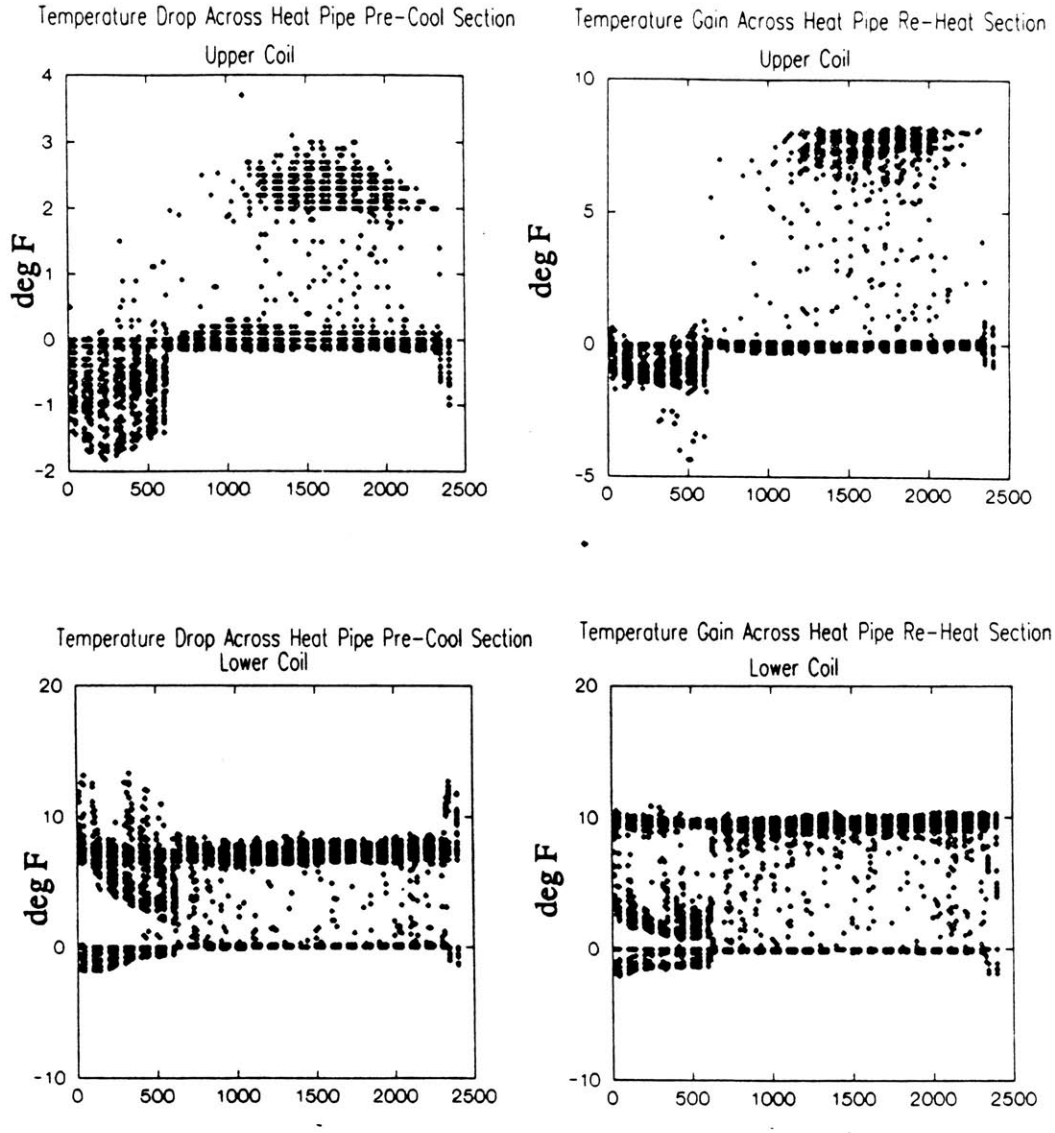

Figure 36. Temperature Differences Across Heat Pipe Sections vs. Time of Day.

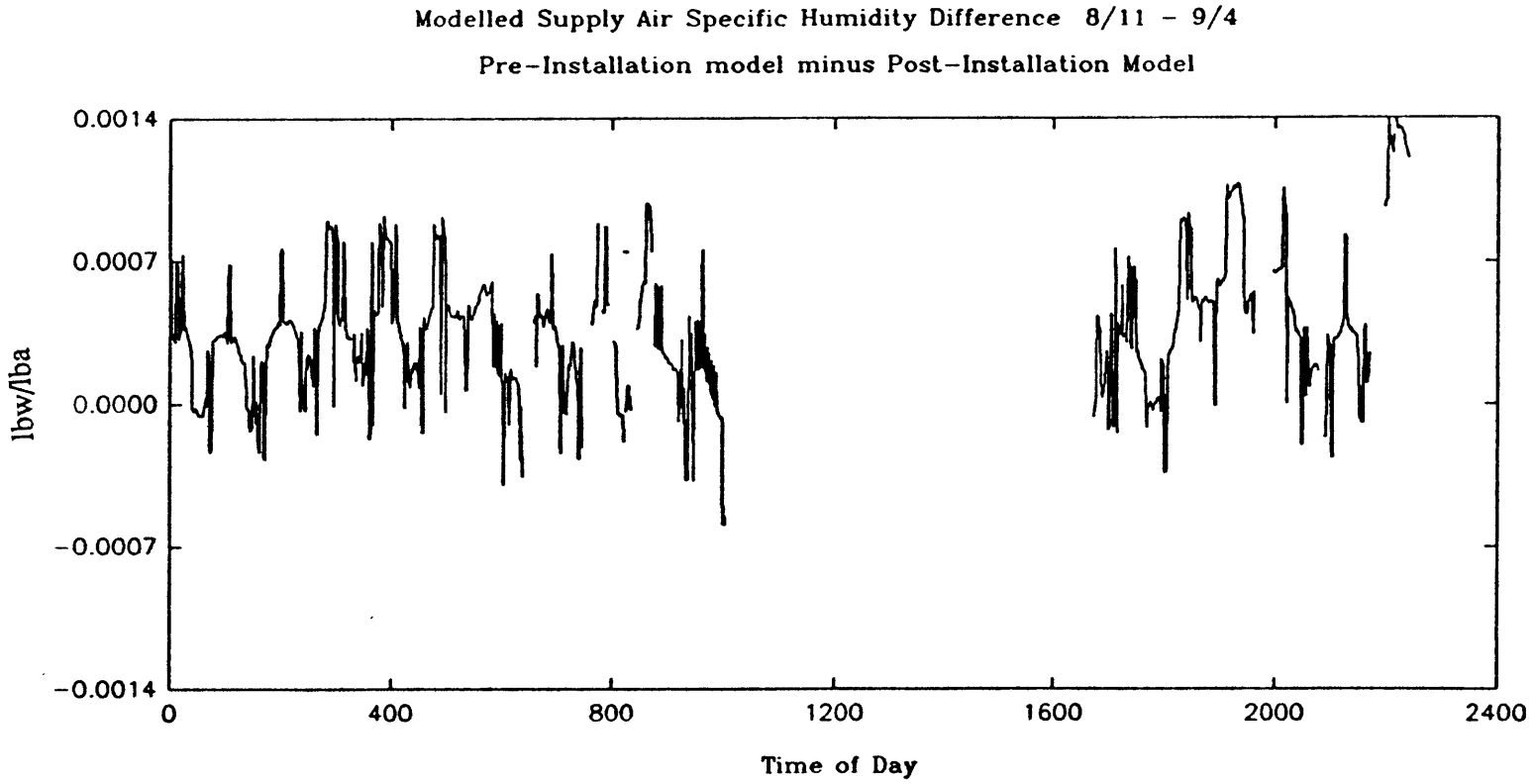

Figure 37. Supply Air Specific Humidity Difference Between Pre-Installation Model and Post-Installation Model.

Chapter 8 Refrigeration System Model

With the air flow model resolved, the next step is to model the refrigeration system and attempt to relate the two. Due to limitations of resources and cost-cutting, it was only feasible to monitor one rack of compressors and one circuit in that rack. Our decision of which rack to analyze was based on the circuit we chose to monitor. We chose circuit 4 on rack A, because it was serving a low temperature open coffin style case which required a significant amount of refrigeration. Also, the effects of dehumidification of inside air would be most evident in this type of case. which infiltrates a lot of inside air and quickly condenses ambient moisture on the low temperature coils. As was explained in section 1.2, frost buildup on the refrigeration coils decreases the efficiency for three reasons - one, the ice serves as an added insulation which decreases the heat transfer from air to coils, two, the ice buildup adds surface area to the coils, which adds resistance to the airflow through the coils, and three, the latent heat of phase change due to freezing condensate creates an unnecessary load on the system. ASHRAE equations provide helpful insight on the energy balances in a Carnot cycle, but not on variations in the cycle which may be due to varying ambient conditions.

It is expected that reducing the specific humidity of air in the display case will affect all three of these factors. When there is less moisture per pound of dry air, there is less condensation for a given dew point temperature, resulting in a slower rate of frost buildup. Therefore, the heat transfer rate doesn't decrease as much, the surface area doesn't expand as much, and the latent heat loss decreases because there is less water by mass to freeze.

This chapter addresses both the energy balances and the variations in the cycle. The first section models the display case load based on temperature and pressure measurements in circuit 4. The second section analyzes the pressure variances in the rack A evaporator and condenser sections, to show how this cycle varies from an ideal Carnot cycle (for which pressures are constant for these sections). The final section shows the results of numerous regression analyses attempting to link display case load and ambient conditions, and display case load and compressor power and a summary of step five. Chapter nine will address regression analyses linking compressor power to ambient conditions and the energy consumption analysis.

8.1 Display Case Load

Display case load for circuit 4 was calculated using the gain in refrigerant enthalpy across the evaporators and the measured mass flow. The pressure vs enthalpy path for the circuit corresponds to points 3, 4 and 1 on the diagram of the Carnot cycle shown in Figure 38. Point 3 on the figure corresponds to the location where the temperature and pressure sensors were located after the liquid manifold. The refrigerant then enters the expansion valve, where the pressure decreases at constant enthalpy to point 4. The refrigerant enters the display cases and evaporates along the path from point 4 to point 1, where it enters the suction manifold.

The flow of refrigerant in the circuit is controlled by a valve located at the opening from the liquid manifold. When the circuit is shut off, the suction end of the circuit continues to maintain a negative pressure, until all of the refrigerant has been drawn out of the line. When refrigeration is needed in the circuit again, the valve is opened and the negative pressure created by compressor suction draws refrigerant in from the liquid manifold.

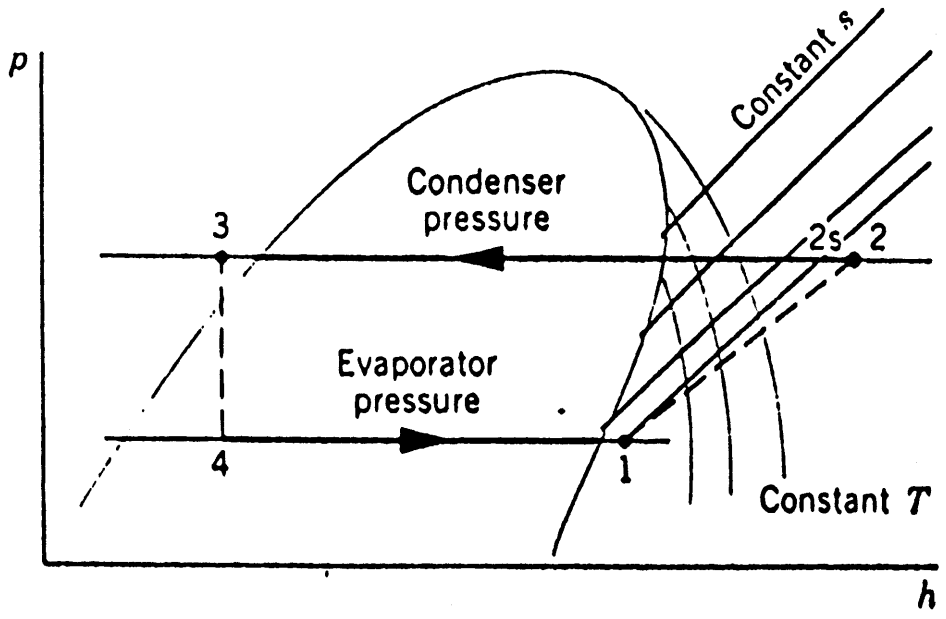

Figure 38. Carnot Cycle on Pressure vs. Enthalpy Diagram.

The enthalpy of the refrigerant at point 3 before the expansion valve is a function only of refrigerant temperature for a single state, condensed refrigerant. Properties of saturated R-502 can be found in Appendix A-1 for temperatures between 70 degrees and 125 degrees Fahrenheit. A regression of liquid saturation enthalpy as a function of temperature using values taken from this table gives the following equation:

$$Enthalpy = 10.98322 + 0.22852(T) + 0.00038(T^2) \text{ [Btu/lbm]} \quad (8.1)$$

$$(R^2 = 1.000)$$

Although the regression error is zero, the statistical error in this calculation based on sensor error is 0.2%, as shown in Appendix D. Since this enthalpy doesn't change after the expansion valve (point 4), it can be used in the calculation of display case load.

The enthalpy of the refrigerant at point 1 is a function of temperature and pressure. The enthalpy quantities for superheated R-502 can be found in Appendix A-2 for pressures between 10.34 psig and 20.26 psig. Figure 39 shows time lines of circuit 4 suction pressure from June 2 through September 18. What this figure shows is that for the majority of the time, the pressure varies between 10 psi and 15 psi. The enthalpy numbers from the tables show that enthalpy varies little over this range of pressures. If the average enthalpy over the range of pressures between 10.34 psi and 15.98 psi is used (see table 9) the margin of error will not be more than ±0.2%. Given this assumption, enthalpy can be approximated as a function of temperature only, as shown in Figure 40. The equation is given by:

$$Enthalpy = 78.668 + 0.158(T) \text{ [Btu/lbm]} \quad (8.2)$$

$$(R^2 = 0.999)$$

The statistical error for this equation is a function of raw temperature measurement and can be expressed as 0.16/T (or 16/T %).

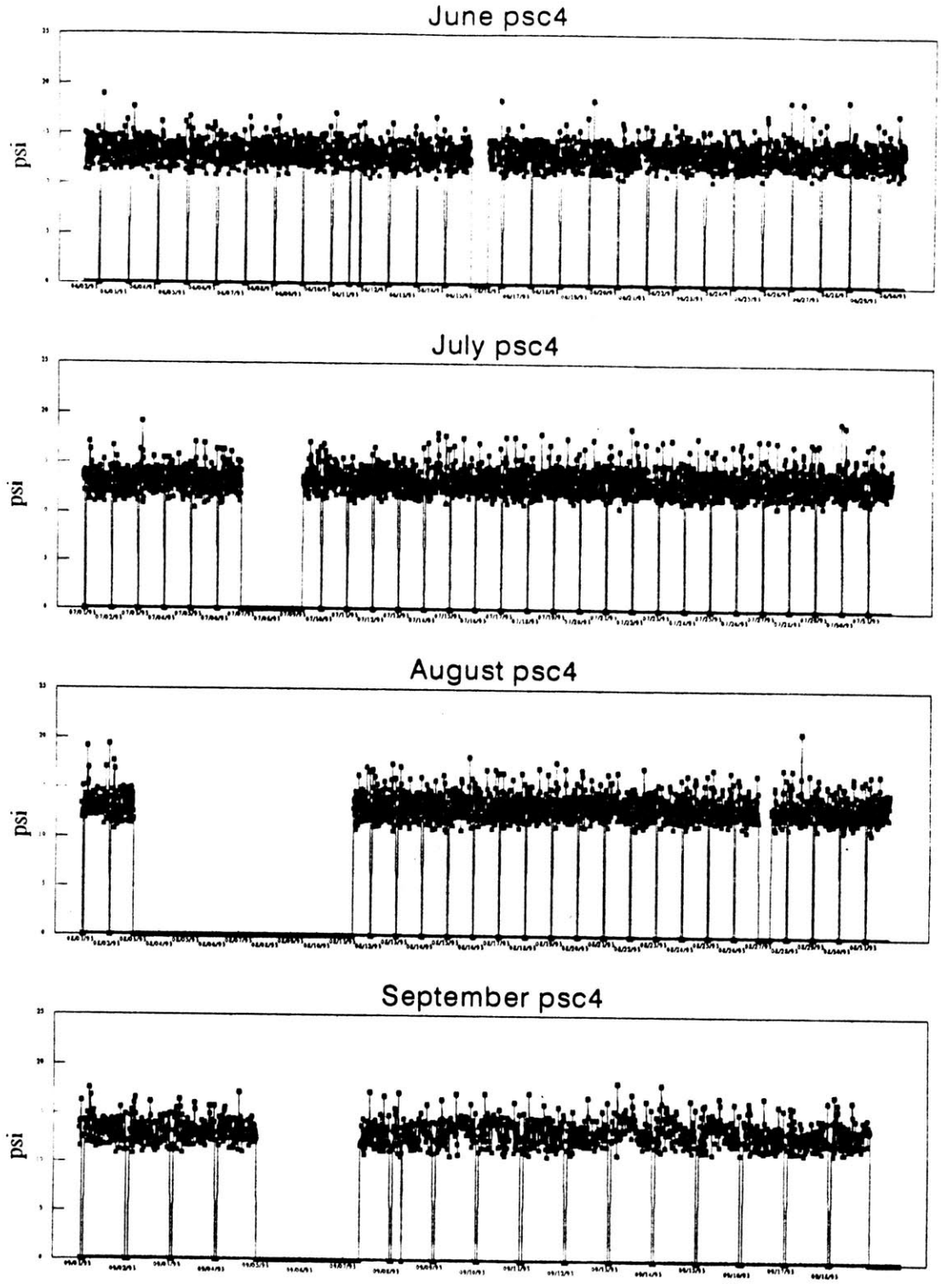

Figure 39. Circuit 4 Refrigerant Flow Suction Pressure.

	Pressure (psig)										Average
Temp.	10.34	10.92	11.52	12.12	12.74	13.36	14.00	14.65	15.31	15.98	13.09
0	78.824	78.793	78.762	78.73	78.698	78.664	78.631	78.596	78.561	78.525	78.68
10	80.385	80.356	80.327	80.297	80.266	80.235	80.203	80.17	80.137	80.103	80.25
20	81.959	81.932	81.904	81.876	81.847	81.817	81.787	81.756	81.725	81.693	81.83
30	83.547	83.521	83.495	83.468	83.441	83.413	83.384	83.355	83.325	82.295	83.32
40	85.149	85.124	85.099	85.074	85.048	85.021	84.994	84.967	84.938	84.91	85.03

Table 9. Enthalpy of R-502 over Circuit 4 Temperature and Pressure Ranges

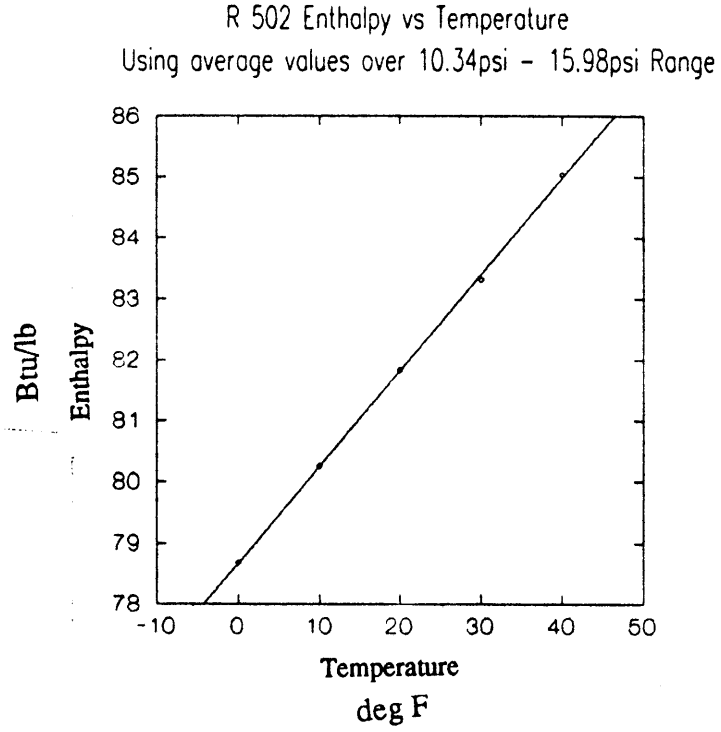

Figure 40. R-502 Enthalpy vs. Temperature for 10.34 psi - 15.98 psi.

Mass flow was monitored over 15 minute averages for the length of the monitoring period. The results of the monitoring show a wide range of values for 15 minute averages between zero and the maximum values. By combining the data into hourly averages the resolution is greatly improved, as can be seen in Figures 41 and 42.

Display case load was calculated by multiplying mass flow by enthalpy difference. The statistical error, as determined in Appendix D, is a function of suction line temperature and can be expressed as $0.4\% + (0.16/T_{suct})$. As was explained earlier, the dominating factor in changes in display case load outside of the defrost cycle is variations in case air humidity. The case air humidity is a function of inside air humidity, which is a function of supply air humidity and outside air humidity, as well as introduction of humidity (customer perspiration, respiration). It is not certain to what extent outside air humidity affects inside air (an entire report could be written on supermarket infiltration), but the difference between return air humidity and supply air humidity should give a good indication of the effect.

The difference between supply air and return air specific humidity should be based on many factors. Moisture is introduced into the circulating air by people breathing and perspiring, which is a function of store occupancy. The constant opening and closing of doors allows humid outside air in if the building is not properly pressurized. Moisture is condensed on refrigeration coils and then evaporated off during defrost cycles. Water from sinks and hoses may work its way into the air system. Despite these factors, a comparison of supply air and return air and display case load may give some indication of whether or not the differences are related to the rate of frost buildup, and subsequently display case load. The calculated load was compared to supply air specific humidity and return air specific humidity using scatter plots for the months of June through September. These graphs are shown in Figure 43 as a comparison of display case load for on-peak hours (between 8:00 am and 8:00 pm, when load should be affected the most) against

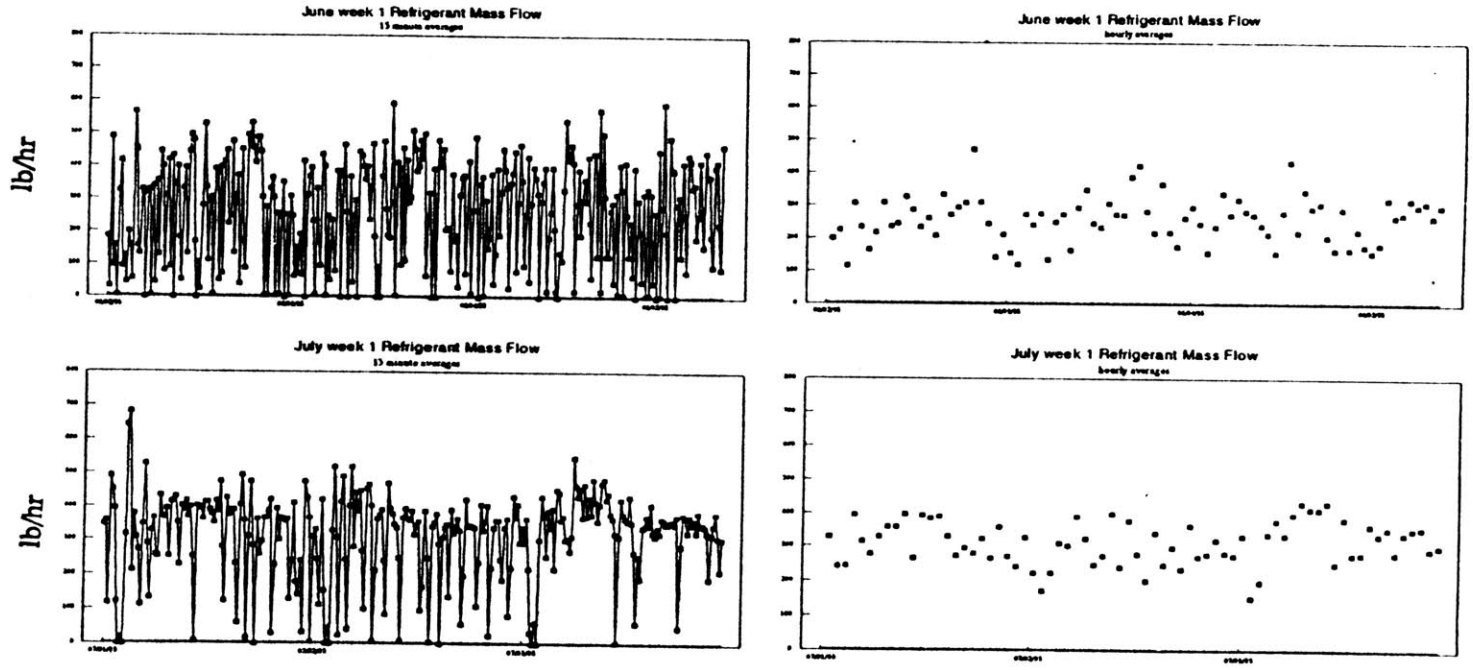

Figure 41. Circuit 4 Refrigerant Mass Flow - 15 Minute and Hourly Averages.

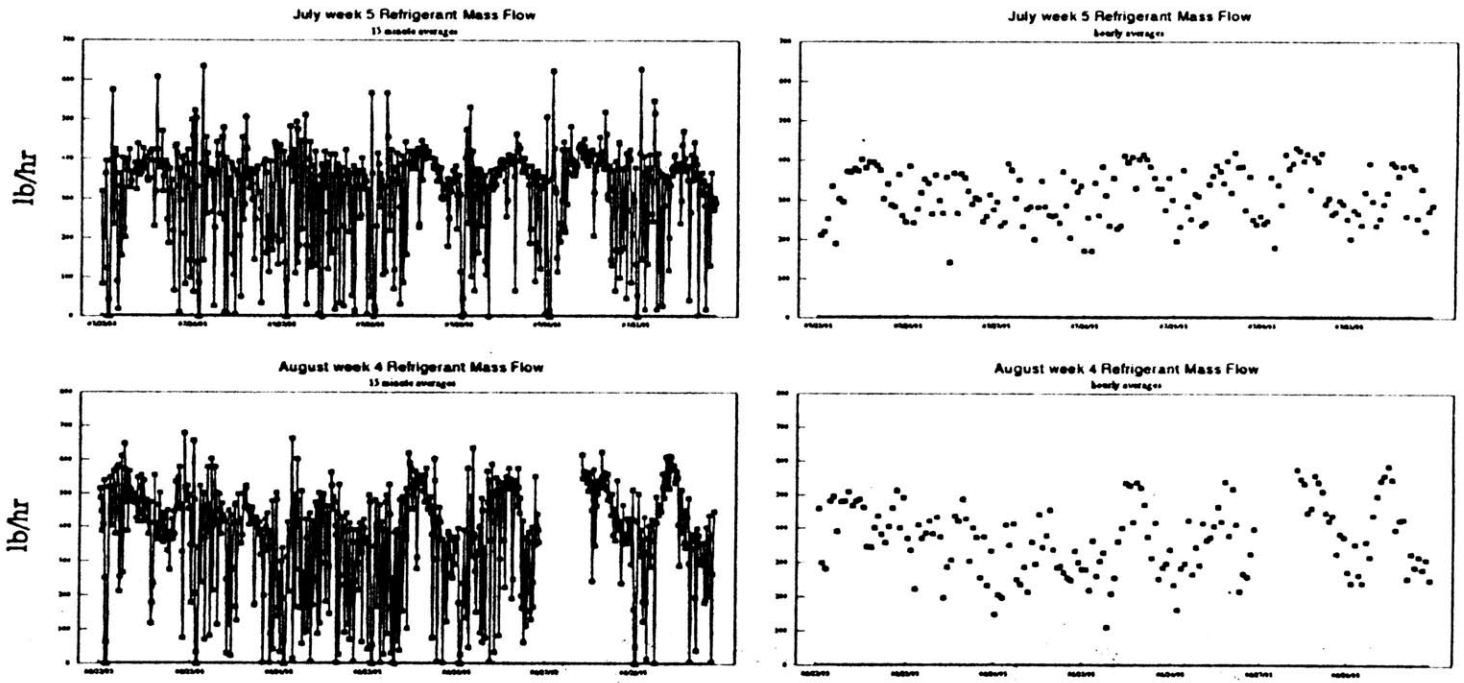

Figure 42. Circuit 4 Refrigerant Mass Flow - 15 Minute and Hourly Averages.

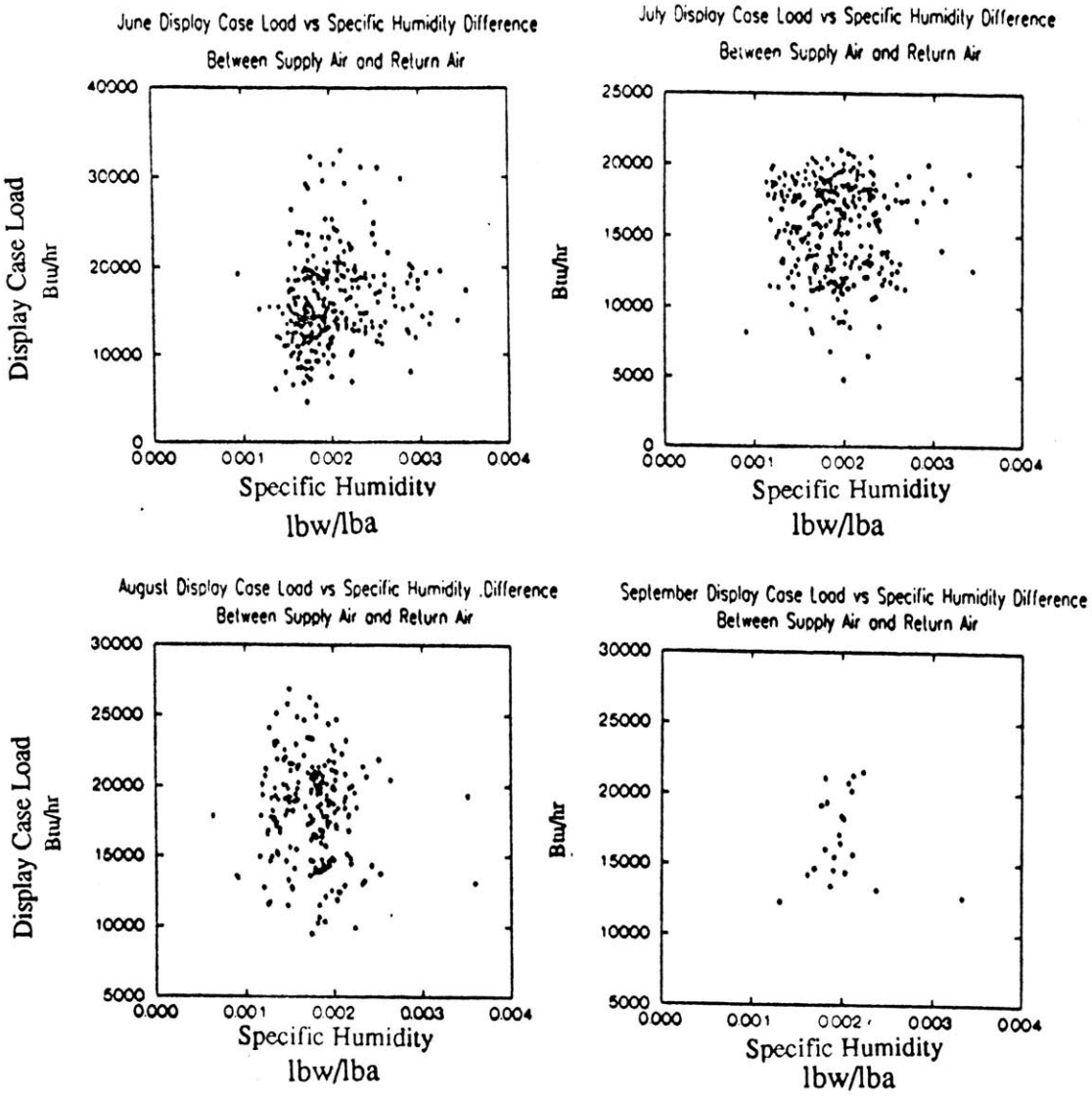

Figure 43. Display Case Load vs. Specific Humidity Difference Between Supply and Return Air.

specific humidity difference between supply air and return air. What these graphs show is that there seems to be very little correlation between display case load and humidity levels. What this means is either that changes in humidity are too subtle to affect this set of display cases, other factors affecting display case load (inventory, store occupancy, evaporator efficiency, defrost control) outweigh humidity differences, or monitoring errors of all the points involved cloud the actual relationship.

Theoretically there should be a noticeable relationship between display case load and ambient conditions. Further analysis shows that the daily range of circuit 4 liquid refrigerant temperatures (measured before the display cases) follows a similar pattern as the range of daily outside temperatures. The top left graph in Figure 44 shows the daily range of refrigerant temperatures and the top right graph shows outside temperatures. The bottom graphs show temperature time lines over the course of the day for every day in July. Both graphs follow a sinusoid curve, with the refrigerant graph lagging the outside air graph by about six hours. However, attempted regressions comparing liquid enthalpy (a function only of refrigerant temperature) to outside temperature and a sine curve of time (R^2=0.273) and outside temperature with a time shift of six hours (R^2=0.251) produced unfavorable results. The reasons for lack of correlation are the same as the ones explained above for the comparison with specific humidity.

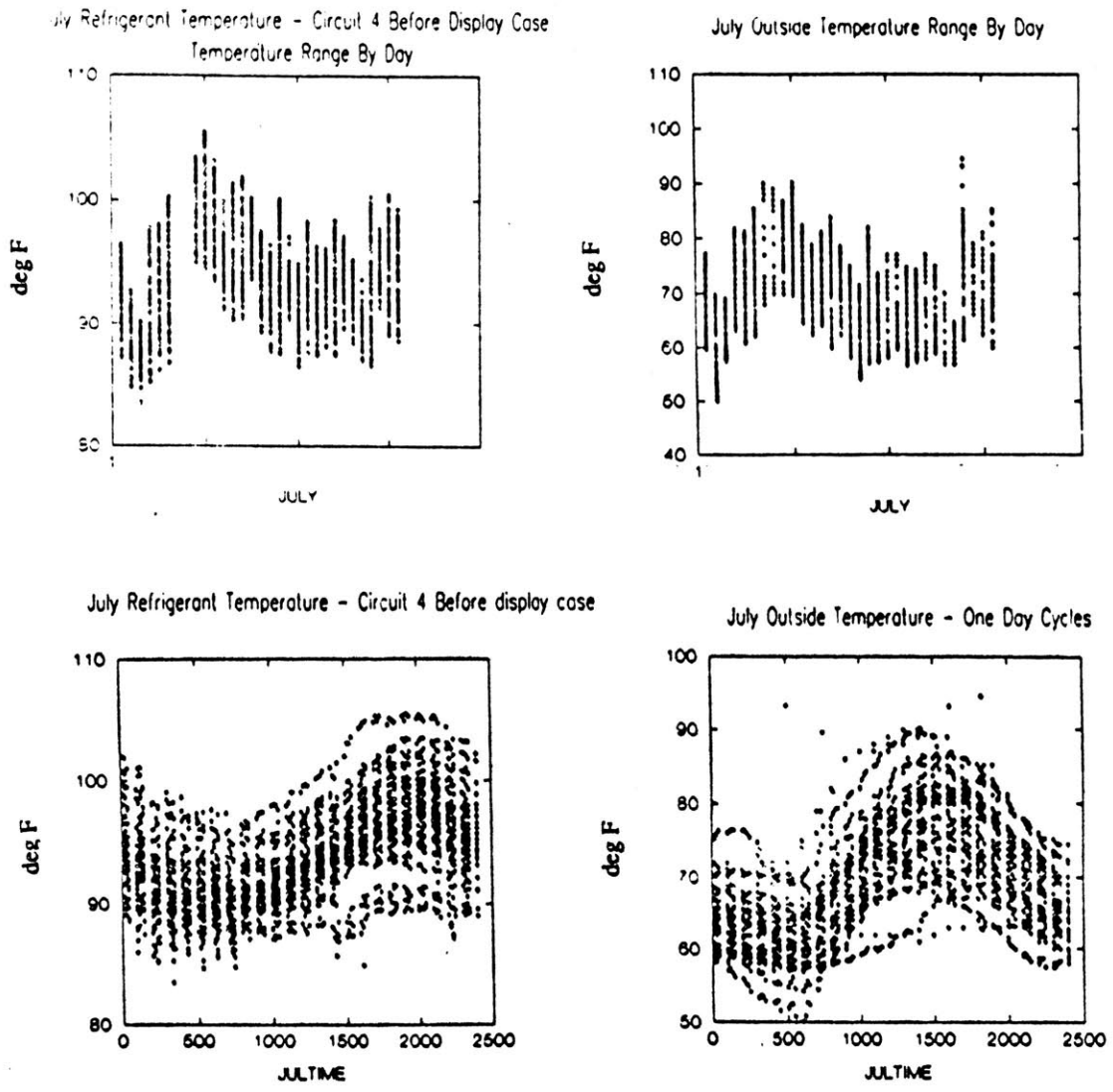

Figure 44. Liquid Refrigerant and Outside Temperatures, July.

8.2 Refrigeration Line Pressures

For an ideal vapor compression circuit, pressure remains constant through the condensing and compression stages. In actual applications, though, there are piping entrance and exit pressure drops as well as friction line losses. This section analyzes these losses as they occur in the monitored refrigeration cycle. With these losses quantified, it will be possible to model the refrigeration system as a Carnot cycle with these differences added.

Figure 45 is a scatter plot of the relationship between circuit 4 liquid pressure, located after the liquid manifold before the expansion valve, and rack A discharge pressure, located after the compressor. This shows that discharge pressure remains relatively constant over the range of circuit 4 liquid pressures above 50 psi and below 170 psi. When the liquid pressure rises above 170 psi, the discharge pressure increases in a linear correlation. A regression of this line for liquid pressure values over 170 psi gives the following equation:

$$Pliqc4 = -5.304 + 0.990(Pdis)$$

$$Standard\ error = 0.9415 + 0.004(Pdis)$$

Pliqc4 : pressure of refrigerant off liquid manifold [psi]

Pdis : pressure of refrigerant after compressor [psi]

The standard error for the range of 170 psi to 210 psi (the maximum and minimum of this regression) is ±1.78 psi (about 1%). Equipment error (0.4%) is ±0.84 psi. What the regression tells us is that the combined pressure losses across the condensing section and through the liquid manifold valves come to 5.3 psi ±2.6 psi.

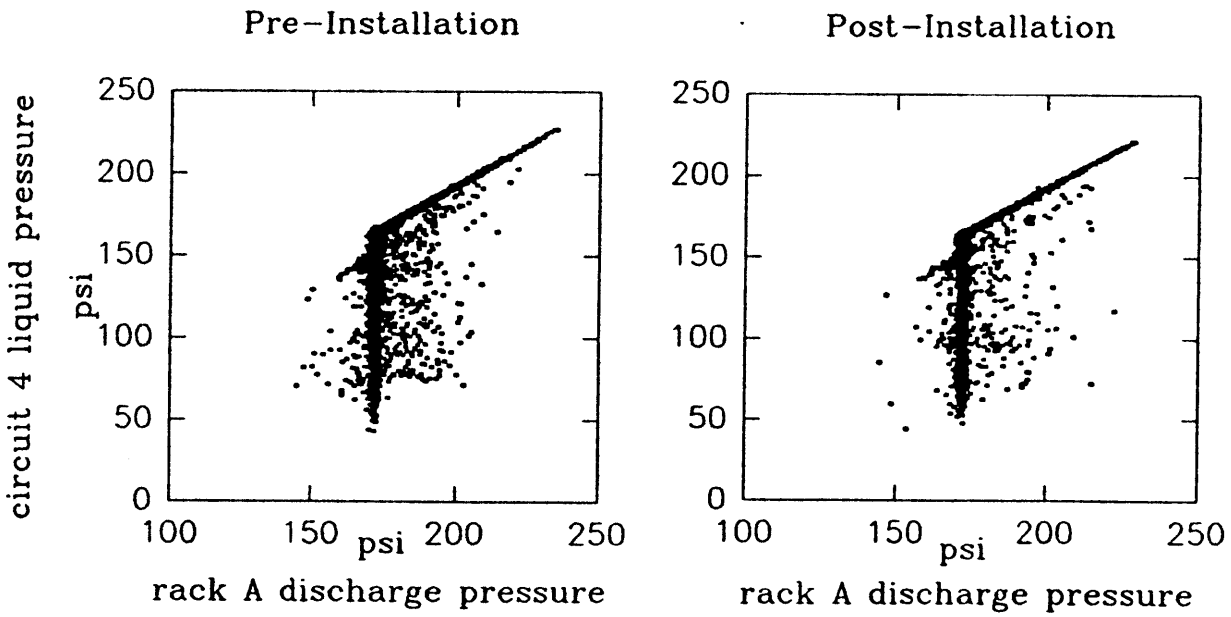

Figure 45. Circuit 4 Liquid Pressure vs. Rack A Discharge Pressure.

The same analysis can be applied to the circuit 4 suction pressure and the suction manifold pressure. These graphs are shown in Figure 46. The groups of points above 50 psi are monitored points during the defrost cycles, and are not included in this analysis. A regression of the remaining points would tell us what the suction manifold entrance valve pressure loss is. An analysis for the range between 10 psi to 20 psi (which excludes the higher circuit 4 defrost cycle pressures) gives the following equation:

$$Psuctc4 = -0.548 + 0.981(PsuctA)$$

$$Standard\ error = 0.0137 + 0.001(PsuctA)$$

Psuctc4 : suction pressure of refrigerant in circuit 4 [psi]

PsuctA : pressure of refrigerant at rack A suction manifold [psi]

The standard error for the range of 10 psi to 20 psi is ±.03 psi (about 0.1%). Equipment error (0.4%) is ±0.08 psi. Therefore, the entrance loss is 0.5 psi ±0.1 psi.

8.3 Refrigeration Compressor Power vs Display Case Load

At this point in the refrigeration model, the point 3 pressure (monitored) and enthalpy (section 8.1), the point 4 enthalpy (same as point 3), the point 1 pressure (monitored) and enthalpy (section 8.1), and the point 2 pressure (monitored) are known. The enthalpy difference between points 4 and 1 (through the evaporator) is known for circuit 4, and on the pressure-enthalpy chart the difference between this line and the line for all of circuit A is a vertical drop characterized by the pressure drop calculated in the previous section (as shown in Figure 47). If compressor power can be predicted using display case load, the point 2 enthalpy can be modelled and the cycle will be complete.

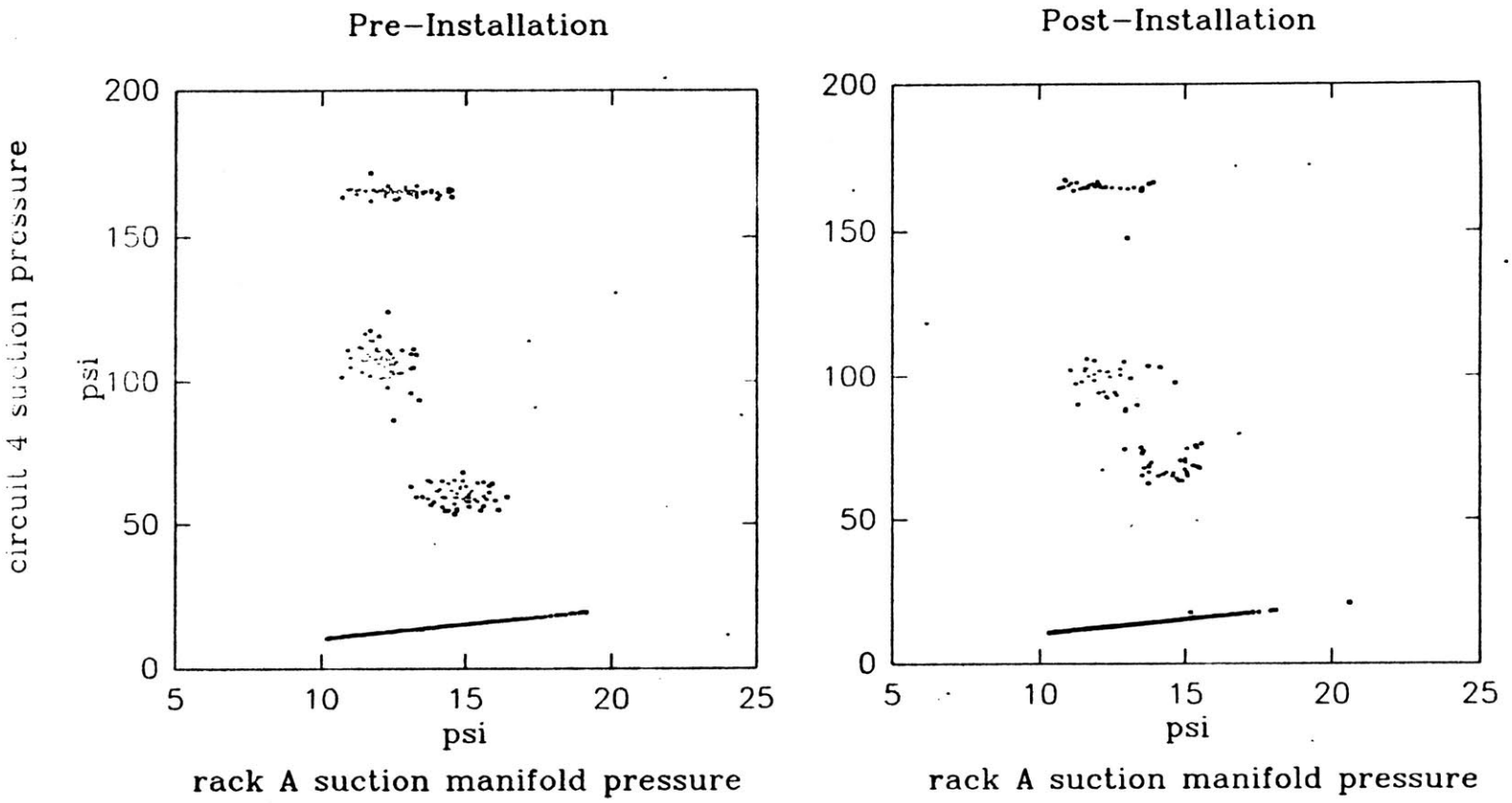

Figure 46. Circuit 4 Suction Pressure vs. Rack A Suction Manifold Pressure.

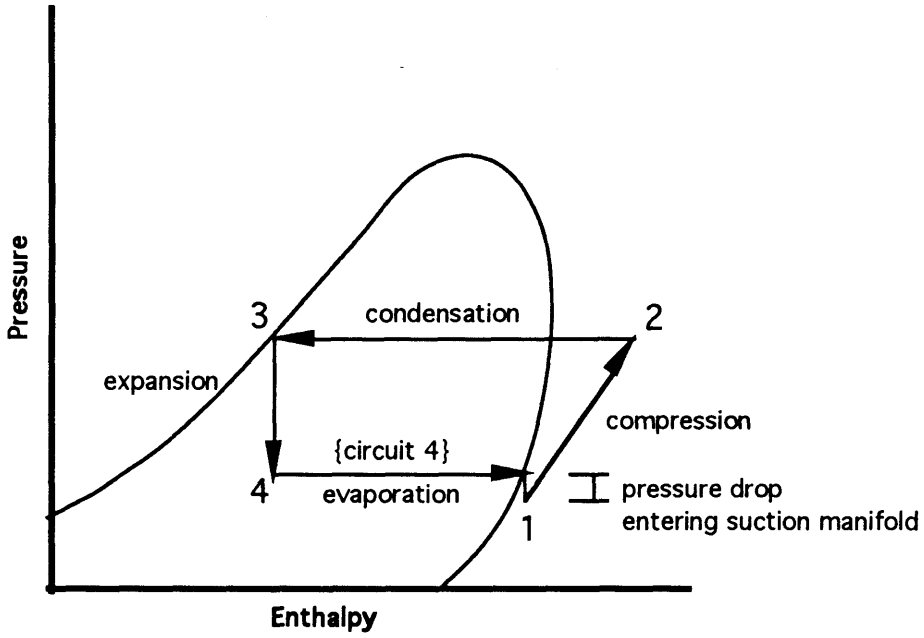

Figure 47. Pressure-Enthalpy Chart Showing Carnot Cycle with Suction Manifold Pressure Drop

Compressor power for rack A was compared to display case load for circuit 4 both before and after installation. Since all display case circuits start at the same liquid manifold and empty into the same suction manifold, it is unrealistic that changes in any one circuit would significantly affect compressor load, and therefore compressor power. It is expected, though, that factors affecting the cooling load in a given circuit would similarly affect load in the other same-temperature circuits served by that rack. Relationship of amount and type of product being cooled can be expected to be different, but ambient humidity and temperature, which should be a stronger factor in load, should be similar.

Due to the rack configuration, compressor power is not expected to fall in any particular pattern, or relate very accurately to the other variables. There are two different types of compressors in the rack, four 10-horsepower models and one 6-horsepower model. The control of these compressors is linked to suction pressure. Different

compressors are cycled on and off based on fluctuations in suction pressure, as compressors are turned on when suction pressure increases.

Figure 48 shows scatter plots of rack A compressor power vs circuit 4 load both before and after installation. There is clearly no definite relationship between these two variables. One can only conclude that, for the majority of the time before installation, display case load fell between 10,000 Btu/hr and 20,000 Btu,hr, a range for which compressor power mostly fell anywhere between 25 kW and 33 kW. After installation, there seems to be a greater grouping of points in this same range, but there also seems to be an extension of points past 20,000 Btu/hr for which compressor power stays around 33 kW.

8.4 Summary

It is clear that this method of refrigeration modelling will not work for this configuration, partly due to my naivete of refrigeration systems when deriving the original strategy, but also due to insufficient monitoring points. It was originally planned that modelling the refrigeration cycle would allow us to create a spreadsheet similar to the one created for the air system, where temperature and pressure points could be input as columns, enthalpy difference across the evaporator (display cases) would be input (similar to the way temperature difference across the cooling coils was used in the airflow model), and the output would be compressor load, which could be translated into power consumption. Unfortunately, the lack of ability to relate compressor power to display case load statistically would cause any model to be incomplete. For a rack configuration, it is necessary to monitor power for each compressor individually, and to use manufacturers equations for each compressor in conjunction with suction and discharge temperature and

pressure to model the compression stage. Ideally, all circuits in the rack would need to be monitored and modelled to calculate the total effect of the evaporation section.

Nevertheless, the air model showed that the changes in supply specific humidity were small (and statistically inconclusive), so it is expected that by the time these changes reached the display case refrigeration coils, they would be insignificant. Any savings, as is discussed in section 9.4, would result from changes in the energy management system reducing equipment power due to expected dew point reduction.

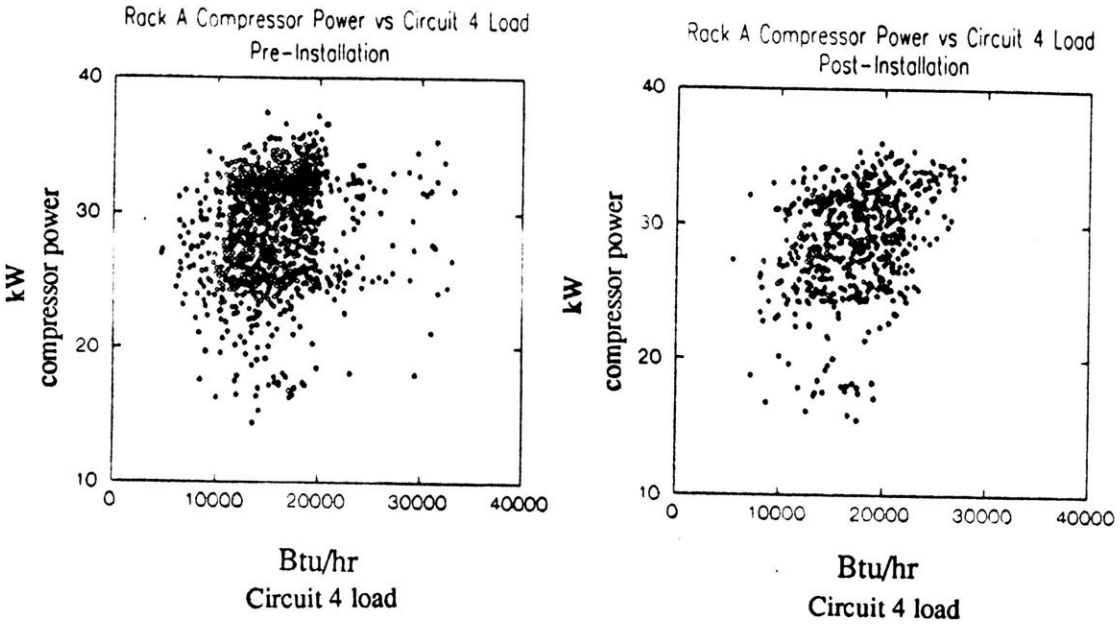

Figure 48. Rack A Compressor Power vs. Circuit 4 Evaporator Load.

Chapter 9 Energy Analysis

This chapter summarizes the final step in the thesis, the energy analysis. The previous step showed that humidity reduction and display case load cannot be predicted from monitored data and regression and engineering equations; this step will attempt to recognize energy savings based on actual monitored power before and after installation. The first section of this chapter analyzes refrigeration compressor power, and attempts to normalize changes in consumption based on ambient conditions. Although defrost cycles are timer activated, meaning that energy consumption for this function would not change as long as the timer didn't change, an increase in heat transfer efficiency at the display case due to dehumidification (explained in chapter 8), would cause compressors to cycle on less often. Also, there would be less latent load of freezing condensate absorbed by the refrigerant if moisture were accumulating less rapidly. The second section addresses the issue of increased air flow resistance due to the presence of the heat pipe and how it affects air conditioning unit performance. The third section looks at unrealized savings, which would require changes to the existing system.

9.1 Refrigeration Compressor Power

The power measurements taken over the course of the monitoring period were the combined power consumption of all of the compressors in a rack. In a multiplex refrigeration system, the capacity of a compressor rack is designed for maximum refrigeration load. When less refrigeration is needed, individual compressors cycle on and off to provide adequate load. Factors which affect the load for a specific case type include ambient temperature, inventory, type of product being refrigerated, and time of day. This

fact turned out to be a major problem in the monitoring scheme. As will be shown later, total rack energy consumption varied considerably from one fifteen minute span to the next, and the variations could not be linked to any ambient trends. As was shown in the previous chapter, compressor power could not be linked to trends in display case load either. An analysis of trends in daily consumption (in kWh) may give a better look at what affects consumption.

Daily energy consumption of rack A, rack B, rack C, and condenser fan energy consumption for rack A is shown in figures 49 through 52. Compressor power for rack B, the medium temperature rack, does not vary much from day to day, and from the beginning of the summer to the end of the summer. The low and high temperature racks, A and C, have significant daily changes in energy consumption, which seem to peak in July and August and drop considerably towards the end of September.

Realized energy savings without changing building operating conditions are expected to be small. The majority of potential savings are unrealized, as explained further in section 9.3. There will be a slight increase in efficiency in the display cases, as frost buildup accumulates at a slower rate due to ambient dehumidification, but since the majority of the defrost cycles are timer activated (including the one on the monitored circuit), there will be no defrost cycle savings without a change in setpoints. An examination of compressor

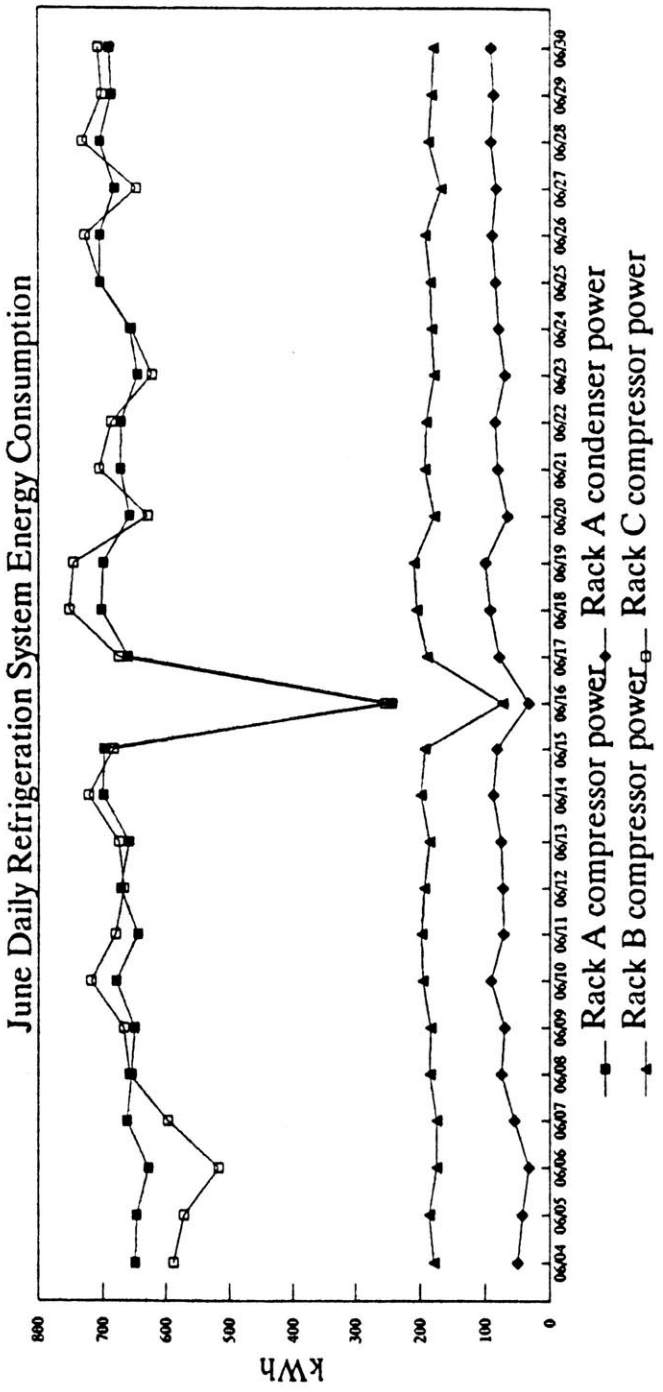

Figure 49. June Daily Refrigeration System Energy Consumption.

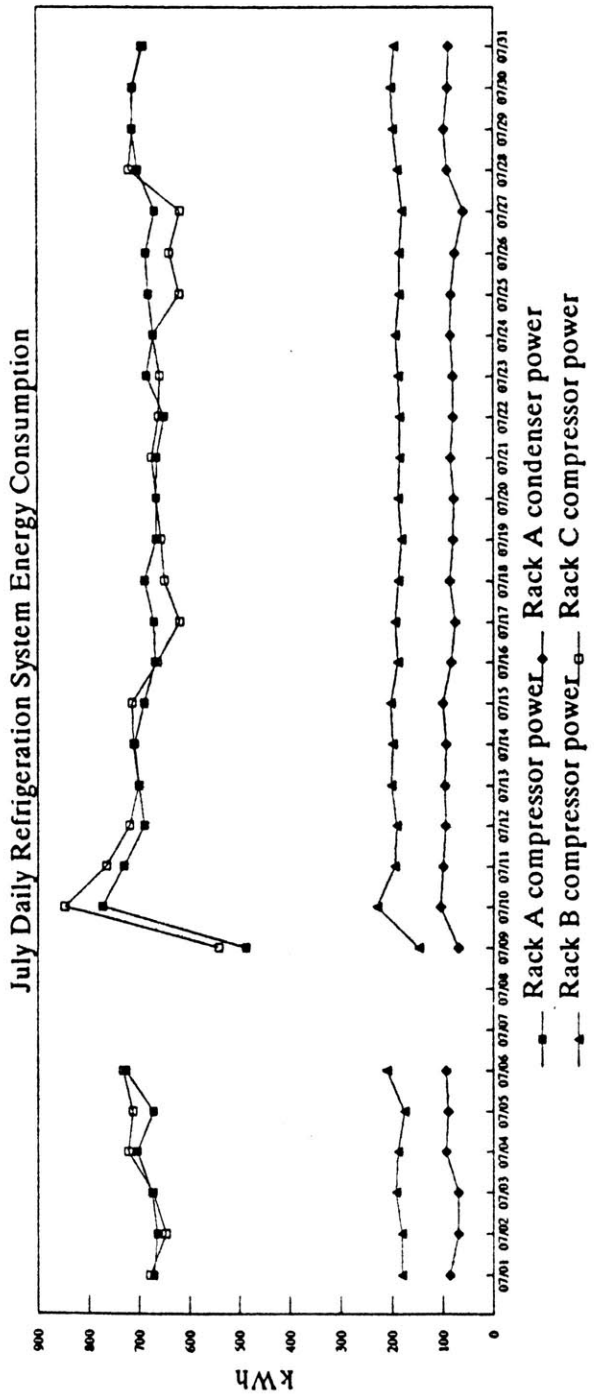

Figure 50. July Daily Refrigeration System Energy Consumption.

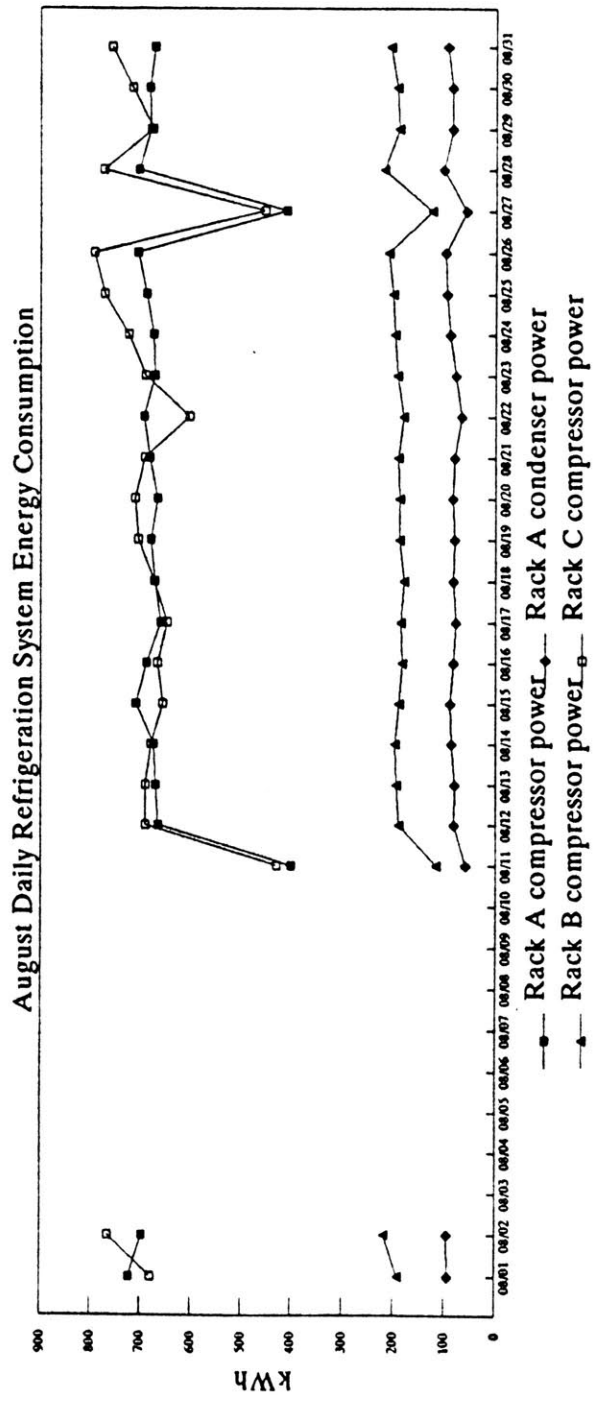

Figure 51. August Daily Refrigeration System Energy Consumption.

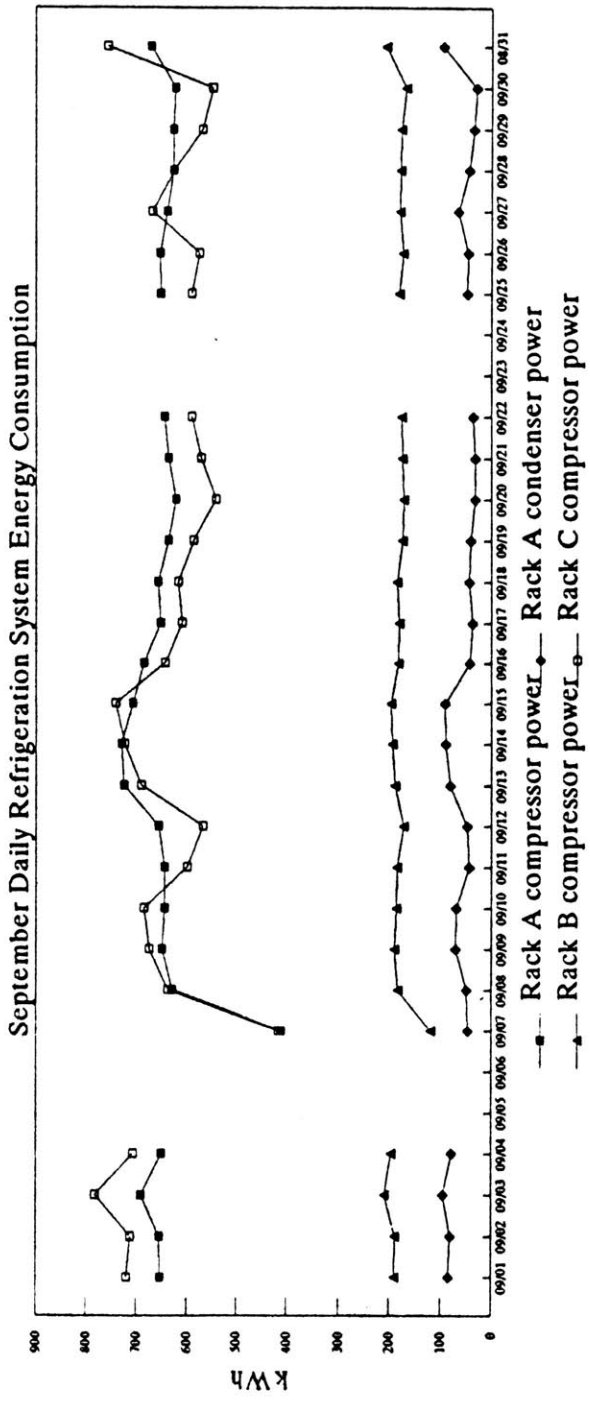

Figure 52. September Daily Refrigeration System Energy Consumption.

power before and after installation, which would give an indication of any efficiency increases, is attempted below.

9.1.1 Daily Consumption

A regression analysis was performed comparing daily energy consumption of each compressor rack in kiloWatt-hours to average outside temperature (Figure 53). What was discovered is that the compressor power of each rack increased as outside temperature increased, and that after the heat pipe was installed, compressor power was lower for a given outside temperature. The regression equations are only accurate for rack C, and are not so obvious for racks A and B. The resulting equations for compressor power in kWh/day are as follows:

Pre-installation

$$CMPA\ power = 3.871 * (AVE\ T\_OUT) + 421.563$$

$$(R^2 = 0.696)$$

$$Standard\ error = 14.4\ kWh/day$$

$$CMPB\ power = 1.154 * (AVE\ T\_OUT) + 112.180$$

$$(R^2 = 0.345)$$

$$Standard\ error = 8.8\ kWh/day$$

$$CMPC\ power = 8.334 * (AVE\ T\_OUT) + 120.376$$

$$(R^2 = 0.776)$$

$$Standard\ error = 25.2\ kWh/day$$

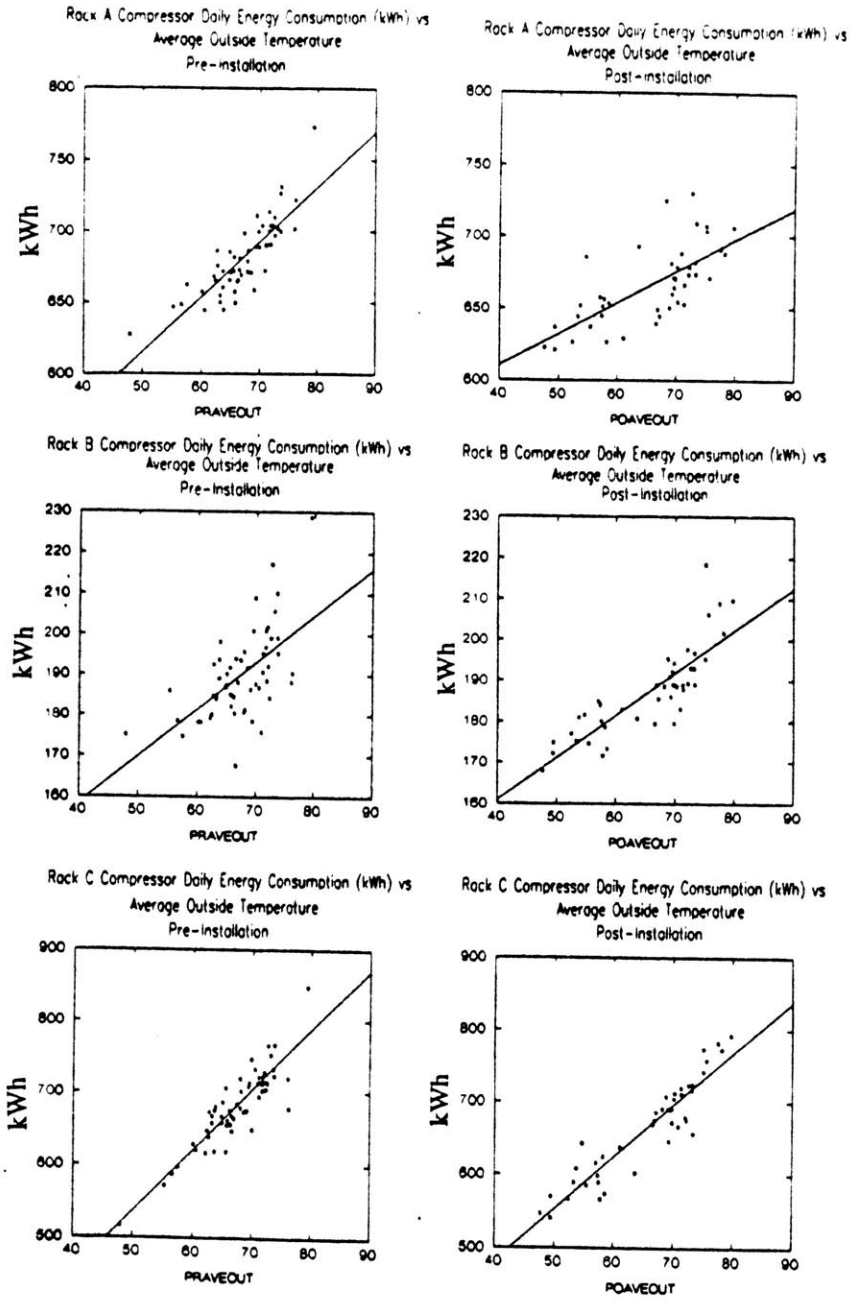

Figure 53. Compressor Daily Energy Consumption vs. Average Outside Temperature.

Post-installation

CMPA power=2.175(AVE T_OUT) + 523.394*

(R^2=0.479)

Standard error = 19.6 kWh/day

CMPB power=1.033(AVE T_OUT) + 119.527*

(R^2=0.689)

Standard error = 6.0 kWh/day

CMPC power=7.113(AVE T_OUT) + 197.731*

(R^2=0.856)

Standard error = 25.4 kWh/day

Figures 54, 55, and 56 show the relationship between daily energy consumption and predicted consumption based on outside temperature for each of the racks. The top graph in each figure shows actual and predicted consumption for the period from the beginning of monitoring to the installation of the heat pipe. Missing sections in the actual consumption line are due to sensor failure or maintenance, or bad data. The lower graph shows actual and predicted consumption from the installation of the heat pipe to the end of September; but it also shows what energy consumption would have been if it had followed the predicted path from before the installation. This path, shown by the short dashed line, assumes what energy consumption would have been if the heat pipe had never been installed. This also assumes that none of the other potential factors affecting consumption changed from pre-installation to post-installation. The section where pre-installation predicted consumption is lower than post-installation predicted consumption reflects errors in the predictions. For rack A, this line is noticeably higher than predicted consumption using the post-installation equation up until the end of September, when the cooling season

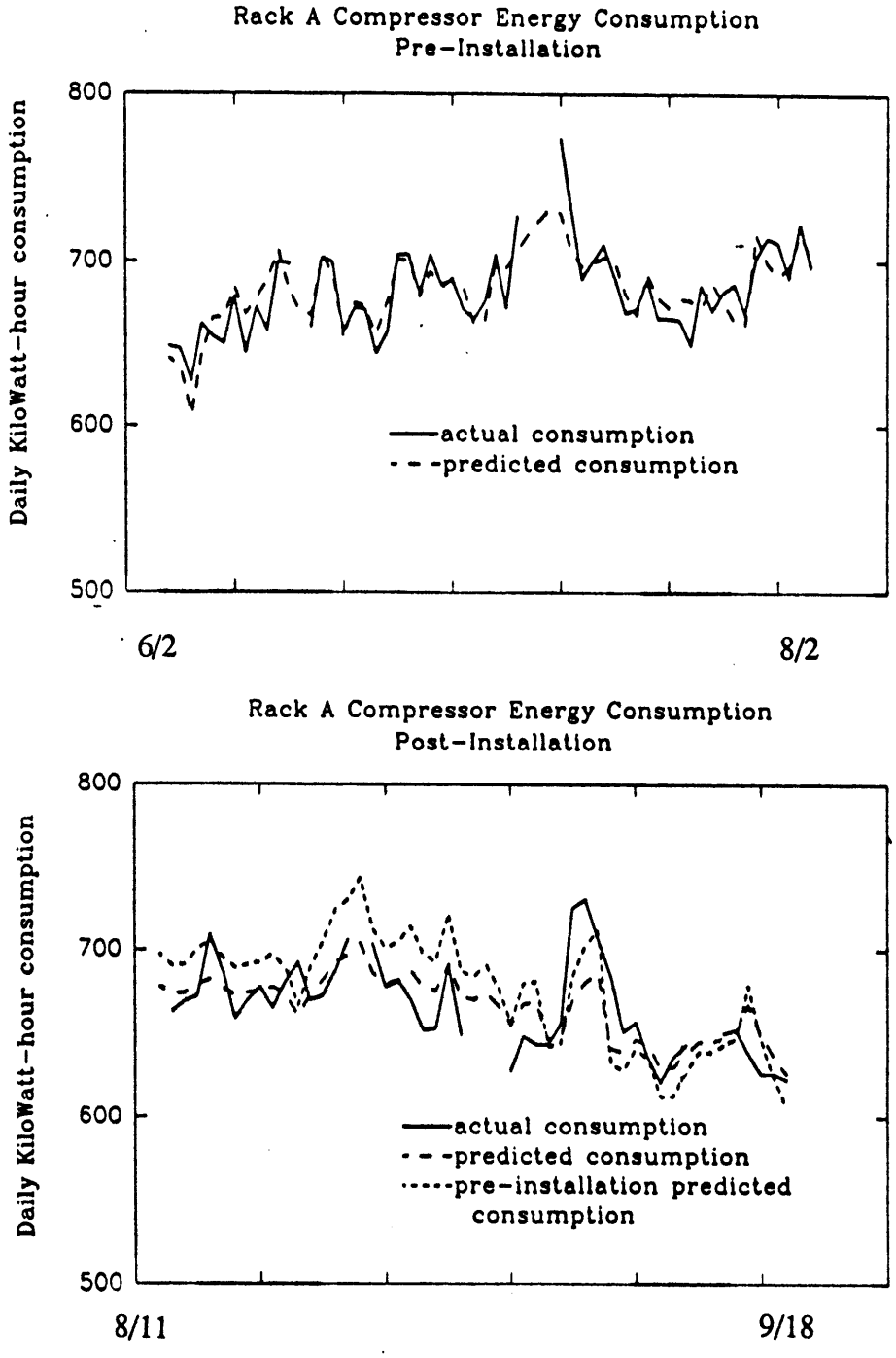

Figure 54. Rack A Actual and Predicted Energy Consumption.

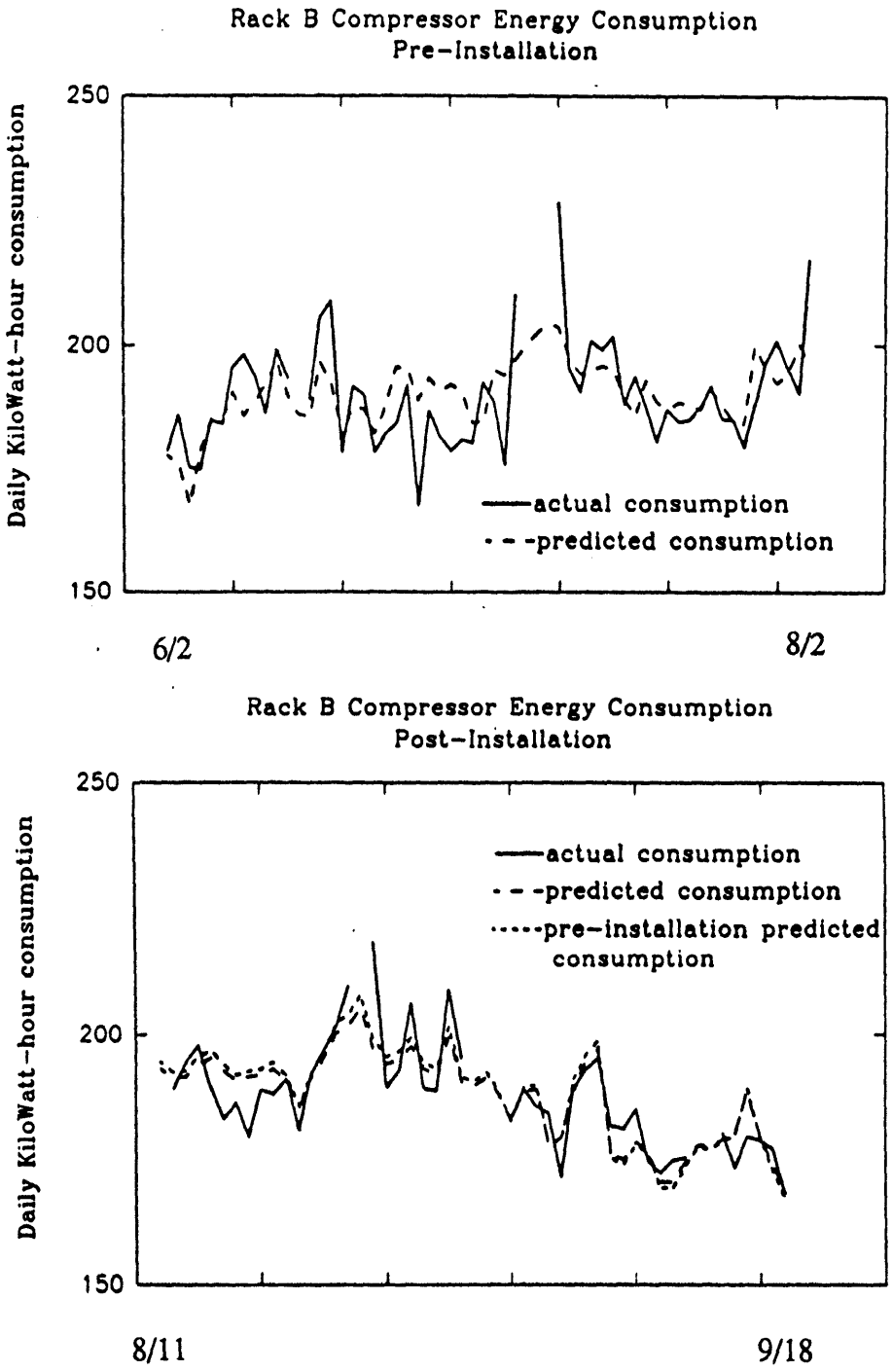

Figure 55. Rack B Actual and Predicted Energy Consumption.

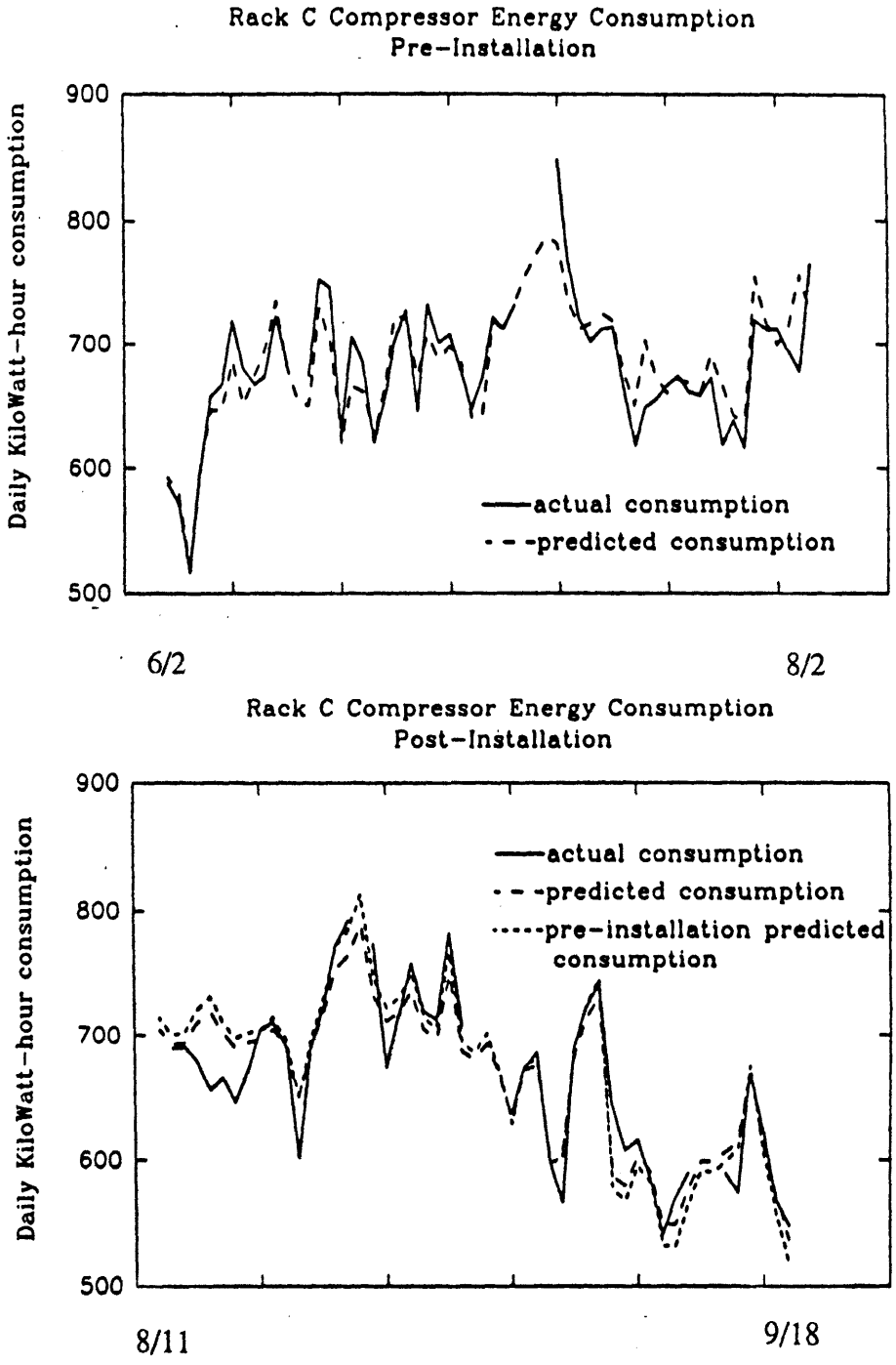

Figure 56. Rack C Actual and Predicted Energy Consumption.

was winding down. For racks B and C, the difference is not as great but the line using the pre-installation equation is higher than the one using the post-installation equation. This analysis shows that although compressor energy consumption did not decrease much after the installation of the heat pipe, consumption for a given outside temperature did decrease.

Table 8 below shows actual and predicted compressor total energy consumption for the period before the installation, and actual, predicted, and without heat pipe predicted energy consumption for the period after the installation until the end of September. Using the regression equations, the total predicted kiloWatt-hour consumption after installation of the heat pipe can be compared to what it would have been if the heat pipe wasn't installed. Equipment errors are 0.25% for the power meter and ±1 degree for the temperature sensor. Combined equipment and regression errors result in the following accuracies:

CMPA Pre = ±20.0 kWh/day

CMPB Pre = ±10.4 kWh/day

CMPC Pre = ±35.3 kWh/day

CMPA Post = ±23.5 kWh/day

CMPB Post = ±7.5 kWh/day

CMPC Post = ±34.1 kWh/day

As shown on table 10, an estimated 426 kWh (8.5 kWh/day) was saved from rack A, 27 kWh (0.5 kWh/day) from rack B, and 130 kWh (2.6 kWh/day) from rack C due to the installation of the heat pipe . Obviously, these estimates are well within calculation errors, rendering them inconclusive.

Table 10. Actual and predicted pre- and post- installation compressor energy consumption.

June 4 to August 2	kWh
actual rack A consumption	38,196
actual rack B consumption	10,632
actual rack C consumption	38,150
August 11 to September 30	
actual rack A consumption	29,323
predicted rack A consumption	29,321
predicted rack A consumption without heat pipe	29,747
actual rack B consumption	8,249
predicted rack B consumption	8,248
predicted rack B consumption without heat pipe	8,274
actual rack C consumption	29,277
predicted rack C consumption	29,277
predicted rack C consumption without heat pipe	29,406

9.1.2 Monitored Compressor Power vs Ambient Conditions

Another factor which is expected to affect compressor power other than outside temperature is inside air dew point. Dew point is more important than dry bulb temperature and specific humidity because it describes the actual temperature that moisture begins to condense on the refrigeration coils. Dew point temperature was calculated using return air temperatures and relative humidities as described above in section 7.2.1. Although return

air is not an exact representation of inside air conditions (section 7.3), changes in dew point should follow the same trends. Figure 57 shows a time line of inside dew point temperature and outside dry bulb temperature for the pre-installation and post-installation periods. Outside temperature is included because dew point varies considerably over time, and to notice any reduction it is necessary to have a controlled variable to compare it to. Excluding the last block of post-installation data, when sensor performance was inconsistent, there is a wider gap between outside temperature and inside dew point. A regression of these two variables was inconclusive, but the difference is visible. Further analysis would be necessary to determine the actual reduction in dew point for given conditions. A regression analysis of rack A compressor power (CMPA) vs inside dew point and outside temperature results in the following equations:

Pre-Installation

$$CMPA = 15.41 + 0.08051(dewpt) + 0.1382(Tout)$$

$$Standard\ error = 0.6016 + 0.0133(dewpt) + 0.0059(Tout)$$

Post-Installation

$$CMPA = 18.85 - 0.01321(dewpt) + 0.140(Tout)$$

$$Standard\ error = 0.7254 + 0.0094(dewpt) + 0.0088(Tout))$$

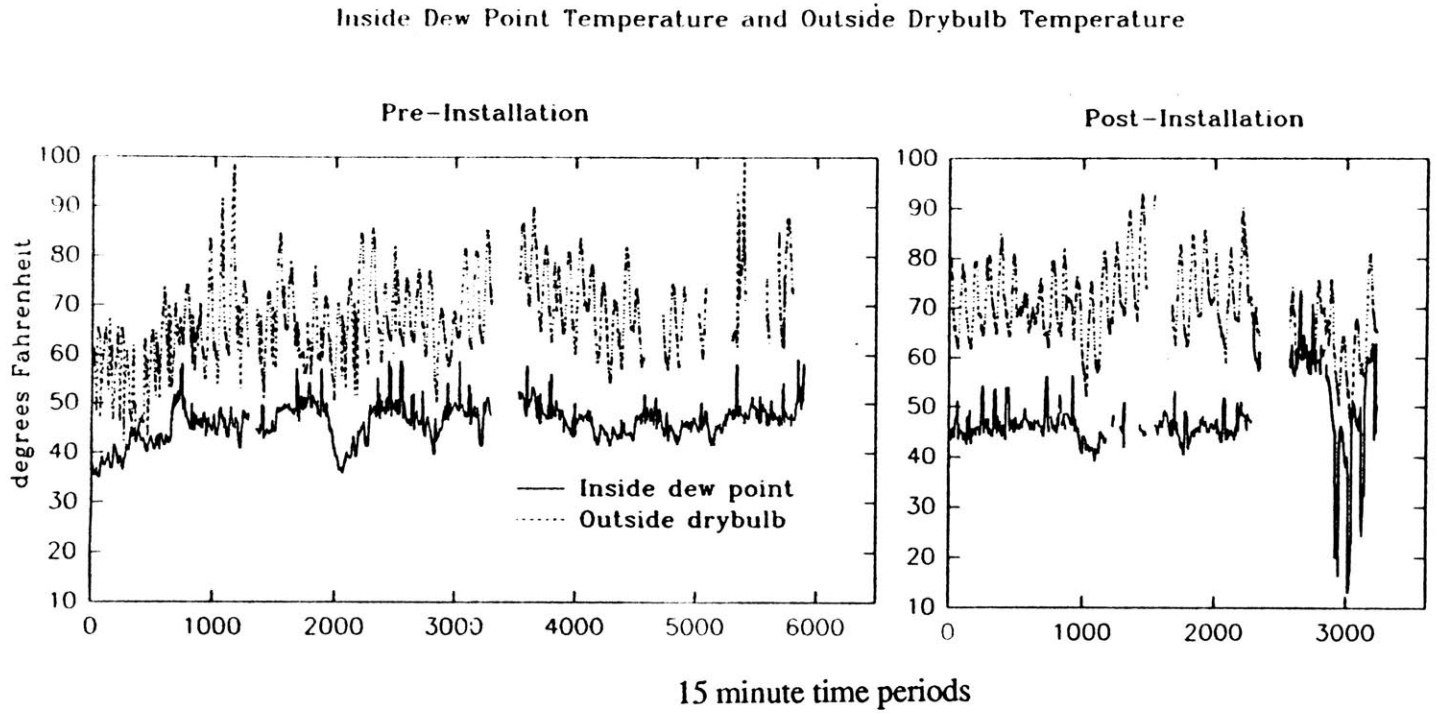

Figure 57. Inside Dew Point Temperature and Outside Dry Bulb Temperature.

Statistical error in this calculation, shown in Appendix D, is ±0.25 kW pre-installation and ±0.16 kW post-installation. The standard error in the equations results in an accuracy of ±1.8 kW pre-installation and ±1.6 kW post-installation. Figure 58 shows a time line of actual and predicted rack A compressor power demand for the four day period starting July 16. Figure 59 shows the same graph for the four day period beginning August 11 (the first day of monitoring after the installation). As expected, there are sharp fluctuations in actual compressor power for fifteen minute averages, which means that the compressors are probably cycling too much. The line of predicted points seems like a good estimate of the mean consumption for the period, but the calculation errors (38 kWh/day) outweigh the accuracy and savings estimates.

Regression equations attempting to predict compressor power as a function of evaporator load and condenser power (R^2=0.517) were inconclusive. Compressor power as a function of outside temperature, relative humidity, and supply air specific humidity (R^2=0.135), results in too significant an error (about 3.4 kW). Therefore, it would be fruitless to attempt to model the refrigeration cycle based on data acquired for this installation. Further measurements are necessary, in which individual compressor power consumption, and display case air temperature and humidity and/or frost accumulation could be additional variables in an analysis.

9.2 Air Conditioning Fan Penalties

To determine the effect of the heat pipe on air flow, it was necessary to perform the same air flow analysis as was done before the installation (see section 5.1). Using the same vane anemometer as in the first test, we measured the air flow at the reheat coil and

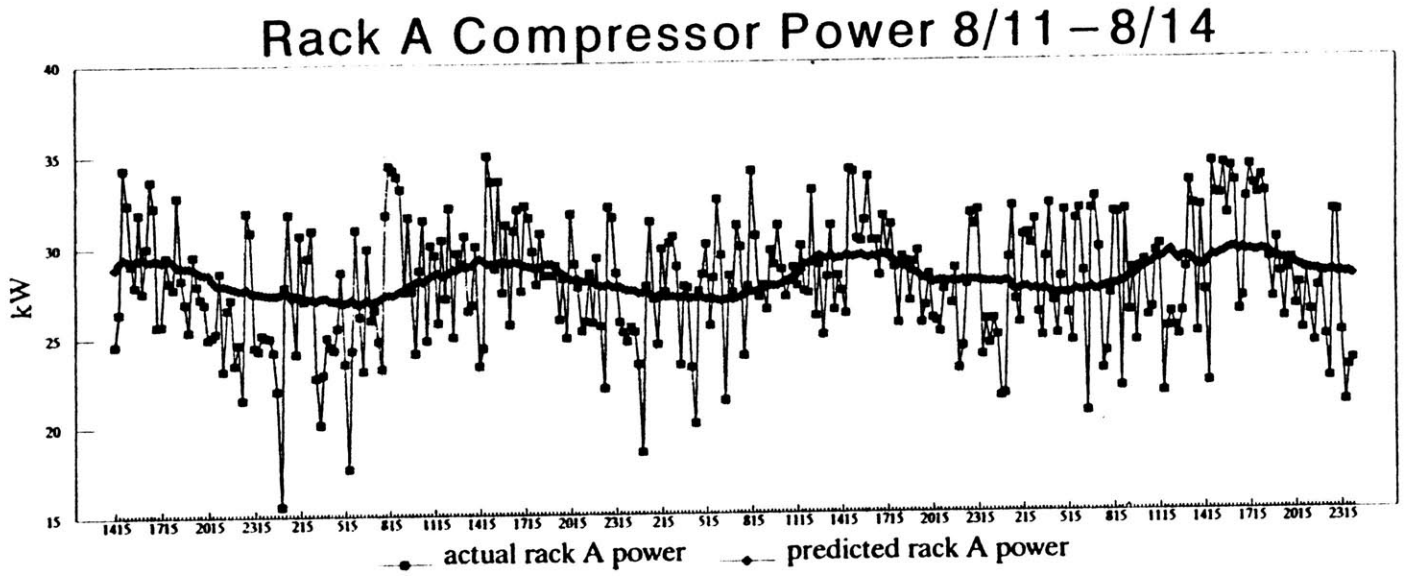

Figure 58. Rack A Actual and Predicted Compressor Power July 16-19.

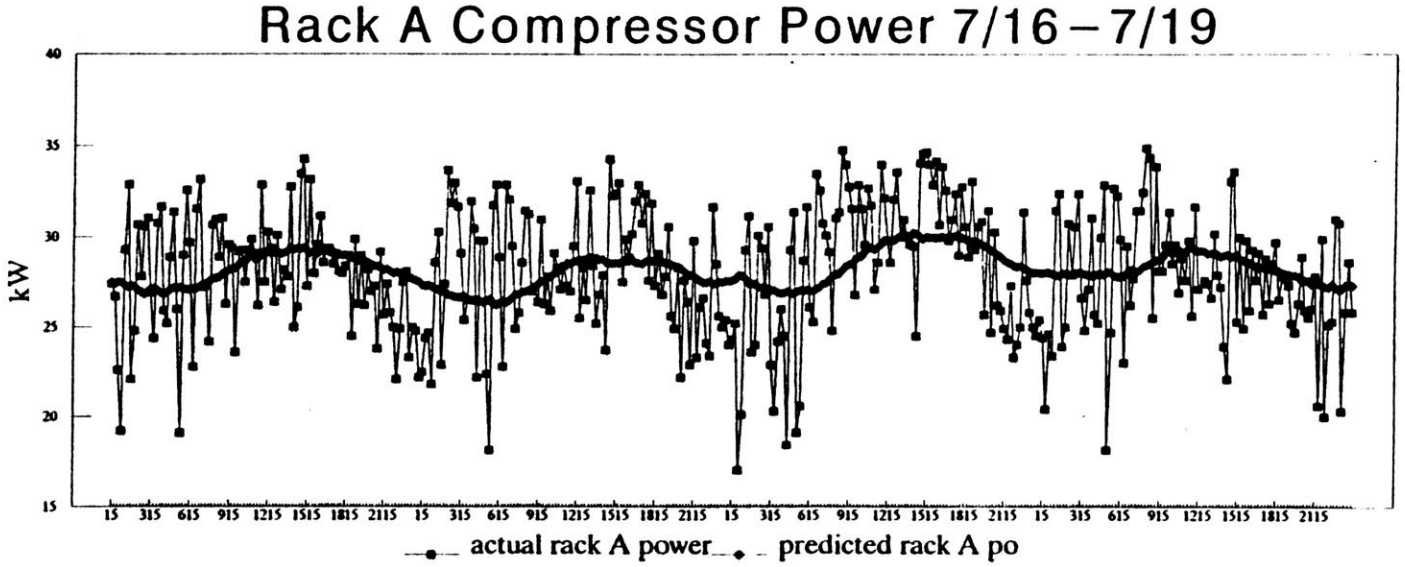

Figure 59. Rack A Actual and Predicted Compressor Power August 11-14.

by-pass damper on September 10. As a result of the test, we estimate the airflow to be 32,400 cfm (approximately a 2.4 percent decrease) as calculated in Table 11 below.

Table 11. Air Flow Measurements - September 10.

	Over Heat Reclaim Coils - Upper Half		Bypass Damper-Lower Half		
	Test 1	**Test 2**	**Test 1**	**Test 2**	**Test 3**
Feet measured	187	147	330	340	290
Seconds	23.7	21.1	18.8	19.5	17.1
Ft/Sec	7.9	7.0	17.6	17.4	17.0
Ft/min	473.4	418.8	1053.0	1046.4	1017.6
CFM	9174	8116	24,061	23,910	23,252

Average of readings over upper half 8,645 cfm

Average of readings over lower coil 23,741 cfm

Total Airflow 32,400 cfm

This is a small difference from the pre-installation measurement (800 cfm = 2.4% of 33,200 cfm). The measurement error for the vane anemometer is estimated for this airflow as 9,980 cfm (see Appendix D). Ideally a more accurate method would be used to measure airflow before and after installation. The reason this device was used is that it was originally expected that the heat pipe installers would measure airflow immediately before and after installation. Unfortunately, they were unprepared to perform this measurement,

and an alternate last-minute method became necessary. At that time a representative of HEC Corp. was hired to make the measurement with a vane anemometer, the most accurate device available within the time frame, and the original measurements were made. The fact that the pre-installation measurement was so close to the post-installation measurement means that reduction in airflow is statistically inconclusive.

However, on October 24 , we performed an air balancing test at the request of the supermarket's managers to determine whether or not the store was running at positive air pressure or not. Normally, the amount of outside air intake at the air conditioning unit is sized to maintain a positive pressure in the building, to reduce the amount of infiltration. If the air in the building is at a higher pressure than outside air, the opening of doors and windows will lead to exfiltration, and not infiltration of humid outside air. For this test we looked for infiltration through the front doors when the store was closed, the supply fan was operating, and all entrances and exits to the store were closed. With the outside air dampers fully opened, we observed that there was still a negative air pressure inside the building, as air was leaking in through the crack between the front doors. This meant that more than the volume of air drawn in through the outside dampers was leaking through another location. After checking all exhaust fans, exits, and windows, we could not come up with a noticeable leak. The only possibility was that air was being drawn in by adjoining stores (a pharmacy and a liquor store abutted the supermarket on either side), but this has not been proven. It was determined, though, that this was a problem before the heat pipe was installed and therefore outside the scope of this project.

Although this resulted in no penalty for this installation, the potential penalty can be calculated by the drop in airflow or air pressure in the duct, and fan curves for this fan. The previous three studies, summarized in section 2.2, did not adjust the fan blower to accommodate this added resistance. The Georgia power study made no mention of it,

while the other two studies maintained the lower air flow rates, and concluded that there was no compromise in building performance with the lower airflow.

9.3 Unrealized Energy Savings

The majority of energy savings associated with the installation of the heat pipe are unrealized at this point. The main aspect of dehumidification is the potential for decreasing the frequency of defrost cycles due to a decrease in average inside dew point. In order to determine the extent to which defrost cycles could be changed, it would be necessary to perform a mass flow balance, to determine the rate at which frost forms on the coils for a given display case air temperature and humidity level. It would also be necessary to analyze the infiltration of ambient air into the display case to determine the effect of dehumidification of inside air. When these are accomplished, it can be estimated how much frost forms on the coils for the existing defrost cycle period, and how long it would take to accumulate the same amount of frost for dehumidified levels. Then the defrost cycle could be adjusted accordingly. As this is an extremely difficult process, it is recommended that the defrost cycles be changed to demand control through the EMS, by which the heat transfer efficiency at the coils is monitored, and when it drops to a certain point, the defrost cycle comes on. This will result in significant savings, which would require further research to predict.

Another source of energy savings occurs in the anti-sweat heaters, which use hot air to heat display case doors above the dew point when condensation starts to form. These were not monitored due to the fact that it was expected that the heaters were monitored by the store's engineers and this information would be supplied to us, which did not occur. With a reduction in inside dew point, the anti-sweat heaters would need to work less often, as the temperature at which 'sweat' would begin to form is lower. For the Duke Power

study, anti-sweat heaters were completely disabled and approximately 350 kWh/day was saved without condensation problems (Abrams et al 1992).

9.4 Summary

It can be determined from these results that any savings which may have occurred due to an increase of efficiency at the display case were too small to quantify. Future savings will be based on changes in how the refrigeration system operates, to make it more efficient without compromising performance. With reductions in inside dew point caused by dehumidification, it is recommended that the following changes be made to the refrigeration system before the next cooling season:

Demand Defrost Control Defrost cycles can be controlled by monitoring refrigerant temperature and pressure just before and after the display case. When the difference between the enthalpy at these locations drops below a specified setpoint, it means that the heat transfer from coil to air is insufficient and the defrost cycle should be activated. This would assure that display cases would be defrosted only when necessary.

Deactivate Anti-sweat Heaters With a lower dew point in the building, the anti-sweat heaters do not need to function as often as was originally designed. Anti-sweat heaters can also be controlled by demand as with the defrost cycle recommendation, but judging by the success of the deactivation in the Duke Power study (in a much more humid climate), it is safe to assume that they can be completely deactivated.

Other energy saving features, such as multideck operation, are already in service or would require further investigation to warrant a recommendation.

Chapter 10 Conclusions

By analyzing the basic theory behind heat pipe dehumidification, which is the alternate cooling and reheating of air due to evaporation and condensation of the refrigerant contained within the heat pipe, it has been determined that if there is any dehumidification performed by a cooling coil, there will be more dehumidification with a heat pipe installed. For supermarket applications, it was determined that the heat pipe can reduce humidity levels while keeping supply air dry bulb temperature the same, and reducing the amount of heat reclaim necessary to bring the air to supply conditions after super-cooling (chapter 2). With the inability of this study to accomplish the original goal of predicting energy savings due to the installation of the heat pipe (relative to experimental uncertainties), the thesis should not be used for its results, but rather for how it can assist further studies and justify heat pipes qualitatively.

There are several ways that this study could have been improved, some I've learned with experience, and some with further knowledge of refrigeration and air systems; these will be discussed in the next section. For this application, it was shown that humidity reduction and energy savings estimates are small, and a significant amount of energy savings are unrealized at this point. Part of the conclusions of this report are recommendations and results for the supermarket air system and refrigeration system; these will be discussed in the following section. The other part of the conclusions is a theoretical analysis that relates heat pipe heat transfer to inside dew point reduction and uses the Duke Power study estimates to generate a normalized refrigerations system energy savings for 1993 weather conditions.

Conclusions of the Methods

Originally, the experiment was designed to use monitored data to track the airflows and refrigerant flows in order to predict supply air conditions, display case load, and subsequently compressor power consumption using only outside air temperature and relative humidity as a variable. Points to be monitored were based on covering as many stages in the air system and refrigeration system while keeping monitoring costs down. Monitoring mass flow for example, usually an expensive process, was provided for one location by the contractor at almost no cost due to the availability of a device from another project. We felt then, and still feel now, that given one location the one we picked - in circuit 4 after the liquid manifold - was the best. Ideally a mass flow meter would have been installed after the compressor section also, to better predict compressor load, and possibly in another circuit. For the air system, the final conclusion is the more temperature readings the better, since the cross section of air airflow is far from isothermal. Also, given the dual-coil configuration of the cooling section, a more in-depth analysis of the difference in airflows across the upper coil and lower coil might have reduced some of the calculation errors.

Several factors forced us to change our method of analysis midway through the project. One factor was the outside air intake. We were told at the beginning of monitoring that the supply fan was on 24 hours a day, and a constant outside air intake was maintained. Based on data examination (explained in chapter six), it was discovered that the supply blower shut off at night, except for times when the night setpoints triggered the air conditioning compressor when cooling was needed. Since the outside air sensors were placed just inside the dampers to protect them from the elements, when the fan was not on the sensors read return air conditions, because there was no airflow to draw in outside air. The resulting sensor relocations and failures warranted an extra source for weather data,

from a national service. Therefore, a new part of the analysis, in which weather station data was integrated into monitored data (section 6.4.3) was added.

Another factor in changing the method was readings which did not make sense, as in the calculations in which supply air specific humidity levels derived from monitored data were higher than mixed air specific humidity levels (sections 7.1 and 7.2). As a result of this discovery, it became necessary to create a model of mixed air conditions, post-cooling coil conditions, and supply air conditions based on known psychrometric equations combined with monitored data. This model, based on the one created in section 2.3, concluded that supply air specific humidity levels did in fact decrease after installation of the heat pipe for given mixed air temperature and humidity levels, but by a small enough amount that savings were determined to be statistically inconclusive (section 7.4).

The refrigeration cycle was originally expected to be a small part of the analysis, since variations in compressor power were expected to be a function of changes in ambient conditions (as this was the method used by the previous studies to predict savings). However, mainly due to the multideck configuration of the compressors (and partly due to my lack of knowledge about refrigeration systems), any comparisons to ambient conditions were inconclusive (sections 8.3 and 8.4). An attempt to model the refrigeration cycle based on variations from the Carnot cycle which could be predicted were informative. The unpredictability of the compressor rack power consumption, due to on/off cycles and varying compressor types, led to the demise of the model (chapter 8).

The inside air conditions, in retrospect, deserved a more detailed analysis than was provided in this study. The temperature recorded for the store's energy management system (EMS) should have been hand checked several times against a hand held reader over many different locations in the store. If this temperature reading were to be used in the analysis, a relationship between this temperature, the average store temperature, and the

temperature of the air inside the display cases should be used to relate supply humidity levels to display case load. If the other studies concluded that reductions in airflow and relative humidity went unnoticed (or without complaint) by store employees and customers, this amount of reduction should be a separate energy saving measure in tandem with the installation of the heat pipe.

With the above observances in mind, there are several recommendations for future studies which will improve the results and savings estimates, which are listed below:

• Improved relative humidity data.

The accuracy of the sensor is vital to the accuracy of specific humidity, and a 2% error is too large for our purpose. As explained above, an accuracy of 0.2% would have been satisfactory for our equations, but an accuracy of 1% at the most is recommended. It is also recommended that relative humidity sensors be calibrated on a regular basis against a high humidity salt solution and a low humidity salt solution.

• Increase number of monitoring locations

The minimum recommended locations should be:

Four temperature and relative humidity sensors per location - return air, mixed air, supply air.

One temperature and relative humidity sensor - outside air.

Thirty two thermocouples around cooling coil - four each in a grid before and after each heat pipe section.

Two power meters - compressors and fan blower.

One power meter per refrigeration compressor - all compressors.

Temperature and pressure sensors - at all four points in refrigeration cycle for at least one circuit, and possibly all circuits in a rack.

Air temperature - before and after display case coils (relative humidity, although it would be helpful, is extremely difficult for sub-freezing temperatures).
Temperature and relative humidity - at least four indoor locations, supply area (usually entrance), refrigerated food sales area, dry food sales area, return air area.
Power meters on anti-sweat heaters if possible.

Monitoring a minimum of these points with accurate instrumentation and sufficient calibration will allow air system and refrigeration system models to be accurate enough to predict humidity reduction and energy savings within error.

Conclusions of the Energy Savings

With the model, it was possible to predict daily total refrigeration compressor power based on average daily temperature (section 9.1.1). By comparing equations using pre-installation equations and post-installation equations, it was determined that daily savings due to increased evaporation section efficiency were 9 kWh for rack A, 1 kWh for rack B, and 3 kWh for rack C. Statistical errors for these predictions were 24 kWh/day for rack A, 8 kWh/day for rack B, and 34 kWh/day for rack C. Therefore, savings estimates cannot be differentiated from possible sensor and regression errors. Regression errors account for most of the statistical error (20 kWh/day for rack A, 6 kWh/day for rack B, and 25 kWh/day for rack C), so more accurate sensors would not have helped the study significantly.

The spreadsheet model was able to predict supply air specific humidity using return and outside air monitored temperature and relative humidity, temperature differences across the cooling coil, temperature differences across the heat pipe, and psychrometric equations (sections 7.2 and 7.4). The modelled difference for supply air specific humidity with and without the heat pipe for given mixed air conditions is shown in Figure 37, and varies

based on how much dehumidification is needed. The difference generally falls between 0 (for no dehumidification) and 0.007 lbw/lba. The statistical error for the analysis is 0.0007 lbw/lba, meaning that the reduction estimates are statistically inconclusive. It is expected, though, that with more dehumidification (due to either more humid ambient conditions or a heat pipe designed for a greater heat transfer), the savings estimates would be greater.

As was explained in section 9.3 with an estimated 350 kWh/day savings from ati-sweat heaters, most of the energy savings are unrealized at this point. It is recommended that, for the next cooling season, defrost cycles be controlled by demand setpoints, and anti-sweat heaters be deactivated for display case doors. It is recommended that, along with these measures, monitoring related to these functions be performed over the cooling season. This would include monitoring inside dry bulb and dew point temperature, display case air temperature, refrigeration line temperatures and pressures (similar to the points monitored in this study) and individual compressor power.

Theoretical Savings Expectations

If we do a psychrometric chart analysis, using the energy drop across the pre-cooling section of the heat pipe to predict drop in dew point, we can use the Duke Power study's estimate of 1.7% savings per degree drop in dew point to determine the magnitude of what range of savings we expect from our site.

Assuming the heat pipe removes 200,000 Btu/hr of energy from the air, this is also the amount of extra latent and sensible energy removal being done by the cooling coil, provided the latent/sensible cooling ratio without the heat pipe is above zero. If the cooling coil provides the same amount of cooling as if the heat pipe weren't present, the heat pipe simply shifts 200,000 Btu/hr of sensible load from the cooling coil to 200,000 Btu/hr of latent and sensible load along the line of saturation. With a volumetric flow of 33,200 cfm,

air with a dew point of 50 degrees would have a specific volume of 12.8 ft^3/lb, and therefore a mass flow of 155,625 lb/hr, and 200,000 Btu/hr would correspond to an enthalpy drop of 1.4 Btu/lb, as shown below:

$$33{,}200 \times (1/12.8) \times 60\ [\text{cfm} \times \text{lb/ft}^3 \times \text{min/hr}] = 155{,}625\ \text{lb/hr}$$

$$200{,}000 \times (1/155{,}625)\ [\text{Btu/hr} \times \text{hr/lb}] = 1.4\ \text{Btu/lb}$$

Although the drop in dew point corresponding to this enthalpy drop varies on the psychrometric chart along the line of saturation, an iteration using ASHRAE equations and 100% relative humidity, as shown in table 12, for temperatures starting with 50 degrees, gives a temperature drop of 2.6 degrees (50 - 47.4). The table also shows that this drop corresponds to a specific humidity drop of 0.0005 lbw/lba, which is within our statistical error comparing calculated mixed air specific humidity and supply air specific humidity of 0.0007 lbw/lba, and therefore savings are expected to be statistically inconclusive. Using Duke Power's savings estimates, the maximum drop in dew point would give 4.4% energy savings for the refrigeration system. For a mean rack A compressor power of 28 kW, this corresponds to 1.2 kW savings.

A quick analysis similar to the one used in the Duke Power study based on the relationship between average daily inside dew point and average daily outside temperature with and without the heat pipe will give us insight as to how much the heat pipe reduced dew point. With this information, we can use the savings estimate of 1.7% per degree drop in dew point and 1993 weather bin data to estimate savings for the 1993 cooling season. Figure 60 in Appendix F shows a scatter plot of average daily inside dew point vs average daily outside temperature both before and after heat pipe installation. The trend of post-installation data (the solid circles) show that average dew points were lower than the pre-installation data (hollow circles) for a given outside temperature. The lines on the graph are

linear regressions for the two cases. For all points above 65 degrees outside temperature (minimum cooling degree-day temperature), the post-installation line is lower than the pre-installation line as described by the equation:

$$\text{drop in dew point} = -14.75 + 0.23(\text{outside temp.})$$

As calculated previously, for this heat pipe design the maximum drop in dew point of supply air is 2.6 degrees. For identical ambient conditions, the inside air dew point difference would be no more than 2.6 degrees (the ratio of supply air dew point drop to return air dew point drop can be no more than 1:1). Therefore the actual line representing post-installation dew point drop would start at the pre-installation line, and continue along the above equation until the difference between the lines was 2.6 degrees, then the post-installation line would run parallel to the pre-installation line at a difference of 2.6 degrees.

Figure 61 shows weatherly bin data for 1993, showing how many hours of each month the outside temperature was within a certain range. For the column marked (1), the post installation regression of dew point and outside temperature was used to calculate dew point for a bin average outside temperature. The column marked (2) gives the average dew point drop due to the presence of the heat pipe based on the above equation, with a maximum of 2.6 degrees. A regression of refrigeration compressor power vs outside temperature with the heat pipe installed (from section 9.1.1) gives the quantities in the column marked (3) as estimated compressor demand. The row at the bottom giving total kWh savings was calculated based on a formula multiplying 1.7% times average dew point drop for each temperature bin times total hours in each bin. The result is an estimated kiloWatt-hour savings for each month. As is shown in Figure 61, annual savings for 1993 can be estimated as 6,700 kWh.

Therefore, for this heat pipe design, savings are expected to be small (using the estimates from the Duke Power study), and drops in specific humidity are expected to be within our margin of error. As is shown in the error calculations for specific humidity in Appendix D, the error based on manufacturers accuracies is dominated by the relative humidity sensor error, so a more accurate sensor would lower the error to within the expected savings range. The regression error, however, is 0.00045 lbw/lba, so in order for the error to remain below 0.0005, the sensor specific humidity error must be below 0.000025 lbw/lba, corresponding to about 0.25% of average conditions. A relative humidity sensor error of 0.2% will keep the specific humidity error below this level.

Summary

The importance of this thesis is that it is the most in depth study to date of supermarket heat pipe applications. It has become evident that energy savings from other studies could end up varying considerably from estimates, because the are so many variables between the extra condensation on cooling coils due to the installation of the heat pipe (which is proven given any dehumidification), and refrigeration compressor power reduction. This process is one of many new, creative ways to expand the fields of energy conservation in general, and demand side management in particular, to include non-standard measures. As the buildings targeted for DSM become saturated with the most energy efficient lighting, motors, and appliances, it is these custom measures which will become the focus of DSM planning.

References

References

1. Blatt, Morton H, "Conference Overview", Proceedings: Electric Dehumidification- State-of-the-art Humidity Control for Supermarkets Seminar, EPRI TR-101154 October 1992

2. Banks N.J., "Utilization of Condenser Heat for Dessicant Dehumidifiers in Supermarket Applications", Dessicant Cooling and Dehumidification, ASHRAE ISBN 0-910110-90-5, 1992

3. Khattar, Mukesh, "Humidity Control in Supermarkets Technologies and Economics", Proceedings: Electric Dehumidification- State-of-the-art Humidity Control for Supermarkets Seminar, EPRI TR-101154, October 1992

4. Keebaugh, D., "Heat Pipe Dehumidification System", EPRI TR-101154 Project 2569-14, October 1992

5. ASHRAE Handbook, 1993 Fundamentals, American Society of Heating Refrigeration and Air conditioning Engineers

6. EPRI CU-7379 Project 2569-9, "Supermarket Refrigeration Assessment for the Commonwealth Electric Company", Electric Power Research Institute, July 1991

7. EPRI CU-7378 Project 2569-8, "Supermarket Refrigeration Assessment for the New England Electric System", Electric Power Research Institute, July 1991

8. Thornton, Jeff W., "Supermarket Refrigeration Options", Thermal Storage Applications Research Center Report No. TSARC 91-1, Electric Power Research Institute, September 1991

9. Abrams, Donald and Wahler, Robert, "Evaluation of HVAC System with Enhanced Dehumidification Capacity", Prepared for Duke Power Company, April 15, 1992

10. Bittner, Robert, "Energy Use in Supermarkets", Proceedings: Electric Dehumidification- State-of-the-art Humidity Control for Supermarkets Seminar, EPRI TR-101154, October 1992

11. Hill, J.M. and Lau, A.S., "Performance of Supermarket Air-Conditioning Systems Equipped with Heat Pipe Heat Exchangers", ASHRAE Transactions v 99, 1993

12. Taylor,John R., "An Introduction to Error Analysis", University Science Books, Mill Valley, California, 1982

13. Olgyay, Victor, "Design with Climate", Princeton University Press, Princeton, N.J., 1963

14. Walker, D and Deming, G, "Supermarket Refrigeration Modeling and Field Demonstration", EPRI CU-6268 Project 2569-2, Electric Power Research Institute, March 1989

Appendix A: R-502 Properties

"FREON" 502 SATURATION

TEMP. °F	PRESSURE		VOLUME cu ft/lb		DENSITY lb/cu ft		ENTHALPY Btu/lb			ENTROPY Btu/(lb)(°R)		TEMP. °F
	PSIA	PSIG	LIQUID	VAPOR	LIQUID	VAPOR	LIQUID	LATENT	VAPOR	LIQUID	VAPOR	
70	152.32	137.62	0.012976	0.26769	77.051	3.7356	29.569	55.114	84.554	0.05978	0.16529	70
71	154.57	139.87	0.013003	0.26367	76.893	3.7933	29.359	55.176	84.636	0.06037	0.16523	71
72	156.84	142.15	0.013029	0.25961	76.737	3.8517	29.219	55.269	84.717	0.06085	0.16519	72
73	159.14	144.44	0.013056	0.25568	76.578	3.9110	29.539	55.258	84.798	0.06139	0.16512	73
74	161.46	146.77	0.013083	0.25181	76.429	3.9711	29.830	55.047	84.878	0.06192	0.16507	74
75	163.81	149.11	0.013111	0.24801	76.269	4.0319	30.122	54.835	84.958	0.06246	0.16502	75
76	166.18	151.49	0.013139	0.24428	76.109	4.0936	30.414	54.622	85.037	0.06299	0.16496	76
77	168.58	153.88	0.013167	0.24060	75.947	4.1561	30.706	54.408	85.115	0.06353	0.16491	77
78	171.00	156.30	0.013195	0.23699	75.784	4.2194	30.999	54.193	85.193	0.06406	0.16485	78
79	173.45	158.75	0.013223	0.23344	75.621	4.2836	31.292	53.977	85.270	0.06460	0.16480	79
80	175.92	161.22	0.013252	0.22995	75.457	4.3487	31.586	53.759	85.346	0.06513	0.16474	80
81	178.41	163.72	0.013281	0.22651	75.292	4.4146	31.880	53.541	85.421	0.06566	0.16469	81
82	180.94	166.24	0.013310	0.22313	75.126	4.4815	32.175	53.321	85.496	0.06620	0.16463	82
83	183.48	168.79	0.013340	0.21981	74.959	4.5492	32.470	53.100	85.570	0.06673	0.16458	83
84	186.06	171.36	0.013370	0.21654	74.791	4.6179	32.766	52.878	85.644	0.06726	0.16452	84
85	188.66	173.96	0.013400	0.21333	74.622	4.6874	33.062	52.654	85.717	0.06780	0.16446	85
86	191.28	176.59	0.013431	0.21017	74.453	4.7580	33.359	52.430	85.789	0.06833	0.16441	86
87	193.94	179.24	0.013462	0.20705	74.282	4.8295	33.656	52.204	85.860	0.06886	0.16435	87
88	196.62	181.92	0.013493	0.20399	74.111	4.9020	33.953	51.977	85.930	0.06939	0.16429	88
89	199.32	184.62	0.013524	0.20098	73.938	4.9755	34.251	51.748	86.000	0.06992	0.16423	89
90	202.05	187.36	0.013556	0.19801	73.764	5.0500	34.550	51.519	86.069	0.07045	0.16418	90
91	204.81	190.12	0.013588	0.19509	73.590	5.1255	34.849	51.288	86.137	0.07098	0.16412	91
92	207.60	192.90	0.013621	0.19222	73.414	5.2021	35.148	51.055	86.204	0.07151	0.16406	92
93	210.41	195.72	0.013654	0.18939	73.237	5.2798	35.448	50.822	86.271	0.07205	0.16400	93
94	213.25	198.56	0.013687	0.18661	73.059	5.3585	35.749	50.587	86.336	0.07258	0.16394	94
95	216.12	201.43	0.013721	0.18387	72.880	5.4384	36.050	50.350	86.401	0.07311	0.16388	95
96	219.02	204.32	0.013755	0.18117	72.700	5.5194	36.352	50.113	86.465	0.07364	0.16382	96
97	221.94	207.25	0.013789	0.17852	72.519	5.6015	36.654	49.874	86.528	0.07417	0.16375	97
98	224.90	210.20	0.013824	0.17590	72.336	5.6848	36.956	49.633	86.590	0.07470	0.16369	98
99	227.88	213.18	0.013859	0.17333	72.152	5.7693	37.259	49.391	86.651	0.07522	0.16363	99
100	230.89	216.19	0.013895	0.17079	71.967	5.8550	37.563	49.147	86.711	0.07575	0.16356	100
101	233.93	219.23	0.013931	0.16829	71.781	5.9419	37.867	48.902	86.770	0.07628	0.16350	101
102	237.00	222.30	0.013967	0.16583	71.593	6.0301	38.172	48.656	86.828	0.07681	0.16343	102
103	240.09	225.40	0.014004	0.16340	71.405	6.1196	38.477	48.407	86.885	0.07734	0.16337	103
104	243.22	228.52	0.014042	0.16101	71.214	6.2104	38.783	48.158	86.941	0.07787	0.16330	104
105	246.38	231.68	0.014079	0.15866	71.023	6.3026	39.090	47.906	86.997	0.07840	0.16323	105
106	249.56	234.87	0.014118	0.15634	70.829	6.3961	39.398	47.653	87.051	0.07893	0.16316	106
107	252.78	238.08	0.014157	0.15405	70.635	6.4910	39.705	47.398	87.103	0.07946	0.16309	107
108	256.02	241.33	0.014196	0.15180	70.439	6.5873	40.013	47.142	87.155	0.07998	0.16302	108
109	259.30	244.60	0.014236	0.14958	70.241	6.6851	40.322	46.883	87.206	0.08051	0.16295	109
110	262.61	247.91	0.014277	0.14739	70.042	6.7843	40.631	46.623	87.255	0.08104	0.16288	110
111	265.94	251.25	0.014318	0.14523	69.841	6.8851	40.942	46.361	87.303	0.08157	0.16281	111
112	269.31	254.62	0.014359	0.14311	69.639	6.9875	41.252	46.098	87.350	0.08210	0.16273	112
113	272.71	258.02	0.014401	0.14101	69.435	7.0914	41.564	45.832	87.396	0.08263	0.16265	113
114	276.15	261.45	0.014444	0.13894	69.229	7.1970	41.876	45.564	87.441	0.08316	0.16258	114
115	279.61	264.91	0.014488	0.13690	69.022	7.3042	42.189	45.294	87.484	0.08368	0.16250	115
116	283.10	268.41	0.014532	0.13489	68.812	7.4132	42.503	45.022	87.525	0.08421	0.16242	116
117	286.63	271.94	0.014576	0.13290	68.601	7.5239	42.817	44.748	87.566	0.08474	0.16234	117
118	290.19	275.50	0.014622	0.13095	68.388	7.6364	43.132	44.472	87.605	0.08527	0.16225	118
119	293.78	279.09	0.014668	0.12902	68.173	7.7507	43.448	44.194	87.642	0.08580	0.16217	119
120	297.41	282.71	0.014715	0.12711	67.956	7.8669	43.765	43.913	87.678	0.08633	0.16208	120
121	301.07	286.37	0.014762	0.12523	67.737	7.9850	44.082	43.630	87.713	0.08686	0.16199	121
122	304.76	290.06	0.014811	0.12337	67.515	8.1052	44.401	43.344	87.746	0.08739	0.16190	122
123	308.49	293.79	0.014860	0.12154	67.292	8.2274	44.720	43.056	87.777	0.08792	0.16181	123
124	312.25	297.55	0.014910	0.11973	67.066	8.3516	45.040	42.766	87.807	0.08845	0.16172	124

Table A-1. Freon 502 Saturation Properties.

TABLE II "FREON" 502 SUPERHEATED VAPOR—CONSTANT PRESSURE TABLES AT SATURATION TEMPERATURE INTERVALS

V = volume, cu ft/lb; H = enthalpy, Btu/lb; S = entropy, Btu/(lb)(°F)

Sat.	SATURATION TEMPERATURE, °F												Sat.
psia	−20			−19			−18			−17			psia
psig	15.01			15.68			16.35			17.03			psig
TEMP. °F	V	H	S	V	H	S	V	H	S	V	H	S	TEMP. °F
−20	1.3172	75.442	0.17178	—	—	—	—	—	—	—	—	—	−20
−10	1.3543	76.996	0.17527	1.3227	76.958	0.17482	1.2919	76.919	0.17437	1.2619	76.879	0.17391	−10
0	1.3911	78.561	0.17872	1.3587	78.525	0.17827	1.3273	78.488	0.17782	1.2966	78.451	0.17737	0
10	1.4274	80.137	0.18211	1.3944	80.103	0.18166	1.3623	80.069	0.18122	1.3310	80.033	0.18077	10
20	1.4634	81.725	0.18545	1.4297	81.693	0.18501	1.3969	81.661	0.18457	1.3650	81.627	0.18413	20
30	1.4992	83.325	0.18876	1.4648	83.295	0.18832	1.4313	83.264	0.18788	1.3987	83.233	0.18745	30
40	1.5346	84.938	0.19202	1.4995	84.910	0.19158	1.4653	84.881	0.19115	1.4321	84.851	0.19072	40
50	1.5698	86.564	0.19524	1.5340	86.537	0.19481	1.4992	86.510	0.19438	1.4653	86.481	0.19395	50
60	1.6048	88.203	0.19842	1.5683	88.178	0.19799	1.5328	88.151	0.19757	1.4982	88.124	0.19714	60
70	1.6395	89.856	0.20157	1.6024	89.831	0.20115	1.5662	89.806	0.20072	1.5310	89.780	0.20030	70
80	1.6741	91.521	0.20469	1.6363	91.498	0.20426	1.5994	91.474	0.20384	1.5635	91.450	0.20342	80
90	1.7086	93.200	0.20777	1.6700	93.178	0.20735	1.6324	93.155	0.20693	1.5959	93.132	0.20651	90
100	1.7428	94.892	0.21082	1.7036	94.871	0.21040	1.6653	94.849	0.20998	1.6281	94.827	0.20956	100
110	1.7770	96.598	0.21384	1.7370	96.578	0.21342	1.6981	96.557	0.21301	1.6602	96.536	0.21259	110
120	1.8110	98.318	0.21683	1.7703	98.298	0.21642	1.7307	98.278	0.21600	1.6922	98.258	0.21559	120
130	1.8449	100.051	0.21980	1.8035	100.032	0.21938	1.7632	100.013	0.21897	1.7240	99.994	0.21855	130
140	1.8786	101.797	0.22274	1.8366	101.779	0.22232	1.7956	101.761	0.22191	1.7558	101.743	0.22150	140
150	1.9123	103.557	0.22565	1.8696	103.540	0.22523	1.8279	103.522	0.22482	1.7874	103.505	0.22441	150
160	1.9459	105.330	0.22853	1.9025	105.314	0.22812	1.8601	105.297	0.22771	1.8190	105.280	0.22730	160
170	1.9794	107.117	0.23139	1.9353	107.101	0.23098	1.8923	107.085	0.23057	1.8504	107.069	0.23016	170
180	2.0129	108.917	0.23423	1.9680	108.902	0.23382	1.9243	108.886	0.23341	1.8818	108.870	0.23300	180
190	2.0462	110.730	0.23704	2.0006	110.715	0.23663	1.9563	110.700	0.23622	1.9131	110.685	0.23582	190
200	2.0795	112.556	0.23983	2.0332	112.542	0.23942	1.9882	112.527	0.23901	1.9444	112.513	0.23861	200
210	2.1127	114.395	0.24260	2.0658	114.382	0.24219	2.0201	114.368	0.24178	1.9756	114.353	0.24138	210
220	2.1459	116.247	0.24534	2.0982	116.234	0.24493	2.0518	116.220	0.24453	2.0067	116.207	0.24412	220
230	2.1790	118.112	0.24806	2.1307	118.099	0.24766	2.0836	118.086	0.24725	2.0378	118.073	0.24685	230
240	2.2121	119.989	0.25077	2.1630	119.977	0.25036	2.1153	119.964	0.24996	2.0688	119.951	0.24955	240
250	2.2451	121.879	0.25345	2.1953	121.867	0.25304	2.1469	121.855	0.25264	2.0998	121.842	0.25224	250
260	2.2781	123.781	0.25611	2.2276	123.770	0.25571	2.1785	123.758	0.25530	2.1307	123.746	0.25490	260
270	2.3110	125.696	0.25875	2.2599	125.685	0.25835	2.2101	125.673	0.25794	2.1616	125.662	0.25754	270
280	2.3439	127.623	0.26138	2.2921	127.612	0.26097	2.2416	127.601	0.26057	2.1924	127.589	0.26017	280
290	2.3768	129.561	0.26398	2.3242	129.551	0.26357	2.2731	129.540	0.26317	2.2233	129.529	0.26277	290
Sat.	−16			−15			−14			−13			Sat.
psia	32.76			33.48			34.21			34.95			psia
psig	18.07			18.78			19.52			20.26			psig
TEMP. °F	V	H	S	V	H	S	V	H	S	V	H	S	TEMP. °F
−10	1.2327	76.839	0.17346	1.2042	76.797	0.17301	1.1766	76.755	0.17256	1.1496	76.712	0.17210	−10
0	1.2668	78.413	0.17692	1.2377	78.374	0.17647	1.2095	78.334	0.17603	1.1819	78.294	0.17558	0
10	1.3005	79.998	0.18033	1.2708	79.961	0.17989	1.2420	79.924	0.17945	1.2138	79.886	0.17901	10
20	1.3339	81.594	0.18369	1.3036	81.559	0.18326	1.2741	81.524	0.18282	1.2454	81.488	0.18239	20
30	1.3669	83.201	0.18701	1.3360	83.169	0.18658	1.3060	83.135	0.18615	1.2767	83.101	0.18571	30
40	1.3997	84.821	0.19029	1.3682	84.790	0.18986	1.3375	84.758	0.18943	1.3076	84.726	0.18900	40
50	1.4323	86.453	0.19352	1.4001	86.423	0.19309	1.3688	86.394	0.19267	1.3383	86.363	0.19224	50
60	1.4646	88.097	0.19671	1.4318	88.069	0.19629	1.3999	88.041	0.19587	1.3688	88.012	0.19545	60
70	1.4967	89.755	0.19987	1.4633	89.728	0.19945	1.4308	89.701	0.19903	1.3991	89.674	0.19861	70
80	1.5286	91.425	0.20300	1.4946	91.400	0.20258	1.4614	91.374	0.20216	1.4292	91.348	0.20174	90
90	1.5603	93.108	0.20609	1.5257	93.084	0.20567	1.4920	93.060	0.20526	1.4591	93.035	0.20484	80
100	1.5919	94.805	0.20915	1.5566	94.782	0.20873	1.5223	94.759	0.20832	1.4889	94.735	0.20791	100
110	1.6234	96.515	0.21218	1.5875	96.493	0.21176	1.5525	96.470	0.21135	1.5185	96.448	0.21094	110
120	1.6547	98.238	0.21517	1.6182	98.217	0.21476	1.5826	98.195	0.21435	1.5480	98.174	0.21394	120
130	1.6859	99.974	0.21814	1.6487	99.954	0.21773	1.6126	99.934	0.21732	1.5774	99.913	0.21692	130
140	1.7170	101.724	0.22109	1.6792	101.704	0.22068	1.6424	101.685	0.22027	1.6066	101.665	0.21986	140
150	1.7480	103.486	0.22400	1.7096	103.468	0.22359	1.6722	103.449	0.22319	1.6358	103.430	0.22278	150
160	1.7789	105.263	0.22689	1.7399	105.245	0.22648	1.7019	105.227	0.22608	1.6649	105.208	0.22568	160
170	1.8097	107.052	0.22975	1.7700	107.035	0.22935	1.7314	107.017	0.22895	1.6938	107.000	0.22854	170
180	1.8404	108.854	0.23259	1.8002	108.838	0.23219	1.7609	108.821	0.23179	1.7227	108.804	0.23139	180
190	1.8711	110.669	0.23541	1.8302	110.654	0.23501	1.7904	110.637	0.23461	1.7516	110.621	0.23421	190
200	1.9017	112.498	0.23820	1.8602	112.482	0.23780	1.8197	112.467	0.23740	1.7803	112.451	0.23700	200
210	1.9323	114.339	0.24097	1.8901	114.324	0.24057	1.8490	114.309	0.24017	1.8090	114.294	0.23977	210
220	1.9627	116.193	0.24372	1.9199	116.178	0.24332	1.8783	116.164	0.24292	1.8377	116.149	0.24252	220
230	1.9932	118.059	0.24645	1.9497	118.045	0.24605	1.9074	118.031	0.24565	1.8663	118.017	0.24525	230
240	2.0235	119.938	0.24915	1.9795	119.925	0.24875	1.9366	119.911	0.24835	1.8948	119.898	0.24796	240
250	2.0539	121.830	0.25184	2.0092	121.817	0.25144	1.9657	121.804	0.25104	1.9233	121.790	0.25065	250
260	2.0842	123.734	0.25450	2.0388	123.721	0.25410	1.9947	123.708	0.25371	1.9517	123.695	0.25331	260
270	2.1144	125.650	0.25714	2.0685	125.637	0.25675	2.0237	125.625	0.25635	1.9802	125.613	0.25596	270
280	2.1446	127.578	0.25977	2.0980	127.566	0.25937	2.0527	127.554	0.25898	2.0085	127.542	0.25858	280
290	2.1748	129.518	0.26237	2.1276	129.506	0.26198	2.0816	129.495	0.26158	2.0369	129.483	0.26119	290
300	2.2049	131.469	0.26496	2.1571	131.458	0.26456	2.1105	131.447	0.26417	2.0652	131.436	0.26378	300

Table A-2. Freon 502 Superheated Vapor-- Constant Pressure Tables at Saturation Temperature Intervals.

TABLE II "FREON" 502 SUPERHEATED VAPOR—CONSTANT PRESSURE TABLES AT SATURATION TEMPERATURE INTERVALS

V = volume, cu ft/lb; H = enthalpy, Btu/lb; S = entropy, Btu/(lb)(°F)

SATURATION TEMPERATURE, °F

Sat. psia / psig / TEMP. °F	−28 V	−28 H	−28 S	−27 V	−27 H	−27 S	−26 V	−26 H	−26 S	−25 V	−25 H	−25 S	Sat. psia / psig / TEMP. °F
	15.03			15.67			16.31			16.97			
	0.34			0.97			1.62			2.28			
−20	1.5979	75.739	0.17549	1.5593	75.705	0.17502	1.5218	75.670	0.17456	1.4853	75.634	0.17409	−20
−10	1.6413	77.275	0.17894	1.6018	77.243	0.17848	1.5635	77.210	0.17802	1.5262	77.176	0.17756	−10
0	1.6843	78.824	0.18235	1.6440	78.793	0.18189	1.6048	78.762	0.18143	1.5667	78.730	0.18098	0
10	1.7269	80.385	0.18571	1.6857	80.356	0.18525	1.6457	80.327	0.18480	1.6068	80.297	0.18435	10
20	1.7692	81.959	0.18903	1.7272	81.932	0.18857	1.6863	81.904	0.18813	1.6465	81.876	0.18768	20
30	1.8112	83.547	0.19230	1.7683	83.521	0.19185	1.7266	83.495	0.19141	1.6860	83.468	0.19096	30
40	1.8530	85.149	0.19554	1.8092	85.124	0.19509	1.7666	85.099	0.19465	1.7252	85.074	0.19421	40
50	1.8945	86.764	0.19874	1.8498	86.741	0.19830	1.8064	86.717	0.19786	1.7642	86.693	0.19742	50
60	1.9358	88.393	0.20191	1.8903	88.371	0.20146	1.8460	88.348	0.20103	1.8030	88.325	0.20059	60
70	1.9769	90.036	0.20504	1.9305	90.015	0.20460	1.8854	89.994	0.20416	1.8415	89.972	0.20373	70
80	2.0178	91.693	0.20814	1.9705	91.673	0.20770	1.9246	91.653	0.20726	1.8799	91.632	0.20683	80
90	2.0586	93.364	0.21120	2.0104	93.345	0.21077	1.9636	93.325	0.21034	1.9181	93.306	0.20990	90
100	2.0992	95.049	0.21424	2.0502	95.031	0.21381	2.0025	95.012	0.21338	1.9562	94.993	0.21295	100
110	2.1396	96.748	0.21725	2.0898	96.731	0.21682	2.0413	96.713	0.21639	1.9941	96.695	0.21596	110
120	2.1800	98.462	0.22023	2.1292	98.445	0.21980	2.0799	98.428	0.21937	2.0319	98.410	0.21895	120
130	2.2202	100.189	0.22319	2.1686	100.172	0.22276	2.1184	100.156	0.22233	2.0696	100.139	0.22190	130
140	2.2604	101.929	0.22611	2.2079	101.914	0.22569	2.1568	101.898	0.22526	2.1072	101.882	0.22483	140
150	2.3004	103.684	0.22902	2.2470	103.669	0.22859	2.1951	103.654	0.22816	2.1447	103.639	0.22774	150
160	2.3403	105.453	0.23189	2.2861	105.438	0.23147	2.2334	105.424	0.23104	2.1821	105.409	0.23062	160
170	2.3802	107.235	0.23475	2.3251	107.221	0.23432	2.2715	107.207	0.23390	2.2194	107.192	0.23347	170
180	2.4200	109.030	0.23757	2.3640	109.017	0.23715	2.3095	109.003	0.23673	2.2566	108.990	0.23631	180
190	2.4597	110.839	0.24038	2.4028	110.826	0.23996	2.3475	110.813	0.23953	2.2938	110.800	0.23911	190
200	2.4993	112.661	0.24316	2.4416	112.649	0.24274	2.3855	112.636	0.24232	2.3309	112.624	0.24190	200
210	2.5389	114.497	0.24593	2.4803	114.485	0.24550	2.4233	114.473	0.24508	2.3679	114.460	0.24466	210
220	2.5785	116.345	0.24867	2.5190	116.334	0.24824	2.4611	116.322	0.24782	2.4049	116.310	0.24741	220
230	2.6179	118.207	0.25138	2.5576	118.196	0.25096	2.4989	118.184	0.25054	2.4418	118.173	0.25013	230
240	2.6574	120.081	0.25408	2.5961	120.070	0.25366	2.5366	120.059	0.25324	2.4787	120.048	0.25283	240
250	2.6967	121.968	0.25676	2.6346	121.958	0.25634	2.5742	121.947	0.25592	2.5155	121.936	0.25550	250
260	2.7361	123.868	0.25942	2.6731	123.858	0.25900	2.6119	123.847	0.25858	2.5523	123.837	0.25816	260
270	2.7754	125.780	0.26206	2.7115	125.770	0.26164	2.6494	125.760	0.26122	2.5890	125.750	0.26080	270
280	2.8146	127.704	0.26468	2.7499	127.694	0.26426	2.6870	127.685	0.26384	2.6258	127.675	0.26342	280
290	2.8539	129.640	0.26728	2.7883	129.631	0.26686	2.7245	129.621	0.26644	2.6624	129.612	0.26603	290

Sat. psia / psig / TEMP. °F	−24 V	−24 H	−24 S	−23 V	−23 H	−23 S	−22 V	−22 H	−22 S	−21 V	−21 H	−21 S	Sat. psia / psig / TEMP. °F
	27.43			28.06			28.70			29.35			
	12.74			13.36			14.00			14.65			
−20	1.4498	75.597	0.17363	1.4153	75.559	0.17316	1.3817	75.521	0.17270	1.3490	75.482	0.17224	−20
−10	1.4899	77.141	0.17710	1.4546	77.106	0.17664	1.4203	77.070	0.17619	1.3868	77.034	0.17573	−10
0	1.5296	78.698	0.18052	1.4935	78.664	0.18007	1.4584	78.631	0.17962	1.4243	78.596	0.17917	0
10	1.5689	80.266	0.18390	1.5321	80.235	0.18345	1.4962	80.203	0.18300	1.4613	80.170	0.18255	10
20	1.6079	81.847	0.18723	1.5703	81.817	0.18678	1.5337	81.787	0.18634	1.4981	81.756	0.18590	20
30	1.6466	83.441	0.19052	1.6082	83.413	0.19008	1.5708	83.384	0.18963	1.5345	83.355	0.18919	30
40	1.6850	85.048	0.19377	1.6458	85.021	0.19333	1.6077	84.994	0.19289	1.5707	84.967	0.19245	40
50	1.7231	86.668	0.19698	1.6832	86.643	0.19654	1.6444	86.617	0.19611	1.6066	86.591	0.19567	50
60	1.7611	88.302	0.20015	1.7204	88.278	0.19972	1.6808	88.253	0.19929	1.6423	88.229	0.19885	60
70	1.7989	89.949	0.20329	1.7574	89.926	0.20286	1.7170	89.903	0.20243	1.6778	89.880	0.20200	70
80	1.8364	91.610	0.20640	1.7942	91.589	0.20597	1.7531	91.567	0.20554	1.7131	91.544	0.20511	80
90	1.8739	93.285	0.20947	1.8308	93.264	0.20905	1.7889	93.243	0.20862	1.7482	93.222	0.20819	90
100	1.9111	94.974	0.21252	1.8673	94.954	0.21209	1.8247	94.934	0.21167	1.7832	94.913	0.21124	100
110	1.9483	96.676	0.21553	1.9036	96.657	0.21511	1.8603	96.638	0.21468	1.8180	96.618	0.21426	110
120	1.9853	98.392	0.21852	1.9399	98.374	0.21810	1.8957	98.356	0.21767	1.8528	98.337	0.21725	120
130	2.0221	100.122	0.22148	1.9760	100.105	0.22106	1.9311	100.087	0.22064	1.8874	100.069	0.22022	130
140	2.0589	101.866	0.22441	2.0120	101.849	0.22399	1.9663	101.832	0.22357	1.9219	101.815	0.22315	140
150	2.0956	103.623	0.22732	2.0479	103.607	0.22690	2.0014	103.591	0.22648	1.9563	103.574	0.22606	150
160	2.1322	105.394	0.23020	2.0837	105.378	0.22978	2.0365	105.363	0.22936	1.9906	105.347	0.22895	160
170	2.1687	107.178	0.23305	2.1194	107.163	0.23264	2.0715	107.148	0.23222	2.0248	107.133	0.23180	170
180	2.2051	108.976	0.23589	2.1551	108.961	0.23547	2.1064	108.947	0.23505	2.0590	108.932	0.23464	180
190	2.2415	110.787	0.23870	2.1906	110.773	0.23828	2.1412	110.759	0.23786	2.0930	110.745	0.23745	190
200	2.2778	112.611	0.24148	2.2261	112.597	0.24107	2.1759	112.584	0.24065	2.1271	112.570	0.24024	200
210	2.3140	114.448	0.24425	2.2616	114.435	0.24383	2.2106	114.422	0.24342	2.1610	114.409	0.24301	210
220	2.3502	116.298	0.24699	2.2970	116.286	0.24657	2.2452	116.273	0.24616	2.1949	116.260	0.24575	220
230	2.3863	118.161	0.24971	2.3323	118.149	0.24930	2.2798	118.137	0.24888	2.2287	118.125	0.24847	230
240	2.4224	120.037	0.25241	2.3676	120.025	0.25200	2.3143	120.013	0.25158	2.2625	120.002	0.25117	240
250	2.4584	121.925	0.25509	2.4029	121.914	0.25468	2.3488	121.903	0.25427	2.2963	121.891	0.25386	250
260	2.4944	123.826	0.25775	2.4381	123.815	0.25734	2.3833	123.804	0.25693	2.3300	123.793	0.25652	260
270	2.5303	125.739	0.26039	2.4732	125.729	0.25998	2.4177	125.718	0.25957	2.3636	125.707	0.25916	270
280	2.5662	127.665	0.26301	2.5083	127.654	0.26260	2.4520	127.644	0.26219	2.3972	127.633	0.26178	280
290	2.6021	129.602	0.26561	2.5434	129.592	0.26520	2.4864	129.582	0.26479	2.4308	129.572	0.26438	290

Table A-3. Freon 502 Superheated Vapor-- Constant Pressure Tables at Saturation Temperature Intervals.

Appendix B: Equipment Specifications

CAMPBELL SCIENTIFIC OV6.1 SPECIFICATIONS 21X MICROLOGGER

The following electrical specifications are valid for an ambient temperature range of -25 deg. C to +50 deg. C unless otherwise specified

ANALOG INPUTS

NUMBER OF CHANNELS: 8 differential or up to 16 single ended using one differential channel for each two single ended channels.

CHANNEL EXPANDABILITY: The Model AM32 Relay Scanner multiplexes 32 differential channels through a single 21X differential channel. Up to 6 AM32 scanners can be added for a total of 192 additional analog channels.

VOLTAGE MEASUREMENT TYPES: Single-ended or differential. A thermistor at the input terminals provides reference junction compensation for thermocouple measurements.

ACCURACY OF VOLTAGE MEASUREMENTS AND ANALOG OUTPUT VOLTAGES: 0.1% of FSR, 0.05% of FSR (0 to 40 deg. C).

RANGE AND RESOLUTION: Ranges are software selectable for any channel. Resolution for single ended measurements is twice the value shown.

Full Scale Range	Resolution
±5 volts	333 microvolts
±0.5 volts	33.3 microvolts
±50 millivolts	3.33 microvolts
±15 millivolts	1 microvolt
±5 millivolts	0.33 microvolts

INPUT SAMPLE RATES: The fast A-D conversion uses a 250us signal integration time and the slow conversion uses a 16.666ms signal integration time (one power line cycle period). Differential measurements include a second sampling with reversed input polarity to reduce thermal offset and common mode errors. The following intervals do not include the self-calibration measurement which occurs once per instruction. Input sample rates should not be confused with system data throughput rates.

Fast single-ended voltage:
2.4 milliseconds/channel
Fast differential voltage:
3.7 milliseconds/channel
Slow single-ended voltage:
18.8 milliseconds/channel
Slow differential voltage
37.0 milliseconds/channel
Fast differential thermocouple
7.3 milliseconds/channel

INPUT NOISE VOLTAGE:
Fast differential — 0.63 microvolts RMS
Slow differential — 0.1 microvolts RMS

COMMON MODE RANGE: ±5 volts

DC COMMON MODE REJECTION: >100 dB

NORMAL MODE REJECTION: 70 dB (60 Hz with slow differential measurement)

INPUT CURRENT: 2 nanoamps max.

INPUT RESISTANCE: 200 gigohms

ANALOG OUTPUTS

NUMBER OF ANALOG OUTPUTS: 4 switched, 2 continuous

DESCRIPTION: Switched and continuous. A switched output is active only during a measurement and is switched off (high impedance) immediately following the measurement. Only one switched output can be active at any one time. The 2 continuous outputs hold a preset voltage until updated by an analog output command.

RANGE: ±5 volts

RESOLUTION: 0.67 millivolts

ACCURACY: Same as voltage input

OUTPUT CURRENT:
Switched: 20 mA @ ±5V, 50 mA @ ±2.5 V
Continuous: same @ -V, 5 mA @ +V

RESISTANCE AND CONDUCTIVITY MEASUREMENTS

ACCURACY: 0.035% (0.02% 0 to 40 deg. C) of full scale of bridge output provided the matching bridge resistors are not the limiting factor. The excitation voltage should be programmed to match the bridge output with a full scale input voltage range.

MEASUREMENT TYPES: 6 wire full bridge, 4 wire full bridge, 4 wire, 3 wire and 2 wire half bridge. High accuracy low impedance bridge measurements are ratiometric with dual polarity measurements of excitation and output to eliminate thermal emfs. AC resistance and conductivity measurements use a 750us excitation pulse with the signal integration occurring over the last 250us. An equal duration pulse of opposite polarity is applied for ionic depolarization.

PULSE COUNTERS

NUMBER OF PULSE COUNTER CHANNELS: 4 eight bit or 2 sixteen bit, software selectable

MAXIMUM COUNT RATE: 2550 Hz eight bit counters; 250 kHz, sixteen bit counters. Pulse counter channels are scanned at a maximum rate of 10 Hz.

MODES: Programmable modes are switch closure, high frequency pulse and low level AC.

SWITCH CLOSURE MODE
MINIMUM SWITCH CLOSED TIME
3 milliseconds
MINIMUM SWITCH OPEN TIME
4 milliseconds
MAXIMUM BOUNCE TIME
1 millisecond open without being counted.

HIGH FREQUENCY PULSE MODE
MINIMUM PULSE WIDTH:
2 microseconds
MAXIMUM INPUT FREQUENCY:
250 kilohertz
VOLTAGE THRESHOLDS
The count is incremented when the input voltage changes from below 1.5 volts to above 3.5 volts
MAXIMUM INPUT VOLTAGE:
±20 volts

LOW LEVEL AC MODE
This mode is used for counting frequency of AC signals from magnetic pulse flow transducers or other low voltage, sine wave outputs.

MINIMUM AC INPUT VOLTAGE
6 millivolts RMS
INPUT HYSTERESIS
11 millivolts
MAXIMUM AC INPUT VOLTAGE:
20 volts RMS
FREQUENCY RANGE

AC Input Voltage (RMS)	Range
20 millivolts	1 Hz to 100 Hz
60 millivolts	0.5 Hz to 100 Hz
150 millivolts to 20 volts	0.3 Hz to 1000 Hz

(consult factory if higher frequencies are desired)

DIGITAL CONTROL OUTPUTS

The 21X provides 8 digital control outputs that can be set or reset on command.

OUTPUT VOLTAGES
(nominal) high — 5 volts ± 1 volt
low — 0 volt

OUTPUT RESISTANCE
400 ohms

TRANSIENT PROTECTION

All input and output connections are protected using spark gaps connected directly to a heavy copper on the circuit card between the two input terminals. The 12 volt power input and charger inputs are protected with transzorbs.

CPU AND INTERFACE

PROCESSOR: HITACHI 6303 CMOS 8 bit microprocessor

MEMORY: 16K ROM, 40K RAM, expandable to 24K ROM with an extended software option. Standard 21X stores 19,328 low resolution data points in Final Memory.

DISPLAY: 8 digit LCD (0.5" digits)

PERIPHERAL INTERFACE: 9 pin D-type connector on the panel for connection to cassette recorder, modem, printer, or RS232 adapter. The serial interface can be programmed for baud rates of 300, 1200, 9600 and 76,800.

CLOCK ACCURACY: ± 1 minute per month

MAXIMUM PROGRAM EXECUTION RATE: The 21X Programming Table can be executed in sync with real time at a maximum rate of 80 per second. Typical throughput rates allow 1 measurement with linear scaling and transfer to tape at this rate with no interruption.

SYSTEM THROUGHPUT: Data throughput is the rate at which a signal can be measured, processed and stored in Final Memory. The rate is reduced by additional processing or when data is transferred to Cassette Tape or through the 21X serial port.

Throughput to the cassette tape is 100 data values per second. During tape transfer 2[illegible] the CPU's time is required. Therefore program execution is uninterrupted if the user's program requires less than 75% of the CPU time.

ASCII data values (10 characters per value) can be transmitted via the serial port at 9600 baud with a throughput of approximately 100 values per second with 15% CPU utilization. Faster throughput rates are possible if CSI's binary format is transmitted (consult factory).

Each time a new measurement instruction is specified, time for two additional measurements is required for self-calibration. Therefore using more repetitions in fewer instructions increases throughput.

SYSTEM POWER REQUIREMENTS

VOLTAGE: 9.6 to 15 volts

TYPICAL CURRENT DRAIN: 1.0 mA quiescent, 25 mA during processing, and 60 mA during analog measurement.

INTERNAL BATTERIES: 8 Alkaline D cells with 7 amp-hour capacity. The Model 21XL includes sealed lead acid batteries with 2.5 amp hour capacity per charge.

EXTERNAL BATTERIES: Any 12 volt external battery can be connected as a primary power source with the internal batteries providing backup while changing external batteries.

OPERATION FROM OTHER SOURCES: The Model 21XL includes a battery charging circuit that can be connected to 15 to 30 VDC indefinitely to maintain a full charge on the batteries without degradation. The charging circuit includes temperature compensation for maintaining optimum charging voltage at temperature extremes. A 110 VAC to 15 VDC wall transformer is provided with the 21XL.

PHYSICAL SPECIFICATIONS

SIZE: 8.2" X 5.7" X 3.3" (input terminal strips extend 0.45" above the panel surface)

WEIGHT: 6.2 lbs.

Printed January 1989
Copyright © 1988

In Europe: K-Flow ApS, Hasselvangen 27, DK-2970 Grow Skovd, Denmark. Phone 45 42 891 900, FAX 45 42 890 366

SUPPLEMENTAL SPECIFICATION SHEET

MODEL NUMBER GW5-006CX959

THIS MODEL HAS THE SAME SPECIFICATIONS AS MODEL GW5-006CX5

WITH THE FOLLOWING REQUESTED CHANGES.

SPECIFICATION CHANGES:

Input		
Current Range: (Using the supplied, external, current transformers)		0-37.5A
Over-Range:	With linearity	45A
	W/O damage	75A
Output		
Scaling:		0-5V = 0-30KW Input
Accuracy:		± 0.25% F.S.

REMARKS:
Supplied with 2 pieces #13747 current transformers.

ALL SPECIFICATIONS LISTED FOR STANDARD MODEL NUMBER WILL APPLY EXCEPT FOR CHANGES LISTED ABOVE.

OHIO SEMITRONICS, INC. [illegible]
TO PLACE AN ORDER: 1-800-537-6732

FLOW SENSOR SPECIFICATIONS

- ***Wetted Parts:*** 316L Stainless Steel & Hastelloy™ C-22
  Non Wetted Parts - 304 Stainless Steel
- ***Welding Procedures:*** Automatic tube weld, no filler metals used
- ***Accuracy:*** ± 0.2% of rate ± zero stability value
- ***Operating Temperature:*** -400°F (-240°C) to 400°F (204°C)
- ***Operating Pressure:*** 1800 - 2000 psi (higher ratings available)
- ***Flow Range:*** From 0 - 2500#/minute
- ***Process Connections:*** ANSI, DIN, Sanitary, NPT
- ***FM & CSA Approvals:*** K2 through K100 - Class I, Div. 1, Groups A, B, C, & D, K250 through K2500 - Class I, Div. 1, Groups C & D. All flow sensors - Class II, Groups E & F
- ***CENELEC Approval:*** All flow sensors - CENELEC EEx ib IIb T2
- ***Transmitter Approval:*** Class I, Div. 2, Groups A, B, C, & D
- ***Options:*** Rupture disk, secondary enclosures, insulation jacket and heat kit

FLOW SENSOR FEATURES

- Direct mass flow measurement
- Density measurement
- Non intrusive sensor in hermetically sealed case
- Larger O.D., heavy wall sensor tubes
- No moving parts, no fouling or plugging
- Low pressure drop design
- Low stress on sensor tubes
- Completely independent of temperature, pressure, density, viscosity flow profile or air entrainment

Model No.	K2	K20	K100	K250	K500	K2500
Sizes: In./ANSI 150#:	¼" NPT	½"	½"	1"	1"	2"
mm/DIN:		DN15	DN15	DN25	DN25	DN50
Typical Flow Range:						
lbs/min	0-2	0-20	0-100	0-250	0-500	0-2500
kg/min	0-1	0-9.09	0-45.45	0-113	0-227	0-1136
Density Accuracy: g/cc	±0.015	±0.003	±0.0010	±0.0010	±0.0005	±0.0005
Zero Stability:						
lbs/min	0.0002	0.004	0.015	0.03	0.1	0.32
kg/min	0.0001	0.002	0.007	0.014	0.05	0.15

Mass flow accuracy: 0.2% ± zero stability — Repeatability: 0.1%

SPECIFICATIONS: SERIES 1200 TRANSMITTER

- ***Housing Material:*** Epoxy coated diecast aluminum
- ***Power:*** 115/230 VAC, 50/60 Hz ± 10%, 24 VDC, 13 watts
- ***Temperature Range:*** 20°F (-7°C) to 140°F (60°C)
- ***Housing Rating:*** NEMA 4 design
- ***Area Rating:*** Class I, Division II, Groups A, B, C & D

USER INPUT & OUTPUT

- 2, 4-20 mA outputs
- 1 frequency/pulse output
- RS 232/485 communications
- 2 relay outputs
- 2 status lines out
- 2 contact closure inputs

SERIES 1200 TRANSMITTER FEATURES

- Mass flow
- Volumetric flow
- Mass & Volumetric totalization
- Batching (multi-mode)
- PID
- % Solids/Liquids/Mass
- Temperature
- Density
- Micro processor based electronics
- Two line, 16 character each display
- Full system diagnostics display
- Keyboard programmability
- Keyboard selection and scaling of all outputs
- One button zeroing

95515

Hastelloy™ is a registered trademark of Haynes International, Inc.

Factory Mutual Approved

K-FLOW

K-Flow Corporation
P.O. Box 849
Millville Airport • Millville, NJ 08332
Phone 1-800-635-5569 • or 1-609-825-FLOW
FAX 1-609-825-1616

In Europe: K-Flow APS, Maarslevvej 37, DK-2630 Taastrup, Denmark, Phone 45 43 99 11 00, FAX 45 43 99 20 66

SUPPLEMENTAL SPECIFICATION SHEET

MODEL NUMBER GW5-006EGX958

THIS MODEL HAS THE SAME SPECIFICATIONS AS MODEL GW5-006EG

WITH THE FOLLOWING REQUESTED CHANGES.

SPECIFICATION CHANGES:

Input	
Current Range: (Using the supplied, external, current transformers)	0-100A
Over-Range: (W/O damage)	200A
Output	
Scaling:	4-20mA = 0-80KW Input
Accuracy:	± 0.25% F.S.

REMARKS:

Supplied with 2 pieces #13747 current transformers.

ALL SPECIFICATIONS LISTED FOR STANDARD MODEL NUMBER WILL APPLY EXCEPT FOR CHANGES LISTED ABOVE.

OHIO SEMITRONICS, INC. 1205 CHESAPEAKE AVENUE COLUMBUS OHIO 43212-2981
PHONE (614) 486-4451 FAX (614) 486-0643
TO PLACE AN ORDER: 1-800-537-6732

SUPPLEMENTAL SPECIFICATION SHEET

MODEL NUMBER GW5-006CX957

THIS MODEL HAS THE SAME SPECIFICATIONS AS MODEL GW5-006CX5

WITH THE FOLLOWING REQUESTED CHANGES.

SPECIFICATION CHANGES:

Input

Current Range:
(Using the supplied, external, current transformers) 0-56A

Over-Range: With linearity 65A
W/O damage 112A

Output

Scaling: 0-5V = 0-45KW Input

Accuracy: ± 0.25% F.S.

REMARKS:

Supplied with 2 pieces #13747 current transformers.

ALL SPECIFICATIONS LISTED FOR STANDARD MODEL NUMBER WILL APPLY EXCEPT FOR CHANGES LISTED ABOVE.

OHIO SEMITRONICS, INC. [illegible] TO PLACE AN ORDER: 1-

Relative Humidity/ Temperature Transmitter

HX10 Series

MADE IN USA

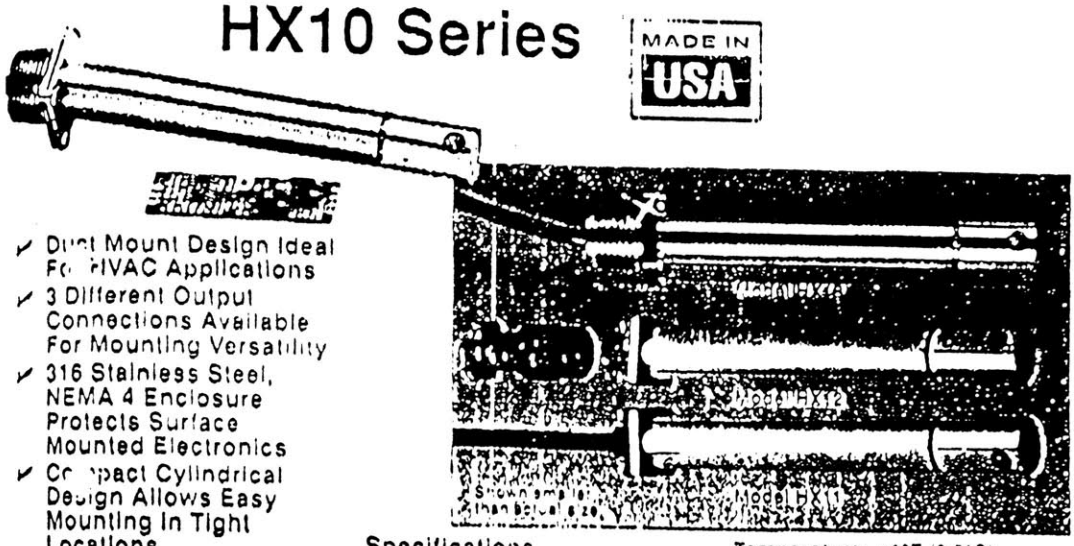

- Duct Mount Design Ideal For HVAC Applications
- 3 Different Output Connections Available For Mounting Versatility
- 316 Stainless Steel, NEMA 4 Enclosure Protects Surface Mounted Electronics
- Compact Cylindrical Design Allows Easy Mounting In Tight Locations
- Two Standard 4-20 mA or 1-5 V Outputs
- 2% RH, 0.6°C Accuracy

The HX10 series two wire transmitters continuously measure relative humidity and temperature of duct air, and provide two separate and simultaneous analog outputs of 4-20 mA or 1-5 Vdc. Housed in a stainless steel, water tight enclosure, the HX10 models are very compact and ideally suited for duct mounting. For added versatility and easy installation, three common connection configurations are available including three foot lead wires, quick disconnect or 1/2" NPT with three foot lead wires.

The HX10 transmitters measure humidity using a thin film capacitor, while a precision integrated circuit senses temperature. Relative humidity measurements are temperature compensated.

A stainless steel mesh filter protects the sensors, which is easily removable for cleaning. An unregulated 24 Vdc power supply powers the HX10 transmitters, which may be placed anywhere in the series current loop for 4-20 mA models.

Specifications

Input Voltage Range: 24Vdc nominal (12-35Vdc)
RH Time Constant: 100 sec. 20 to 90% RH; 60 sec. 90 to 20% RH
Repeatability: ±1% RH, 0.5°F
Enclosure: 316 Stainless Steel, NEMA 4
Dimensions: 5.10" L x 0.625" Dia. (130 x 16 mm)
Weight: 0.6 lb (270 gr)

MEASUREMENT RANGES
Relative Humidity: 5 to 95%
Temperature: 32 to 212°F (0 to 100°C)

ACCURACY
Relative Humidity: ±2%
Temperature: ±1°F (0.5°C)
RH Temperature Compensation: -4 to 140°F (-20 to 60°C).

OUTPUTS
Current Output Models: 4 to 20mA for 0 to 100% RH and 32 to 212°F (0 to 100°C)
Voltage Output Models: 1 to 5Vdc for 0 to 100% RH and 32 to 212°F (0 to 100°C)

CONNECTIONS
HX11: 36" braided and shielded cable, PVC sheathing
HX12: Bendix 4-pin PTO2A-8-4P, mating connector optional
HX13: ½" male NPT conduit with 36" braided shielded cable

To Order (Specify Model Number)

Model No.	Price	Description
HX11(*)	$205	RH/Temperature transmitter with 3 lead wires
HX12(*)	225	RH/Temperature transmitter with Bendix 4-pin connector
HX13(*)	215	RH/Temperature transmitter with ½" male NPT fitting and 3 leads
PT06F-8-4S	24	Mating Bendix 4-pin connector for HX12
U24Y100	120	24Vdc, 1000mA, unregulated power supply
PSU-24B	40	24Vdc, 200mA, unregulated power supply

To order, specify "V" for voltage outputs, or "C" for current outputs.
Ordering Example: *HX11C, transmitter with current outputs, 3 lead wires, $205.*

Twisted/Shielded Thermocouple Wire

MADE IN USA

- Maintains Electrical Ground from Probe Sheath to Instrument
- Polyvinyl and Teflon Insulations Available
- Complements OMEGA Low Noise Thermocouple Probes and Connectors
- Extension and Thermocouple Grades
- Custom Wire Designs Available
- Consult Sales for Large Quantity Discounts

From $220 1000 ft. Spool

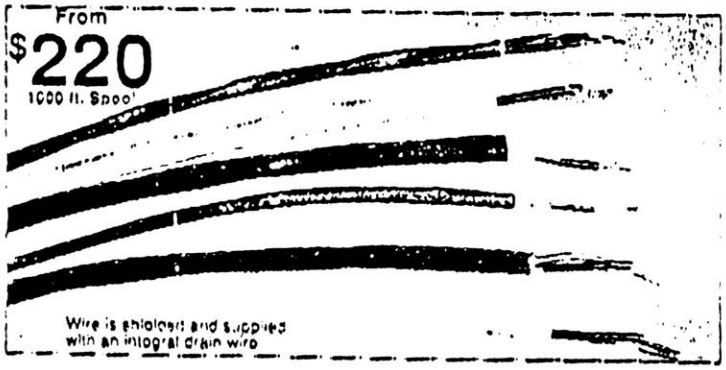

Wire is shielded and supplied with an integral drain wire

Thermocouple Grade PFA Teflon Insulation

AWG	Model No.	Thermocouple Calibration	Price 1000'
20	TT-J-20-TWSH	J	$ 760
	TT-K-20-TWSH	K	875
	TT-T-20-TWSH	T	750
	TT-E-20-TWSH	E	925
20S*	TT-J-20S-TWSH	J	915
	TT-K-20S-TWSH	K	1050
	TT-T-20S-TWSH	T	900
	TT-E-20S-TWSH	E	1110
24	TT-J-24-TWSH	J	450
	TT-K-24-TWSH	K	525
	TT-T-24-TWSH	T	430
	TT-E-24-TWSH	E	555
24S*	TT-J-24S-TWSH	J	540
	TT-K-24S-TWSH	K	630
	TT-T-24S-TWSH	T	516
	TT-E-24S-TWSH	E	670

Extension Grade Polyvinyl Insulation

AWG	Model No.	Thermocouple Calibration	Price 1000'
18	EXPP-J-18-TWSH	J	$ 420
	EXPP-K-18-TWSH	K	615
	EXPP-T-18-TWSH	T	395
	EXPP-E-18-TWSH	E	825
18S*	EXPP-J-18S-TWSH	J	695
	EXPP-K-18S-TWSH	K	995
	EXPP-T-18S-TWSH	T	665
	EXPP-E-18S-TWSH	E	1010
20	EXPP-J-20-TWSH	J	220
	EXPP-K-20-TWSH	K	320
	EXPP-T-20-TWSH	T	225
	EXPP-E-20-TWSH	E	305
20S*	EXPP-J-20S-TWSH	J	345
	EXPP-K-20S-TWSH	K	545
	EXPP-T-20S-TWSH	T	345
	EXPP-E-20S-TWSH	E	560

*Solid wire

Thermocouple Grade FEP Teflon Insulation — ***IN STOCK FOR FAST DELIVERY!***

AWG	Model No.	Thermocouple Calibration	Price 1000'
20	FF-J-20-TWSH	J	$ 575
	FF-K-20-TWSH	K	695
	FF-T-20-TWSH	T	565
	FF-E-20-TWSH	E	715
20S*	FF-J-20S-TWSH	J	690
	FF-K-20S-TWSH	K	840
	FF-T-20S-TWSH	T	680
	FF-E-20S-TWSH	E	860
24	FF-J-24-TWSH	J	340
	FF-K-24-TWSH	K	395
→	FF-T-24-TWSH	T	325*
	FF-E-24-TWSH	E	425
24S*	FF-J-24S-TWSH	J	410
	FF-K-24S-TWSH	K	475
	FF-T-24S-TWSH	T	390
	FF-E-24S-TWSH	E	505

Extension Grade FEP Teflon Insulation — PFA Teflon insulation also available. Consult sales for pricing.

AWG	Model No.	Thermocouple Calibration	Price 1000'
16	EXFF-J-16-TWSH	J	$ 725
	EXFF-K-16-TWSH	K	1195
	EXFF-T-16-TWSH	T	685
	EXFF-E-16-TWSH	E	1225
16S*	EXFF-J-16S-TWSH	J	870
	EXFF-K-16S-TWSH	K	1430
	EXFF-T-16S-TWSH	T	825
	EXFF-E-16S-TWSH	E	1470
20	EXFF-J-20-TWSH	J	490
	EXFF-K-20-TWSH	K	590
	EXFF-T-20-TWSH	T	480
	EXFF-E-20-TWSH	E	605
20S*	EXFF-J-20S-TWSH	J	590
	EXFF-K-20S-TWSH	K	710
	EXFF-T-20S-TWSH	T	580
	EXFF-E-20S-TWSH	E	730

Extension grade wire also available in R and S calibrations. Consult Sales for pricing information.

THIN FILM PRESSURE SENSOR

OMEGA

100 mV OUTPUT

EXCELLENT LONG TERM STABILITY

3 YEAR WARRANTY | MADE IN USA | NIST

PX602 - PX612 Series
15 PSI TO 20,000 PSI

From

$198

- All Stainless Steel Case
- Small and Lightweight
- NEMA 4 Cable or Connector Models

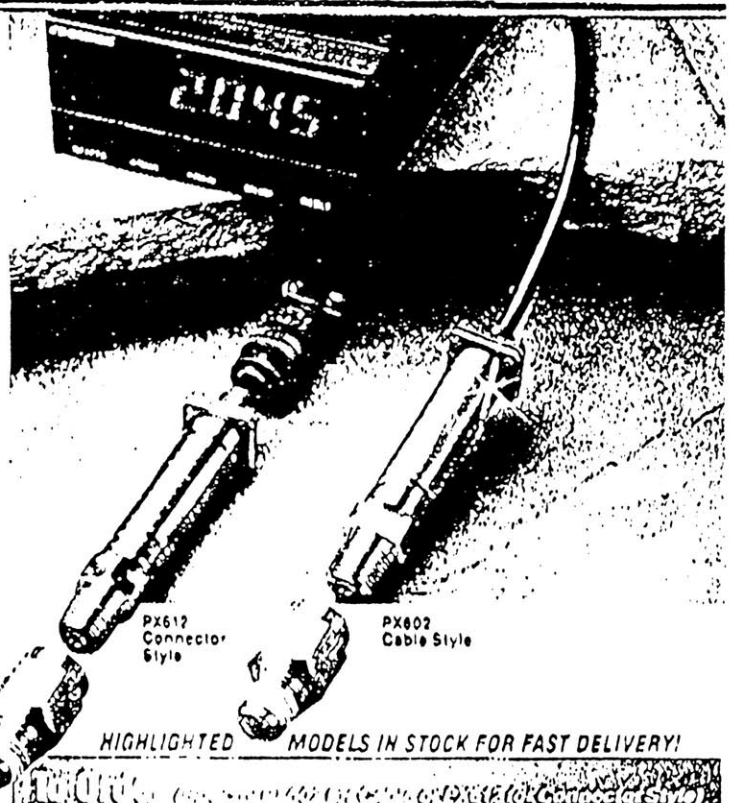

Ordering Example:
DP41-S Meter $395
PX602-100GV $198
PX612-100GV $225
PT06F8-4S Connector (not included) $24
PB-4 snubber $10

SPECIFICATIONS

Excitation: 10 Vdc (5 to 10 Vdc limits)
Output: 0 to 100 mV @ 10 Vdc
Sensitivity: 10 mV/V
Input Impedance: 1500Ω ohms
Output Impedance: 100Ω ohms
Insulation Resistance: 100M ohms @ 50 Vdc
Accuracy: ±0.4% BFSL
Hysteresis: ±0.2%
Repeatability: ±0.05%
Stability: ±1%/year
Zero Balance: ±1%
Durability: 100 million cycles
Operating Temp.: –55 to 195°F
Compensated Temp.: –20 to 180°F
Thermal Zero Effect: ±0.04% FS/°F
Thermal Span Effect: ±0.04% FS/°F
Proof Pressure: 15 to 2000 PSI = 200%; 3000 to 5000 = 150%; 7500 to 20000 = 120%
Burst Pressure: 15 to 2000 PSI = 800%; 3000 to 20000 = 500%
Gages: Thin film polysilicon
Diaphragm: 17-4PH stainless steel
Case: 300 Series stainless steel
Pressure Connection: 15 to 10,000 PSI ¼ NPT, 15,000 and 20,000 PSI = 9/16-18 UNF Aminco fitting
Electrical Connection: 36" braided shield PVC Cable or connector
Weight: 2.5 oz without cable
Response time: 1 ms
Construction: Sealed units (except PX602 ≤ 500 PSI is vented to room)

HIGHLIGHTED MODELS IN STOCK FOR FAST DELIVERY!

0-15	PX6[ ]2-015GV	$198	$225	DP41-S, DP205-S, DP350
0-30	PX6[ ]2-030GV	198	225	DP41-S, DP205-S, DP350
0-60	PX6[ ]2-060GV	198	225	DP41-S, DP205-S, DP350
0-100	PX6[ ]2-100GV	198	225	DP41-S, DP205-S, DP350
0-150	PX6[ ]2-150GV	198	225	DP41-S, DP205-S, DP350
0-200	PX6[ ]2-200GV	198	225	DP41-S, DP205-S, DP350
0-300	PX6[ ]2-300GV	198	225	DP41-S, DP205-S, DP350
0-500	PX6[ ]2-500GV	198	225	DP41-S, DP205-S, DP350
0-1000	PX6[ ]2-1KGV	198	225	DP41-S, DP205-S, DP350
0-2000	PX6[ ]2-2KGV	198	225	DP41-S, DP205-S, DP350
0-3000	PX6[ ]2-3KGV	198	225	DP41-S, DP87, DP110-R1
0-5000	PX6[ ]2-5KGV	198	225	DP41-S, DP87, DP110-R1
0-7500	PX6[ ]2-7.5KGV	198	225	DP41-S, DP87, DP110-R1
0-10,000	PX6[ ]2-10KGV	198	225	DP41-S, DP87, DP110-R1
0-15,000	PX6[ ]2-15KGV*	198	225	DP41-S, DP87, DP110-R1
0-20,000	PX6[ ]2-20KGV*	198	225	DP41-S, DP87, DP110-R1

*15,000 and 20,000 PSI Models Supplied With female AMINCO fitting.

Appendix C : Constants and Variables For Equations

Appendix C-1. Saturated Air Tables

Temp	RH	W	mass flow	spec vol	enthalpy	Energy Flow
52.15	100	0.008252	154574	12.8870	21.4627	3317576
52.145	100	0.008251	154576	12.8869	21.4598	3317170
52.14	100	0.008249	154578	12.8867	21.4569	3316764
52.135	100	0.008248	154580	12.8865	21.4540	3316359
52.13	100	0.008246	154582	12.8864	21.4511	3315953
52.125	100	0.008245	154584	12.8862	21.4482	3315548
52.12	100	0.008243	154586	12.8861	21.4453	3315142
52.115	100	0.008241	154587	12.8859	21.4425	3314736
52.11	100	0.00824	154589	12.8857	21.4396	3314331
52.105	100	0.008238	154591	12.8856	21.4367	3313925
52.1	100	0.008237	154593	12.8854	21.4338	3313520
52.095	100	0.008235	154595	12.8853	21.4309	3313115
52.09	100	0.008234	154597	12.8851	21.4280	3312709
52.085	100	0.008232	154599	12.8850	21.4252	3312304
52.08	100	0.008231	154601	12.8848	21.4223	3311899
52.075	100	0.008229	154603	12.8846	21.4194	3311493
52.07	100	0.008228	154604	12.8845	21.4165	3311088
52.065	100	0.008226	154606	12.8843	21.4136	3310683
52.06	100	0.008225	154608	12.8842	21.4107	3310278
52.055	100	0.008223	154610	12.8840	21.4079	3309872
52.05	100	0.008221	154612	12.8839	21.4050	3309467
52.045	100	0.00822	154614	12.8837	21.4021	3309062
52.04	100	0.008218	154616	12.8835	21.3992	3308657
52.035	100	0.008217	154618	12.8834	21.3963	3308252
52.03	100	0.008215	154620	12.8832	21.3935	3307847
52.025	100	0.008214	154621	12.8831	21.3906	3307442
52.02	100	0.008212	154623	12.8829	21.3877	3307037
52.015	100	0.008211	154625	12.8828	21.3848	3306632
52.01	100	0.008209	154627	12.8826	21.3819	3306228
52.005	100	0.008208	154629	12.8824	21.3791	3305823
52	100	0.008206	154631	12.8823	21.3762	3305418
51.995	100	0.008205	154633	12.8821	21.3733	3305013
51.99	100	0.008203	154635	12.8820	21.3704	3304608
51.985	100	0.008202	154637	12.8818	21.3675	3304204
51.98	100	0.0082	154638	12.8817	21.3647	3303799
51.975	100	0.008198	154640	12.8815	21.3618	3303394
51.97	100	0.008197	154642	12.8813	21.3589	3302990
51.965	100	0.008195	154644	12.8812	21.3560	3302585
51.96	100	0.008194	154646	12.8810	21.3532	3302181
51.955	100	0.008192	154648	12.8809	21.3503	3301776

Appendix C-1. Saturated Air Tables

Temp	RH	W	mass flow	spec vol	enthalpy	Energy Flow
48.45	100	0.007181	155965	12.7721	19.4015	3025958
48.449	100	0.007181	155965	12.7721	19.4010	3025882
48.448	100	0.00718	155966	12.7720	19.4005	3025805
48.447	100	0.00718	155966	12.7720	19.3999	3025729
48.446	100	0.00718	155966	12.7720	19.3994	3025652
48.445	100	0.00718	155967	12.7719	19.3988	3025576
48.444	100	0.007179	155967	12.7719	19.3983	3025499
48.443	100	0.007179	155968	12.7719	19.3978	3025422
48.442	100	0.007179	155968	12.7719	19.3972	3025346
48.441	100	0.007179	155968	12.7718	19.3967	3025269
48.44	100	0.007178	155969	12.7718	19.3962	3025193
48.439	100	0.007178	155969	12.7718	19.3956	3025116
48.438	100	0.007178	155969	12.7717	19.3951	3025040
48.437	100	0.007177	155970	12.7717	19.3945	3024963
48.436	100	0.007177	155970	12.7717	19.3940	3024887
48.435	100	0.007177	155971	12.7716	19.3935	3024810
48.434	100	0.007177	155971	12.7716	19.3929	3024734
48.433	100	0.007176	155971	12.7716	19.3924	3024657
48.432	100	0.007176	155972	12.7715	19.3919	3024580
48.431	100	0.007176	155972	12.7715	19.3913	3024504
48.43	100	0.007176	155972	12.7715	19.3908	3024427
48.429	100	0.007175	155973	12.7715	19.3902	3024351
48.428	100	0.007175	155973	12.7714	19.3897	3024274
48.427	100	0.007175	155974	12.7714	19.3892	3024198
48.426	100	0.007174	155974	12.7714	19.3886	3024121
48.425	100	0.007174	155974	12.7713	19.3881	3024045
48.424	100	0.007174	155975	12.7713	19.3876	3023968
48.423	100	0.007174	155975	12.7713	19.3870	3023892
48.422	100	0.007173	155975	12.7712	19.3865	3023815
48.421	100	0.007173	155976	12.7712	19.3859	3023739
48.42	100	0.007173	155976	12.7712	19.3854	3023662
48.419	100	0.007173	155977	12.7712	19.3849	3023585
48.418	100	0.007172	155977	12.7711	19.3843	3023509
48.417	100	0.007172	155977	12.7711	19.3838	3023432
48.416	100	0.007172	155978	12.7711	19.3832	3023356
48.415	100	0.007172	155978	12.7710	19.3827	3023279
48.414	100	0.007171	155978	12.7710	19.3822	3023203
48.413	100	0.007171	155979	12.7710	19.3816	3023126
48.412	100	0.007171	155979	12.7709	19.3811	3023050
48.411	100	0.00717	155980	12.7709	19.3806	3022973

Appendix C-1. Saturated Air Tables

Temp	RH	W	mass flow	spec vol	enthalpy	Energy Flow
45.7	100	0.006467	156992	12.6886	17.9610	2819735
45.699	100	0.006467	156992	12.6885	17.9605	2819661
45.698	100	0.006467	156992	12.6885	17.9600	2819588
45.697	100	0.006467	156993	12.6885	17.9595	2819514
45.696	100	0.006466	156993	12.6884	17.9590	2819441
45.695	100	0.006466	156994	12.6884	17.9585	2819367
45.694	100	0.006466	156994	12.6884	17.9580	2819294
45.693	100	0.006466	156994	12.6884	17.9575	2819220
45.692	100	0.006465	156995	12.6883	17.9570	2819147
45.691	100	0.006465	156995	12.6883	17.9564	2819074
45.69	100	0.006465	156995	12.6883	17.9559	2819000
45.689	100	0.006465	156996	12.6882	17.9554	2818927
45.688	100	0.006464	156996	12.6882	17.9549	2818853
45.687	100	0.006464	156997	12.6882	17.9544	2818780
45.686	100	0.006464	156997	12.6881	17.9539	2818706
45.685	100	0.006464	156997	12.6881	17.9534	2818633
45.684	100	0.006463	156998	12.6881	17.9529	2818559
45.683	100	0.006463	156998	12.6881	17.9524	2818486
45.682	100	0.006463	156998	12.6880	17.9519	2818412
45.681	100	0.006463	156999	12.6880	17.9513	2818339
45.68	100	0.006462	156999	12.6880	17.9508	2818266
45.679	100	0.006462	157000	12.6879	17.9503	2818192
45.678	100	0.006462	157000	12.6879	17.9498	2818119
45.677	100	0.006462	157000	12.6879	17.9493	2818045
45.676	100	0.006461	157001	12.6878	17.9488	2817972
45.675	100	0.006461	157001	12.6878	17.9483	2817898
45.674	100	0.006461	157001	12.6878	17.9478	2817825
45.673	100	0.006461	157002	12.6878	17.9473	2817752
45.672	100	0.00646	157002	12.6877	17.9467	2817678
45.671	100	0.00646	157003	12.6877	17.9462	2817605
45.67	100	0.00646	157003	12.6877	17.9457	2817531
45.669	100	0.00646	157003	12.6876	17.9452	2817458
45.668	100	0.006459	157004	12.6876	17.9447	2817384
45.667	100	0.006459	157004	12.6876	17.9442	2817311
45.666	100	0.006459	157004	12.6875	17.9437	2817238
45.665	100	0.006459	157005	12.6875	17.9432	2817164
45.664	100	0.006458	157005	12.6875	17.9427	2817091
45.663	100	0.006458	157006	12.6875	17.9422	2817017
45.662	100	0.006458	157006	12.6874	17.9416	2816944
45.661	100	0.006458	157006	12.6874	17.9411	2816870

Appendix C-2. Constants Used in Analysis

Equation 2.11.

$C_0 = -10440.4$

$C_1 = -11.2946669$

$C_2 = -0.02700133$

$C_3 = 0.12897060 \times 10^{-4}$

$C_4 = -0.2478068 \times 10^{-8}$

$C_5 = 6.5459673$

Appendix D. Uncertainties in Variables and Equations

In this appendix, the issue of uncertainties and errors in measurement, equations, and regressions will be addressed. The errors calculated in this section are to be used throughout the thesis, and will be referred to therein. Uncertainties in sums, differences, products, and quotients are calculated using the following equations (Taylor 1982):

Measured X	(measured)X = X best $\pm \delta X$
$Z = X + Y, Z = X - Y$	$\delta Z = \delta X + \delta Y$
$Z = XY, Z = X/Y$	$\delta Z/Z = \delta X/X + \delta Y/Y$
$Z = aX$	$\delta Z = a\delta X$
$Z = X^n$	$\delta Z/Z = n\delta X/X$
$Z = f(X)$	$\delta Z = (dZ/dX)\delta X$

I. Measured Data

For monitored measurements, the manufacturers errors for the sensors are:

$\delta T = \pm 1^o$ F	Temperature
$\delta RH/RH = \pm 2\%$	Relative Humidity
$\delta P/P = \pm 0.4\%$	Pressure
$\delta M/M = \pm 0.2\%$	Mass Flow

II. Psychrometeric Variables

Specific Humidity: $W = 0.62198\ (p_w / p\text{-}p_w)$ [lb water/lb air] (2.1)

p = atmospheric pressure (psi)

p_w = partial water vapor pressure (psi)

Error : $\delta W/W = 0.62198(\delta p_w/p_w + \delta p/p + \delta p_w/p_w)$

$= 0.62198(\ 2\% + 2\%)$ $\quad [\delta p/p=0]$

$= 2.5\%$

$$p_w = p_{ws}\ x\ RH \tag{2.2}$$

RH = relative humidity

p_{ws}=partial water vapor saturation pressure (psi)

Error : $\delta p_w/p_w = \delta p_{ws}/p_{ws} + \delta RH/RH$

$= 0.02\% + 2\%$

$= 2\%$

$$p_{ws}=C_0+C_1(T)+C_2(T^2)+C_3(T^3)+C_4(T^4)+C_5(lnT) \tag{2.3}$$

T = dry bulb temperature (R)

Error : $\delta p_{ws}/p_{ws} = C_1(\delta T/T)+2C_2(\delta T/T)+3C_3(\delta T/T)+4C_4(\delta T/T)+1/T(C_5(\delta T/T))$

$= (C_1+2C_2+3C_3+4C_4+1/T(C_5))(1/T)$

Constants are found in Appendix C-2, error is a function of T

$= -11.349(1/T) + 6.546(1/T^2)$

which, for the range of T = 529.6 R - 579.6 R (50 F - 100 F) is

$= 0.02\%$

Dew Point Temperature:$T_d = 79.047 + 30.5790\alpha + 1.8893\alpha^2$ [F] (7.1)

Error : $\delta T_d = 30.5790\delta\alpha + 1.8893(2)\delta\alpha$

$= 30.5790(.04) + 3.7786(.04)$

$=1.37$ [F]

$$\alpha = ln(p_W) \tag{7.2}$$

Error : $\delta\alpha = (1/p_W)\delta p_W$

$= \delta p_W/p_W = 4\%$

$$p_W = (p*W) / (0.62198 + W) \tag{7.3}$$

Error : $\delta p_W/p_W = \delta p/p + \delta W/W + \delta W/W$

$= 4\%$ [$\delta p/p= 0$]

W = specific humidity

p = atmospheric pressure [in. Hg]

p_W = water vapor partial pressure [in. Hg]

III. Refrigeration System Equations

The enthalpy of the refrigerant before the expansion valve can be expressed by the following equation:

Enthalpy : $h = 10.98322 + 0.22852(T) + 0.00038(T^2)$ [Btu/lb] (8.1)

$(R^2=1.000)$

T = dry bulb temperature (F)

Error : $\delta h/h = 0.22852(\delta T/T) + 0.00038(2)(\delta T/T)$

$= 0.22926(1/T)$

Since the temperature range falls between 80 F - 110 F, and the value of the error is small enough not to vary much between these points, it can be estimated as 0.002, or 0.2%.

and for the enthalpy of the refrigerant after the evaporator:

Enthalpy : $h = 78.668 + 0.158(T)$ [Btu/lb] (8.2)

$(R^2=0.999)$

T = dry bulb temperature (F)

Error : $\delta h/h = 0.158(\delta T/T)$

$= 0.158(1/T)$

so the error for the display case load (evaporator load) is:

Display Case Load ; $Q = m\,(h_2 - h_1)$ [Btu/hr] (4.1)

m = mass flow (lb/hr)

h_2=enthalpy of suction gas (Btu/lb)

h_1=enthalpy of liquid (Btu/lb)

Error : $\delta Q/Q = \delta m/m + \delta h_2/h_2 + \delta h_1/h_1$

$= 0.2\% + (0.16/T_2 + 0.002)$

$= 0.4\% + (0.16/T_2)$

IV. Section 7.1.1 Calculated vs Monitored Mixed air

The equation comparing calculated mixed air temperature to monitored mixed air temperature has an error (0.6 degree) which is close to the sensor error (1 degree), therefore the uncertainty is the root mean square, or the square root of the sum of the

squares of the deviations divided by the number of deviations. For two deviations the equation looks like this:

$$RMS = \sqrt{[(\delta T_1)^2+(\delta T_2)^2]} / 2$$

which for δT_1=0.6 and δT_2=1, RMS = 0.8 degrees

V. Section 7.2.3 Calculated Mixed air vs Supply air

The uncertainties in this analysis occur in the calculation of dew point, and the monitored temperature difference across the cooling coils. Since the dew point is not a factor in the calculation, but a checkpoint for what equations will be used, it is only a factor when the calculated post-cooling coil temperature is closer to the dew point than the statistical error. Since this rarely occurs, it can be ignored. Since the error in temperature difference is twice the error for one sensor, the error for specific humidity is the same calculated above with twice the temperature error. Yet since that error is dominated by the error in the relative humidity sensor, the difference is small (the difference between 2.02% and 2.04%), and the estimate of 2% can be used

VI. Section 9.1.2 Rack A Compressor Power vs Dew Point and Outside Temperature

The regression equations for pre-installation and post-installation compressor power result in the following equations:

Pre-Installation

$$CMPA = 15.41 + 0.08051(dewpt) + 0.1382(Tout) \text{ [kW]}$$

Post-Installation

$$CMPA = 18.85 - 0.01321(dewpt) + 0.140(Tout) \text{ [kW]}$$

Pre-installation error : $\delta CMPA = 0.08051(\delta T_d) + 0.1382(\delta T)$

$= 0.08051(1.37) + 0.1382(1)$

$= 0.25$ [kW]

Post-installation error : $\delta CMPA = 0.01321(\delta T_d) + 0.140(\delta T)$

$= 0.16$ [kW]

VII. Section 9.2 Air Conditioning Fan Penalties

The accuracy of the volumetric airflow measurement can only be approximated using the measurement errors of its parts, as the flow was measured using a vane anemometer, a device which uses fan blades to measure distance traveled by the air in feet (with an error of ±1 foot). A stopwatch was used to time the readings (with an error of ±0.1 second), and the cross-sectional area was used with these readings (error of ±.01 ft^2) to calculate cfm. However, there are other, unmeasurable errors associated with this calculation, since the method was to have one person inside the duct, transversing the whole area with the meter while another person outside starts and stops the stopwatch at a verbal cue. Therefore, there are potential errors relating to possible differences in starting times, stopping times, and areas covered by the metering person. The metering error can be calculated as follows:

Error : $\delta CFM/CFM = \delta(\text{velometer})/\text{velometer} + \delta(\text{stopwatch})/\text{stopwatch} \times 60 + \delta(\text{area})/\text{area}$

which, for the upper half, comes to $1/167 + (0.1/22.4)60 + .01/19.38 = 0.274 = 27.4\%$

and for the lower half, $1/320 + (0.1/18.5)60 + .01/19.38 = 0.324 = 32.4\%$

giving an airflow estimation of $32{,}400 \pm 9.980$ cfm

Appendix E. Sensor Calibrations

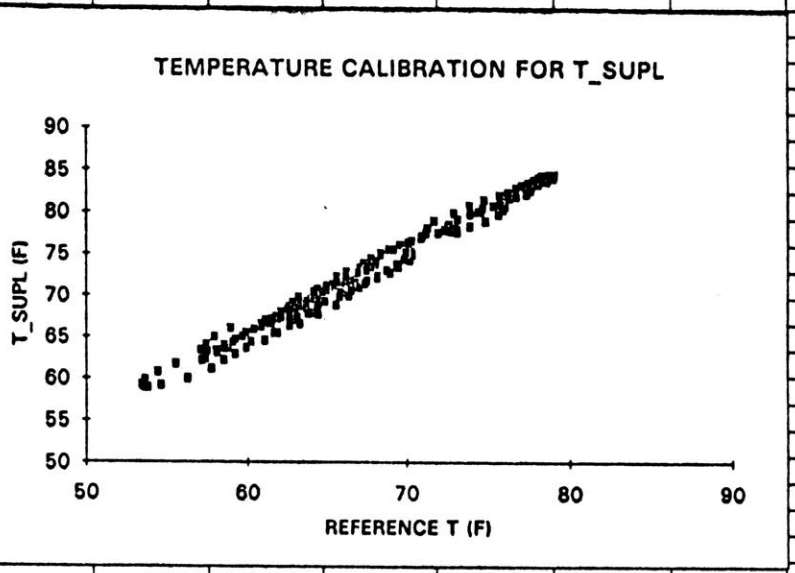

		AVERAGE TREF-T_SUPL =			-5.36189		
Regression Statistics							
	Multiple R	0.99092					
	R Square	0.981923					
	Adjusted R	0.98183					
	Standard E	0.857105					
	Observatio	196					
Analysis of Variance							
		df	*m of Squares*	*Mean Square*	*F*	*Significance F*	
	Regression	1	7741.568	7741.568	10538.06	5E-171	
	Residual	194	142.518	0.734629			
	Total	195	7884.086				
		Coefficients	*tandard Error*	*t Statistic*	*P-value*	*Lower 95%*	*Upper 95%*
	Intercept	-3.08728	0.682273	-4.525	1.05E-05	-4.43291	-1.74166
	x1	0.968422	0.009434	102.6551	1.1E-171	0.949816	0.987028
CORRECTION FOR ALL DATA							
	ACTUAL T_SUPL = 0.97*(MEASURED T_SUPL) - 3.1 F						
OR	ACTUAL T_SUPL = MEASURED T_SUPL - 5.4 F						

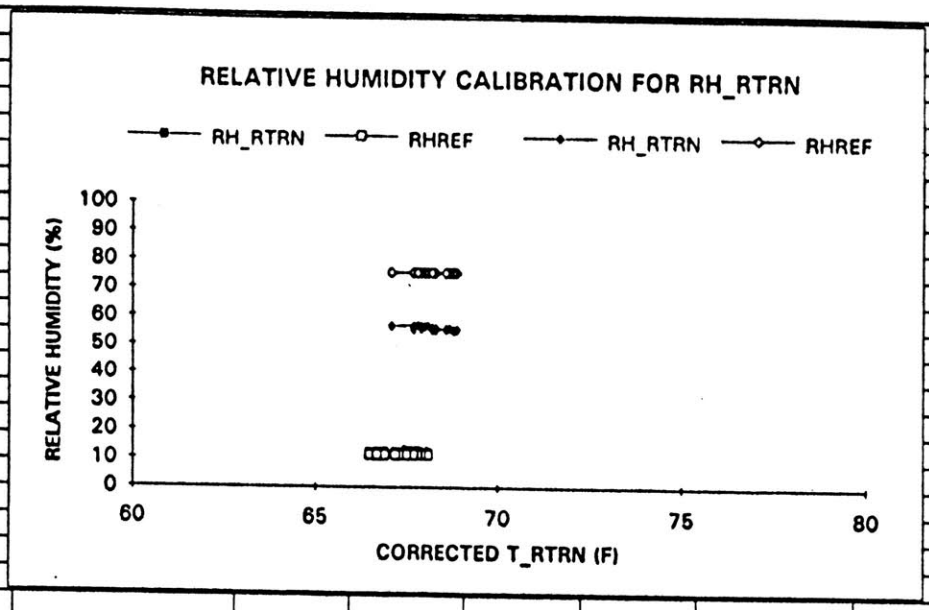

		AT RHREF = 75.5		AVERAGE (RHREF - RH_RTRN) =			19.223226
		AT RHREF = 11.3		AVERAGE (RHREF - RH_RTRN) =			-0.967083
	Regression Statistics						
	Multiple R	0.999839					
	R Square	0.999677					
	Adjusted R Square	0.999665					
	Standard Error	0.58832					
	Observations	55					
	Analysis of Variance						
		df	*m of Squares*	*Mean Square*	*F*	*Significance F*	
	Regression	2	55736.55	27868.28	80516.2	1.70882E-91	
	Residual	52	17.99825	0.34612			
	Total	54	55754.55				
		Coefficients	*tandard Error*	*t Statistic*	*P-value*	*Lower 95%*	*Upper 95%*
	Intercept	-44.5976	11.61239	-3.84051	0.000325	-67.899501	-21.29561
	x1	0.564929	0.172513	3.27471	0.00185	0.21875722	0.9111006
	x2	1.450276	0.004366	332.1652	4.46E-91	1.441514648	1.4590372

CORRECTION FOR DATA UP TO 16:45 ON 9/22/93

ACTUAL T_RTRN = MEASURED T_RTRN - 5.8 F

ACTUAL RH_RTRN = 0.565*(T_RTRN) + 1.450*(MEASURED RH_RTRN) - 44.6

ALTERNATE CORRELATION WITH NO TEMPERATURE DEPENDENCE

Regression Statistics

Multiple R	0.999805
R Square	0.999611
Adjusted R Square	0.999603
Standard Error	0.640017
Observations	55

Analysis of Variance

	df	*m of Squares*	*Mean Square*	*F*	*Significance F*
Regression	1	55732.84	55732.84	136059.3	4.81796E-92
Residual	53	21.70994	0.409622		
Total	54	55754.55			

	Coefficients	*tandard Error*	*t Statistic*	*P-value*	*Lower 95%*	*Upper 95%*
Intercept	-6.57379	0.170078	-38.6516	4.92E-41	-6.91492369	-6.232657
x1	1.458202	0.003953	368.8622	1.56E-93	1.450272402	1.4661308

CORRECTION FOR DATA UP TO 16:45 ON 9/22/93

ACTUAL RH_RTRN = 1.458*(MEASURED RH_RTRN) - 6.6

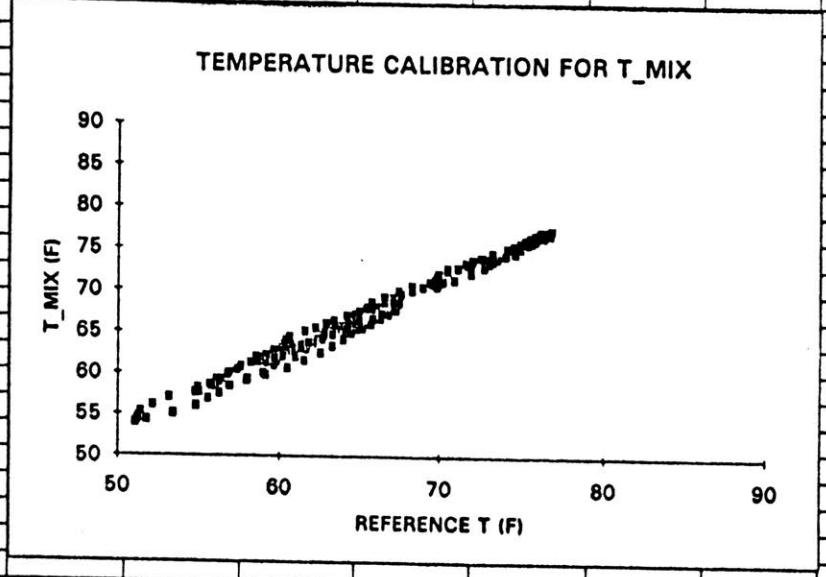

		AVERAGE TREF - T_MIX =			-1.76643		
Regression Statistics							
	Multiple R	0.991826					
	R Square	0.983719					
	Adjusted R	0.983635					
	Standard E	0.806442					
	Observatio	196					
Analysis of Variance							
		df	*m of Squares*	*Mean Square*		*F Significance F*	
	Regression	1	7623.334	7623.334	11721.93	2E-175	
	Residual	194	126.1675	0.650348			
	Total	195	7749.501				
		Coefficients	*tandard Error*	*t Statistic*	*P-value*	*Lower 95%*	*Upper 95%*
	Intercept	-7.93945	0.670412	-11.8426	9.95E-25	-9.26168	-6.61722
	x1	1.093329	0.010098	108.2679	4.1E-176	1.073412	1.113246
CORRECTION FOR DATA FROM 8/11/93							
		ACTUAL T_MIX = 1.09*(MEASURED T_MIX) - 7.9					
OR		ACTUAL T_MIX = MEASURED T_MIX - 1.8					

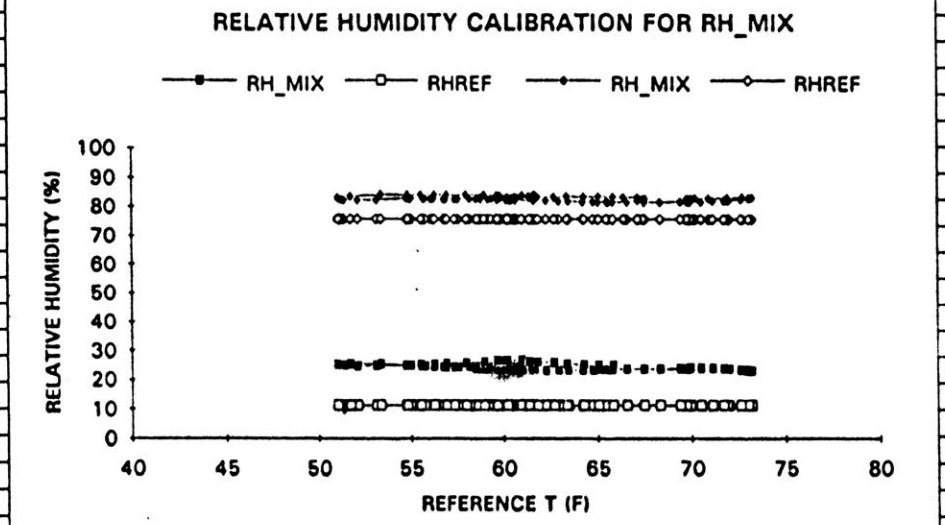

AT RHREF = 11.3	AVERAGE (RHREF - RH_MIX) =				-13.1336	
AT RHREF = 75.5	AVERAGE (RHREF - RH_MIX) =				-6.98785	
Regression Statistics						
Multiple R	0.99968					
R Square	0.999359					
Adjusted R Square	0.999353					
Standard Error	0.81541					
Observations	196					
Analysis of Variance						
	df	*m of Squares*	*Mean Square*		*F*	*Significance F*
Regression	2	200128.7	100064.4	150496.8		0
Residual	193	128.3245	0.664894			
Total	195	200257				
	Coefficients	*tandard Error*	*t Statistic*	*P-value*	*Lower 95%*	*Upper 95%*
Intercept	-19.4224	0.616183	-31.5205	1.82E-78	-20.6377	-18.2071
x1	0.061553	0.009896	6.219728	2.97E-09	0.042034	0.0810719
x2	1.103764	0.002024	545.2788	0	1.099772	1.1077566

CORRECTION FOR DATA FROM 8/11/93

ACTUAL RH_MIX = 0.062*(T_MIX) + 1.104*(MEASURED RH_MIX) - 19.4

ALTERNATE CORRELATION WITH NO TEMPERATURE DEPENDENCE

Regression Statistics	
Multiple R	0.999615
R Square	0.999231
Adjusted R Square	0.999227
Standard Error	0.891095
Observations	196

Anelysis of Variance	*df*	*m of Squares*	*Mean Square*	*F*	*Significance F*
Regression	1	200103	200103	252002.7	5.1E-304
Residual	194	154.0459	0.794051		
Total	195	200257			

	Coefficients	*tandard Error*	*t Statistic*	*P-value*	*Lower 95%*	*Upper 95%*
Intercept	-15.6724	0.138979	-112.769	1.6E-179	-15.9465	-15.39834
x1	1.105011	0.002201	501.9987	2.3E-305	1.10067	1.1093528

CORRECTION FOR DATA FROM 8/11/93

ACTUAL RH_MIX = 1.105*(MEASURED RH_MIX) - 15.7

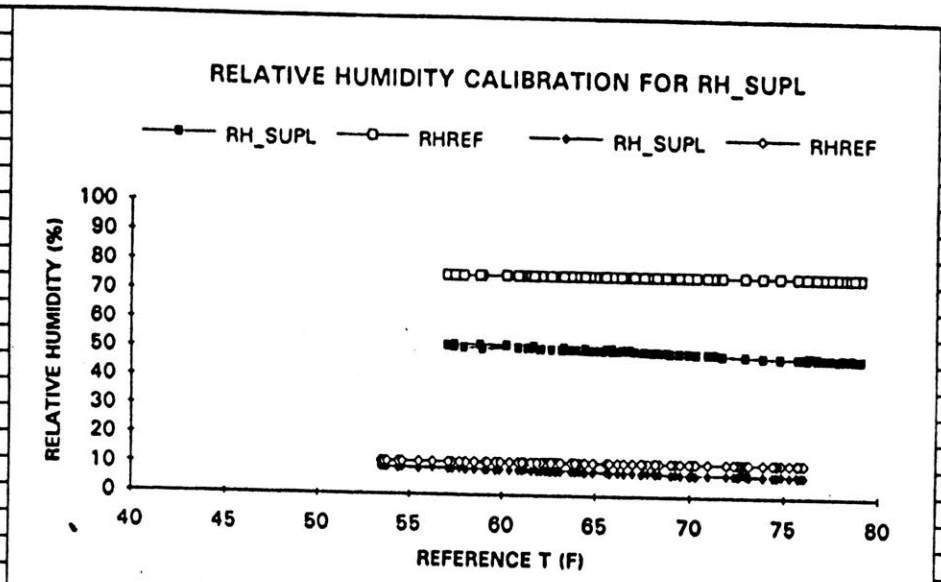

	AT RHREF = 75.5	AVERAGE (RHREF - RH_SUPL) =				26.04517	
	AT RHREF = 11.3	AVERAGE (RHREF - RH_SUPL) =				3.102617	
	Regression Statistics						
	Multiple R	0.999826					
	R Square	0.999653					
	Adjusted R Square	0.999649					
	Standard Error	0.600291					
	Observations	196					
	Analysis of Variance						
		df	*m of Squares*	*Mean Square*	*F*	*Significance F*	
	Regression	2	200187.5	100093.7	277768.3	0	
	Residual	193	69.5475	0.36035			
	Total	195	200257				
		Coefficients	*tandard Error*	*t Statistic*	*P-value*	*Lower 95%*	*Upper 95%*
	Intercept	-14.8029	0.453899	-32.6129	6.79E-81	-15.6982	-13.9077
	x1	0.206438	0.006892	29.95177	7.02E-75	0.192844	0.2200324
	x2	1.54064	0.002126	724.678	0	1.536447	1.5448329
CORRECTION FOR ALL DATA							
	ACTUAL RH_SUPL = 0.206*(T_SUPL) + 1.541*(MEASURED RH_SUPL) - 14.8						

ALTERNATE CORRELATION WITH NO TEMPERATURE DEPENDENCE

Regression Statistics						
Multiple R	0.999019					
R Square	0.998038					
Adjusted R Square	0.998028					
Standard Error	1.422971					
Observations	196					
Analysis of Variance						
	df	*m of Squares*	*Mean Square*	*F*	*Significance F*	
Regression	1	199864.2	199864.2	98705.84	1.4E-264	
Residual	194	392.8203	2.024847			
Total	195	200257				
	Coefficients	*tandard Error*	*t Statistic*	*P-value*	*Lower 95%*	*Upper 95%*
Intercept	-1.3736	0.167493	-8.20092	3.15E-14	-1.70394	-1.043258
x1	1.55303	0.004943	314.1749	1E-265	1.543281	1.5627796

CORRECTION FOR ALL DATA

ACTUAL RH_SUPL = 1.553*(MEASURED RH_SUPL) - 1.4

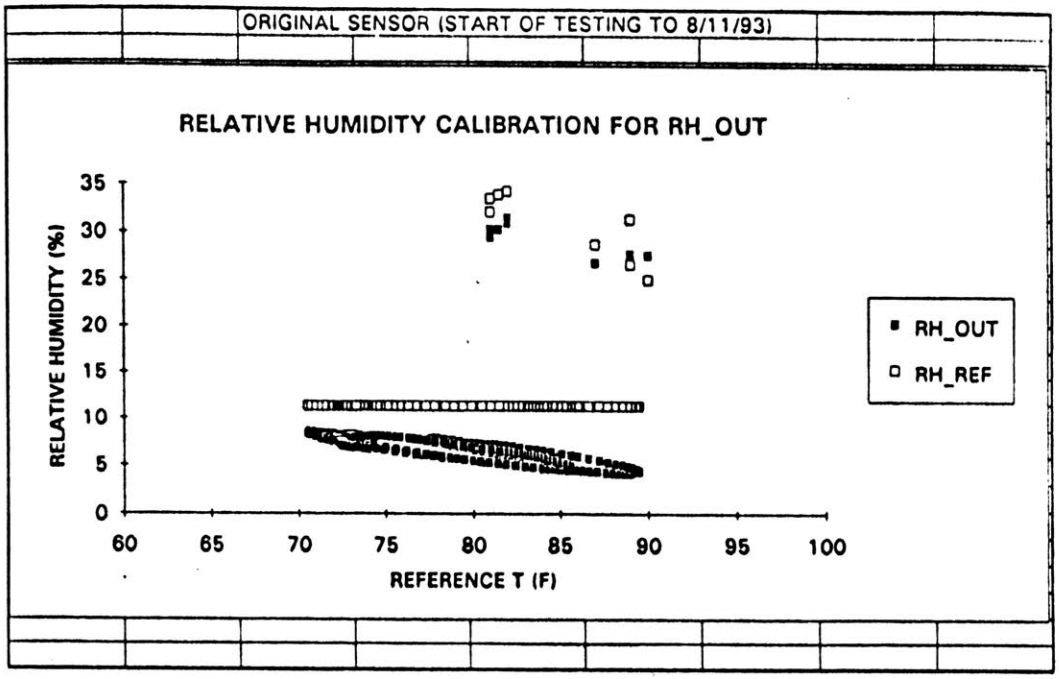
ORIGINAL SENSOR (START OF TESTING TO 8/11/93)
RELATIVE HUMIDITY CALIBRATION FOR RH_OUT
RELATIVE HUMIDITY (%)
35
30
25
20
15
10
5
0
60
65
70
75
80
85
90
95
100
REFERENCE T (F)
RH_OUT
RH_REF

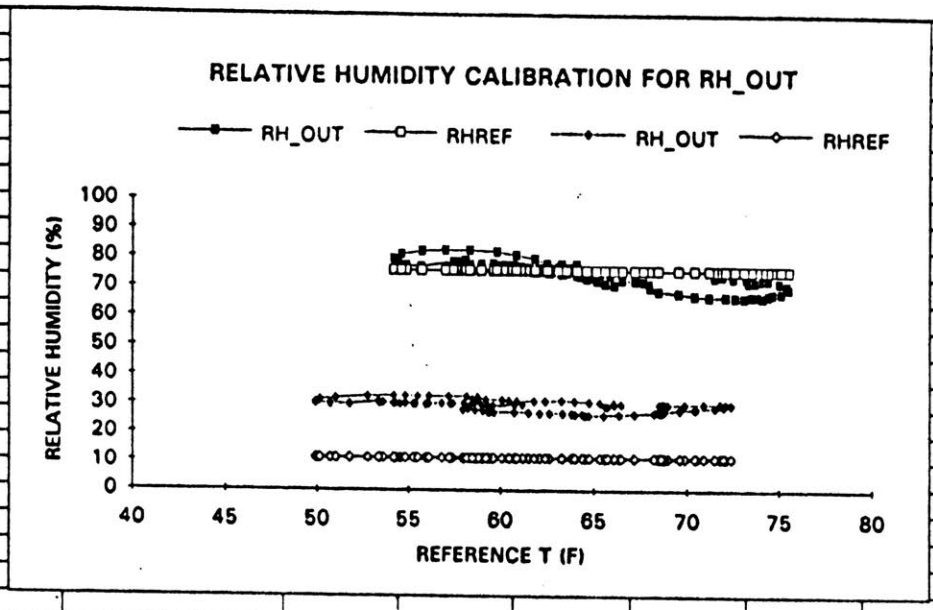

AT RHREF = 75.5	AVERAGE (RHREF - RH_OUT) =				1.112135	
AT RHREF = 11.3	AVERAGE (RHREF - RH_OUT) =				-18.2625	
Regression Statistics						
Multiple R	0.994887					
R Square	0.989801					
Adjusted R Square	0.989695					
Standard Error	3.253059					
Observations	196					
Analysis of Variance						
	df	*m of Squares*	*Mean Square*	*F*	*Significance F*	
Regression	2	198214.6	99107.31	9365.3	6.7E-193	
Residual	193	2042.402	10.5824			
Total	195	200257				
	Coefficients	*tandard Error*	*t Statistic*	*P-value*	*Lower 95%*	*Upper 95%*
Intercept	-58.3383	2.370599	-24.6091	1.03E-61	-63.0139	-53.66267
x1	0.472106	0.03799	12.42695	1.71E-26	0.397176	0.5470352
x2	1.382704	0.010483	131.8952	1.3E-192	1.362027	1.4033807

CORRECTION FOR DATA FROM 16:15 on 8/27/93

ACTUAL RH_OUT = 0.472*(T_OUT) + 1.383*(MEASURED RH_OUT) - 58.3

ALTERNATIVE CORRELATION WITH NO TEMPERATURE DEPENDENCE

Regression Statistics	
Multiple R	0.990778
R Square	0.98164
Adjusted R Square	0.981546
Standard Error	4.353356
Observations	196

Analysis of Variance	*df*	*m of Squares*	*Mean Square*	*F*	*Significence F*
Regression	1	196580.4	196580.4	10372.7	2.3E-170
Residual	194	3676.632	18.95171		
Total	195	200257			

	Coefficients	*tandard Error*	*t Statistic*	*P-value*	*Lower 95%*	*Upper 95%*
Intercept	-29.7276	0.755986	-39.323	1.19E-94	-31.2186	-28.23663
x1	1.405931	0.013804	101.8464	5E-171	1.378705	1.4331565

CORRECTION FOR DATA FROM 16:15 on 8/27/93

ACTUAL RH_OUT = 1.406*(MEASURED RH_OUT) - 29.7

Appendix F Figures for Annual Savings Estimates

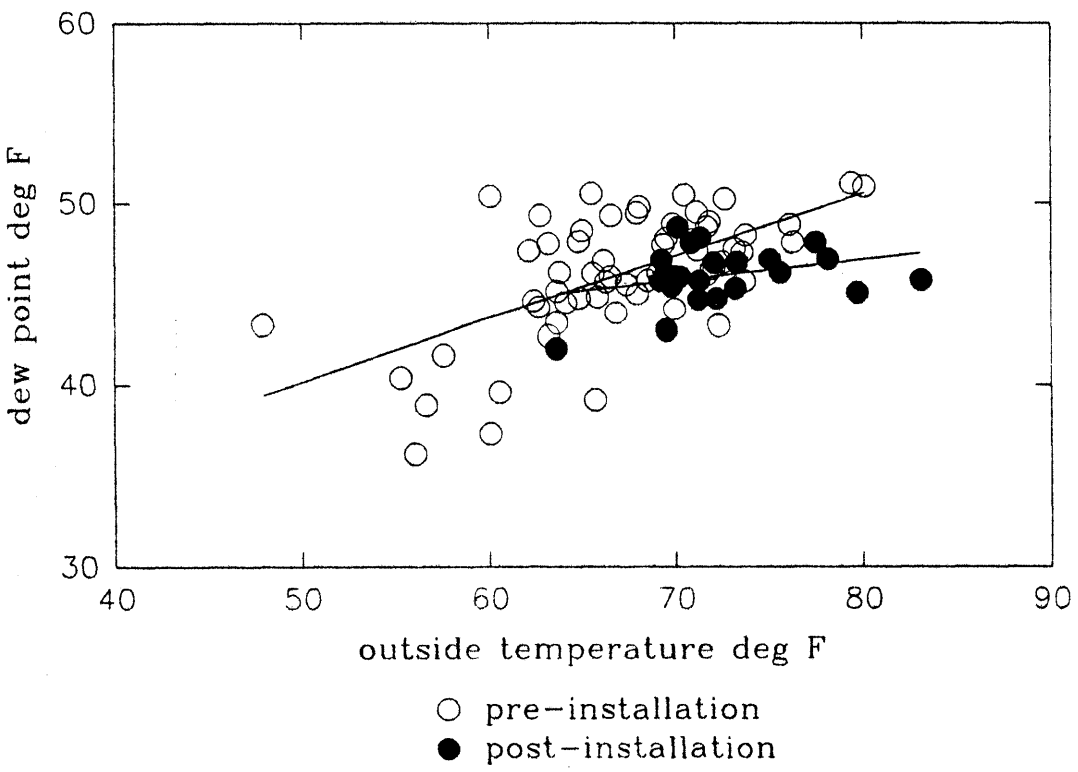

Figure 60. Pre- and Post-installation Daily Average Dew Point vs Average Outside Temperature

Figure 61. Annual Savings Estimates based on Weatherly Bin Data for 1993

Weatherly Bin Data - Boston Massachusetts 1993

Outside Dry Bulb Temperatures (F)		Bin Average	Dew Pt Average [1]	Ave Dew Pt Drop [2]	Ref. Comp kW [3]	Jan hrs	Feb hrs	Mar hrs	Apr hrs	May hrs	June hrs	July hrs	Aug hrs	Sept hrs	Oct hrs	Nov hrs	Dec hrs	Annual Total
95	99	97	48.3	2.6	118.7412	0	0	0	0	0	0	7	0	0	0	0	0	7
90	94	92	47.7	2.6	116.591	0	0	0	0	1	0	20	7	5	0	0	0	33
85	89	87	47.2	2.6	114.4408	0	0	0	0	9	1	48	29	13	0	0	0	100
80	84	82	46.6	2.6	112.2906	0	0	0	0	17	16	87	81	22	0	0	0	223
75	79	77	46.1	2.6	110.1404	0	0	0	1	31	48	119	121	42	6	2	0	370
70	74	72	45.5	1.8	107.9902	0	0	2	11	46	76	174	159	81	16	8	0	573
65	69	67	45	0.7	105.84	0	0	2	18	75	126	199	200	142	47	13	0	822
Total Hours						0	0	4	30	179	267	654	597	305	69	23	0	2128
Total kWh saved [4]						0	0	9	64	532	728	2219	1951	852	141	53	0	6549

[1] Average inside dew point, based on post-installation curve fit
[2] Average drop in inside dew point due to heat pipe, based on comparison of pre-installation and post-installation data
[3] Refrigeration system compressor power consumption as a function of outside temperature
[4] KWh savings based on 1.7% kW reduction per 1 degree drop in dew point